Design of Teleoperated Surgical Instruments for Minimally Invasive Surgery

by

Akhil Jiten Madhani

B.S. Mechanical Engineering
University of California at Berkeley, 1989

S.M. Mechanical Engineering
Massachusetts Institute of Technology, 1991

Submitted to the Department of Mechanical Engineering
in partial fulfillment of the requirements for the degree of

Doctor of Philosophy in Mechanical Engineering

at the

MASSACHUSETTS INSTITUTE OF TECHNOLOGY

February 1998

© 1998 Massachusetts Institute of Technology. All rights reserved.

Author . . . .
Department of Mechanical Engineering
September 22, 1997

Certified by . . . .
Dr. J. Kenneth Salisbury Jr., Thesis Supervisor
Principal Research Scientist, Mechanical Engineering, MIT

Accepted by . . . .
Professor Ain A. Sonin
Chair, Department Graduate Committee

JUN 03 1998

Design of Teleoperated Surgical Instruments
for Minimally Invasive Surgery
by
Akhil Jiten Madhani

Submitted to the Department of Mechanical Engineering
on September 22, 1997, in partial fulfillment of the
requirements for the degree of
Doctor of Philosophy in Mechanical Engineering

Abstract

Minimally invasive surgery (MIS) is performed today using hand held instruments passed through small incisions into the body. The internal surgical site and instruments are viewed remotely on a monitor using images obtained with an endoscopic camera. It is well recognized that the marked therapeutic benefits of MIS must be weighed against the increased technical difficulty for the surgeon and the ensuing risk of surgical errors.

Here I describe the design, construction, and operation of teleoperated surgical instruments that solve several key problems in current minimally invasive surgical practice. These improvements are primarily achieved through 1) an increase in dexterity and degrees of freedom, 2) force feedback to allow surgeons to feel instrument-tissue interactions, and 3) the elimination of geometrical discrepancies between actual and observed tool motions.

I present the design of two teleoperator slave manipulators for minimally invasive surgery, the seven-degree-of-freedom Silver Falcon and the eight-degree-of-freedom Black Falcon. Both systems were tested using an existing PHANToM™ haptic interface which was modified for use as a master manipulator. Position based bilateral force-reflecting teleoperation was implemented using sound cable design principles, without force sensors. Through the design of system dynamics that accommodate a macro-micro control scheme, a substantial reduction was achieved in slave endpoint inertia and friction reflected to the user.

The Black Falcon was successfully used to drive surgical sutures along arbitrarily oriented paths, a task which is rarely feasible using today's instruments. This test demonstrates successful kinematic design and range of motion, although the quality of force reflection was not sufficient to be helpful when suturing soft tissue. Force reflection was found to be more useful during rigid contact tasks where force information is not already available to the operator via visual cues.

Thesis Supervisor: Dr. J. Kenneth Salisbury, Jr.
Title: Principal Research Scientist

Thesis Committee:

Dr. J. Kenneth Salisbury, Jr., Chairperson
Principal Research Scientist, Department of Mechanical Engineering, MIT.

Professor David Wallace
Assistant Professor of Mechanical Engineering, MIT.

Dr. Mandayam Srinivasan
Principal Research Scientist, Department of Mechanical Engineering, MIT.

Dr. Joseph Rosen, M.D. Associate Professor of Plastic Surgery, Department of Surgery, Dartmouth University.

Acknowledgments

My most sincere and heartfelt thank you goes to my advisor, J. Kenneth Salisbury Jr. This last year and a half has been very exciting for both Ken and me. I feel tremendously fortunate to have had the opportunity and freedom to embark on this project and to have such a supportive, intelligent, and creative friend and ally with whom to see this project forward. I only hope that we will continue to know each other as friends and colleagues in the years to come.

On this project I have had the privilege of working with one of the best controls/dynamics/software people at MIT, and probably the planet, Günter Niemeyer. After receiving his Ph.D., Günter did postdoctoral work on this project, writing the control code for both the Silver Falcon and the Black Falcon teleoperator slaves and the PHANToM and Toolhandle master manipulators. I learned far more about control systems by working alongside Günter than I did in any of my MIT controls classes.

A number of other former graduate students also deserve thanks. Evangelos Papadopolous, Joe Deck, and Bert Hootsmans from Building 3, and Brian Eberman and Erik Vaaler at the AI lab showed me the ropes at MIT.

I would like to thank Rob Younge at Intuitive Surgical, Inc. for giving me the opportunity to participate and contribute to their efforts in what promises to be an exciting endeavor. Rob is a gentleman with remarkable integrity and talent and I can think of no one more likely to make such a project successful.

Several people deserve special thanks for making the MIT AI Lab a much better place. Jacqui Taylor, Ron Wiken, Bruce Walton, and Laurel Simmons have all spent countless hours helping me during my years at the AI lab. I know for a fact that graduate students at the lab universally appreciate their efforts and their cheerful and supportive attitude.

There are those friends to whom I will always be indebted for sharing life in and around the Institute. Nick Patrick, Archie Roberts, KrisZtina Holly, John Morrell and most especially my dear friend Laurel Simmons have and continue to make life worthwhile and rewarding. My brother, Hiten, and my parents, Dhanvant and Minakshi, deserve thanks for their unwavering support.

Finally, special thanks goes to Craig Latimer and Brian Anthony for putting in many hard hours on my most ridiculous of automotive projects. And to Z for letting me leave my truck on jackstands in her garage for six weeks while we did it.

5

6

:

Contents

List of Figures

Chapter 1

Introduction

Minimally Invasive Surgery (MIS) is the practice of performing surgery through small incisions or "ports" using specialized surgical instruments in order to reduce the size of incisions required to access human internal tissues during surgery. During conventional "open" surgery, the trauma created at the wound is typically greater than at the operating site. Therefore it is argued that procedures performed using MIS will have reduced bleeding, discomfort, patient recovery time, and cost.

However, MIS is technically more difficult for the surgeon. Surgeons must train extensively, and there still remains an increased risk of surgical complications which must be traded off against the opportunity for reduced morbidity. MIS is therefore limited to a number of relatively simple procedures such as cholecystecomy (gall bladder removal) for which there seems to be a consensus within the medical community that it is in fact beneficial, (NIH, 1993). Due in part to the changing landscape of medical reimbursement in the United States, there is a substantial push from medical payer organizations (insurance companies, health maintainance organizations, and hospitals) to introduce MIS to other procedures in order to reduce hospital stays and therefore costs. Recoveries are typically faster and less painful which also means patients are asking for these procedures.

In this thesis, I study and develop the design of a new class of surgical instruments which I hope will relieve the surgeon of key difficulties in current MIS practice. The goal is to perform current procedures more safely and with better results, but moreover to allow new MIS procedures to be performed which are currently impossible and by doing so to improve patient satisfaction and reduce the overall cost of these procedures.

As new technology is introduced, we as a society must ascertain whether or not this new technology is beneficial. In medical care, we must weigh the quality of patient care

19

against increased financial costs and possibly new risks. As an example, consider that there has recently been a great deal of interest in minimally invasive coronary artery bypass grafting, (Winslow, 1997), and several new approaches have been recently introduced. In Appendix A, we try to estimate whether these approaches will be beneficial by reviewing cost-effectiveness studies of several past cases: laparoscopic cholecystectomy, coronary angioplasty, and open coronary artery bypass grafting. These studies may give some insight as to how technology introduced in this thesis will be treated.

1.1 Current Minimally Invasive Surgery

Perhaps the most common form of MIS is laparoscopy, which is minimally invasive surgery within the abdominal cavity. Another common form is arthroscopy, minimally invasive surgery within the knee. A rapidly emerging field is MIS cardiac surgery for coronary artery bypass graft surgery (CABG). Others are being named as they are developed with the prefix referring to the body cavity under investigation (hysteroscopy, sinoscopy, pelviscopy, etc.) During laparoscopy, a patient's abdomen is insufflated with CO_2, and cannulas (essentially metal tubes) with pneumatic check valves are passed through small (approximately 1-2 cm) incisions to provide entry ports for laparoscopic surgical instruments.

The instruments include an endoscope for viewing the surgical site (a CCD camera/lens combination with a slender shaft), and tools such as needle-holders, graspers, scissors, clamps, staplers, and electrocauteries. The instruments differ from conventional instruments in that the working end is separated from its handle by an approximately 30 cm long, 4-13 mm diameter shaft, see Figure 1-1.

The surgeon passes these instruments through the cannula and manipulates them inside the abdomen by sliding them in and out, rotating them about their long axis and pivoting them about centers of rotation defined roughly by their incision site in the abdominal wall. Typically a one-degree-of-freedom (DOF) device (gripper, scissors, etc.) can be actuated with a handle via a tension rod running the length of the instrument. The surgeon monitors the procedure by means of a television monitor which displays the abdominal worksite image provided by the laparoscopic camera.

There are several disadvantages to current MIS technology.

1. Visualization of the surgical site is reduced. The operating site is viewed on an upright, two-dimensional video monitor placed somewhere in the operating room. The surgeon is deprived of three-dimensional depth cues and must learn
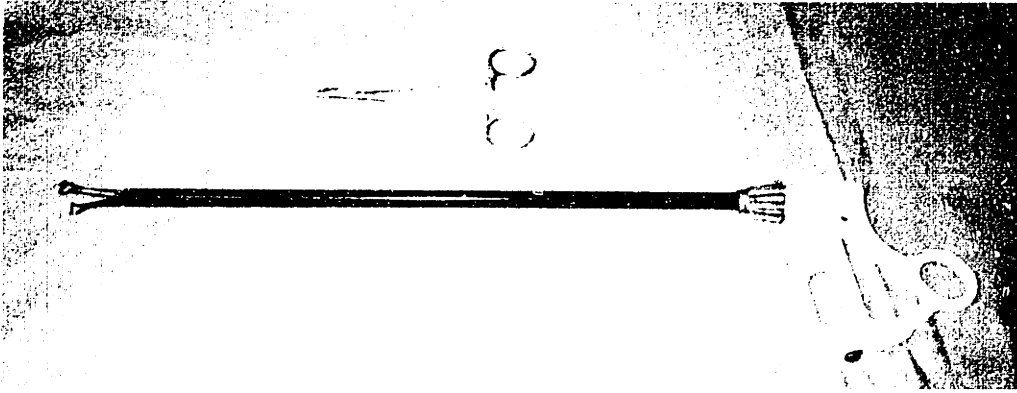
Figure 1-1: Above: A typical needle holder for open surgery. Below: A typical MIS instrument, an Ethicon disposable Babcock (soft tissue grasper).

the appropriate geometrical transformations to properly correlate hand motions to tool tip motions.

2. The surgeon's ability to orient the instrument tip is reduced. The incision point/cannula restricts the motions of the instrument from six DOF to four. As a result, the surgeon can no longer approach tissue from an arbitrary angle and is often forced to use secondary instruments to manipulate the tissue in order to access it properly or to use additional incision sites. Suturing become particularly difficult.

3. The surgeon's ability to feel the instrument/tissue interaction is nearly eliminated. The instruments are somewhat constrained from rotating and sliding within the cannula due to sliding friction from the air seal, and the body wall constrains pivoting motions of the instrument shaft. The mechanical advantage designed into MIS instruments reduces the ability to feel grasping/cutting forces at the handle.

Despite surgeons' considerable skill and ability to work within the constraints of current MIS technology, the expansion of minimally invasive medical practice remains limited by the lack of dexterity with which surgeons can operate while using current MIS instruments.

1.2 Teleoperators as the next step in MIS

We propose *teleoperation* as a general solution to these problems. Our goal is to improve the dexterity possible during MIS procedures through the use of *teleoperated*

surgical instruments and in certain cases to improve the surgeon's dexterity over that when using conventional instruments during open surgery.

1.2.1 What are Teleoperators?

Teleoperators are machines designed to allow a user to manipulate objects in a location remote from his own. They have historically been used to allow people to work remotely in dangerous or inaccessible environments such as nuclear reactors, the deep sea, and space.

A teleoperator consists of two mechanical systems of linkages, a master manipulator and a slave manipulator, (typically arms with grippers on the ends). These are connected either (a) mechanically, for example by cables or linkages, or (b) by servoactuating both the master and slave (e.g. using electric motors) and controlling each manipulator via computer. Motions are transmitted from the master to the slave so the user may manipulate the slave environment remotely.

There are many variations on this basic idea including the addition of other sensory modalities and inputs. For example sound, and tactile stimulus can be transmitted from the slave environment to the user. In particular, it is useful to transmit forces and motions from the master to the slave, and forces and motions from the slave back to the master. This is known as bilateral force-reflecting teleoperation.

1.2.2 Teleoperators used for MIS

What follows is our vision for how teleoperators will be used for MIS, see Figure 1-2. First, instead of standing at the operating table, the surgeon will sit at a console where they will view the procedure via monitors which provide them with a three-dimensional image of the operating site. Mounted within this console will be a pair of master manipulators, one for each hand, which will control a pair of slave manipulators at the operating site. On the patient side of the system, the slave manipulators will be mounted adjacent to the operating table and positioned such that the distal end of the slave passes through a cannula in the body wall in order to access the surgical site. Different quick-release slave end-effectors would be available to duplicate the surgeon's current array of instruments such as needle drivers, tissue graspers, and clamps. In addition there will be a seperate slave arm which holds an endoscopic camera through which the image of the operating site will be transmitted to the surgeon.

The surgeon will have several advantages when using such a system:

Traditional Minimally Invasive Surgery

Teleoperated Minimally Invasive Surgery
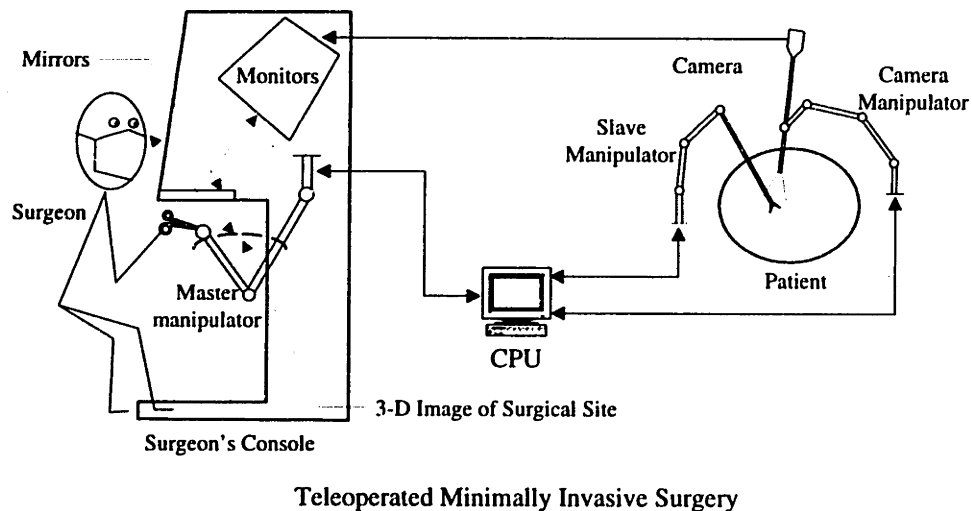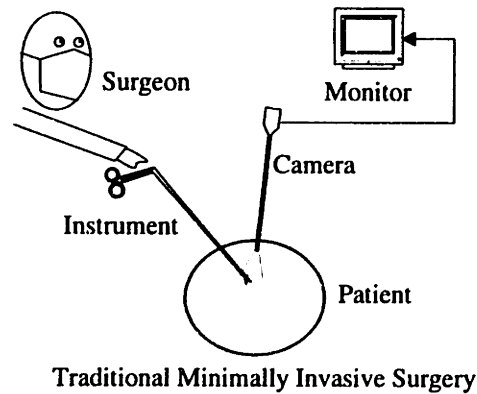
Figure 1-2: In MIS Telesurgery, the surgeon will sit at a *surgeon's console* within the OR.. He will remotely control a *surgical slave manipulator* and a *camera slave manipulator* using a *master manipulator*. Most likely, he will control two surgical slaves using two surgical masters. The monitors and console will be arranged such that his hand and wrist motions are similar to those used during open procedures. The slave must be designed with sufficient degrees of freedom to perform these motions. The goal is to create the illusion, with the accompanying increase in manual dexterity, that he *is* performing open surgery. The door is opened to enhanced modes of surgery where motion scaling, force scaling, and visual and haptic overlays are used to make dexterity better than that possible during open surgery.

1. By viewing a three-dimensional image of the slave instruments geometrically aligned with his own hands which are manipulating the master manipulators, the illusion is created for the surgeon that he in fact directly manipulating the slave instruments. The surgeons hands appear connected to the actual instruments which he views, since hand motions are directly correlated to the instrument motions as they are when a surgeon manipulates conventional instruments during open procedures. This illusion was created very successfully by SRI with their open surgical teleoperation system, (Hill et al., 1994).

2. We will show that the slave can be designed with additional degrees of freedom by adding additional "wrist" joints beyond the cannula. It is easier for the designer to do this than in the case of hand-held instruments because the joints are servoactuated. The endpoint mobility of the instruments can then be increased to six degrees of freedom to provide greater access to the tissue and hence greater dexterity. The goal is for the surgeon to be able to suture naturally, that is in the same fashion as when performing open surgery.

3. Finally, if accurate force and tactile information can be transferred back to the surgeon, this will improve the illusion by making him feel as though he were manipulating the surgical instruments or the tissue itself directly by hand. We will find that this goal, in particular in a system with 7 or 8 degrees of freedom, is by far the most difficult.

Success in these areas would give back to the surgeon dexterity which was lost when procedures were converted from open to minimally invasive, and would expand the type and number of MIS procedures possible. But the door to additional capabilities is opened. Consider that:

1. Motions and forces could be scaled. For example, if a 1 mm slave motion is made to correspond to a 5 mm master motion and if the image of the operating site is magnified correspondingly, it will appear to the surgeon that the operating site has been enlarged, thereby allowing finer absolute motions. 1 mm vessels would appear to be 5 mm vessels. Also, if forces between the instrument and tissue are scaled up and accurately transferred to the surgeon, the illusion will be even more convincing.

2. Semi-autonomous behaviors could be introduced into the slave manipulators and the camera, if it were mounted on a seperate controllable arm. For example, the camera and slave manipulators could be programmed to track moving tissue such as a beating heart. In the case of beating heart surgery, the heart would now appear stationary, thus allowing the surgeon to perform delicate tasks such

as suturing without having to stop the heart from beating and using cardio pulmonary bypass as in conventional heart surgery.

3. Graphic overlays could be placed in the surgical workspace to aid visualization of the operating site. For example, if a liver tumor must be removed but is viewable only using MRI, an image of the tumor could be overlayed on the surgeon's actual image of the liver so that he would know where to operate. This concept has been used sucessfully in brain surgery (Grimson et al., 1996), where the images are overlaid on a 2-D monitor placed in the operating room.

4. Haptic overlays could be placed into the surgical workspace to help guide the surgeon by feel. For example, since the master manipulator will be actuated, we could implement a virtual funnel to guide the surgeon towards a tumor. Or if some part of the anatomy such as a nerve bundle must be avoided, a virtual tube could be placed around the nerve bundle so that the surgeon cannot cut it with the slave manipulator.

We refer to the overall package as *enhanced teleoperation*. All of these areas present a variety of exciting research topics in the next generation of surgery, in teleoperation, and in haptic and force feedback devices.

1.3 Thesis Scope and Overview

This thesis concentrates on teleoperator slave design. Control methods are studied for such systems in order to better design them. We present designs of two force-reflecting teleoperators for minimally invasive telesurgery, the Silver Falcon and the Black Falcon. We discuss the important issues involved with making such systems work from both controls and mechanisms perspectives, and focus in particular on design for force reflection. Our goal is not to use these systems on humans, thereby relieving us of certain safety, sterilization, and tool interchangeability requirements. These issues are kept in mind, however, in particular during our second design, to allow future extension to human surgical practice.

1.3.1 The Silver Falcon Teleoperator Slave

Our first system is called the Silver Falcon and is described in Chapter 5, and shown in Figure 1-3. This is a seven-degree-of-freedom teleoperator slave which consists of two major subsystems, a wrist unit and a base positioner. The wrist unit incorporates five motors to actuate a small three-degree-of-freedom-wrist and gripper mechanism
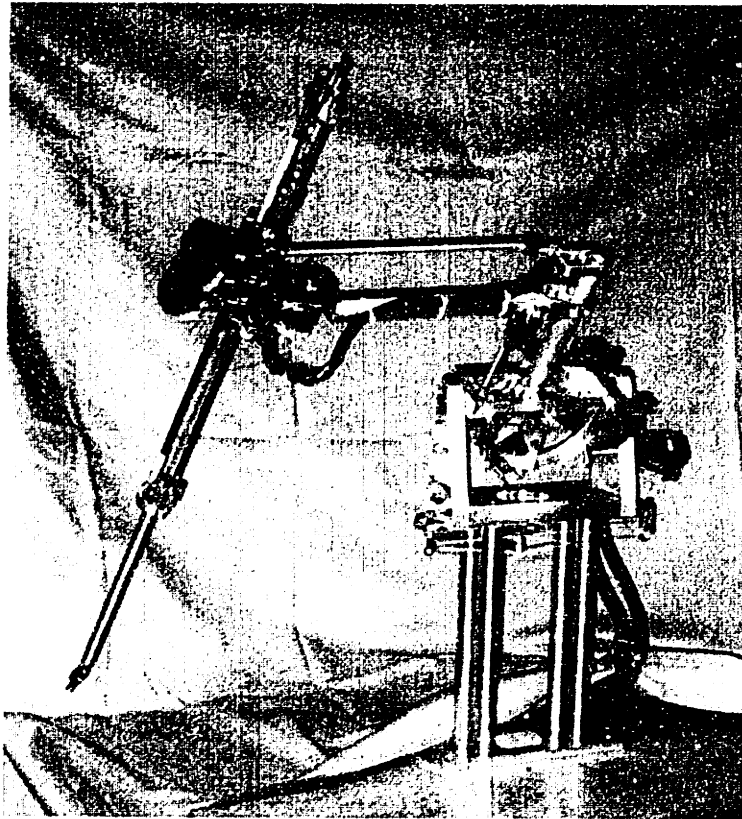
Figure 1-3: Our first teleoperator slave, the Silver Falcon.

which is placed at the end of a long slender shaft. This instrument shaft is designed to pass through an incision into the patient. The wrist unit also rotates the shaft about its long axis and controls insertion of the shaft into the patient. Power is transmitted from the motors to the wrist through a series of miniature stainless steel cables.

The second subsystem is a two-degree-of-freedom base positioner which orients the wrist unit in pitch and in yaw about the incision point. It is designed to keep one point on the shaft stationary and coincident with the incision point.

This system was connected via a controller to a PHANToM Haptic Interface which we modified to allow us to use it as a master manipulator for our slaves. This complete master-slave system allowed us to prove that macro-micro control would enable force reflection on a full master-slave system designed for minimally invasive surgery. It also showed us that using a small dextrous wrist coupled to a larger positioning mechanism would allow us to perform intricate tasks such as suturing.

There were a number of areas where the Silver Falcon was limited however. The wrist kinematics allowed us to use macro-micro control in only two out of three

directions meaning that there was always one direction in which the surgeon could not feel forces. Obviously we would like the surgeon to feel forces in all three directions equally well. There were also practical issues such as excessive structural flexibility, insufficient base servo performance, and the lack of sufficient grip strength to hold needles securely. Finally the wrist was designed as an integral part of the system and is not interchangable with other instruments or sterilizable. All of these are important problems to be solved if we intend to understand teleoperated minimally invasive surgery in an actual operating room environment.

1.3.2 The Black Falcon Teleoperator Slave

Our second telesurgical slave, the Black Falcon, is shown in Figure 1-4 and is fully described in Chapter 7. This eight-degree-of-freedom system is structurally stiffer and stronger in terms of actuator capacity. The system is counterbalanced for safety by placing all of its actuators at its base and using a combination of stainless steel and Spectra fiber cable transmissions to actuate the wrist and gripper. This also allows the wrist unit to be detatchable to allow future development of wrist-units which perform other functions, such as cutting, grasping tissue instead of needles, and cauterizing. This basic concept also allows the wrist-unit to be sterilized. The wrist was redesigned with an additional degree of freedom to allow forces to be felt in all three directions.

We found that the system had the appropriate kinematics and range of motion to allow suturing along arbitrarily oriented suture lines. Force reflection was however inadequate to help the suturing task. Force reflection is more useful during rigid contact tasks where force information is not available to the operator via visual cues.

During the course of this work and experimentation with both the Silver Falcon and the Black Falcon, we learned a great deal about how a master should be designed for surgery. While we did not design a new master, some of our observations have been recorded in Chapter 9 as this is logically on the critical path towards developing a complete and more refined teleoperator for minimally invasive surgery.

1.3.3 Outline

In Chapter 2 we discuss past work in teleoperator hardware, haptic interfaces, and telesurgery systems. We then discuss several methods of force control and of actuator and transmission design.

Chapter 3 outlines the relevant objectives and constraints on the design of a slave
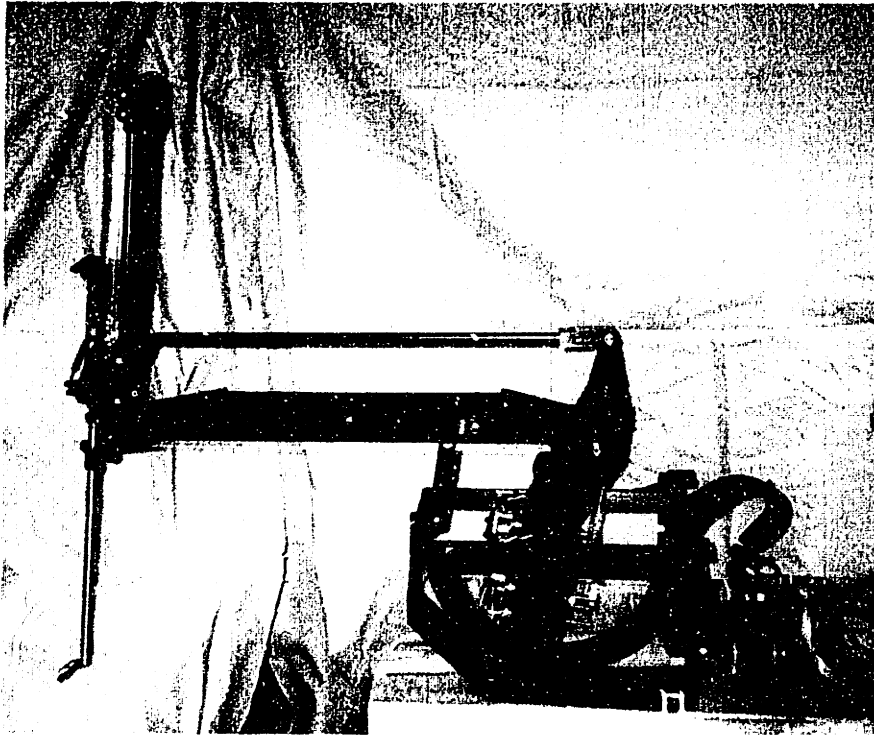
Figure 1-4: Our second teleoperator slave, the Black Falcon.

manipulator for minimally invasive surgery.

In Chapter 4 we describe basic position based bilateral force reflecting teleoperator control, and discuss certain physical limiations involved. We then investigate several ways to control a system with widely different base and end-effector inertias, which we refer to in general as macro-micro control. This chapter demonstrates the effects of different types of controllers on a three-degree-of-freedom master-slave testbed, and shows that a Jacobian Inverse control takes advantage of this inertia difference to improve performance.

Chapters 5 and 6 give a detailed description of our first teleoperator design, performance results and areas for improvement.

Chapters 7 and 8 address these issues by presenting the design of a new teleoperator slave, the Black Falcon. Again we give performance results and areas for improvement.

Finally, In Chapter 9, we summarize our work and present further areas for improvement and future research with this system.

Chapter 2

Background

In this chapter, we discuss background in telemanipulator design, haptic interface design, and telesurgical systems. We then discuss several methods of force control and actuator and transmission design.

2.1 Manipulator and Telemanipulator Hardware

There are several excellent books on telerobotics and human-in-the-loop computer control of mechanisms such as (Sheridan, 1992) and (Vertut and Coiffet, 1986). There are scores of different manipulators and books on them. Here we mention a few systems which we find interesting, in particular to give a little historical perspective on cable driven designs.

The field of telerobotics is by now not new, having its beginning in purely mechanical master-slave manipulators used in radioactive hot-cells. (For a more extensive history, see (Vertut and Coiffet, 1986)). The first mechanical master-slave system, the M1, was developed by Raymond Goertz at Argonne National Laboratory in mid 1948. The M1 and roughly a dozen later models used a series of mechanical linkages and steel cables to connect a master manipulator to a kinematically identical slave manipulator on the other side of a lead-glass barrier. (Goertz, 1954) briefly describes the Model 8. Later, the advent of servomechanisms allowed the mechanical linkages to be replaced by servomotors, though the kinematically identical nature of the manipulators remained, (Goertz and Thompson, 1954). These manipulators were force reflecting.

It is interesting to note that the prior to the development of mechanical teleoperators, (and after the dangers of radiation were discovered), nuclear laboratories used

remote handling tongs which passed through a spherical joint in a lead wall to handle radioactive materials. A mirror arrangement was used to view samples. These tongs were nearly identical in design to modern minimally invasive (laparoscopic) graspers and needle drivers, (Vertut and Coiffet, 1986) (p.25) states that: "There are clearly a number of difficulties that arise from the inversion of the movements of the gripper in relation to those of the handle, and from working with the mirror image of the scene. The need for a method of manipulation, which involved little training and provided complete dexterity for handling the first radioactive metallic or chemical samples in laboratory experiments, was clear." These motivations completely parallel those for teleoperation in minimally invasive surgery.

In the 60's and 70's, Carl Flatau, originally of Brookhaven National Laboratory, championed cable drive manipulators for teleoperation with such designs as that proposed for the MIT A.I. lab mini-robot project (Flatau, 1973), the MA-22-A Arm (Flatau et al., 1972), and the Telemac, designed to perform nuclear facility maintenance.[1] (Vertut and Coiffet, 1986) also describes another interesting arm developed at CEA in France, the MA-23M. This is a descendent of the MA-22-A which uses cable and tape drives exclusively as speed reductions, that is no gearing in the shoulder, in order to make the system more backdrivable and to eliminate backlash. It uses existing motor weight to counterbalance the weight of the arm.

The Salisbury hand and the Utah/MIT hand are both examples of cable/tendon driven manipulators, (Salisbury, 1982), (Narasimhan, 1988). The Salisbury hand uses three fingers with three degrees of freedom each. The fingers are actuated by cables (four for each finger in an N+1 configuration) which run through telfon-lined flexible metal conduits to a motor package which can be placed remotely, on the forearm of a PUMA arm for example. The Utah/MIT hand has four four-degree-of-freedom fingers actuated using polyethyl ne tendons (originally these were Kevlar) strung through a tendon remotizer to a remote pneumatic actuator package. The remotizer is essentially a separate arm consisting of links and pulleys over which the tendons are routed to maintain a constant cable length as the hand is moved. Both hands incorporate tendon tension sensors to better modulate output forces.

The WAM (Whole Arm Manipulator) is a four-degree-of-freedom arm developed at the MIT A.I. Lab which is again entirely cable driven, , (Townsend, 1988), (Salisbury et al., 1989). This arm is also backdrivable, has no backlash in the joints and can perform very fast motions without disturbances which would normally accompany a gear drivetrain. Another cable driven arm is the WHOI (Woods Hole Oceanographic Institution)/MIT arm developed for the ARGO/JASON project, (DiPietro, 1988).

---

[1]By personal communication (phone conversation), Carl Flatau, Director, The Bartholemew Co., Telerobotic Division, Westbury, N.Y., 1991.

For an extensive treatment of robotic transmissions, see (Schempf, 1990). Cable designs specifically allow many degrees of freedom to be packaged in a compact space, without backlash, and with low friction. These are good dynamics from a control point of view.

2.2 Haptic Interfaces

Haptic Interfaces are used either as the master side of a master-slave telerobot, or as an interface to a virtual environment where the sense of touch or force is imparted to the user. Again, there are many examples of hardware and we mention only a few. (Burdea, 1996) and (Minsky, 1995) give extensive historical bibliographies on haptic interfaces. Note our emphasis is on imparting forces to the user as opposed to tactile senses using tactile displays and on higher-degree-of-freedom systems as opposed to force reflecting joysticks.

Salisbury developed a cable driven six-degree-of-freedom hand controller at JPL. This system used revolute joints and a single sliding joint in a gravitationally counter-balanced configuration. A description of the device is given in (Bejczy and Jr., 1983), and performance analyses were done by (Hannaford et al., 1991). Unfortunately, the slave used in these experiments was PUMA arm mounted with a wrist force/torque sensor.

In 1992 and 1993 EXOS, Inc, led by Dr. Beth Marcus, developed two force reflecting exoskeletal devices. The SAFiRE™ is a seven-degree-of-freedom (2 DOF index, 3 DOF thumb, 2 DOF wrist) hand exoskeleton designed to work with "glove-box" simulations of shuttle experiments in 0 g.[2] The Force ArmMaster™ is a four-degree-of-freedom (3 dof shoulder, 1 dof elbow), arm exoskeleton. Both systems use combinations of planetary gear reductions and cable reductions to achieve the necessary speed reduction.

In 1993, Thomas Massie and Ken Salisbury at the MIT A.I. Lab developed the PHANToM haptic interface, (Massie and Salisbury, 1994). This interface is essentially a three- degree-of-freedom powered arm which gives force, but not torque, feedback to a user. A passive three-degree-of-freedom quarter-gimbal mounted at the end of the arm allows the user's fingertip (or a stylus) to attach to the end of the arm without constraining rotations. Several nice features include gravitational counterbalancing, low friction cable drive speed reductions, and relatively isotropic friction and inertia through much of its workspace.

---

[2]The photograph of SAFiRE shown in Burdea's book is of a preliminary prototype of the SAFiRE. The final version is not shown.

These devices all use actuators which emulate good effort (force/torque) sources. They control output force by commanding motor currents and relying on low friction, high efficiency transmissions to transmit these forces to the user. They do not explicitly present tactile feedback to the user. Nor are they "gloves" in the sense of the VPL Dataglove, which is an open loop sensing glove. They are each precision manipulators which the users either grasps or attaches to their hand or arm and which has the ability to exchange power with the user.

2.3 Teleoperators for Surgery

Teleoperators for surgery incorporate work in manipulators, telerobots and haptic interfaces. There are two areas which have received focus within the past three years, largely due to the efforts of Col. Richard Satava, M.D., formerly a project leader at DARPA. The first, championed by Col. Satava is the idea of battlefield surgery where surgeons well back from the front lines perform surgery using telerobots installed in armored vehicles on the front lines. These systems are for performing open surgery in a remote location. The second area which is gaining ground in the commercial sector and which is the focus of this thesis, is that of minimally invasive surgery.

SRI's open telesurgical system, was at the forefront of this movement (Hill et al., 1994). This system uses two five-degree-of-freedom slaves, and two kinematically identical masters mounted within a surgeon's console. The arms use spherical kinematics and a gripper (pitch, yaw, in/out, roll, and grip). The console uses a video monitor which is mounted so that a mirror reflects the image to a surgeon wearing polarized 3-D glasses. The monitor uses an LED screen to polarize the images from two CCD cameras mounted at the operating site alternately vertically and horizontally. The user wears glasses with similarly polarized lenses to generate a stereo image. The surgeon places their hands beneath the mirror such that, if everything is aligned correctly, the instruments which they hold (attached to the masters) coincide visually with the slave instruments. The most striking thing about this system is that the effect of the illusion created in this way is extremely effective. The system has some degree of force reflection. The author found that it was difficult to distinguish the difference in stiffness between, for example, the fleshy part of the hand and a hard knuckle being pressed on by the slave.

At JPL, a microdexterity robot was developed, (Schenker and Charles, 1995). This robot has a needle at the output, as opposed to a gripper which would be needed to actually perform surgical tasks. It uses gear reductions and cables to drive its joints. The wrist used is a variant of the Rosheim wrist (Rosheim, 1989). The focus here is microsurgery, as opposed to remote or minimally invasive surgery.

In the corporate sector, substantial efforts are now being made to commercialize telerobotics for minimally invasive surgery. Perhaps the two most important companies in this area are Intuitive Surgical, Inc., Mountain View, CA, and and Computer Motion, Inc., Goleta. CA. Intuitive Surgical is developing a two arm master-slave system for MIS, and Computer Motion is developing an MIS system code-named ZUES. Neither company has yet released a product. Computer Motion has been selling for several years a robotic endoscopic camera holder known as AESOP, (Mehta, 1997).

2.4 Methods of Force Control

The art of manipulator design and control is largely concerned with addressing manipulator and actuator dynamics. Force control in particular is concerned with accurately generating interaction forces between the endpoint of a manipulator and its environment. Below we discuss just a few methods by which this has been implemented. We emphasize that the environment of the master is the human operator. As a result we must understand how humans perceive forces. We will discuss this briefly below in section 2.7.

2.4.1 Commanded Motor Currents

The simplest form of manipulator endpoint force control is to command motor currents open loop. We may be able to command joint torques in this way with a Lorentz force actuator such as a D.C. electric motor because torque is typically proportional to input current, and because we can command current using servo amplifiers which operate closed loop. The quality of the output force depends on the quality of the actuator. We are limited (as always) by amplifier bandwidth, and friction in the motor bearings and brushes. If a brushless motor is used with electronic commutation, the limit is typically in the electronics. The controller can introduce cogging even if the motor rotor intrinsically has none, (Paul, 1987), (Levin, 1990).

This approach forces us to design manipulators with low transmission friction and low inertia. However, the approach is stable and will feel smooth (subject to the quality of the actuator), since there is no additional force control loop to add vibrations. This is a substantial benefit, especially when considering that a human will be directly interacting with the system.

2.4.2 Basic Closed Loop Force Control

Another common approach is to close a force control loop about a manipulator between a force sensor or sensors and the actuators. In colocated force control, a force sensor is placed very near the motor in an effort to minimize the dynamics between the force sensor and actuator. The goal is to make the motor/sensor appear as a perfect torque source. If motors were perfect Lorenz devices, this would be unnecessary, but in the presence of brush friction or non-ideal electronics, the sensor can be used to hide these unwanted dynamics. For example, (Paul, 1987) used a torque sensor on the output of a brushless d.c. servomotor in order to control out ripple induced by the motor controller caused by imperfect electronic commutation. He concluded that the best way to compensate was to use feedforward compensation because the disturbances were position dependent and could be effectively mapped with much less mechanical complexity than implementing a torque sensor.

In another related effort, (Levin, 1990) designed a reaction torque sensor into a housing custom designed for a frameless brushless d.c. torque motor. He found that with such a design he could achieve 200 Hz to 300 Hz bandwidths when commanding a step response in torque. A major problem was eliminating noise picked up by the sensors generated by the motor's PWM servo amplifiers. This was eventually solved using hardware and software filters. Transmission dynamics, distal from the motor, cannot be compensated for with such a system, so that transmission design is still an important issue.

In a non-colocated arrangement, the sensor is placed near the end of a robot, separated from the motor by the linkages and transmissions that make up the robot. The difference is a matter of degree. More dynamics are introduced between the actuator and sensor, and kinematic transformations are involved in mapping endpoint force/torques onto the joints. Also, dynamic feedforward elements have been used to cancel manipulator dynamics. The goal is again to use the controller to hide these dynamics so that the entire robot appears to be a perfect force/torque source. This of course becomes increasingly difficult as the dynamics increase.

Examples can be found in (Mason and Salisbury, 1985) where strain gage based tendon tension sensors are used to hide friction in cable conduits used in the Salisbury (NASA/JPL) Hand. Force control and the stability problems involved have been discussed by (Eppinger, 1988), (Whitney, 1985), (Kazerooni, 1985), (An, 1986), (Colgate and Hogan, 1989), (Volpe and Khosla, 1992), and others.

(Pratt and Williamson, 1995) gives another example of using a force sensor on the output of a motor to control output torques. This is a non-colocated arrangement where a brushed d.c. servomotor applies torque through a planetary gear/cable drive
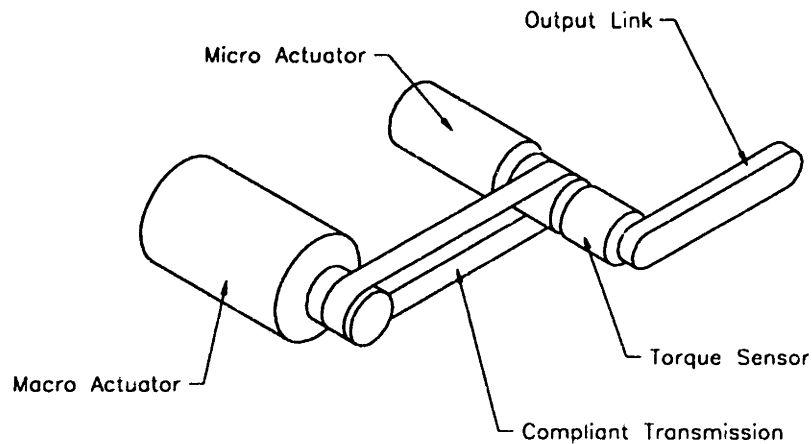
Figure 2-1: Parallel-coupled micro-macro control uses two actuators connected in parallel via a flexible transmission. A force sensor is required to sense the sum of the torques output by each actuator.

speed reduction and then through an output torque sensor. This sensor is a steel torsional spring mounted with strain gages. The spring adds a substantial compliance to the system which improves stability when contacting rigid surfaces. Positioning bandwidth is also decreased, but this was not a concern as their system is typically run in a joint compliance control mode with soft positioning gains. The compliance of the force sensor has the advantage that it shields the planetary gear reductions which they use from external shock loads.

2.4.3 Parallel-Coupled Micro-Macro Control

The idea of using two motors coupled in parallel to drive a load was studied by (Morrell, 1996). The goal is to increase the ratio of maximum to minimum controllable force, a measure known as the dynamic range, over that of either actuator used individually. Figure 2-1 shows the concept. Because a flexible transmission is used to couple the macro motor to the load, its bandwidth in applying forces is limited by its position control bandwidth, that is how quickly it can produce a desired deflection in the flexible transmission. It can, however, apply large torques. The micro motor, on the other hand, will typically have a high bandwidth, but it can apply only small forces. At the output, torque must be sensed and fed back to the controller to allow the micro motor to compensate for disturbances introduced by the macro motor. If the motors, transmission stiffness, and controller are selected and designed properly, the advantages of each motor can be capitalized upon to increase dynamic range during force control while maintaining good position control.
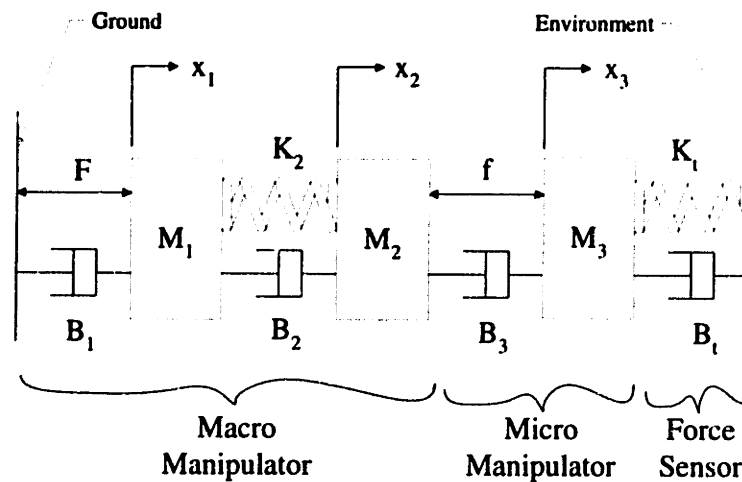
Figure 2-2: Sharon's macro-micro model. The macro manipulator is assumed flexible. K_t and B_t represent stiffness and damping of a force sensor mounted to ground upon which the micro manipulator pressed during force control contact tests.

2.4.4   Series-Coupled Macro-Micro Control

(Sharon, 1988) studied the idea of coupling two manipulators in series, with one grounded on the other. The base manipulator (macro manipulator) is presumed to be larger and potentially flexible, but has a large range of motion. The distal manipulator (micro manipulator) is presumed to be smaller and have a higher position servo bandwidth. It is assumed that absolute endpoint position measurement of the tip of the macro-micro system is available. Figure 2-2 shows a model used for the study. The results were confirmed on a two-degree-of-freedom macro-micro manipulator. The macro manipulator consisted of a d.c. electric motor with a cable reduction and a flexible beam link structure. The micro actuator consisted of a high bandwidth dual-acting hydraulic actuator capable of 45 g accelerations, (3000 psi fluid with 1 in bore pistons). While controlling the position of the endpoint of the robot in freespace, $(K_t, B_t = 0)$, Sharon showed he could use the micro manipulator to compensate for positioning inaccuarcies of the flexible macro manipulator using the following control:

$$f = -G_1 x_3 - G_2 \dot{x}_3 \qquad (2.1)$$

x_1 is assumed to be zero, that is exactly tracking the desired position/velocity. Also, it is assumed that the micro actuator has a limited positioning range, and is programmed to stop when it reaches the end of its workspace limit. The result is that the micro manipulator "jumps out ahead" of the macro manipulator and "locks on" to the desired endpoint position when the macro manipulator brings it within its workspace.

Positioning bandwidth is thereby improved over the macro manipulator alone.

To study force control, Sharon attached a piezoelectric sensor to ground and covered it with a soft (15 lbs/in, 2600 N/m) covering. The manipulator pressed on this surface. The control was:

$$F = -G_1 x_1 - G_2 \dot{x}_1 \qquad (2.2)$$

$$f = -G_3 F_t - G_4 \dot{x}_3 \qquad (2.3)$$

The gain G_2 was chosen based on impedance matching with the micro manipulator in order to remove energy from the system. The gains G_1, G_3 and G_4 were tuned to give the best stable response based on classical frequency domain analysis. It was found both in simulation and in experiments that stable force control could be maintained with the caveat that the environmental stiffness be sufficiently soft. This was attributed to the use of a hydraulic micro manipulator whose output force could not be directly commanded, that is which acts like a flow source. Sharon suggests that a micro actuator which acts like an effort (force) source may be able to interact more successfully with a hard surface. He also suggests that if the micro actuator acts like an effort source and is therefore backdrivable, the macro-micro manipulator will be able to present a low impedance to the environment.

2.4.5 Force Measurements

As described above, there are certain cases where force measurements are beneficial. For example, in the case where large gear type reductions are necessary and substantial friction is therefore unavoidable, the use of force sensing might be appropriate to help compensate for this friction. In the case of parallel-coupled micro-macro control a substantial increase in dynamic range is achieved using multiple actuators in conjunction with force sensing. However, several specific problems with force sensing should be discussed:

- Noise in the measurements. If measurements contain noise, either the system bandwidth must be maintained below the frequency of the noise, or the noise must be filtered. Inputing noisy signals into a controller at best will introduce vibrations which the human operator can feel and will find annoying. At worse, noisy signals can excite unmodelled system dynamics and drive a system unstable. However, if force signals are filtered, the filter will introduce lag into the controller which will limit the achievable gains and hence the controller's ability to reject disturbances.

- Drift in force sensor readings will make system "walk". For example, if the slave is commanded to output zero torques, but sensors on the slave drift slightly from zero, the slave motors will be commanded to move in order to zero these sensors. The master robot will track the positions of the slave robot. If the user prevents the master robot from moving, phantom forces will be felt corresponding to the drift forces in the sensor.

    This is similar to having uncompensated gravity terms in the controller. However, force sensor drift may occur in any direction and will likely be time varying since it is typically caused by changes in temperature. Temperature changes are abundant in the surgical environment due to body fluids, saline for irrigation, and hot lights for endoscopy which will contribute to sensor drift, even if full bridges and thin sensor elements with high heat conductivity are used.

- Sensors introduce additional cost and complexity. Extra wiring and packaging is required as are A/D boards, bridge electronics and filtering circuitry.

- Force sensors typically consist of flexible elements whose deformation (strain) is sensed and from which force is inferred. As a result, they tend to be delicate if they are sensitive and have a limited range based on allowable deflections before permanent deformations are introduced. Implementing force sensors in high-degree-of-freedom systems is in itself a challenge and expensive. As an example, Assurance Technologies, Inc. (Garner, North Carolina, formerly Lord Industrial Automation) sells a fairly small six axis force/torque sensor (14.4 × 17 mm diamter) which sells for $6225.00 plus $350.00 for the highly recommended thermistor-based temperature compenstion module.

2.5 Actuators

Actuator technology is another field unto itself, but a few comments are warranted concerning teleoperators in particular. In bilateral force reflecting systems, we typically want our actuators to behave as pure force/torque (effort) sources. As described above, much research has been focussed on this goal. Lorenz force actuators such as d.c. servomotors or voice coils have the potential to behave this way, converting input current into output effort. Since current may be controlled accurately at frequencies well above typical mechanical frequencies, this is a good choice.[3] A voice coil mounted

---

[3]For example, the off the shelf PWM current amplifiers (Copley Controls, model 303) which we use have a measured bandwidth of 400 Hz.

on a frictionless flexure provides a high quality effort source. For example, Hi-Fi audio speakers using high quality audio amplifiers have low distortion in the tens of kHz range. There are obviously many other types of actuators such as hydraulics servoactuators, pneumatics, shape memory alloys, and piezo-electric devices. For small convenient effort sources, however, we maintain our focus on electric servomotors.

Typically, at the joint of a manipulator we require substantial torque outputs over roughly a one revolution range of motion. Several schools of thought have arisen to implement this. One is to use direct drive motors such as Inland Corp.'s frameless torque motors. These motors use iron cores and have a large diameter to increase output torque. Hence they have high rotor inertia, can have substantial cogging, occupy a large volume, and operate at low speeds. Early work in direct drive motor manipulator design was done by (Asada and Kanade, 1982), (Asada and Youcef-Toumi, 1984). Manipulators designed with current direct drive technology tend to be massive and therefore not well suited for a system which must interact with a delicate environment. Another school of thought is to not worry too much about the actuator and to compensate by using a combination of distal force sensing and mapping to eliminate friction and torque ripple. Some of these attempts were desribed above in Sections 2.4.2. Finally, we can use fast, low inertia actuators, and high quality transmissions and speed reductions. This idea is in fact not new, coming from the original mechancal master-slave manipulators which required high quality transmissions to enable force reflection. For example, (Vertut and Coiffet, 1986) discusses the use of block-and-tackle cable transmissions used to reduce friction and inertia and to eliminate backlash on the French MA-23M bilateral force reflecting teleoperator.

If we use this last approach, then it is beneficial to have low rotor inertia because the effective output inertia contribution of the motor rotor is equal to the rotor inertia multiplied by the square of the reduction ratio. Therefore, with any substantial reduction, rotor inertia can dominate the total inertia. Ironless core (basket or disk) d.c. brushed motors then become a good choice for two reasons. First, they have low rotor inertia, and second, they have no cogging. This is because there are no pole pieces on the rotor to line up with permanent magnets which creates cogging. They have one important disadvantage: they have poor thermal properties. Because the rotor consists of wire encased in an epoxy resin, the rotor has low thermal inertia and must dissipate heat across an air gap to the motor stator (housing). Peak torque capacity for a good motor is typically 10× greater than the thermally limited continuous torque capacity. In Chapter 7 we show an example where water cooling a basket motor (Maxon Motors RE-035) can increase continuous torque limits by a factor of two.

Permanent magnet materials are critical when determining power and stall torque.

The best magnets today are the Neodymium-Iron-Boron variety, with Samarium-Cobalt being slightly weaker and Alnico being 4 to 5 times weaker. There are a number of manufacturers of basket motors (Maxon Motors, Micro-Mo, Escap) and disk motors (PMI), but Maxon Motors have typically been our favorite, largely because their "RE series" was the first of these to use NeFeBo magnets.

A significant percentage of friction in a well designed system will be contributed by motor brushes. This is a function of the brush and commutator design. Brushless motors (sometimes called electronically commutated motors) have the coils mounted in the stator, and permanent magnets on the rotor. The advantage is there is no brush friction and no brush-life limitation, and thermal dissipation is improved because the coils dissipate heat directly to the housing. In fact with water cooling, these motors may be able to run at peak torque values continuously.[4] The disadvantage is the motor rotor inertia is typically higher since they carry magnets, the commutation electronics can be expensive, and the commutation electronics themselves can contribute cogging even if the rotors intrinsically have none, (Levin, 1990). For these reasons, we have chosen in this thesis to use brushed motors, though it is not inconceivable that with improved brushless technology one would consider brushless motors. Reducing friction is critical in our systems and would be the primary motivation for this change.

2.6 Cable Design

Given the need to design high efficiency transmissions with substantial speed reduction, how does one go about doing so? In my experience, the best method for implementing a low friction, backlash free transmissions in a high-degree-of-freedom manipulator with severe space constraints is to use mechanically cabled transmisions. There are a number of examples of systems which take this route, (Flatau, 1973), (Salisbury, 1982), (Vertut and Coiffet, 1986), (Townsend, 1988), (DiPietro, 1988), (Salisbury et al., 1989), (Salisbury et al., 1990), (Schempf, 1990), (Massie and Salisbury, 1994).

2.6.1 Cable properties

Cable (also called wire rope) is used commonly to support loads and transmit power in large equipment such as cranes, elevators, tramways and suspension bridges, and

---

[4]Underwater manipulators such as those used at Woods Hole Oceanographic Institute use the cold seawater as a motor heat sink and are designed to run at peak torques continuously.

much of the information available refers to large sizes, from 3/16 in to 3 in diameter. In the designs presented in this thesis, we use "miniature cable" in sizes which range from 0.018 in to 0.032 in diameter.

A number of different materials can be used. Stainless steel is most commonly used for miniature cable. Tungsten may also be used, as tungsten wire drawing is well developed for light bulb filaments. Tungsten has an elastic modulus which is roughly twice that of steel and in cable form has improved fatigue properties.[5] There are also other materials available, notably Spectra fiber, a high-density polyethelene (sold commerically in fused strand and braided varieties as Spiderwire™ Fishing Line), Kevlar, and Vectran polymer, though these materials behave differently and the discussion below does not apply to them. Critical design factors for metallic cable are:

- Construction: This refers to the number and arrangement of individual fibers. For example 7×19 wire consists of 7 individual bundles of 19 fibers each. 6 of these bundles are wrapped helically around a central bundle.

- Minimum fiber size: Wire is made by drawing through a series of mandrels of decreasing size. A typical small fiber size would be 0.0012 in diameter. To draw to a 0.0009 in diameter requires several additional drawings steps, increasing cost. However, flexibility and fatigue strength increase as fiber size decreases. Ideally we like to have a large number of small diameter fibers within a cable. For example, 7×7×7 cable is typically more desirable than 7×19, though it is more expensive and available in fewer sizes.

- Lubricants: Lubricants, typically oil, impregnated within the fibers of a cable reduces friction and hence abrasion between individual fibers and reduces corrosion. In particular, stainless steel tends to gall when rubbing on itself. Lubricants prevent this, thereby increasing overall life.

- Coatings: Coatings are typically made of plastic such as nylon or teflon and can increase the fatigue life of a cable substantially by reducing external abrasion and by retaining lubrication. However, coatings tend to add substantial viscous friction to a miniature cable drive. This is most likely due to the compression of the coating as it goes over pulleys. The result is we typically do not use coated cables in our designs.

- Pulley diameter: Pulley diameter is a critical factor in cable design. Bending of individual fibers creates stress which increases sharply as bending radius of

---

[5]SAVA Industries, Riverdale, N.J. makes stainless cable, and Baird Industries, Hohokus, N.J. makes stainless and tungsten cable.

curvature decreases, (Costello, 1985). All cable manufacturers specify minimum pulley diameters for their cable which is a function of construction, cable diameter, and desired life. For example, SAVA Industries specifies that pulley diameters be 25× cable diameter for maximum life in a 7×19 construction cable, but states that at this ratio strength will be reduced to 92% of the catalog value for that cable.

- Pulley Groove Shape: Cable will tend to compress from a round to an elliptical cross section as it rolls onto and off of pulleys. This compression results in increased stresses within the cable and lost energy as the individual fibers rub on each other. This can be minimized by designing radiused pulley grooves to better support the cable. Ideally, the design will have cables approach pulleys directly along the tangent of their circumference. If however the cable approaches at a slight angle ("fleet angle"), then the cable can rub agains the edges of the pulley groove adding friction and abrasion. In these cases it is helpful to design shallow pulley grooves to avoid this interference.

- Pulley Material: Very hard pulley materials, such as anodized aluminum or "hardcoat" can abrade cable rapidly. We recommend using pulley materials which are softer than the cable material such as non anodized aluminum, or plastics such as nylon, which is soft yet tough.

- Reverse Bending: Cable which is routed over multiple pulleys may be subject to reverse bending. In a complex mechanism, this is almost inevitable, but the designer must be aware that fatigue life will be reduced.

2.6.2   Speed reduction

There are many options available to implement speed reductions in cabled mechanisms. A common example would be a block-and-tackle arrangement, as used by (Vertut and Coiffet, 1986) in the MA-23M. A "chinese windlass" is a way of producing essentially arbitrarily large speed reductions using a cable drive. More commonly, one can use a combination of large and small pulleys as as an analog to spur gear trains. Figure 2-3 shows how a motor can be coupled to a ring to drive it. A larger center to center distance may be used between the motor capstan and the driven drum, but if they are kept near, as shown in the figure, then the overhanging loads on the motor shaft are reduced because the cable exits the capstan in opposing directions. Rotary motion of a motor can also be converted to linear motion using a similar technique as shown in Figure 2-4. Note that in both these examples a frictional connection is shown between the motor and the cable. Usually only a few wraps are required
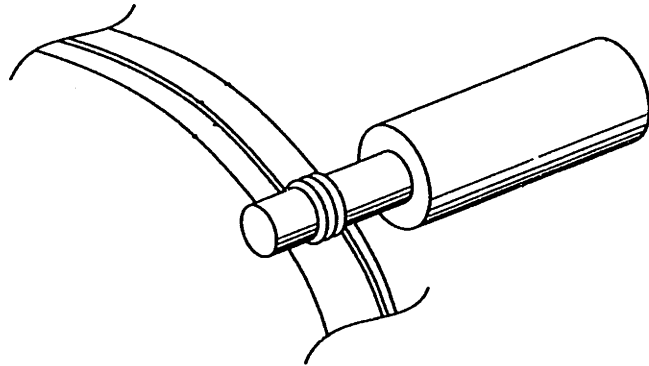
Figure 2-3: Cable used to couple a motor capstan to a ring in order to drive it. The cable must be terminated at its end in the ring which is being driven. As shown, the cable is frictionally connected to the motor capstan.
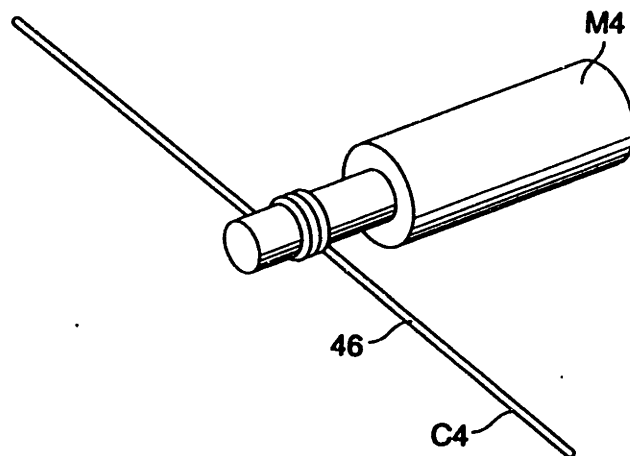
Figure 2-4: Cable drive used to convert rotatary to linear motion.
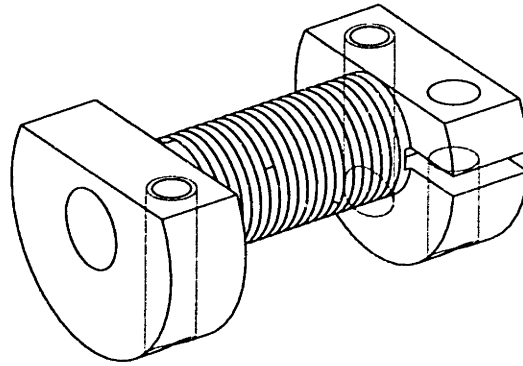
Figure 2-5: The driving capstan can be designed such that the cable terminates on the capstan itself to avoid the possibility of slippage. Here flats are machined into the capstan so that the cable ends can be held under screw heads. Each cable segment then winds towards the center of the capstan before exiting. Threads are machined into the capstan to guide the cable and prevent it from rubbing on adjacent wraps. This capstan also has a flexure clamp designed into it to secure it to the motor shaft.

because friction increases exponentially with wrap angle:

$$\frac{T_1}{T_2} = e^{\mu\theta}$$

where T_1 is the high tension side, T_2 is the low tension side, μ is the coefficient of friction, and θ is the wrap angle. This relation holds for the case of impending slip where the tangential frictional force between the cable and the capstan is proportional to the normal force multiplied by the coefficient of friction μ. Note that this requires that a pretension be maintained so that one side of the cable does not go slack.

Alternatively, to ensure that the cable does not slip, we can also terminate the cable on the motor pinion, as shown in Figure 2-5.

2.7   Comments on Human Perception

Since humans will interact directly with our manipulator, it is helpful to understand how humans perceive inertia, stiffness, and vibration. Human perception and haptic perception in particular are broad fields of research, see for example (Boff et al., 1986). Here we intend only to make a few general comments.

- Humans cannot distinguish finite stiffnesses above roughly 25,000 N/m between infinite stiffnesses, according to experiments by (Tan et al., 1994). These ex-

periments were performed by placing a flexible aluminum bar in the vise of a milling machine and pushing on the bar (with eyes closed) at distances increasingly close to the vise, which is effectively completely rigid. This was done with fingers, the palm of the hand and the forearm with similar results. Above a stiffness of 25,000 N/m, the bar was indistinguishable from the vise itself, despite deflections of as much as several cm.

- Humans are very sensitive to vibrations. During the same experiments by (Tan et al., 1993), tapping on the bar and sensing the resulting vibrations allowed the subjects to move within several cm of the vise and discern the difference in stiffness with much greater resolution. (Bolanowski et al., 1988) showed that humans can detect vibrations nearly as small as 0.1 μm amplitude at 300 Hz on the thenar eminence (the group of muscles at the base of the thumb between the thumb and the wrist). (Sherrick and Cholewiak, 1986) gives a value of between 0.2 μm and 0.5 μm at 200 Hz to 400 Hz again for stimulation of the thenar eminence. While sensitivity decreases at lower or higher frequencies, amplitudes of 5 μm to 20 μm can still be detected at frequencies as low as 30 Hz.

- Humans are sensitive to changes in stimulus, but are relatively insensitive to constant stimulus. To some extent, we are "AC coupled". As a result, the notion of isotropy is important in teleoperator design in order to provide transparency. Friction and inertia present disturbance forces to the human user of a teleoperator. However, if these disturbances are not time varying, are distributed evenly in space, and are the same in all directions, hence isotropic, then humans will be much less sensitive to them than otherwise.

  Also, a system with non-isotropic friction and inertia will have preferred directions of motions. That is, motions in certain directions will be easier than in others. This is distracting and confusing to a user especially when making fine motions.

- Gravitational forces, though constant, cause fatigue. A system can have a considerable amount of inertia which, if isotropic, may not be bothersome to a user. But if the user must carry the weight of the system, they will quickly become fatigued and consequently annoyed. This comment is based on personal experience co-designing the SAFiRE force-reflecting hand interface for Exos, Inc.[6] A constant weight of as little as 2 lbs carried on the user's forearm caused considerable fatigue. The device was eventually counterbalanced with a table mounted boom.

---

[6]Exos Inc. of Woburn, MA has since been purchased by Microsoft, Inc., Redmond, WA.

2.8 Summary

There has been much work over the years in teleoperation, manipulation, and haptic input devices. We have come to believe through our experience that bilateral force reflecting manipulators should be designed using actuators which emulate high quality effort sources operating through lightweight links with high efficiency transmissions. We have described background work with an emphasis on work which shares these ideas.

In order to achieve force reflecting teleoperation we have to go farther however. In Chapter 4, we will revisit the idea of macro-micro control using a considerably different experimental system than that used by (Sharon, 1988) which more accurately reflects our goals and design techniques, in addition to the fact that it is a master-slave system as opposed to a single manipulator. We show that using a two-degree-of-freedom macro-micro slave manipulator coupled to a one-degree-of-freedom master we can achieve well-behaved force scaled teleoperation with a force scale factor of 50:1 without the use of a force sensor.

While there have been many teleoperators and haptic interfaces designed, there are no systems which allow teleoperated minimally surgery with force reflection and with manual dexterity comparable to that of open surgery. We hope that the systems presented in this thesis will help to fill that gap and lead to a new generation of surgical instruments: teleoperators for minimally invasive surgery.

Chapter 3

Discussion of Teleoperator Slave Design Constraints

In this chapter, we discuss specific constraints which affect the slave manipulator designs presented in Chapters 5 and 7. We ask:

- What type of kinematics, how many degrees of freedom, and what range of motion do we need in order to provide dexterity for surgery?

- How must the kinematics of the slave manipulator be constrained in order to perform minimally invasive surgery?

- How will teleoperator control considerations (which we will discuss in more detail in Chapter 4) affect the desired kinematics and dynamics of our design?

- How will practical issues regarding use in the operating room affect the overall structure of the design?

In this chapter, we focus on the slave manipulator, however the design of the teleoperator *master* is obviously an important aspect of the overall system design. In our work, we will use a modified PHANToM haptic interface (Massie and Salisbury, 1994) to control both slave manipulators which we present. Though we do not present a new master design in this thesis, we will discuss desirable attributes for a master to possess in Chapter 9.
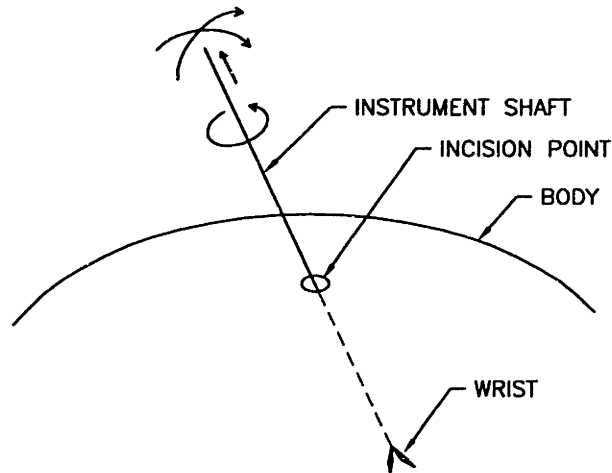
Figure 3-1: The incision point constrains the motions of one link of the slave manipulator to four degrees of freedom.

3.1   Kinematics Requirements

3.1.1   The Incision Point Constraint

A fundamental requirement of MIS is that the instrument must pass through a small incision when entering the body, as shown in Figure 3-1.

If we imagine that some portion of the slave consists of a shaft which passes through the incision point, this shaft will be constrained to have a maximum of four degrees of freedom. Considering that we wish the surgeon to perform as though they were performing open surgery, the tip of the slave manipulator we design should have at least six degrees of freedom plus one gripping freedom, or seven total. In order to achieve seven total degrees of freedom, an additional three-degree-of-freedom mechanism must be placed distally to the incision site (inside the patient). We feel this is best done using a compact wrist mechanism that will not get in the way of other instruments or tissue structures at the operating site. Such a wrist has a number of fairly severe requirements:

- The wrist must have sufficient and appropriate degrees of freedom to allow specific surgical tasks such a suturing.

- The wrist must support substantial loads in order to grip needles and to manipulate tissue.

- In Chapter 4, we will discuss macro-micro control, where a small micro manipu-
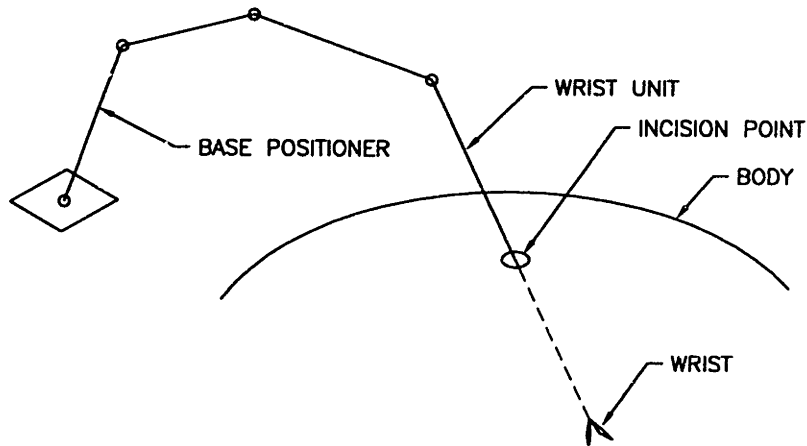
Figure 3-2: The kinematic constraints on the slave manipulator defines its overall structure. While many other general concepts could be formulated (snake robots, parallel robots which assemble through multiple ports), a slave manipulator which consists of a wrist unit coupled to a base positioner is straightforward and will prove effective.

lator is used mounted on a larger macro manipulator. When used in conjunction with this type of control, the wrist would act as the micro manipulator and in doing so will help us achieve force reflection. This imposes certain dynamical constraints on the wrist design in addition to geometric constraints.

The wrist and accompanying mechanism will be referred to as the wrist unit. The wrist unit must naturally be carried by the remainder of the slave manipulator in order to be positioned relative to the surgical site. One possible structure for the slave manipulator is shown in Figure 3-2. Here, an external arm whose base is fixed relative to ground carries and positions the wrist unit. We refer to this portion of the slave manipulator which carries the wrist unit as the base positioner, or base unit. One might consider a number of other general architectures for our system. We might use a highly redundant "snake" type robot which enters the body through a single incision point. We might use a parallel actuated mechanism such as a Stewart Platform, whose linear actuators or links pass through separate incisions in the body and connect inside the body. We will find the idea of having an arm which extends into the body is relatively straightforward and will prove effective.

3.1.2 Suturing Motions

Consider the task of suturing, Figure 3-3. (Hunter and Sackier, 1993) suggest the
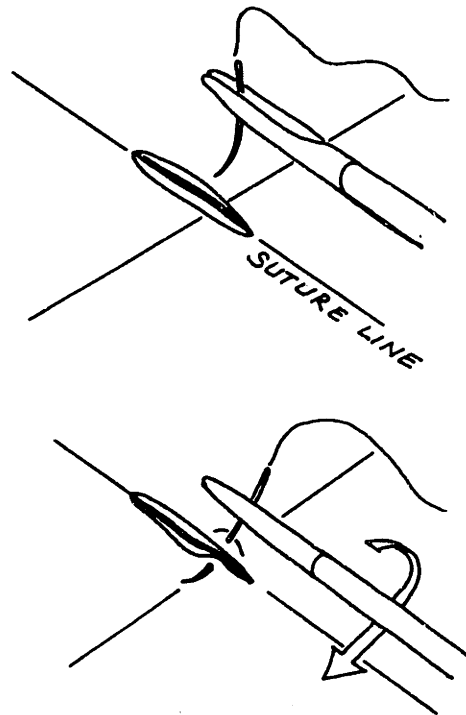
Figure 3-3: The proper positioning of a needle driver with respect to tissue is critical during suturing. Suturing is primarily a rolling motion combined with a push in the direction the needle is driven. Adapted from (Hunter and Sackier, 1993).

proper positioning of an MIS needle driver with respect to the tissue which must be approximated (sutured together). The needle driver should be in a plane vertically above the suture line, and nearly parallel (within 20 degrees) to the tissue. The motion required to suture is largely a rotation about the instrument shaft, combined with a push to drive the needle through the tissue. The tissue may be held with another instrument.

In the absence of a wrist, the orientation of the instrument with respect to the suture line defines the point of entry into the body of the tool. The tissue may be moved to orient the suture line with respect to the tool, but this is not always possible. If the suture line is rotated by 45 degrees with respect to the orientation shown in the figure, then it will be difficult to maintain proper needle orientation. However, a wrist which could reorient by 45 degrees could maintain the correct needle orientation during the suturing motion.

Maintaining such an angle would realistically require more range of motion than

±45 degrees. An educated estimate is that the advantages of having a wrist will probably not be worth the substantial design effort involved unless ±90 degree movements are possible. On the other hand, bending at much more than 90 degrees will likely not be useful given that the wrist would then begin to interfere with the instrument shaft on which it is mounted.

3.2 Wrist Kinematics

Wrist design is a subject unto itself as demonstrated by the many robotic wrists which have been designed. By way of example, we discuss just a few wrist kinematics options below in order to give an idea of the relevant issues involved. Note that there are many more issues involved with actually implementing any of these kinematic types concerning structure, actuation, transmissions, sensing and so forth. These types of issues are addressed within the context of the designs we present and describe fully in Chapters 5 and 7. By way of a preview, the wrist that is implemented in the Silver Falcon is a variation of the roll-pitch-yaw wrist, and the wrist implemented in the Black Falcon is a roll-pitch-pitch-yaw wrist.

3.2.1 Roll-Pitch-Yaw

The shape of an instrument which must pass through an incision might naturally include a long slender shaft. If so, it is natural for the first axis of the wrist to be a rotation about this instrument shaft. If we use the motions for suturing as a guide, a rolling motion seems to be required at the output where the needle is held. One way to do this is through a universal (cardan) joint as used in automotive drive shafts. In this case two intersecting, perpendicular axes are located near the end of the instrument shaft to give the pitch and yaw axes.

This results in a roll-pitch-yaw wrist are shown in Figure 3-4. Roll-pitch-yaw refers to the orientation of revolute joints from the base of the wrist moving outwards towards the tip.

3.2.1.1 Angular Velocity Singularities

Singular configurations are a common problem in wrist design. The traditional differential kinematics mapping between manipulator joint velocities $\dot{q}$ and the angular and/or linear velocity of a point on the manipulator $\dot{x}$ (typically of the end-effector)
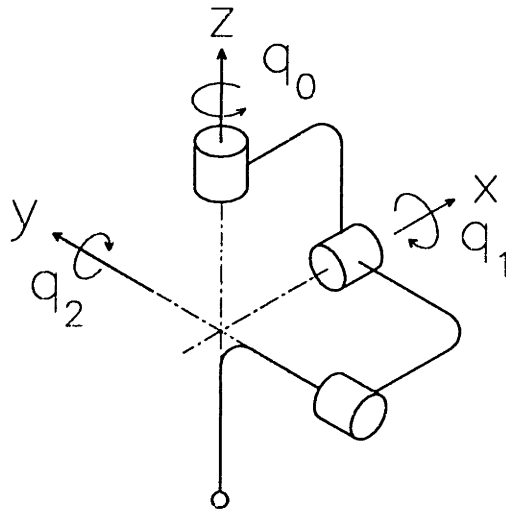
Figure 3-4: Kinematics for a roll-pitch-yaw wrist. The small circle at the lower tip of the structure represents a point where objects might be held by a gripper mounted distally on the wrist.

is:

$$\dot{\mathbf{x}} = J\dot{\mathbf{q}} \tag{3.1}$$

where J is the manipulator Jacobian matrix whose elements are a function of its configuration q. The manipulator is said to be *singular* in configurations where J loses rank. In this case, a manipulator consisting of serially connected links will require infinite joint velocities to produce certain output velocities which are hence impossible. Let:

$$\omega = \begin{pmatrix} \omega_x \\ \omega_y \\ \omega_z \end{pmatrix}, \quad \dot{\mathbf{q}} = \begin{pmatrix} \dot{q}_0 \\ \dot{q}_1 \\ \dot{q}_2 \end{pmatrix} \tag{3.2}$$

be vectors of angular velocities about the coordinate frame axis, shown in Figure 3-4 and joint velocities respectively. Then:

$$\omega = J\dot{\mathbf{q}} = \begin{pmatrix} 0 & c_0 & -s_0 c_1 \\ 0 & s_0 & c_1 c_0 \\ 1 & 0 & s_1 \end{pmatrix} \dot{\mathbf{q}} = \begin{pmatrix} \hat{q}_0 & \hat{q}_1 & \hat{q}_2 \end{pmatrix} \dot{\mathbf{q}} \tag{3.3}$$

where $\hat{\mathbf{q}}_i$ is a unit vector along the ith joint axis. If q_1 is rotated by $\pm\pi/2$

$$J = \begin{pmatrix} 0 & c_0 & 0 \\ 0 & s_0 & 0 \\ 1 & 0 & \pm 1 \end{pmatrix} \tag{3.4}$$

Since $\hat{\mathbf{q}}_0$ and $\hat{\mathbf{q}}_2$ are parallel, rank(J) = 2, and we lose the ability to roll the output of the wrist.

Consider suturing as described above. The primary motion is a rolling motion. As a result, we expect that suturing will become essentially impossible for a roll-pitch-yaw wrist near its singular configurations.

If the range of motion of joints 1 and 2 are $\pm\pi/2$, then the workspace of the wrist is a hemisphere and the two singular points at $q_1 = \pm\pi/2$ are at the edges of the wrist workspace.

3.2.1.2 Linear Velocity Singularities

We may also consider the mapping between joint velocities and linear velocities of a point on the last link of the wrist such as the small circle shown in Figure 3-4. Let $\mathbf{x}$ be a vector along the last link from the intersection of the three joint axes to this point. Then:

$$\dot{\mathbf{x}} = \begin{pmatrix} \hat{\mathbf{q}}_0 \times \mathbf{x} & \hat{\mathbf{q}}_1 \times \mathbf{x} & \hat{\mathbf{q}}_2 \times \mathbf{x} \end{pmatrix} \dot{\mathbf{q}} \tag{3.5}$$

In this case, Rank(J) = 2 for all values of q_0, q_1 and q_2 because all the columns are orthogonal to $\mathbf{x}$. It is impossible to produce a velocity $\dot{\mathbf{x}}$ in a direction along the last link, that is along a vector $\mathbf{x}$.

If the wrist is mounted on a larger arm, this lack of mobility is traditionally not a problem. However we will see that the macro-micro control described in Chapter 4 will require that there be redundant degrees of freedom corresponding to directions in which we would like force reflection. Since this wrist is always singular with respect to motions in one direction, macro-micro control would only provide force feedback in two of three directions when used with a roll-pitch-yaw wrist.

3.2.2 Roll-Pitch-Roll

Another common set of wrist kinematics is roll-pitch-roll, shown in Figure 3-5. This wrist is similar to a roll-pitch-yaw wrist with the final link rotated by $\pi/2$.
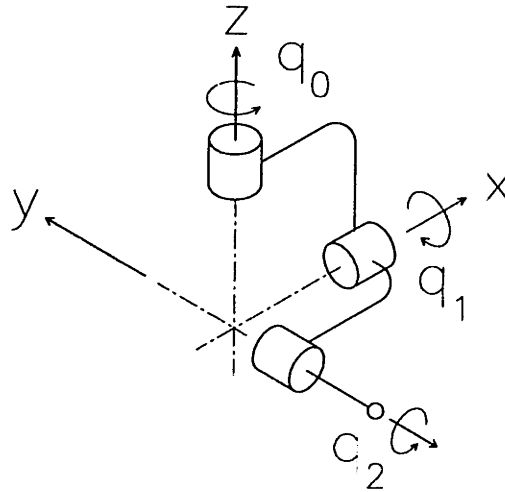
Figure 3-5: Kinematics for a roll-pitch-roll wrist. The small circle at the lower tip of the structure represents a point where objects might be held by a gripper mounted distally on the wrist.

3.2.2.1   Angular Velocity Singularities

Just as in the roll-pitch-yaw wrist, there are two singularities when q_1 is rotated by $\pm\pi/2$ from the orientation shown in the figure.

Again, when singular, angular velocities can only be produced in the plane formed by the axes of joints 0 and 1. The wrist is farthest from its singularities when q_1 is in the orientation shown in the figure, so the wrist therefore operates optimally at a right angle.

The advantage of this wrist is that the output roll which is so critical for suturing is always available. The instrument shaft would ideally be inserted into the body perpendicular to the tissue being sutured instead of parallel to it as in the case of no wrist or the roll-pitch-yaw wrist. The disadvantage compared to the roll-pitch-yaw wrist is that it is considerably more difficult to mechanize. This is due to the fact that if a gripper is added to the end of this wrist, then q_2 will be perpendicular to the axis of gripper. In the roll-pitch-yaw wrist, q_2 and the gripper axis are parallel.

3.2.2.2   Linear Velocity Singularities

The roll-pitch-roll wrist is also singular with respect to linear velocities for all q_0, q_1, and q_2 just as is the roll-pitch-yaw wrist. That is, linear velocities are impossible in a direction along the last link, again making macro-micro control impossible in
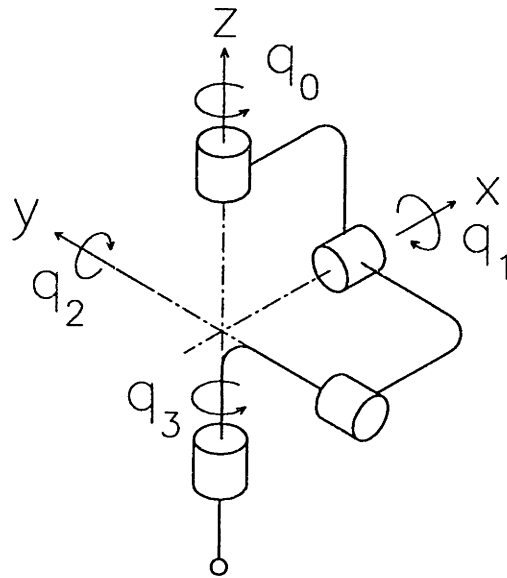
Figure 3-6: Kinematics for a roll-pitch-yaw-roll wrist. The small circle at the lower tip of the structure represents a point where objects might be held by a gripper mounted distally on the wrist.

this direction. However, when q_1 is rotated by $\pm\pi/2$, linear velocities also become impossible along $\hat{q}_1$. So always having output roll available does come at a cost.

3.2.3 Roll-Pitch-Yaw-Roll

In an effort to avoid singularities, more joints can be added. Consider the roll-pitch-yaw-roll wrist shown in Figure 3-6. This wrist avoids angular velocity singularities (losing output roll) by adding an extra roll degree of freedom on the distal link. This can be effective, but we should note that singularities can still be found. A singular configuration for this wrist is shown in Figure 3-7

The interesting point is that by re-orienting q_1 by $\pi/2$, this singular configuration can be avoided while maintaining the same output link orientation. In fact, we can always (ignoring joint range of motion limits) use the redundant degree of freedom to avoid angular velocity singularities. Redundancy resolution of a 4-R wrist (a wrist with four intersecting revolute joints) is discussed in (Long et al., 1989)

A redundant wrist of course has the disadvantage of adding an actuator which we might not otherwise need, and further increasing design complexity.
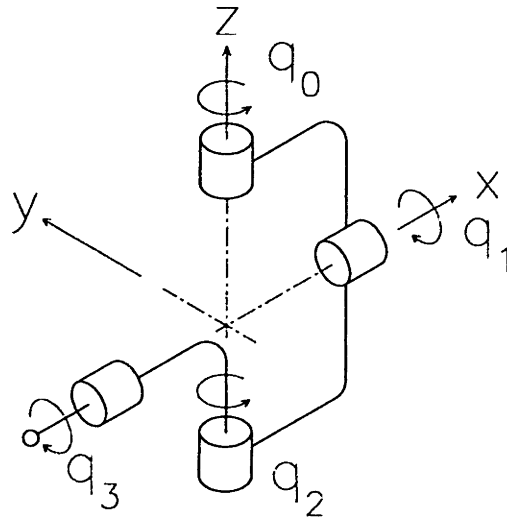
Figure 3-7: The roll-pitch-yaw-roll wrist in a singular configuration. All joint axes lie in a plane. Angular velocities out of the plane are impossible.

3.2.3.1   Rosheim

Mark Rosheim is a creative designer probably best know for his variation of the roll-pitch-yaw wrist known as the omni-wrist, which has no angular velocity singularities, (Rosheim, 1989). This wrist consists of a pair of cardan joints linked in series. The redundant two degrees of freedom are resolved internally to the wrist using a fairly complicated set of gears and rollers so that each bends half of the total reorientation of the wrist. At a wrist limit of 90 degrees, each cardan joint re-orients by 45 degrees so they remain non-singular. Output roll is fed through the wrist using a smaller double cardan driveshaft. While such a complex wrist is difficult to miniaturize, (Schenker and Charles, 1995) describe a Rosheim variant designed at the Jet Propulsion Lab which has an approximately 2.5 cm outside diameter.

3.3   Base Kinematics

The slave manipulator must be designed so that one link always passes through a constrained point, the incision point. The three most logical ways for this to be done are to use 1) controlled redundant kinematics, 2) passive redundant kinematics, or 3) the option which we choose, remote center kinematics.

3.3.1 Controlled Redundant Kinematics

Consider a six-degree-of-freedom robot whose last link is a rigid shaft. If the manipulator is not in a singular configuration, the shaft will have six degrees of freedom. Singular configurations of a manipulator (singularities) are configurations where the Jacobian matrix relating endpoint velocities to joint velocities becomes singular, or loses rank. If we wish to constrain a point on the shaft such that it does not translate, then we write the transformation between $n > 6$ joint velocities, $\dot{q}$ and three linear and three rotational velocities of the point in consideration on the shaft $\dot{x}$ and $\dot{\theta}$ respectively:

$$\begin{pmatrix} \dot{x} \\ \dot{\theta} \end{pmatrix} = J\dot{q} \tag{3.6}$$

If we set:

$$\dot{x} = v \tag{3.7}$$

where v is a vector representing the desired velocity and points in a direction along the axis of the shaft, then the equations above represent a constraint on joint velocities which enforce the incision point constraint.

We therefore constrain the robot to act like a four-degree-of-freedom robot to satisfy the incision point constraint. If additional freedoms are incorporated so that the end-effector has six degrees of freedom plus a gripping freedom after the constraint is applied, then the robot will have a minimum of nine degrees of freedom.

There are two disadvantages to this approach:

- The addition of redundant actuators and degrees of freedom is costly and wasteful if unnecessary. It is our experience that the complexity of a design can increase sharply with increased degrees of freedom and should be avoided if possible.

- We are effectively creating a two-degree-of-freedom gimbal in software using this approach. The structural rigidity of this gimbal is therefore limited by the servo gains we can generate. Servo controlled joints are typically less stiff than actual mechanical bearings, so it is likely that some flexibility will be introduced between the manipulator base and its tip resulting in inaccuracy of motion and placing a limit on the stiffness of the connection between the master and slave manipulators.

3.3.2   Passive Redundant Kinematics

We could alternatively design redundant degrees of freedom into the robot which are uncontrolled; they freely rotate/translate in bearings. Instead of resolving the redundancy actively, we would let the cannula and tissue at the incision point passively constrain these redundant freedoms. This alternative uses the body to constrain the motion of the robot. The approach has the advantage of appearing simple and requires only as many actuators as degrees of freedom being controlled. Also if the patient is accidentally moved, the portion of the robot in the incision point will naturally move out of the way. There are, however several disadvantages to the approach:

- Because the robot will move with body movements, this will result in uncontrolled motions of the robot tip during these movements which might be dangerous.

- Forces applied at the tip of the manipulator will react against the body wall causing deflections which may be unwanted.

- We may use sensors in the uncontrolled joints and use the manipulator forward kinematics to find the manipulator tip position. We may then control the remaining joints in order to maintain a desired endpoint position and orientation. However introducing a flexibility between the actuators and the point whose position is being controlled is not desirable, even if all joint positions are being measured. Positioning bandwidth, given the fact that all real actuators have velocity and torque limits, will be reduced.

3.3.3   Remote Center Kinematics

Our third option is to design a device with no redundant freedoms which, by its kinematic design, always places a part of the robot (the axis of a distal instrument shaft) through the incision point. Such devices exist and are called remote center devices, because they produce a remote center of rotation, unencumbered by mechanism, which can be placed at the incision point. This is the approach which we chose. We use the double parallelogram linkage described below, as further described in Chapter 5.

3.3.3.1   Spherical Linkages

One way of implementing a remote center is to use a spherical linkage such as that shown in Figure 3-8. If a serial linkage of revolute joints is designed such that its axes
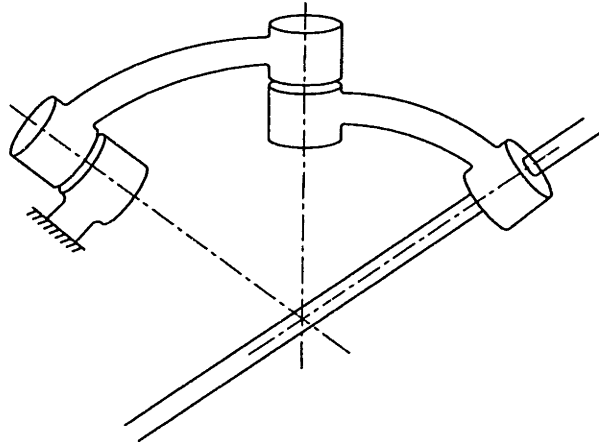
Figure 3-8: A serial linkage whose joint axes intersect at a single point will create spherical (remote center) motion.

intersect at a single point, then the links rotate on a sphere about a remote center of rotation. If a shaft were to be placed in the second link as shown in the figure, it would be constrained to pass through the remote center. Two or more such linkages can be connected in parallel so that the motors of the spherical linkage are fixed with respect to ground.

We can imagine other combinations of linkages with the same property. Linear bearings might also be designed with curved bearings surfaces to follow the surface of a sphere again providing a remote center of rotation.

3.3.3.2 Double Parallelogram

Figure 3-9 shows the double parallelogram mechanism. A similar linkage is described separately in (Hamlin and Sanderson, 1994), and (Taylor et al., 1995). Ralph Mosher used a version in a wrist called the Roticulator, (Rosheim, 1989), it has been used in hand/wrist exoskeletons by Exos, Inc. and Sarcos, Inc., and variations are commonly used in interior cabinet hinges. By combining two parallelogram linkages we can produce a remote center of rotation in a plane. By rotating the entire linkage out of the plane about the axis labeled 0, a spherical remote center is achieved.

This mechanism has several advantages as we will see in Chapters 5 and 7.

- Because the mechanism is essentially planar, mechanizing it is relatively straight forward.

- It is possible to run mechanical transmission cables along a planar linkage,
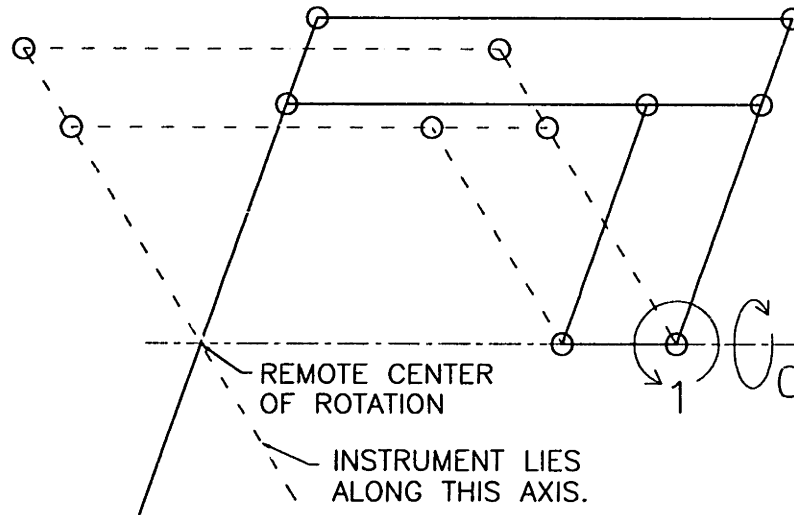
Figure 3-9: The double parallelagram remote center linkage. The circles represent revolute joints whose axes are perpendicular to the page. Axis 0 rotates the linkage out of the plane of the page.

    making it possible to actuate the wrist unit using motors placed on a remote location of the linkage.

- The linkage may be gravitationally counterbalanced.

- The linkage has a natural way of extending over the patient.

3.4 Dynamics

At this point, we turn toward dynamic constraints on our system. Here we comment on the type of dynamics which we would like to see in the slave manipulator. These recommendations are a direct result of our experimentation with teleoperator control, and macro-micro control in particular, as discussed in Chapter 4.

3.4.1 Wrist Dynamics

The wrist dynamics become important when we consider force reflection. If our goal was to only provide additional degrees of freedom to the surgeon, dynamic constraints would be far less important.

3.4.1.1 Wrist Inertia

Macro-micro control will dictate that the inertia of the micro freedoms, in this case the wrist, be low. This is the portion of the robot that interacts with the environment and defines how the slave will appear, dynamically, to the user. Because of the small size of the wrist however, this is not a problem. In fact, the inertia of the motor rotors may be on the order of the inertia of the wrist and gripper components.

We do however have a lower limit on the mass of the wrist components and their actuators which is dictated by the servo stiffness we wish to achieve. We may reduce the mass until achieving a desired servo stiffness becomes impossible given bandwidth limitations on our system, see Section 4.2.1.

3.4.1.2 Wrist Friction

While under macro-micro control, our ability to reflect forces back to the user will be directly limited by friction in the wrist mechanism, (see Chapter 4). During freespace motions, friction in the wrist will be reflected back to the user. If a force scaling factor is used, the frictional forces will be scaled by this factor which, if greater than one, will make freespace motions feel consequently worse. When the slave manipulator makes contact with the environment, forces below the frictional forces in the wrist will not be felt by the user lowering their ability to discriminate contact.

3.4.2 Base Positioner Dynamics

3.4.2.1 Servo Response

The goal of the base positioner will be to move the wrist within the body with good positioning bandwidth and accuracy. Any errors in tracking of the master will be perceived as forces by the user and will be felt during freespace motions of the master and slave.

Unlike the wrist, the base positioner does not necessarily need to be light or have particularly low friction. The most important requirement is that its actuators be matched properly to the slave inertia so that it tracks master movements with little error. We should also generate a sufficient overall stiffness to compensate for external disturbance forces such as those caused by the body wall.

3.4.2.2   Structural Dynamics

Structural dynamics should be minimized in order to achieve good position servo response of the base. Also, the overall stiffness of the connection between the master and slave will be limited by the structural stiffness of both the master and the slave.

3.4.2.3   Counterbalancing

Gravitationally counterbalancing the slave manipulator, if possible, will help reduce the torques required for the base positioner actuators. It also provides a measure of safety. A counterbalanced slave manipulator will not have a tendency to "fall over" if motor power is lost.

3.5   Sizing

Based on the size of current MIS instruments, the stroke of an instrument into and out of the patient should be roughly 23-25 cm (9-10 in). The depth of penetration into the body should be roughly 33 cm (13 in). The volume of the workspace should be consistent with this. Obviously these values will vary with different size patients and with different procedures, but these give good estimates for a general system. The size of the instrument shaft must be comparable with current instruments which range from 5 mm diameter to 13 mm diameter.

3.6   Force Requirements

I spoke with surgeons in order to generate a specification for x, y, z force levels. Surgeons, unfortunately, have a poor quantitative sense of the forces which they apply. I performed a simple experiment where I asked a general surgeon[1] to tug on tissue, in this case a pig stomach, using a hand held force sensor with a digital readout and hook attachment (Mark-10, model BG-2). I asked him to tug on the tissue itself, and on suture which was tied into the tissue, "as hard as he might pull during surgery". The range of forces which ranged from 1/2 to 2 lbs. Based on this very rough experiment, I used 2 lbs as a rough specification for desirable x, y, z force capability.

---

[1]Dr. Barry Gardiner of Oakland, CA

Gripping force is difficult to specify, and yet very important to the ultimate performance of the system. The primary challenge for the gripper is to hold needles. The problem is that different needle sizes and cross sections, and different needle holder grip surfaces change the required grip force. Typically, smaller needles require less gripping force because forces acting at the needle tip create a smaller moment on shorter needles than on longer ones. Again I performed a simple experiment using a needle holder (Miltex 8-50 with stainless steel, not carbide, grip surfaces). I held one finger loop in a table vise, and held a large (approximately 37 mm) tapered needle with an oval cross section in the jaws by pushing down on the other finger loop through a force sensor (Wagner Force Dial, model FDK 160). This is probably the largest needle I expect to encounter during surgery, so the force required should represent an upper limit. Roughly 2 lbs of force was required on the finger loops to hold the needle "firmly". The needle could wiggle slightly, but to my best estimation was held sufficiently well so as not to roll in the grasp during suturing. After considering the mechanical advantage of the needle holder (the needle was held 0.75 inches from the pivot point, and the force was applied 4.25 inches from the pivot point), the resulting grip force on the needle was approximately 11.3 lbs. This is a severe constraint considering that the required tip force is only 2 lbs.

3.7 Practical Operating Room Constraints

There are a number of issues which are to some extent separate from the main design and controls focus of this thesis, but which are critical to the design of an actual product. These issues are discussed below.

3.7.1 Tool Changing

During surgery, many different tools are used. They typically rest in a tray next to the patient, and the surgeon calls for them, to an assistant, as they are needed. The rate at which tools can be interchanged today is high, taking only a few seconds for each tool change.

For a MIS robot to be effective, this cannot change by much. There is nothing intrinsic about using a teleoperator which affects the need to change tools quickly. As a result, some distal portion of the robot will have to disconnect and be replaced by alternate versions in order to have needle holders, scissors, tissue graspers, etc. available to the surgeon.

3.7.2 Fit Over Patient

The system must be able to fit over a patient without obstructing other equipment, other surgeons, and surgical assistants. Access to the patient should not be blocked in the event of an emergency. The general system setup is an important issue if such a system is used as a product. These issues include how the system will be mounted in the OR, how it will be positioned above the patient, what happens if the patient is moved or if the OR table is tilted during a procedure.

Different procedures might require completely different positioning of the slaves over the patient. There will likely be two slaves which operate instruments and one slave which positions the endoscopic camera. All will be occupying a limited space which compounds the problem of setup and mounting within the operating room.

3.7.3 Power Sources

The system should use standard power sources which might be available in the operating room. For example, the use of hydraulic or pneumatic compressors would be impractical. Electric motors are a logical choice for operating room use.

3.7.4 Sterilization and Draping

Surgical instruments must of course be sterile. The portion of the slave manipulator which passes into the body must therefore be sterile. This means typically that it may be subject to the heat of an autoclave or to chemical methods of sterilization. This limits the materials which we may use for the slave and in particular, for the wrist components.

The entire robot need not be sterilized, since a standard solution already exists which is to cover non sterile systems with sterile drapes. Since the portion of the system which enters the body must be sterile, some sort of interface is required in order to allow the draped non-sterile portion of the robot to connect to a sterile removable instrument while maintaining the sterility of the instrument and transmitting power through the drape. Motions of the robot must be unencumbered by the drape. The design of this interconnection and perhaps of the drape is an issue in itself.

3.8 Safety

The most important specification for a surgical system is that it be safe. Typically a commercial system might have a complex software and digital hardware safety protocol built into the control system to ensure fail-safe operation. This would be used in combination with redundant sensors, and brakes or clutches on each axis to prevent uncontrolled motions.

There are also certain mechanical characteristics which we feel make a robot intrinsically safer and which should apply to a system designed for human surgery:

- Counterbalancing of the largest degrees of freedom, either gravitationally or via a spring. This prevents the system from falling under its weight in the event that power is turned off.

- Low link inertia. The energy stored in the system when it is moving is then low. The forces required to dissipate power while stopping a machine can do as much damage to the environment or the machine as forces which the machine can output using its actuators.

- Backdrivability. In the event of a failure, we would like to be able to pull the machine out of the patient under manual control. A simple way to accomplish this is to have backdrivable actuators.

3.9 Summary of Slave Manipulator Goals

To summarize, we have compiled a short list of desirable qualities for a slave manipulator for minimally invasive surgery.

- The system should have at least seven degrees of freedom overall with four outside the body (constrained by the incision point) and the remaining degrees of freedom inside the body in the form of a wrist mechanism and gripper.

- The system should have a compact, slender wrist/shaft which will fit through a cannula inserted in the incision point.

- The system should have the ability to orient the wrist 90 degrees relative to the axis of the shaft.

- Wrist singularities, if they exist, should be located at edge of the wrist's range of motion.

- The wrist should allow independent positioning of a point at the tip of the grippers. This redundancy is to enable macro-micro control (see Chapter 4) of the overall system.

- The system should have particularly low inertia in the wrist to enable macro-micro control (see Chapter 4), but not so low to prevent sufficient servo stiffness from being achieved.

- The system should have particularly low friction in the wrist to enable macro-micro control, (see Chapter 4).

- The system should have a remote center base positioner mechanism which will support the weight of the required motors and wrist unit.

- The base positioner should be designed to have good servo control bandwidth.

- The stroke of the instrument into and out of the body should be roughly 8-10", and the overall workspace should also be on this order.

- We should be able to apply 2 lbs in the $\dot{x}, y, z$ directions.

- We should be able to apply 11 lbs of grip force to hold large needles for suturing.

- A research system should allow tools to be interchanged relatively easily to allow testing of different types of instruments.

- A production system requires that tools be interchanged quickly, within several seconds.

- A production system must fit over a patient without obstructing other equipment and personnel in the operating room.

- A production system must use power sources which are available in the operating room.

- A production system must provide for sterile draping and sterilization of at least the portion which passes through the incision into the human body.

- A production system should be safe to the patient and surgical staff working with it.

Chapter 4

Initial Teleoperator Control Study and Controller Selection

This chapter begins by discussing basic teleoperator control and its limitations. We then investigate several methods to control a master-slave system where a macro-micro manipulator is used as the slave. We define a macro-micro manipulator as one consisting of a lightweight distal manipulator mounted on a heavier proximal manipulator. We study the benefits and difficulties of macro-micro control and find that a Jacobian Inverse type controller allows us to achieve 50:1 scaled force reflection using a three-degree-of-freedom experimental master-slave testbed. This study gives insight which is critical to understanding the telemanipulator slave designs presented in Chapters 5 and 7.

4.1   Basic Force Reflecting Teleoperation

Consider a master manipulator and a slave manipulator, each with its own sensors, actuators, power supplies and amplifiers. Controlling each manipulator is a computer which reads sensor values from each and which commands actuator inputs based on a controller operating on the computer. Using such a system, as shown in Figure 4-1, the human operator can interact with the environment. In our case, this will be a surgeon interacting with tissues at the surgical site.

In our designs, we limit ourselves to force feedback and forego use of other haptic modalities. In particular, we do not consider the use of direct tactile feedback. For example, tactile stimulus may be imparted to the user via direct stimulation of skin cutaneous sensors via devices which produce pressure maps across the fingertips,
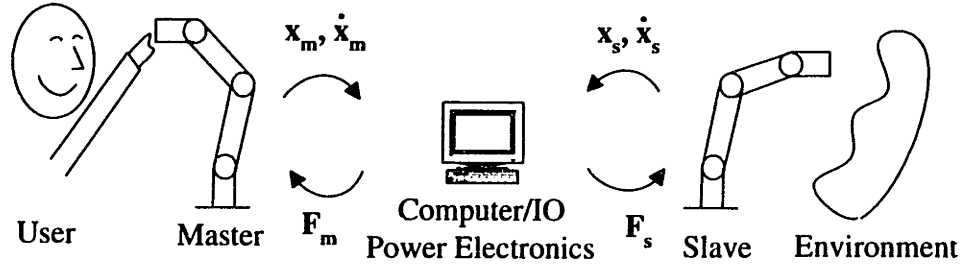
Figure 4-1: A teleoperator consists of a master, slave, and associated computer and electronic hardware to control each.

or via non-directional vibration sources. For example, (Kontarinis, 1995) studies vibration and shape feedback specifically for telemanipulation. Often, teleoperators are used to manipulate objects from a large distance introducing a communications link with time delay between the master and slave manipulators. We will not consider communication delays in our system.

Sections 4.1.1 and 4.1.2 below describe basic position based bilateral force reflecting teleoperator control. These sections are based on (Niemeyer, 1996).

4.1.1   Basic Teleoperator

The dynamics of the master and slave may be expressed as

$$H_m(\mathbf{q}_m)\ddot{\mathbf{q}}_m + C_m(\mathbf{q}_m, \dot{\mathbf{q}}_m)\dot{\mathbf{q}}_m + G_m(\mathbf{q}_m) = -\tau_m \qquad (4.1a)$$

$$H_s(\mathbf{q}_s)\ddot{\mathbf{q}}_s + C_s(\mathbf{q}_s, \dot{\mathbf{q}}_s)\dot{\mathbf{q}}_s + G_s(\mathbf{q}_s) = \tau_s \qquad (4.1b)$$

where $\mathbf{q}$ is the vector of joint positions, H is the inertia matrix, $C\dot{\mathbf{q}}$ are coriolis torques, G are gravitational torques, and τ are motor torques, (Asada and Slotine, 1986).

To control the system, we compensate for gravity by calculating and feeding forward gravitational torques, and use P.D. feedback to force tracking between the master and slave joints.

$$\tau_m = -G_m(\mathbf{q}_m) + \tau_{PD} \qquad (4.2a)$$

$$\tau_s = G_m(\mathbf{q}_s) + \tau_{PD} \qquad (4.2b)$$

$$\tau_{PD} = K(\mathbf{q}_m - \mathbf{q}_s) + B(\dot{\mathbf{q}}_m - \dot{\mathbf{q}}_s) \qquad (4.2c)$$

If the feedback gains K and B are symmetric positive definite matrices, then the
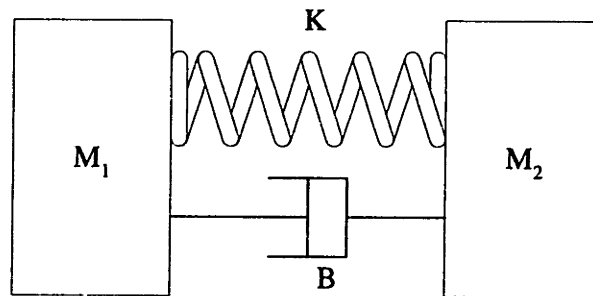
Figure 4-2: The basic teleoperator mimicks two inertias connected via a spring and damper in the one-degree-of-freedom case.

master and slave will appear to be connected via a spring and damper. Figure 4-2 shows the mechanical equivalent for a one-degree-of-freedom system.

4.1.2 Jacobian Transpose Cartesian Control

The above controller assumes that we are using a kinematically similar master and slave. If this is not the case, then the most straightforward method of cartesian control is to implement tracking between the endpoints of each manipulator. To do this, we calculate the endpoint position x and endpoint velocity $\dot{x}$ using the manipulator geometry. We then apply a P.D. controller to find the resulting endpoint forces and torques, F. These are then converted to joint torques τ and commanded to the master and slave motors.

Endpoint velocities are calculated as follows, where J is typically referred to as the manipulator Jacobian:

$$\dot{\mathbf{x}}_m = J_m(\mathbf{q}_m)\dot{\mathbf{q}}_m \qquad (4.3a)$$

$$\dot{\mathbf{x}}_s = J_s(\mathbf{q}_s)\dot{\mathbf{q}}_s \qquad (4.3b)$$

The joint P.D. is replaced with a cartesian version:

$$\mathbf{F}_{PD} = K(\mathbf{x}_m - \mathbf{x}_s) + B(\dot{\mathbf{x}}_m - \dot{\mathbf{x}}_s) \qquad (4.4a)$$

$$\mathbf{F}_m = \mathbf{F}_{PD} \qquad (4.4b)$$

$$\mathbf{F}_s = \mathbf{F}_{PD} \qquad (4.4c)$$

The resulting joint torques are then calculated:

$$\tau_m = -J_m^T(\mathbf{q}_m)\mathbf{F}_m + G_m(\mathbf{q}_m) \qquad (4.5a)$$
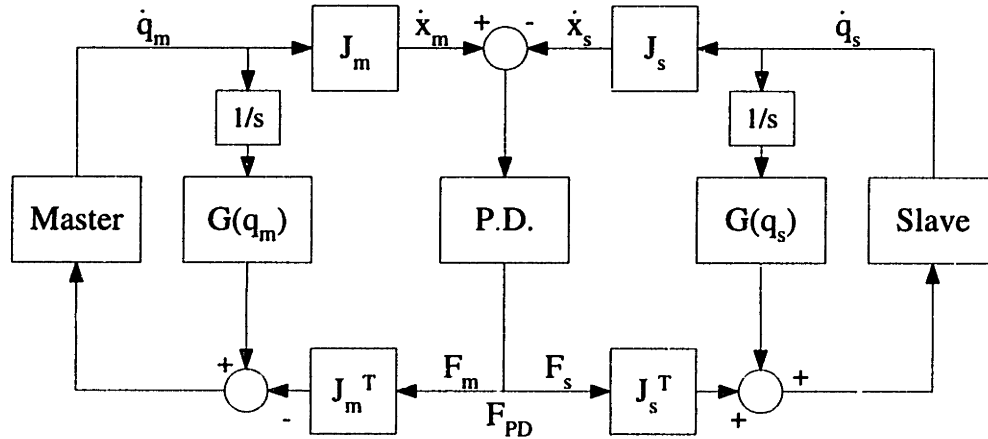
Figure 4-3: Both master and slave robots are gravity compensated, transformed into a cartesian domain, then connected via a P.D. controller mimicking a spring and damper.

$$\tau_s = J_s^T(\mathbf{q}_s)\mathbf{F}_s + G_s(\mathbf{q}_s) \qquad (4.5b)$$

Figure 4-3 shows the system in block diagram form with the kinematic transformations included.

4.1.3 Scaling

One way in which we can change the user's perception of the environment is to scale positions and forces between the master and the slave. We may introduce scaling into the above system in order to change the size of relative motions and to amplify forces between the master and slave. This is done by introducing the scale factors η_P and η_F as shown in Figure 4-4.

Scaling will effect the users perception of the environment and of the teleoperator:

- $\eta_F > 1, \eta_P = 1$ Forces are scaled up from the slave to the master, and velocities remain one to one. In this case, the user will feel an increased slave/environment impedance. Objects in the environment will feel stiffer and heavier. This will make transitions between freespace and contact feel more crisp and noticeable. However, the friction and inertia of the slave will also be amplified and felt by the user. As a result, these undesirable dynamics will have to be very low in the slave if η_F is to be large. Conversely, the environment will feel a reduced master/user impedance. The environment will more easily backdrive the master
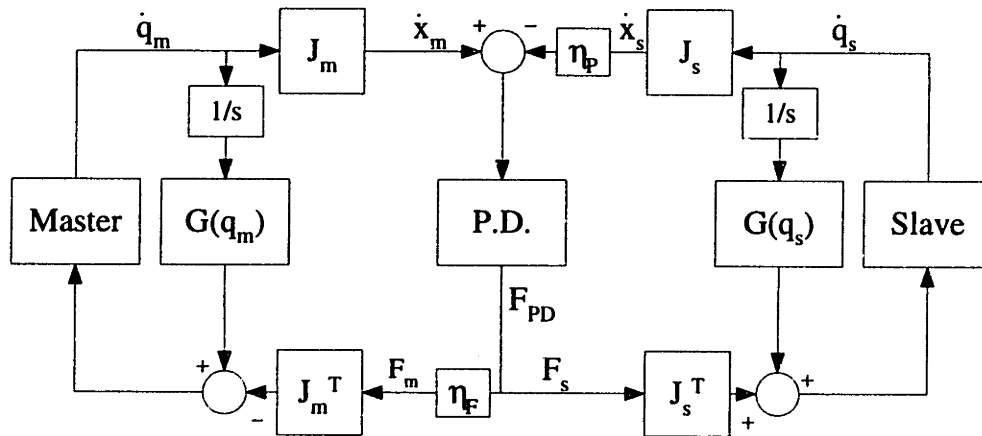
Figure 4-4: Both master and slave robots are gravity compensated, transformed into a cartesian domain, then connected via a P.D. controller mimicking a spring and damper. Scaling is included.

and human operator.

- $\eta_F < 1, \eta_P = 1$ Forces are scaled down from the slave to the master and velocities remain one to one. The situation is inverse of the previous case. Note that as long as $\eta_F > 0$, some level of force reflection will exist.

- $\eta_P > 1, \eta_F = 1$ Positions are scaled up from the slave to the master, and forces remain one to one. In this case, motions made by the human operator are reduced, making fine motions easier to perform. Steady state forces will be equal at the master and slave. Therefore, the user will feel a decrease in slave/environment impedance. Transitions made between freespace and contact will feel softer and will be more difficult to distinguish.

- $\eta_P < 1, \eta_F = 1$ Positions are scaled down from the slave to the master, and forces remain one to one. Fine motion control now becomes more difficult, since errors in the users motions will be amplified. But the slave/environment impedance increases as felt by the master/user so that contacts will be easier to distinguish.

- $\eta_F > 1, \eta_P = 1/\eta_F$ Positions are scaled down from the slave to the master, but forces are scaled up in such a way that the environment stiffness appears unchanged to the user.

4.2 Limitations

Theoretically, if the inertia of the slave and master were zero, and the P.D. gains were infinite, the system would be transparent. In other words, forces and motions at the slave and master would be identical. Or if scaling were implemented, forces and motions would be exact scaled versions of one another. In a real system, of course, infinite gains and massless linkages are impossible. In what follows, we discuss several real world limitations.

4.2.1 Relation of Stiffness to Inertia

Consider again our model for a one-degree-of-freedom teleoperator shown in Figure 4-2. The dynamics can be written as:

$$m_1 \ddot{x}_1 = K(x_2 - x_1) + B(\dot{x}_2 - \dot{x}_1) \tag{4.6}$$

$$m_2 \ddot{x}_2 = -K(x_2 - x_1) - B(\dot{x}_2 - \dot{x}_1) \tag{4.7}$$

Or in Laplace notation where s is the Laplace operator:

$$m_1 x_1 s^2 = K(x_2 - x_1) + B(x_2 - x_1)s \tag{4.8}$$

$$m_2 x_2 s^2 = -K(x_2 - x_1) - B(x_2 - x_1)s \tag{4.9}$$

Which simplifies to:

$$s^2 (m_1 m_2 s^2 + (m_1 + m_2)Bs + (m_1 + m_2)K)x_1 = 0 \tag{4.10}$$

$$s^2 (m_1 m_2 s^2 + (m_1 + m_2)Bs + (m_1 + m_2)K)x_2 = 0 \tag{4.11}$$

The natural frequency is then:

$$\omega_n = \sqrt{\frac{K}{\frac{m_1 m_2}{m_1 + m_2}}} = \sqrt{\frac{K}{M_{eff}}} \tag{4.12}$$

where $M_{eff} = \frac{m_1 m_2}{m_1 + m_2}$ is an effective mass.

In practice a real system will always have a bandwidth limitation, call this ω_b. To ensure stability, we should impose a frequency limit λ below this limitation, say at $\lambda = \omega_b/5$. Typically, ω_b is caused by the finite servo rate of a digital controller, the bandwidth of motor amplifiers, or limited position measurement resolution. As a result, we have the following tradeoff. On one hand, we desire a system with low inertia, so that the teleoperator feels light to the human operator. For a given effective

mass M_{eff}, however, our stiffness is then limited by:

$$K < \lambda^2 M_{eff} \tag{4.13}$$

On the other hand, if we desire a certain stiffness, K, then the effective mass, M_{eff} is limited by:

$$M_{eff} > \frac{K}{\lambda^2} \tag{4.14}$$

We can either (a) design the system to have a high inertia in order to make the connection between the master and slave stiff, or (b) design the system to have low inertia, but have a low stiffness as a result. In practice we compromise in order to have sufficiently high stiffness and sufficiently low inertia to make the system usable.

4.2.2 Position Measurement

There are many effects which contribute to a system bandwidth limit. Typically each gain K and B will be limited for different reasons which makes the situation a bit more complicated. Below we give a simple rule of thumb relating digital position measurement resolution and the gain K which can be achieved.

Digital encoders are very convenient for measuring joint positions. It is typical to differentiate this measurement to infer joint velocities because velocity measuring devices (tachometers) are bulky and costly. Furthermore, digital encoders are relatively immune to outside sources of noise and add very little mass and no friction to a motor when mounted directly to a motor shaft. They are not limited in the number of revolutions which can be measured, and electronics to read encoders are common and straightforward. These are all advantages over using analog potentiometers. They are of course digital, and this causes several problems.

Digital position measurement limits the servo stiffness (position gain K) which can be implemented. Consider the position term for a one-degree-of-freedom P.D. controller:

$$F = -K(x_m - x_d) \tag{4.15}$$

Where the measured position is x_m, the desired position is x_d, the controller force is F, and the position resolution is Δ. If the position sensing is digital, the measured position x_m is quantized to $n\Delta$ where n is an integer. The resulting forces form a staircase as shown in Figure 4-5. In nearly all cases, $x_d \neq x_m$, because this would
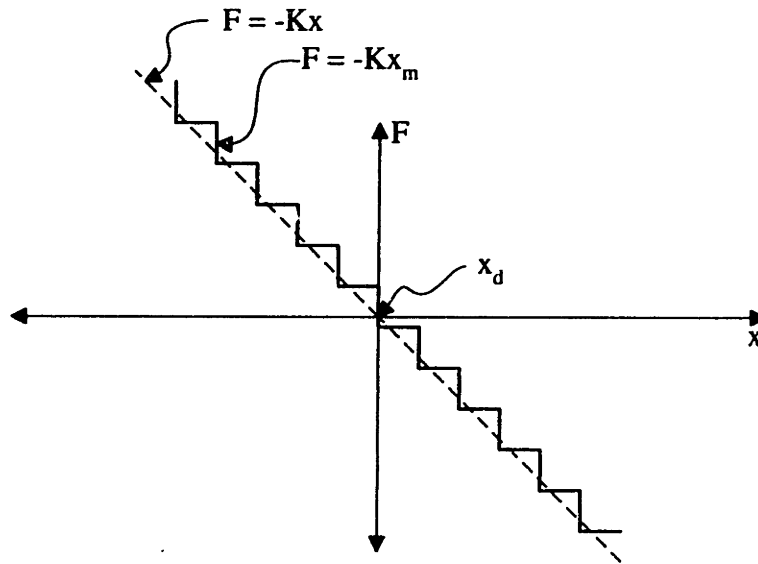
Figure 4-5: Instead of producing a straight line force output, a staircase is produced instead.

require equality to within machine floating point precision. Therefore the smallest F can be is $K\Delta$. In the absence of friction, there will always be a commanded force and the system will continuously bounce between steps without settling to a fixed value.

In the presence of friction, it would seem the energy would approach zero. However, time delay induced by finite servo rate provides a mechanism to add energy to the limit cycle. Consider Figure 4-6. The dotted line shows the path of a system in a one resolution step limit cycle. If we start at the upper left of the loop, labeled 1, the controller pushes the system to the right with a force of, in this case, $K\Delta/2$. At 2, the force should drop to $-K\Delta/2$, however due to the time delay the force is maintained until 3. The same effect is repeated in the other direction. The area of the loop represents the energy added during each cycle.

In practice, while it is usually beneficial to reduce friction in our mechanisms and transmissions, a little static friction helps with this problem. In particular, if the static friction level, F_f is greater than the force step $K\Delta$, then the limit cycle cannot start. Then, given our encoder resolution, and static friction, our gain is limited by:

$$K < \frac{F_f}{\Delta}$$
(4.16)

Increasing encoder resolution is obviously a more attractive solution over increasing static friction.
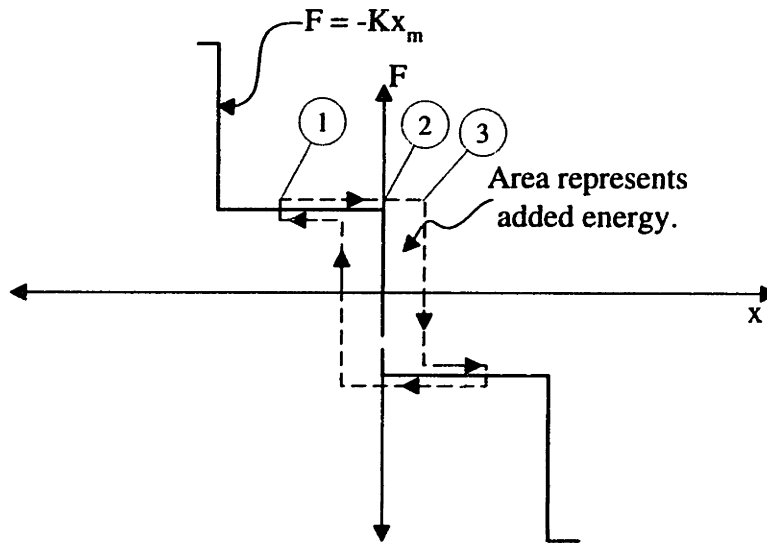
Figure 4-6: Time delay adds what looks like hysteresis to add energy to the limit cycle.

4.2.3 Velocity Estimation

Any time a digital position signal is differentiated in order to estimate velocity, a certain amount of "noise" will be added to the signal. Typically, we filter the velocity signal digitally in order to avoid injecting this noise into the system which would otherwise create unwanted vibrations in the system. The filter cutoff however should be kept above the position servo bandwidth to avoid adding unnecessary lag to the controller which can lead to instability.

4.3 Macro-Micro Control

If we look at the basic force-reflecting teleoperator discussed above, we can see that when moving the teleoperator through free space the human operator will feel the inertia of both the master and the slave. Therefore, to make the system feel as light as possible it seems reasonable to design the master and slave manipulators to be as light as possible. Of course, we are limited because actuators have limited power to weight ratios and materials have limited strength and stiffness.

Here we investigate several methods to control a master-slave system where a macro-micro manipulator is used as the slave. We define a macro-micro manipulator as one consisting of a lightweight distal manipulator mounted on a heavier proximal

manipulator.

The idea is based on the assumption that the slave can be designed to have a "sensitive" end-effector (wrist and fingers) which is lightweight and low in friction. Then we ask: if this wrist is mounted on the end of a larger manipulator, with consequently larger inertia, would it be possible to suppress the reflected inertia of the macro manipulator, and to have an endpoint impedance which approaches that of the micro manipulator? In this chapter, we compare several methods of control as part of this approach.

The master in this study is essentially an actuated rotary turntable with a knob which the user can grasp. The slave has two actuators, a macro actuator base and a micro actuator mounted upon it whose endpoint inertia is 200 times lower than that of the macro actuator. We present data from five different controllers using a three-degree-of-freedom testbed to demonstrate our approach. We demonstrate high quality, force-reflecting teleoperation with force scaling of 50:1, without the use of explicit force sensing. The control effectively (a) hides much of the inertia of the slave manipulator from the user who feels primarily the dynamics of the master and that of the slave micro actuator end-effector, and (b) therefore makes the slave respond more readily to forces from the environment. The goal is to develop an approach which can be extended to our later seven and eight-degree-of-freedom teleoperator designs, the Silver Falcon and Black Falcon.

An interesting question which arises is whether we wish to reduce the inertia of the master as well. After all, the user feels both the inertia of the master and the slave, so if we wish to reduce slave inertia, why not reduce master inertia as well? The reason has to do with force scaling, which breaks the inherent symmetry of the system. If we scale forces such that master forces are magnified with respect to slave forces, as we will in this chapter, then the master must be able to achieve a proportionately higher servo stiffness than the slave. Reducing the inertia of the master reduces the servo stiffness which the master can achieve. In this case, we would like the master to have an inertia larger than the slave micro degree of freedom roughly in proportion to the force scale factor.

4.3.1   Prototype Hardware

These ideas were studied using the testbed shown in Figure 4-7. A schematic drawing is shown in Figure 4-8 where system variables are defined.

The slave has two degrees of freedom, a macro and a micro freedom. The master has one degree of freedom. All three axes are driven by brushed d.c. servomotors (Maxon Motors RE025-055-035EAA200A). In our discussion of the system, we scale
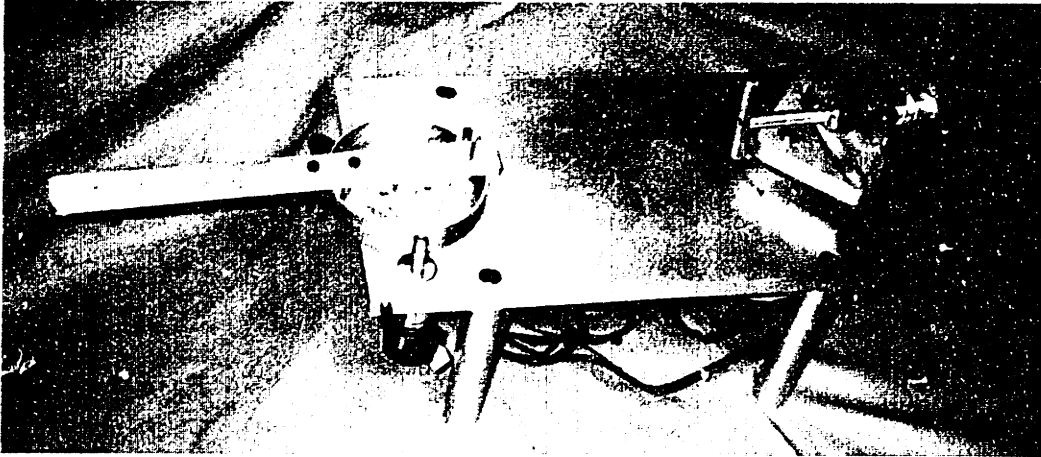
Figure 4-7: Photo of the macro-micro testbed. The master is on the left. The bar was added to increase the master inertia. The macro-micro slave is on the right.

all joint forces and positions by link lengths implicity in order to avoid carrying these values through the calculations. In order to keep with general notation for joint forces and positions, these are labeled τ_i and q_i respectively, and have units of newtons and meters. Inertias are also measured at the endpoint of each joint and have units of kilograms.

The first joint position of the slave is labeled q_1 and the output force for this joint (force at the tip of the link) is τ_1. This first axis is driven by a low friction, one stage cable reduction with a ratio of 13.87:1. The axis one encoder is a Hewlett-Packard optical encoder with 2000 counts per revolution after quadrature. The output resolution is therefore 27,740 counts per revolution. At a link length of $l_1 = .0635$ m (2.5 in), this gives an endpoint resolution of 1.44×10^{-5} m (5.66×10^{-4} in).

The second joint is mounted to the first joint such that its axis is orthogonal to and intersecting with the first. The second joint position is labeled q_2, and the output force of this second joint is labeled τ_2. Mounted to the shaft of the joint 2 motor is a "T" shaped output link[1]. This second joint is direct drive and uses a Canon laser encoder (TR-36) with 14,400 counts per revolution after quadrature. At a link length of $l_2 = 0.025$ m (1 in), this gives an endpoint resolution of 1.11×10^{-5} m (4.36×10^{-4} in).

The master is a single rotary joint whose position is labeled q_3. The force for this joint is τ_3. The master is driven by a single stage cable reduction with a ratio

---

[1]The reason for this "T" shape is to dynamically balance the link as a safety measure. This prevents bending of the motor shaft at high shaft velocities.

$$q_1 = \theta_1 l_1$$
$$q_2 = \theta_2 l_2$$
$$q_3 = \theta_3 l_3$$

$$x_s = q_1 + q_2$$
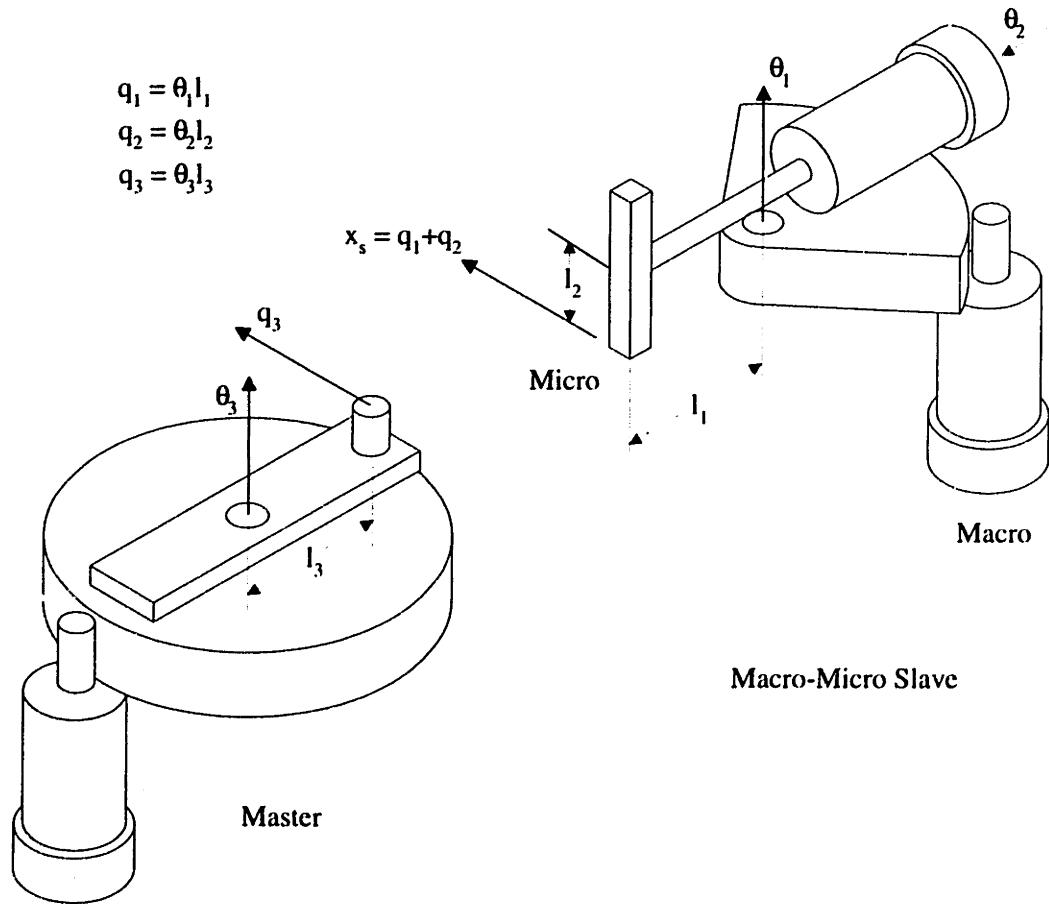
Figure 4-8: The slave consists of a single motor with a "T" shaped output shaft resting on a base turntable driven with a cable reduction. The master is a single turntable driven with a cable reduction.

of 10.67:1. The encoder on this axis is a Hewlett-Packard optical encoder with 2000 counts per revolution after quadrature, giving a total resolution of 21,340 counts per revolution. At a link length (the point where the user holds the master) of $l_3 = .044$ m (1.75 in), this gives an endpoint resolution of 1.29×10^{-5} m (5.1×10^{-4} in).

The inertia for joint 1, the macro axis, is 1.16 kg. The inertia of joint 2, the micro, is .006 kg, and the inertia for joint 3, the master, is 1.53 kg. These values were found by simulating a mass-spring-damper system with the same spring and damping values as programmed into the real system and adjusting the mass until the simulated and experimental responses coincided. The nominal controlled damping value was zero. Some damping was added to the simulation to compensate for friction in the system.

The friction in each axis was measured using a digital force sensor (Mark 10 Model BG2). The friction in joint 1, the macro, is approximately 0.47 N, the friction in joint 2, the micro, is 0.02 N, and the friction in joint 3, the master, is 0.54 N.

The electronics for the system are straightforward. Torques calculated based on control laws are commanded from the computer (Dell P.C., 166 MHz Pentium Processor) to 12-bit D/A boards (SensAble Devices, Cambridge, MA) which in turn command analog voltages to PWM servo amplifiers, (Model 303, Copley Controls, Westwood, MA). The servo loops ran at approximately 6000 Hz for the data presented in this chapter. Encoder counters are mounted on the same board as the D/A converters.

4.3.2   Individual Joint Performance

To give an idea of the performance of each axis acting individually, we looked at individual position control response for each joint. Each axis was controlled with a simple position-derivative (P.D.) controller:

$$\tau_i = -K_i q_i - B_i \dot{q}_i \qquad (4.17)$$

The P.D. gains used for the responses were:

$$K_1 = 7000 \text{ N/m} \quad B_1 = 55 \text{ Ns/m}$$
$$K_2 = 160 \text{ N/m} \quad B_2 = 1.3 \text{ Ns/m}$$
$$K_3 = 8000 \text{ N/m} \quad B_3 = 65 \text{ Ns/m}$$

These gains, or slight variations of these gains, were used in all the controllers presented in this chapter, in order to implement 50:1 force scaling.

In order to reduce the effects of static friction in the system, we used a friction
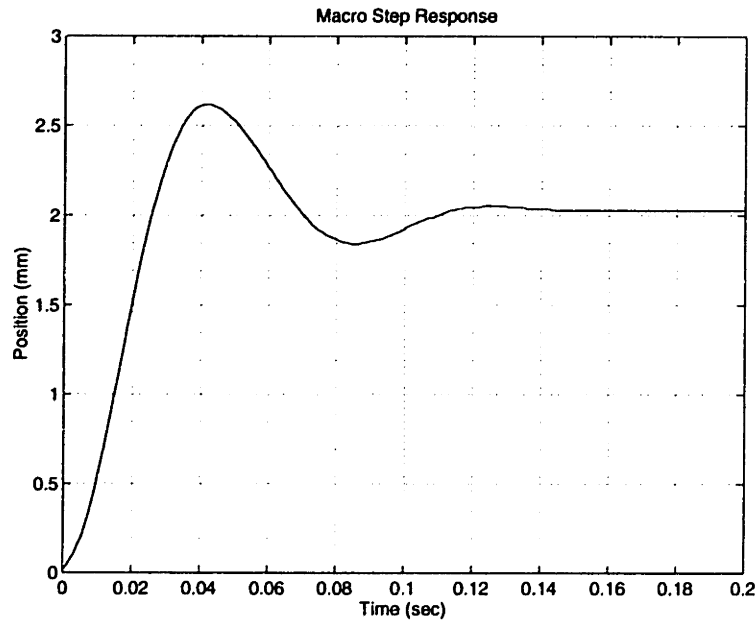
Figure 4-9: Step response for the q_1 macro actuator.

compensation algorithm which feeds forward a constant torque which is slightly less than brush friction. The feed forward torque is increased linearly with velocity until a value of approximately 70% of the measured brush friction in each axis is reached. This corresponds to 0.0072 Nm at the motor. The velocity at which this full feed forward torque is applied was adjusted empirically. If the value is zero, the system will feel "sticky" near zero velocity. If this value is too high, insufficient feedforward torque will be applied.

Step responses for each axis are shown in Figures 4-9, 4-10, and 4-11. Note that the master and macro responses are underdamped, while the micro response is nearly critically damped. This is expected given the gains which were selected. If we ignore for the moment existing natural friction in the system, the damping ratios ζ_i for each axis are given by:

$$\zeta_1 = \frac{B_1}{2\sqrt{K_1 m_1}} = \frac{55 \text{ Ns/m}}{2\sqrt{(7000 \text{ N/m})(1.16 \text{ kg})}} = 0.31 \tag{4.18a}$$

$$\zeta_2 = \frac{B_2}{2\sqrt{K_2 m_2}} = \frac{65 \text{ Ns/m}}{2\sqrt{(8000 \text{ N/m})(1.53 \text{ kg})}} = 0.29 \tag{4.18b}$$

$$\zeta_3 = \frac{B_3}{2\sqrt{K_3 m_3}} = \frac{1.3 \text{ Ns/m}}{2\sqrt{(160 \text{ N/m})(0.006 \text{ kg})}} = 0.66 \tag{4.18c}$$
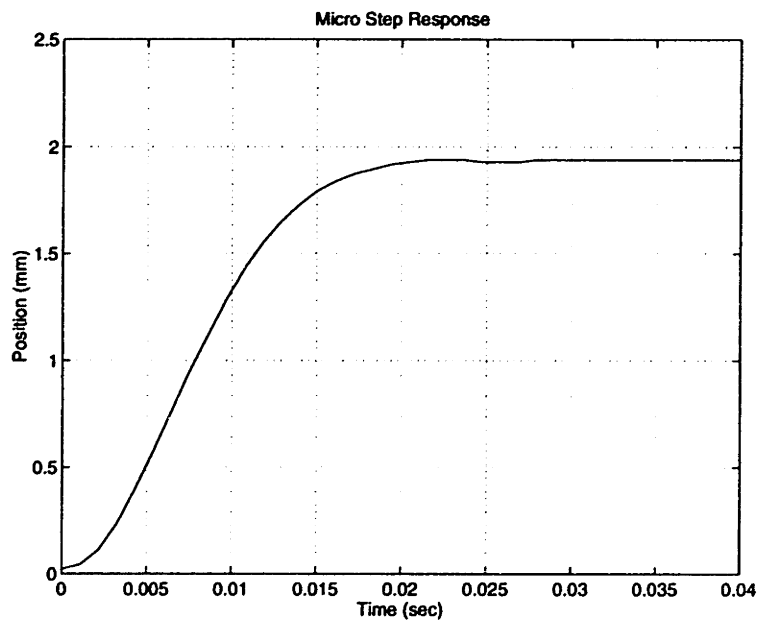
Figure 4-10: Step response for the q_2 micro actuator.
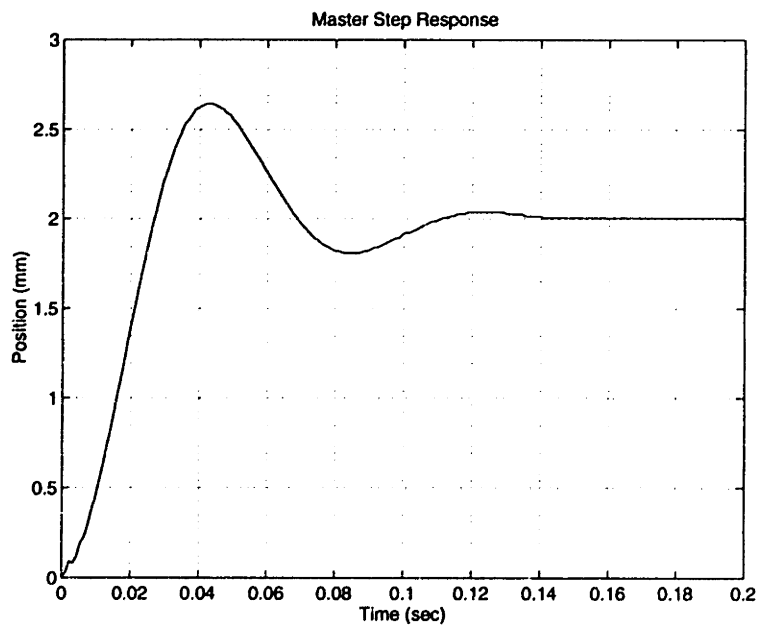
Figure 4-11: Step response for the q_3 master.

In fact, looking at the plots, the damping ratios appear higher which we would expect given that some naturally occuring friction exists in the joints.

These "classic" second order responses show that a cable reduction drive with very little free length of cable (cable which is not wrapped around a drum) can introduce very little additional dynamics even with 10-13 times reduction. This is typically not the case with geared reductions for example. If you look carefully, you can see a small bump at beginning of the master response. This is due to a slight flexibility in the master cable transmission. A similar slight ripple occurs in the other master response plots. Other than that, transmission dynamics are not visible in the plots.

While the macro and micro axes differ by a factor of roughly 200, the positioning bandwidth differs only bv a factor of roughly five. Our primary goal in designing a controller is to take advantage of the large difference in macro and micro inertias, not to compensate for any dramatic difference in their servo bandwidth. Each axis has been designed to be a high quality system with low friction and zero backlash.

4.3.3 Control Methods

Below we describe five different methods for controlling our macro-micro system. In the process, we find out what the relevant benefits and pitfalls of such a system are and demonstrate stable, well-behaved master-slave teleoperation with 50:1 force scaling over a reasonable range of motion.

Two basic tests were done for each controller, a step response and a contact response test. These tests show the speed of response and qualitatively show stability at two extremes of the spectrum, during free space motions and while contacting rigid objects.:

- Step response tests. In these tests, the initial condition for the master and slave are stationary and positioned 2 mm apart. The micro joint q_2 is stationary and positioned at approximately zero. The command is a step in endpoint position such that the desired endpoint positions are identical. The motions of the master q_3, macro q_1 and slave endpoint $q_1 + q_2$ were plotted.

- Contact response tests. In these tests, I moved the master such that the slave moved towards and then contacted a rigid aluminum block. The motions of the master q_3, macro q_1 and slave endpoint $q_1 + q_2$ were plotted.
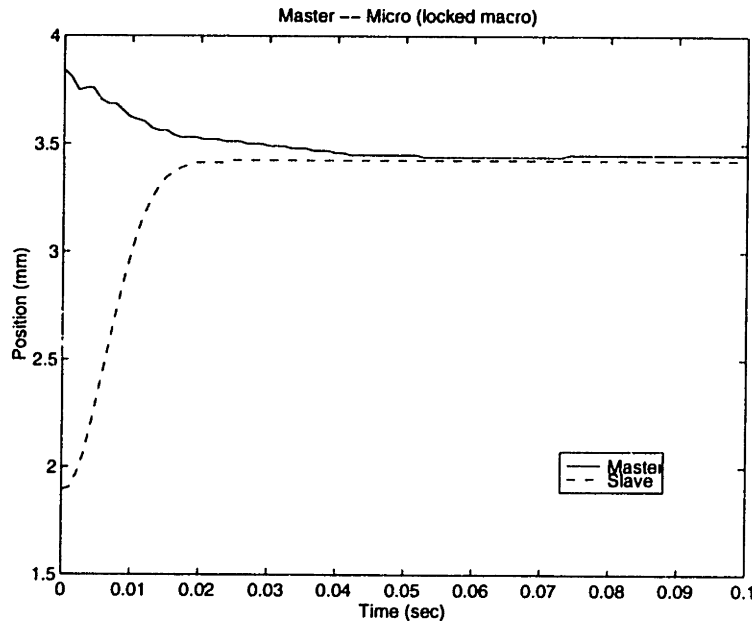
Figure 4-12: Step response for the master and micro axes slaved together using basic teleoperator control.

4.3.3.1 Basic Teleoperator

This is the gold standard by which we compare the other controllers. Here we apply the basic teleoperator control described in Section 4.1.1 to the master and micro actuator alone. The macro actuator is locked in place with clamps. We label the endpoint forces for the master and slave F_m and F_s, and the cartesian stiffness and damping gains as K_m, B_m, K_s, B_s. The controller is given by:

$$F_m = -K_m(q_3 - q_2) - B_m(\dot{q}_3 - \dot{q}_2) \tag{4.19a}$$

$$F_s = K_s(q_3 - q_2) + B_s(\dot{q}_3 - \dot{q}_2) \tag{4.19b}$$

In order to achieve 50:1 force scaling, we set K_m to be 8000 N/m, which is the highest we can reasonably achieve and set $K_s = K_m/50 = 160$ N/m. The damping gains were $B_m = 65$ and $B_s = 1.3$. Because the master and slave have only one degree of freedom each, the joint forces are $\tau_2 = F_s$ and $\tau_3 = F_m$.

The 2 mm step response is shown in Figure 4-12. Because the micro freedom, labelled "Slave" in the figure is so much lighter than the macro freedom, it moves considerably more than the master as they move together to achieve the same endpoint position. Figure 4-13 shows the contact plot for this system. The master is moved by hand and the slave quickly follows. The slave makes contact with an alu-
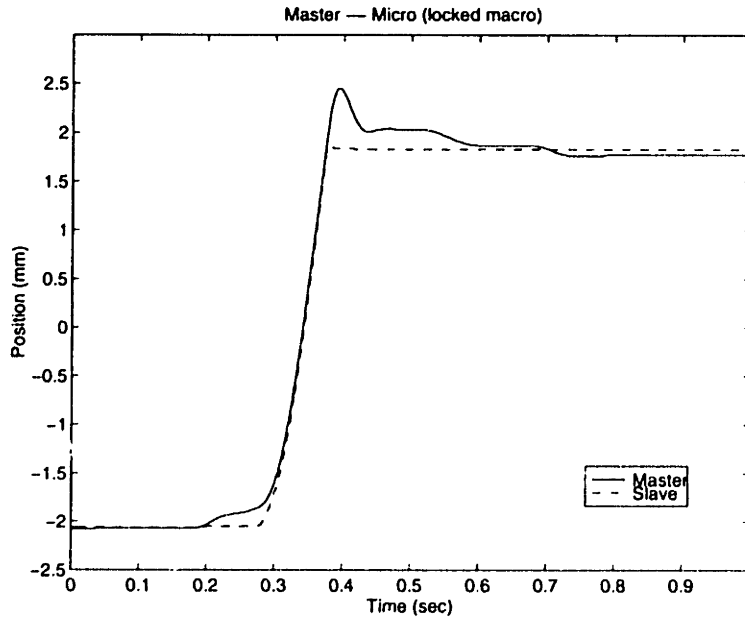
Figure 4-13: Contact response for the master and micro axes slaved together using basic teleoperator control.

minum block and stops abruptly and the contact is well behaved and stable. The master overshoots slightly due to the finite stiffness connection between the master and slave. The force created by the resulting position error however quickly stops the master and its position settles to the slave position value as pressure is released by the user. The commanded output forces which the master applies to the user are 50 times that which the slave applies to the aluminum block. The actual output forces differ by the small amount of friction in the systems and by the forces required to decelerate the very light aluminum micro output link.

The actual feeling which the user experiences is fairly dramatic. Because the position has not been scaled between the master and slave, the effective stiffness of objects in the environment is multiplied by 50 when felt through the master. Contact with the aluminum block is felt sharply and clearly at the master. Another excellent example is poking the slave using soft foam. It is easy to shove the master around (and the user holding on to it) with a piece of very soft foam or kleenex tissue. Trying to push a standard eraser across the table with the slave from the master side of the connection feels like pushing a desktop telephone.

The problem with this system is that the range of motion of the micro actuator is limited in this case to only a few centimeters. The price of having a very light, low friction slave is that it must also be small. As a result, motions of the master

are limited to a small portion of it's workspace. The next four controllers represent different ways to use the macro actuator to increase the range of motion of the entire slave manipulator.

4.3.3.2 Jacobian Transpose Controller

This controller is passive in the same sense as the previous controller and is probably the most straightforward method of cartesian control of a multiple-degree-of-freedom slave manipulator. In this case, a cartesian error is calculated between the master and slave endpoints and is multiplied by a cartesian P.D. to produce desired endpoint forces. Also, because our master has one-degree-of-freedom (it does not include orientation), we set the desired slave endpoint orientation to zero and apply an additional P.D. to maintain this orientation. These endpoint forces will then be mapped to the joint torques via the transposed jacobians for each manipulator. The endpoint forces are given by:

$$F_m = -K_m(q_3 - x_s) - B_m(\dot{q}_3 - \dot{x}_s) \tag{4.20a}$$

$$F_s = K_s(q_3 - x_s) + B_s(\dot{q}_3 - \dot{x}_s) \tag{4.20b}$$

$$F_{q2} = -K_{orient}q_2 - B_{orient}\dot{q}_2 \tag{4.20c}$$

where:

$$x_s = q_1 + q_2 \tag{4.21}$$

Then our Jacobian is given by:

$$\begin{pmatrix} \dot{x}_s \\ \dot{q}_2 \end{pmatrix} = \begin{pmatrix} 1 & 1 \\ 0 & 1 \end{pmatrix} \begin{pmatrix} \dot{q}_1 \\ \dot{q}_2 \end{pmatrix} = J\dot{\mathbf{q}} \tag{4.22}$$

The joint torques are found using the transposed Jacobian:

$$\tau_3 = F_m \tag{4.23a}$$

$$\begin{pmatrix} \tau_1 \\ \tau_2 \end{pmatrix} = \begin{pmatrix} 1 & 0 \\ 1 & 1 \end{pmatrix} \begin{pmatrix} F_s \\ F_{q2} \end{pmatrix} = J^T \begin{pmatrix} F_s \\ F_{q2} \end{pmatrix} \tag{4.23b}$$

We find the controller viewed at the joint level is:

$$\tau_1 = K_s(q_3 - q_1 - q_2) + B_s(\dot{q}_3 - \dot{q}_1 - \dot{q}_2) \tag{4.24a}$$

$$\tau_2 = K_s(q_3 - q_1 - q_2) + B_s(\dot{q}_3 - \dot{q}_1 - \dot{q}_2) - K_{orient}q_2 - B_{orient}\dot{q}_2 \tag{4.24b}$$

$$\tau_3 = -K_m(q_3 - q_1 - q_2) - B_m(\dot{q}_3 - \dot{q}_1 - \dot{q}_2) \tag{4.24c}$$
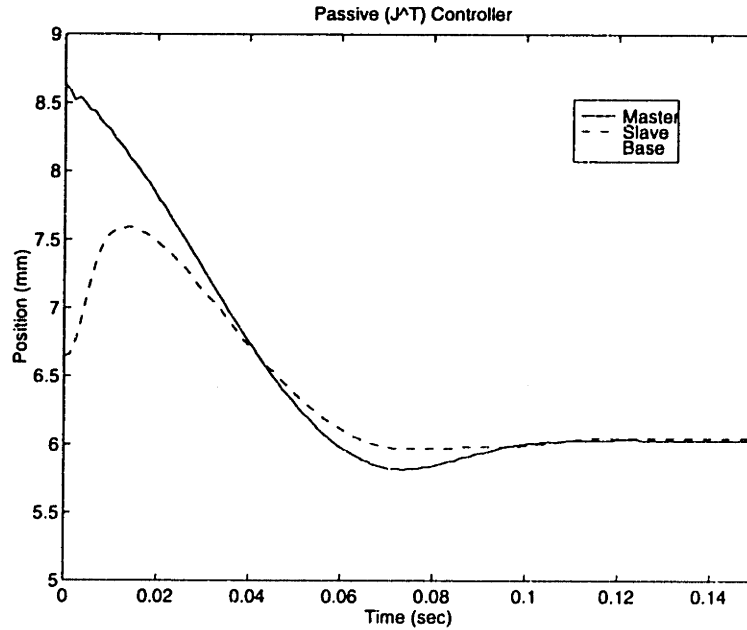
Figure 4-14: Step response for the master and slave using the Jacobian Transpose control.

The individual joint gains used were:

$$K_s = 160 \text{ N/m} \qquad B_s = 1.3 \text{ Ns/m}$$
$$K_m = 8000 \text{ N/m} \qquad B_m = 65 \text{ Ns/m}$$
$$K_{orient} = 50 \text{ N/m} \qquad B_{orient} = 0.5 \text{ Ns/m}$$

The problem with this controller is the gains which are applied to the macro axis are simply too small. A gain of 160 N/m is simply too weak to move the macro axis given its inertia and friction. Figure 4-14 shows the 2 mm step response for the system with the Jacobian Transpose controller. Because of the small macro axis gain, it barely moves and all compensation is done by the master and micro axes. The endpoints come together and are also pulled towards the macro position.

When trying to move the system by pushing on the master, the macro axis is again immovable, see Figure 4-15. The master motor reaches its torque limit after deflecting by about 9 mm and contact with the aluminum block is never made. At an 8000 N/m master stiffness, this means about 72 N of force was applied and the macro axis had yet to move.
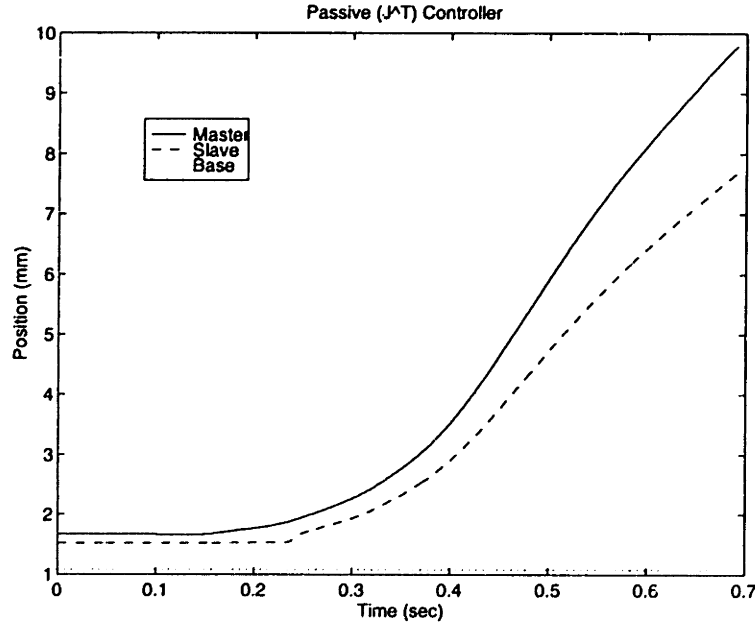
Figure 4-15: Contact response for the master and slave using the Jacobian Transpose control. Contact is never actually made here because the base is essentially immovable and the master hits a torque limit in trying to move it.

4.3.3.3 Jacobian Inverse Controller

In this section, we describe a controller which suppresses the inertia of the macro actuator. We will show in Section 4.3.3.4 that this is in fact standard Jacobian Inverse manipulator control, which reduces to the controller presented below when applied to our system.

The controller is given as follows. First we simply command the master to follow the position of the tip of the slave manipulator:

$$\tau_3 = -K_3(q_3 - x_s) - B_3(\dot{q}_3 - \dot{x}_s) \tag{4.25}$$

where

$$x_s = q_1 + q_2 \tag{4.26}$$

Next we command the macro to follow the position of the master without regards to the micro position:

$$\tau_1 = -K_1(q_1 - q_3) - B_1(\dot{q}_1 - \dot{q}_3) \tag{4.27}$$

Finally, we command the micro actuator to remain at zero:

$$\tau_2 = -K_2 q_2 - B_2 \dot{q}_2 \qquad (4.28)$$

The gains are then tuned to provide as stiff a master and macro as possible and then the micro gains are tuned such that the total endpoint stiffness of the slave is 50 times less than that of the master in order to provide 50:1 scaled force reflection. The gains which provide this are:

$$
\begin{array}{ll}
K_1 = 7000 \text{ N/m} & B_1 = 55 \text{ Ns/m} \\
K_2 = 163.74 \text{ N/m} & B_2 = 1.331 \text{ Ns/m} \\
K_3 = 8000 \text{ N/m} & B_3 = 65 \text{ Ns/m}
\end{array}
$$

The macro and micro stiffnesses form springs in series, so that:

$$(163.74 \times 7000)/(7000 + 163.74) = 160 \text{ N/m}$$

It is important to note that the micro axis is decoupled from the macro axis. Regardless of the position of the master or macro axes, the micro axis simply tries to remain at its zero position.

Figure 4-16 shows the 2 mm step response for this controller. The master and macro respond to each other and come together in straightforward second order responses. Since the inertia and gains of these axes are similar they essentially mirror each others motions. The micro axis barely moves during the motion. The response appears well behaved and stable. Figure 4-17 shows a contact response plot for the Jacobian Inverse controller. Initially the master and slave are moving together towards an aluminum block. The slave hits the block and its tip position comes immediately to rest. The master actuator overshoots the slave tip position due to its finite servo stiffness, but quickly comes to rest. The macro (base) comes to rest at the position of the master. The roughly 0.25 mm offset between the master and slave represents a constant force being applied by the slave against the aluminum block and 50 times that force being applied to the user. The difference in the curves labeled Slave and Base (Macro) represent the relative motion between the micro and macro motions. While the micro stays in contact with the block, it deflects relative to the macro actuator.

This controller is well-behaved during contact and provides crisp feeling scaled force reflection. During freespace motions and during contact, the feel is very similar to that of the basic teleoperator of Section 4.3.3.1. It has the important advantage however that the range of motion is equal to that of the macro actuator.

Let us consider the inertia which the user feels when the system is moved through
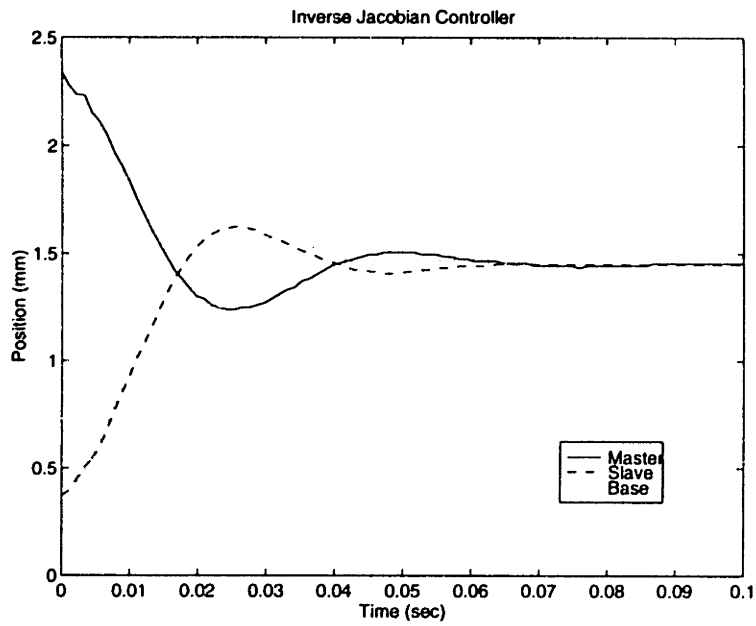
Figure 4-16: Step response for the master and slave using the Jacobian Inverse control.
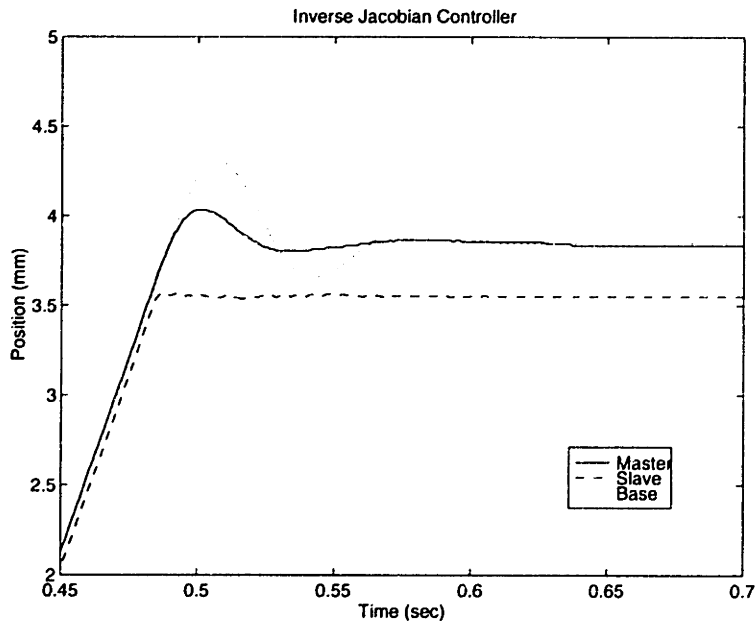
Figure 4-17: Step response for the master and slave using the Jacobian Inverse control.

freespace. If we look and equations 4.25 and 4.27 and consider that in freespace motion, there is no disturbance applied to q_2, then $q_2 = 0$. These equations are then identical to those for the basic teleoperator, 4.19 in Section 4.3.3.1, with q_1 replacing q_2. However, the gain scale is 8000/7000 so that the user feels the inertia of the slave macro freedom multiplied by 8/7. If we could increase the gain of the macro freedom further, the macro freedom would feel lighter. So using this macro-micro approach, while moving through freespace, the user feels the inertia of the master, 1.53 kg, plus 8/7 times the inertia of the macro base, or 1.33 kg. If our slave had consisted of only the macro base and we had implemented 50:1 force scaling, we would have felt a slave inertia of 50 times its actual inertia, or 58.7 kg. So the control effectively suppresses the inertia of the base by 58.7/1.33 = 44 times.

4.3.3.4   Extension to Higher Degrees of Freedom

The Jacobian Inverse controller discussed earlier can be extended to higher degrees of freedom. The general equations are given below.

In Jacobian Inverse control for a single manipulator, we calculate a desired velocity $\dot{\mathbf{x}}_d$ and a desired incremental tip motion $\tilde{\mathbf{x}}$ which will maintain our desired manipulator trajectory. We can combine these into a reference velocity $\dot{\mathbf{x}}_r$ using a factor of λ which represents the bandwidth of the trajectory command and should be selected to be within our positioning servo bandwidth:

$$\dot{\mathbf{x}}_r = \dot{\mathbf{x}}_d - \lambda\tilde{\mathbf{x}} \tag{4.29}$$

where

$$\tilde{\mathbf{x}} = \mathbf{x} - \mathbf{x}_d \tag{4.30}$$

Note that if the cartesian position is lagging the desired cartesian position, $\dot{\mathbf{x}}_r$ increases and if the cartesian position is leading the desired cartesian position, $\dot{\mathbf{x}}_r$ decreases. Thus position feedback is implicitly included in $\dot{\mathbf{x}}_r$. Then we convert our cartesian reference velocity into a desired joint velocity:

$$\dot{\mathbf{q}}_r = J^{-1}\dot{\mathbf{x}}_r = J^{-1}(\dot{\mathbf{x}}_d - \lambda\tilde{\mathbf{x}}) \tag{4.31}$$

Then we apply the following controller:

$$\tau = -B(\dot{\mathbf{q}} - \dot{\mathbf{q}}_r) \tag{4.32}$$

which is effectively a joint space P.D. controller with velocity gain B and position gain λB.

To show that these equations reduce to those given earlier for our two-degree-of-freedom macro-micro slave manipulator, let $\mathbf{x}$ represent the cartesian output vector, let x_s represent the output cartesian position and let θ represent the orientation of the output link. Then $\mathbf{x} = [x_s \ \theta]^T$. Let $\mathbf{q} = [q_1 \ q_2]^T$ represent a vector of joint positions, then:

$$\dot{\mathbf{x}} = J\dot{\mathbf{q}} = \begin{pmatrix} \dot{x}_s \\ \dot{\theta} \end{pmatrix} = \begin{pmatrix} 1 & 1 \\ 0 & 1/l_2 \end{pmatrix} \begin{pmatrix} \dot{q}_1 \\ \dot{q}_2 \end{pmatrix} \tag{4.33}$$

where J is the manipulator Jacobian. Converting our cartesian reference velocity into a joint reference velocity we have:

$$\dot{\mathbf{q}}_r = J^{-1}\dot{\mathbf{x}}_r = J^{-1}(\dot{\mathbf{x}}_d - \lambda\tilde{\mathbf{x}}) = \begin{pmatrix} 1 & -l_2 \\ 0 & l_2 \end{pmatrix} \begin{pmatrix} \dot{x}_{sd} - \lambda\tilde{x}_s \\ \dot{\theta}_d - \lambda\tilde{\theta} \end{pmatrix} \tag{4.34}$$

We may substitute:

$$x_{sd} = q_3 \tag{4.35}$$
$$\tilde{x}_s = q_1 + q_2 - q_3 \tag{4.36}$$
$$\theta = q_2/l_2 \tag{4.37}$$

to get:

$$\dot{\mathbf{q}}_r = \begin{pmatrix} \dot{q}_3 - \lambda q_1 + \lambda q_3 \\ -\lambda q_2 \end{pmatrix} \tag{4.38}$$

Our slave controller is given by:

$$\tau = -B(\dot{\mathbf{q}} - \dot{\mathbf{q}}_r) \tag{4.39}$$
$$\tau_1 = -B(\dot{q}_1 - \dot{q}_3) - B\lambda(q_1 - q_3) \tag{4.40}$$
$$\tau_2 = -B\dot{q}_2 - \lambda B q_2 \tag{4.41}$$

The master has only one degree of freedom, so its controller is straightforward. Its desired position is simply the slave tip position so that its controller is given by:

$$\tau_3 = -K_3(q_3 - q_1 - q_2) - B_3(\dot{q}_3 - \dot{q}_1 - \dot{q}_2) \tag{4.42}$$

If we compare these equations to Equations 4.25, 4.27, and 4.28, we see that they are identical if we substitute $K_1 = \lambda B, K_2 = \lambda B, B_1 = B$, and $B_2 = B$. That is, we would prefer to tune the individual gains separately in order to tailor them to our hardware. In reality the λ and gains required for each axis will be different due to differences in inertia, encoder resolution and friction. Low inertia axes naturally require lower gains than high inertia axes. This can be taken advantage of to achieve

force scaling. Force scaling is implemented by:

1. Designing the master and micro inertias in a ratio similar to the desired force scaling gains.

2. Tuning the gains for good position response.

3. Retuning the gains to achieve our desired force scale factor. If bandwidth limitations were uniform across all axes, then inertia would be the only factor affecting stiffness gains, and our gains would be in the ratio of our force scale factor. However in the presence of other factors such as encoder resolution, we must retune.

4.3.3.5   Modified Jacobian Inverse Controller

This method might be thought of as "traditional macro-micro control" because it was originally developed to increase response times of a slow and/or flexible industrial manipulator by adding a small, high bandwidth micro manipulator to its end. The idea, which was used by (Sharon et al., 1993) for a single manipulator, is to command the micro actuator to null error between the desired slave endpoint position and the actual slave endpoint position. If the micro actuator has a faster servo bandwidth than the macro actuator, then it will tend to "jump out ahead" of the macro actuator and consequently decrease position response times. Its effect on a teleoperator system is discussed below.

The controller is given as follows. As before, the master desired position is that of the slave tip:

$$\tau_3 = -K_3(q_3 - q_1 - q_2) - B_3(\dot{q}_3 - \dot{q}_1 - \dot{q}_2) \qquad (4.43)$$

The macro desired position is equal to that of the master so that:

$$\tau_1 = -K_1(q_1 - q_3) - B_1(\dot{q}_1 - \dot{q}_3) \qquad (4.44)$$

Now the micro position is not servoed to zero, but rather directly to the master position:

$$\tau_2 = -K_2(q_2 - q_3 + q_1) - B_2(\dot{q}_2 - \dot{q}_3 + \dot{q}_1) \qquad (4.45)$$

This is what gives the "jump out ahead" behavior to the micro axis.

Figure 4-18 shows the 2 mm step response for this controller. The gains used
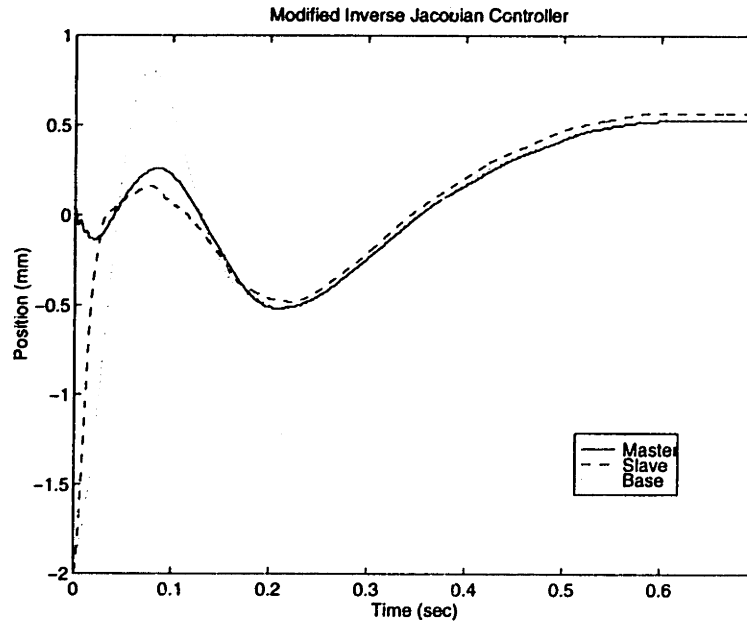
Figure 4-18: Step response for the master and slave using the Modified Jacobian Inverse control.

were:

$$K_1 = 7000 \text{ N/m} \quad B_1 = 55 \text{ Ns/m}$$
$$K_2 = 160 \text{ N/m} \quad B_2 = 1.3 \text{ Ns/m}$$
$$K_3 = 8000 \text{ N/m} \quad B_3 = 65 \text{ Ns/m}$$

The position of the micro is the difference between the curves labeled Slave and Base. The micro initially jumps out ahead of the base (macro) axis. The master does not move a great deal because while the position of the slave tip is negative, its velocity is large and positive. The effects cancel in the master P.D. controller, and as a result, most of the relative motion between the master and slave is caused by the slave which generates substantial momentum. The base overshoots the position of the master while the micro compensates by reversing its direction and tracking the master. The micro effectively locks on to the master position.

However the master is not a fixed target. In fact, it tracks the slave and begins to oscillate with it as they both settle. The result is the overall amount of oscillation is greater due to the added control input caused by the micro actuator. The overall speed of response is roughly 10 times slower than in the previous Jacobian Inverse control case.

The additional oscillation present in the response is more striking in Figure 4-
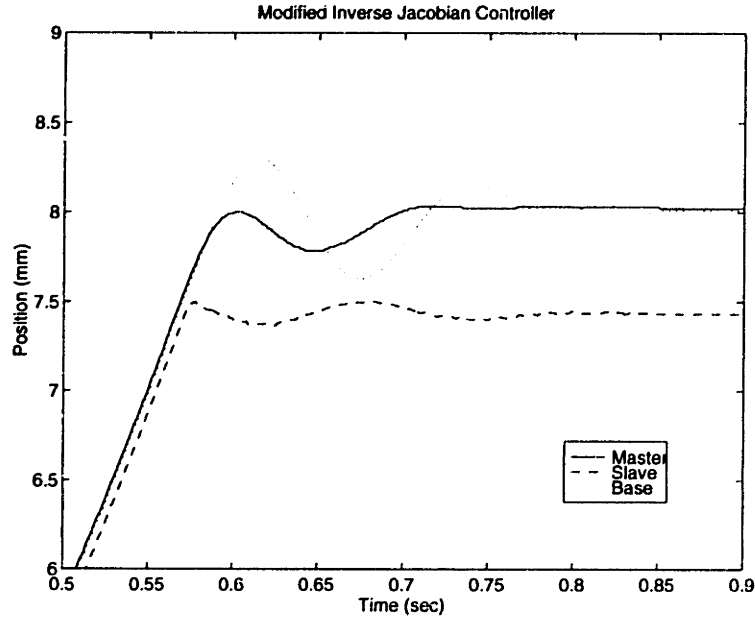
Figure 4-19: Contact response for the master and slave using the Modified Jacobian Inverse control.

19, the Modified Inverse Jacobian contact response plot. The contact in this case is barely stable. The slave tends to bounce on the surface of the aluminum block. This is because the master, which is tracking the slave, tends to overshoot slightly and the micro actuator now wants to track these oscillations. Of course the master tries to track the master oscillations, and the macro tracks the master. Considerable energy is added to the system at this point because the master and macro use much higher gains, hence much larger torques are applied. The fact that the micro axis is directly coupled to the master and macro and reacts to them is critical and causes this behavior. In the previous Jacobian Inverse control, the master and macro track the micro, but the micro does not track them; it simply tries to settle to zero independent of their motions.

We can decrease the overall stiffness gains in order create overdamped responses in order to stabilize the system, but this in turn reduces the overall stiffness of the master-slave connection. The increase in the level of oscillation in the system and the poor contact response make this method of control far less desirable than the previous Inverse Jacobian control.

4.3.3.6 Simulated Force Sensor Controller

A popular method to implement teleoperator force reflection is to use a distal force sensor on the end of the slave manipulator and to feed these forces directly back to the master. The master then tracks the endpoint position of the slave. So it is natural to ask how our system would perform if we were to use the micro actuator simply as a force sensor. In this case, we command the micro actuator to remain at zero:

$$\tau_2 = -K_2 q_2 \tag{4.46}$$

We feed this force back to the master with a 50 times force scaling:

$$\tau_3 = -50\tau_2 \tag{4.47}$$

And we command the macro to track the master:

$$\tau_1 = -K_1(q_1 - q_3) - B_1(\dot{q}_1 - \dot{q}_3) \tag{4.48}$$

The gains were:

$$K_1 = 7000 \text{ N/m} \quad B_1 = 55 \text{ Ns/m}$$
$$K_2 = 163.74 \text{ N/m} \quad B_2 = 1.331 \text{ Ns/m}$$

The 2 mm step response for this system is shown in Figure 4-20. Because there is no contact being made with the micro actuator in this freespace motion, no forces are commanded to the master. The micro also does not move relative to the macro. The base (macro) compensates entirely on its own and eventually reaches the master position in a classic second order response. When contacting a rigid surface, the slave displays a contact instability as shown in Figure 4-21. Because the scaled contact force is fed directly back to the master, the master is forced backwards away from the block. The macro axis tracks this motion and pulls the entire slave away from the aluminum block at which point the force commanded to the master drops to zero. But the user is still pushing the master towards the block, so it re-initiates contact. A violent increase in the amplitude of the oscillations occurs.

This behavior can of course be avoided by reducing gains. But then the same level of force reflection cannot be achieved as with other methods, in particular the Jacobian Inverse method. Another way of looking at this problem is that while the slave is in contact with the aluminum block, a very high position gain exists between the micro position and torques applied to the master. Very small position changes in the micro actuator creates forces which are amplified by the 50:1 force scaling and
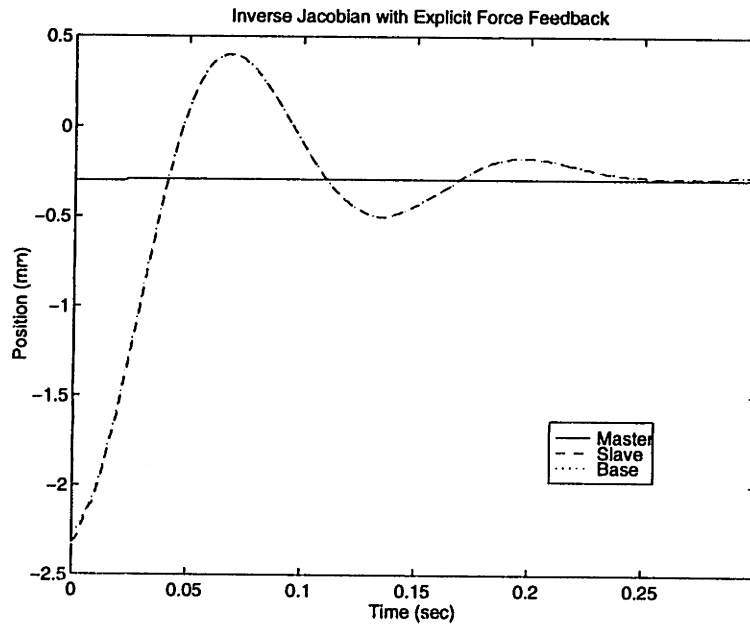
Figure 4-20: Step response for the master and slave using a simulated force sensor controller.
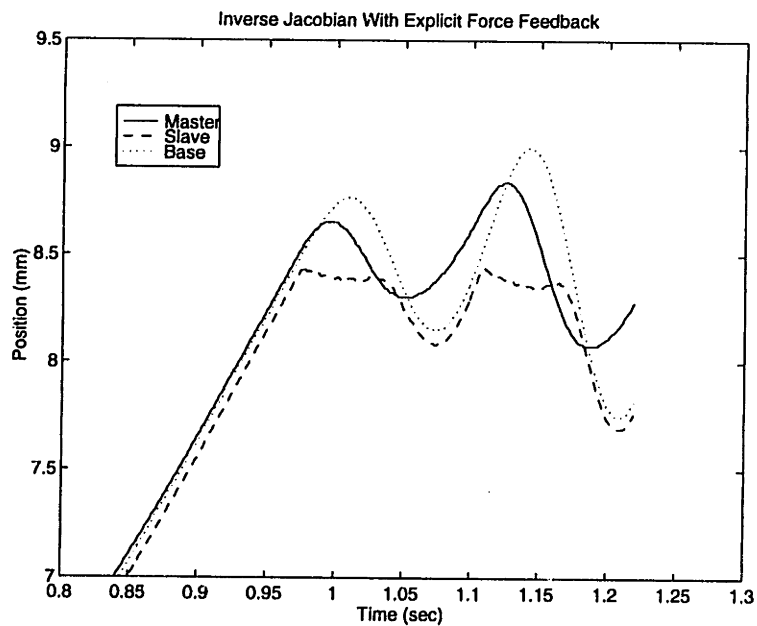
Figure 4-21: Contact response for the master and slave using a simulated force sensor controller. Note the contact instability.

sent to the master. This in turns causes rapid movement of the master which the slave is then forced to track.

4.3.3.7 Friction Instability

There is one other phenomenon which I would like to point out that is common to several of the controllers presented, though in varying degrees. First note that the Inverse Jacobian, Modified Inverse Jacobian and Simulated Force Sensor controllers all use deflections in the micro position to generate force commands to the master axis. Any static friction in the micro actuator will cause a fixed non-zero deflection which is indistinguishable from an actual force. Any of the above controllers will react by commanding torques to the master and macro axes. If these torques overcome the static friction in these axes, the master and macro axes will move, and the system will slowly "walk" until it contacts something and stops. The higher the force scale factor, the more likely that a fixed micro deflection will result in torques which will move the master and macro axes.

Now if the slave tip is placed between two rigid surfaces, an oscillation can develop. If the slave bumps one surface, the micro axis will "flip" through its zero point and get stuck in its friction in the opposite direction. As a result it will move towards the second rigid surface, bump into it, flip back through its zero position, and move towards the first surface. The result is an oscillation which sounds like a clock ticking.

Recall that a joint level friction compensation algorithm was running on all axes during all of the above tests. This effectively lowers the size of the fixed micro deflection. In the case of the Jacobian Inverse controller, this behavior did not develop in our tests with the friction compensation running. However with it off, we could create oscillations between two rigid surfaces like that shown in Figure 4-22. The Modified Inverse Jacobian control would exhibit similar behavior when friction compensation was turned off, Figure 4-23. The Simulated Force Sensor control exhibited this behavior even with friction compensation turned on, as shown in Figure 4-24, and became unstable if friction compensation was turned off, Figure 4-25.

4.3.4 Summary

The idea of using a slave manipulator with macro and micro degrees of freedom which can be used in conjunction to reduce endpoint inertia and improve force reflection is good, but nontrivial to implement. Of the methods that we tried, we found that an Inverse Jacobian type approach yielded the best results. Motions in freespace in fact felt free. The user could feel the inertia of the master, and an inertia due to movement
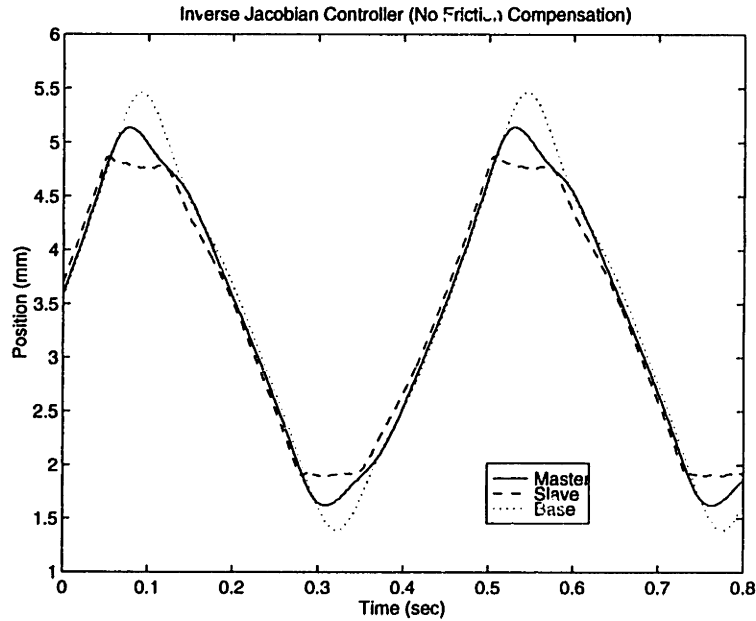
Figure 4-22: A friction induced oscillation using Jacobian Inverse control with friction compensation turned off. The slave oscillates by slowly bouncing between two aluminum blocks.
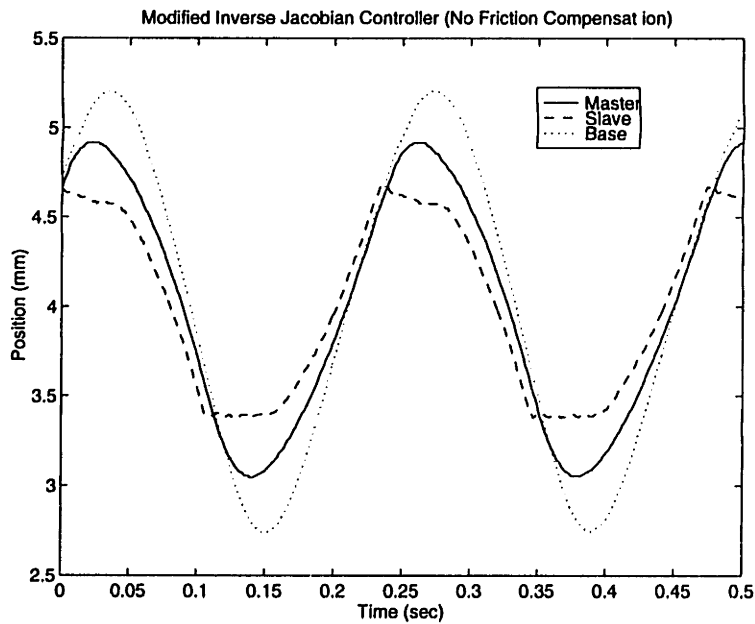
Figure 4-23: A friction induced oscillation using Modified Jacobian Inverse control with friction compensation turned off. The slave oscillates by slowly bouncing between two aluminum blocks.
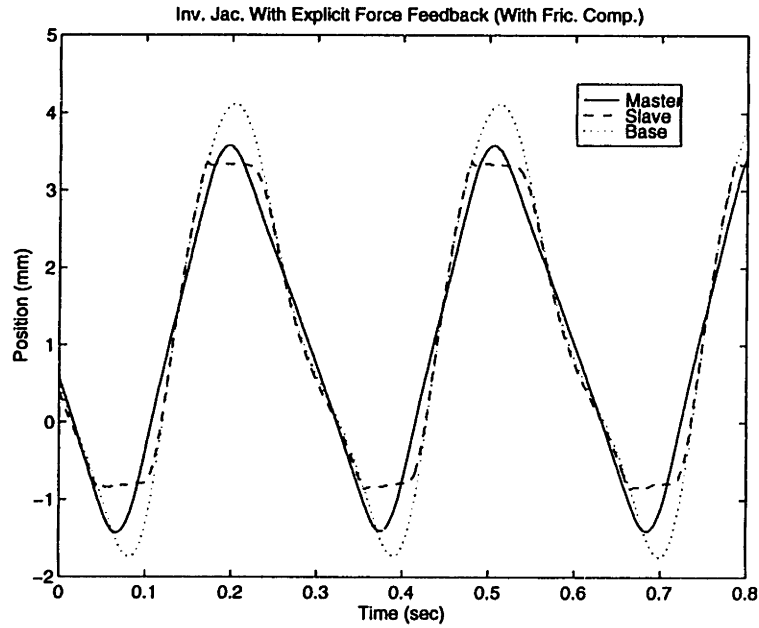
Figure 4-24: A friction induced oscillation using Simulated Force Sensor control with friction compensation turned on. The slave oscillates by slowly bouncing between two aluminum blocks.
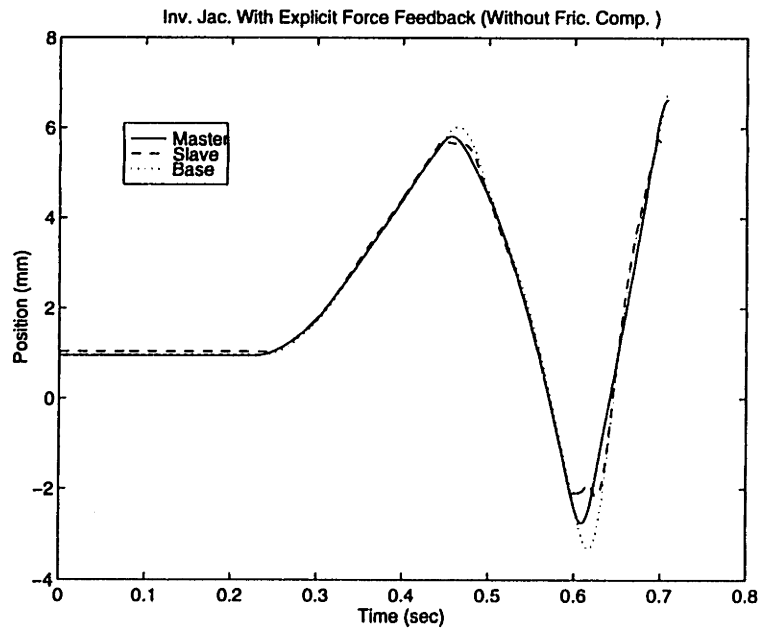
Figure 4-25: A friction induced oscillation using Simulated Force Sensor control with friction compensation turned off. The slave oscillations increase catastrophically.

of the micro axis, but the inertia of the macro axis was essentially hidden. Contacts felt crisp, and remarkably small and soft objects such as erasers and tissue paper could be made to feel heavy and rigid using a force scaling of 50:1. Such behavior existed over the larger workspace of the macro axis.

However friction and inertia in the micro axis were also scaled by a factor of 50. The inertia and friction were not very noticeable using our system, but the absolute values in our system were miniscule by most robot standards. Our friction was dominated by brush friction and was only 0.02 N at the tip of the micro axis. This kind of low friction is not to be expected in a larger manipulator. The level of force reflection and force scaling will be directly limited by the end-effector friction levels which we can achieve when using this approach.

4.4   Implications for Teleoperator Design

Prior to this investigation, I had believed that the limitations imposed by our use of the basic force reflecting teleoperator would prevent us from achieving force reflection without a force sensor. If we were to use only the basic force reflecting teleoperator control, we would conclude that:

- The slave must be very light in order to allow force reflection. Too much inertia will simply overly attenuate force information being conveyed to the user.

- Force scaling where forces are increased to the user would make things even worse. If the slave has a large inertia, such scaling will make it feel even heavier, as we saw in this chapter using the Jacobian Transpose controller.

- Disturbances caused by tissue forces at the incision point would be felt directly by the user.

- The only real option to make the slave feel lighter would be to use a force sensor between the slave and the environment. This has its own set of problems as discussed in Chapter 2 and in this chapter in Section 4.3.3.6. The net effect is that inertia reduction would be limited to low bandwidths in order to maintain stability.

However, in our simple macro-micro testbed, we found that:

- The slave can have a heavy base corresponding to the macro actuator (which will ideally carry all the heavy components like motors) and still achieve good

force reflection. The base can have friction and other disturbances which the user will feel very little of.

- The user will primarily feel the inertia of the end-effector, corresponding to the micro actuator, but this is very low. If forces are scaled up, the effect of this inertia will be correspondingly greater, but if the end-effector can be made sufficiently light, this would not be an issue. In this testbed, the end-effector inertia is very small, that of a small aluminum "T" and the motor rotor inertia.

- Probably the most severe constraint is caused by the fact that the user will feel friction in the end-effector. We will find this constraint severe because due to our desire to miniaturize, this is precisely where friction is difficult to eliminate. In our testbed, the only friction was due to motor brushes and was very small. However, we will find that in the design of a three or four-degree-of-freedom end-effector, minimizing friction becomes a considerable challenge.

- We note that the "right" scaling to have depends on the relative inertias of different components of the system. Since gains can be made higher on higher inertia degrees of freedom, the inertias to some extent dictate the type of scaling possible. Conversely, if we desire a certain type of scaling, the inertias should be designed correspondingly. In the case of the testbed, the master inertia was 200 times larger than that of the micro actuator. The result was that a 50:1 force scaling was achievable and felt quite good.[2]

- We note that this is not meant to be an end all in terms of controller selection, but rather a preliminary study which was required to focus our design efforts. Future work on controllers within the context of our full scale teleoperators will be needed.

We will see that the hard part of the design is the incorporation of a wrist whose primary purpose is to give the added dexterity that we want to allow tasks like suturing, *and* which satisfies the properties of our testbed's one-degree-of-freedom end-effector. If it does however, we should be able to achieve force reflection in a system several orders of magnitude heavier than we previously thought possible. The design of the wrist now becomes doubly important since we give it the responsibility of enabling force reflection.

Up to this point, we have focussed entirely on forces, and not on torques, applied to the end-effector. The reason is that our master, the PHANToM, only allows us

---

[2]We could program a higher force scale factor but the resulting slave stiffness would be unacceptably low. In principle, we could also increase the master stiffness, but limitations in master encoder resolution prevent this.

to feel forces. This is not necessarily a bad thing. We have found that in virtual environments, forces alone can create compelling illusions that the user is touching virtual objects and surfaces, both rigid and deformable. One of the things we will learn is that torque information can be useful for some tasks, but for a first system, this is not at all necessary, even for a surgical teleoperator master.

We conclude this chapter by proposing the following hypothesis, which we will explore as we design and test the two systems described herein, the Silver Falcon and the Black Falcon: We propose that we can use a wrist to achieve orientation degrees of freedom for the system and at the same time allow redundant positional degrees of freedom to enable macro micro force control of a point at the tip of the end-effector.

Chapter 5

The Silver Falcon Teleoperator Slave

This chapter presents our first teleoperator slave, the Silver Falcon. We begin by describing which of our overall goals were satisfied, and which were not. We then proceed with a general description of the design followed by a detailed description of the implementation and the appropriate differential kinematic relationships between motors and joints. Finally, we discuss briefly the master which is used to complete the master-slave system.

5.1 Goals Achieved

Our goal in building the Silver Falcon was to test the feasibility of our ideas for wrist and mechanism design when applied specifically to minimally invasive surgery. The system was built around a novel cable driven wrist and actuator concept which was mounted to a remote center positioning mechanism.[1] We control the system using a modified PHANToM haptic interface. Below is a summary of specifications and goals achieved and not achieved in this design.

- The Silver Falcon allows positioning and orientation of the end effector within

---

[1] At the time of this writing, 3 patents have been filed: Madhani and Salisbury "Force-Reflecting Surgical Instrument and Positioning Mechanism for Performing Minimally Invasive Surgery with Enhanced Dexterity and Sensitivity", Madhani and Salisbury "Wrist Mechanism for Surgical Instrument for Performing Minimally Invasive Surgery with Enhanced Dexterity and Sensitivity", and Madhani and Salisbury "Articulated Surgical Instrument for Performing Minimally Invasive Surgery with Enhanced Dexterity and Sensitivity"

its workspace by using seven degrees of freedom, (six + gripping).

- The system satisfies the incision point constraint by using remote center kinematics. There are no uncontrolled (passive) or redundant degrees of freedom to maintain the incision point constraint.

- The system minimizes friction by using a low friction cable drive design throughout. There are no gears, and no backlash in any of the joints.

- The wrist is designed to allow force reflection in two directions. The backdrive friction in the wrist is 0.30 N, and 0.75 N in each of these two directions measured at the tip of the end effector jaws.

- The wrist can orient ±90 degrees in pitch and yaw (the exact kinematics will described herein). There are two points which are singular at the edges of the wrist workspace.

- Macro-micro control can be achieved in two of three directions, as the wrist provides redundant (micro) motions in only two of three directions.

- The stroke is 7", slightly less than the 8-10" desired.

- The maximum forces achievable at the tip of the Silver Falcon are between 5.4 N (1.2 lbs) and 41 N (9.2 lbs) at the tip of the manipulator depending on the direction of the force and the orientation of the wrist.

- The grip force achievable is 0.48 N (1.0 lb) at the tip of the gripper jaws.

- The system can be operated in one of two counterbalancing modes. Either we can use a spring counterbalance which is designed into the system, or we can actively add gravity compensation terms to the controller and use motor torques which are functions of position.

- The system uses electric motors, which work well within the constraints of an operating room.

- Draping and sterilization were not addressed in this design.

- Safety features such as redundant sensors were not implemented in this design.

- The tool tip (end effector) in this design is fixed and not interchangeable.

- The shaft diameter is 16 mm, somewhat greater than the 10-13 mm desired.
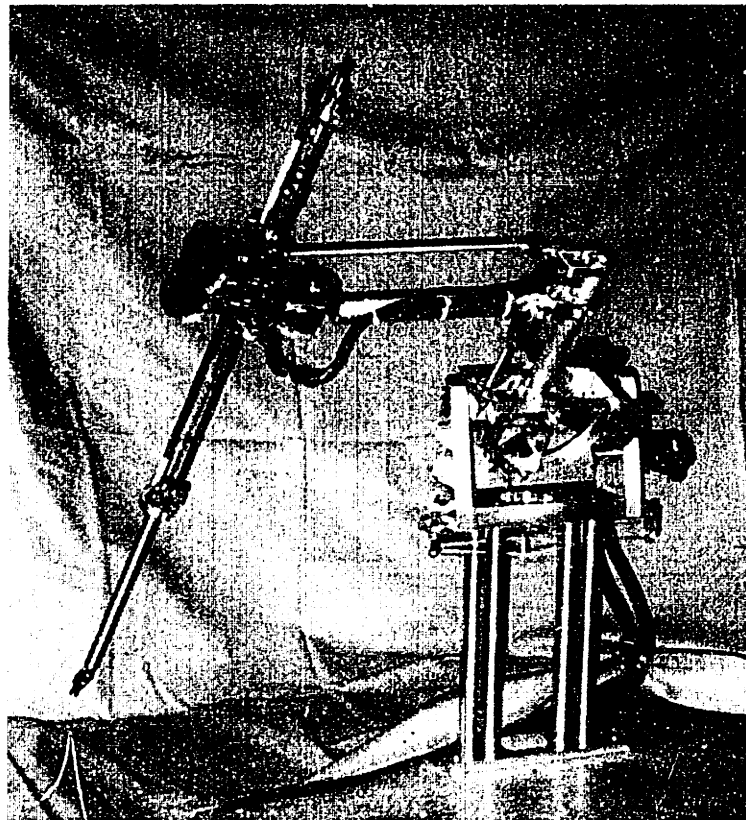
Figure 5-1: The Silver Falcon, our first teleoperator slave prototype for Minimally Invasive Surgery. This system fixed the basic kinematics and layout of the device and allowed initial testing to determine feasibility of the teleoperated MIS concept.

5.2 Silver Falcon Design Description

Figure 5-1 shows a photo of the Silver Falcon. The system has seven degrees of freedom (DOF) which are shown in Figure 5-2.

The Silver Falcon can be broken into two major subsystems which are designed to work together to achieve force reflecting teleoperation. The first is a five-degree-of-freedom wrist unit comprising a wrist, gripper, instrument shaft, and five motors. In the descriptions, I often refer to the wrist unit as the "instrument" and the shaft which passes into the body as the "instrument shaft" in analogy with conventional surgical instruments. The wrist unit is labeled 12 in the figures, and the numbering scheme is consistent throughout all the figures in this chapter. The wrist unit is carried by a second subsystem, a two-degree-of-freedom remote center base positioner, 14, which allows overall pitch/yaw of the wrist unit about the incision point. Figure 5-3 shows
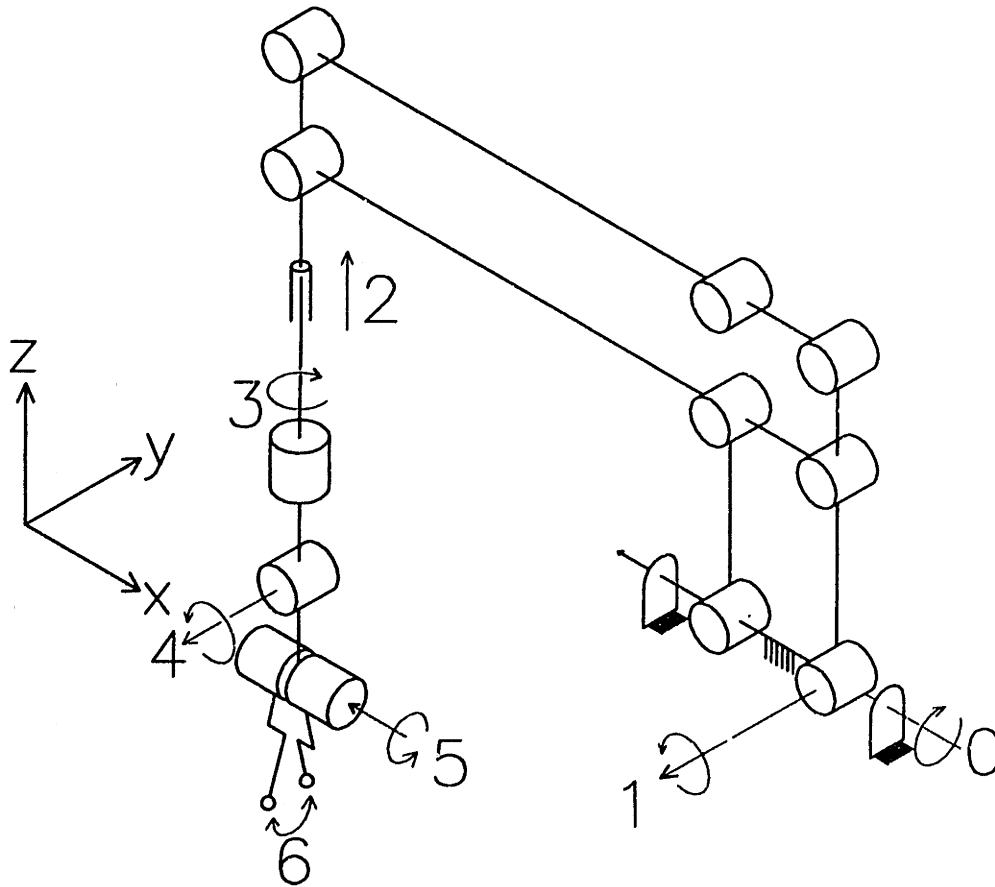
Figure 5-2: Layout of the seven DOF kinematics. The joints are labeled from 0 to 6. Note that joint 5 represents rotation of a point midway between the two fingers about the final yaw axis, and that joint 6 represents gripping motions between the two fingers. Opening of the fingers is defined as positive.

a schematic view of the entire Silver Falcon with components labeled as described above.

Before we begin the detailed description of the base unit and wrist unit, notice that the wrist and fingers are much lower in inertia than is the entire base positioner which must carry the wrist unit including its actuators. As a result of the low end effector inertia, the macro-micro control discussed in Chapter 4 can be applied to the Silver Falcon if we consider the wrist and fingers to be the micro freedoms and the base positioner to be the macro freedoms.

5.2.1 Remote Center Base Positioner

5.2.1.1 Remote Center Kinematics

The purpose of the base positioner is to position the wrist unit with two degrees of freedom (pitch and yaw) inside the human body, without violating the incision point constraint. Combined with a translational degree of freedom which is part of the wrist unit, this provides three-degree-of-freedom (x, y, z) positioning for the wrist and fingers. The kinematics used to do this are shown in Figure 5-4. The parallelogram linkage shown gives the instrument shaft two rotary degrees of freedom about a remote center point.

5.2.1.2 Cable Drives

Figure 5-5 shows the drive system for the base positioner. The drive system must operate smoothly and without backlash, because errors in this drive are amplified by the length of the instrument shaft beyond the remote center. Also vibration or cogging introduced by the drive would excite the entire structure. The cable drives below are backlash free, have low stiction and no cogging. Referring to the figure, two rings, 32 and 42, are fixed to a spindle 57. Motor M0 is fixed to the base, 68, and is coupled to ring 32 via a cable drive as shown in Figure 5-6. This provides yaw motion of the entire remote center structure about axis E. Motor M1 is fixed to the vertical support 56 and is coupled to ring 42 in a similar manner as in the yaw drive. However, now the motor walks around the fixed ring in order to pitch the remote center mechanism forwards and backwards.

One effect of allowing motor M1 to move is that its weight partially counterbalances the entire structure. It acts as a pendulum, in effect, to counteract the weight of the wrist unit and base positioner structure. Unfortunately, in this design the weight of the five wrist unit motors far outweighs that of motor M1, so that a spring
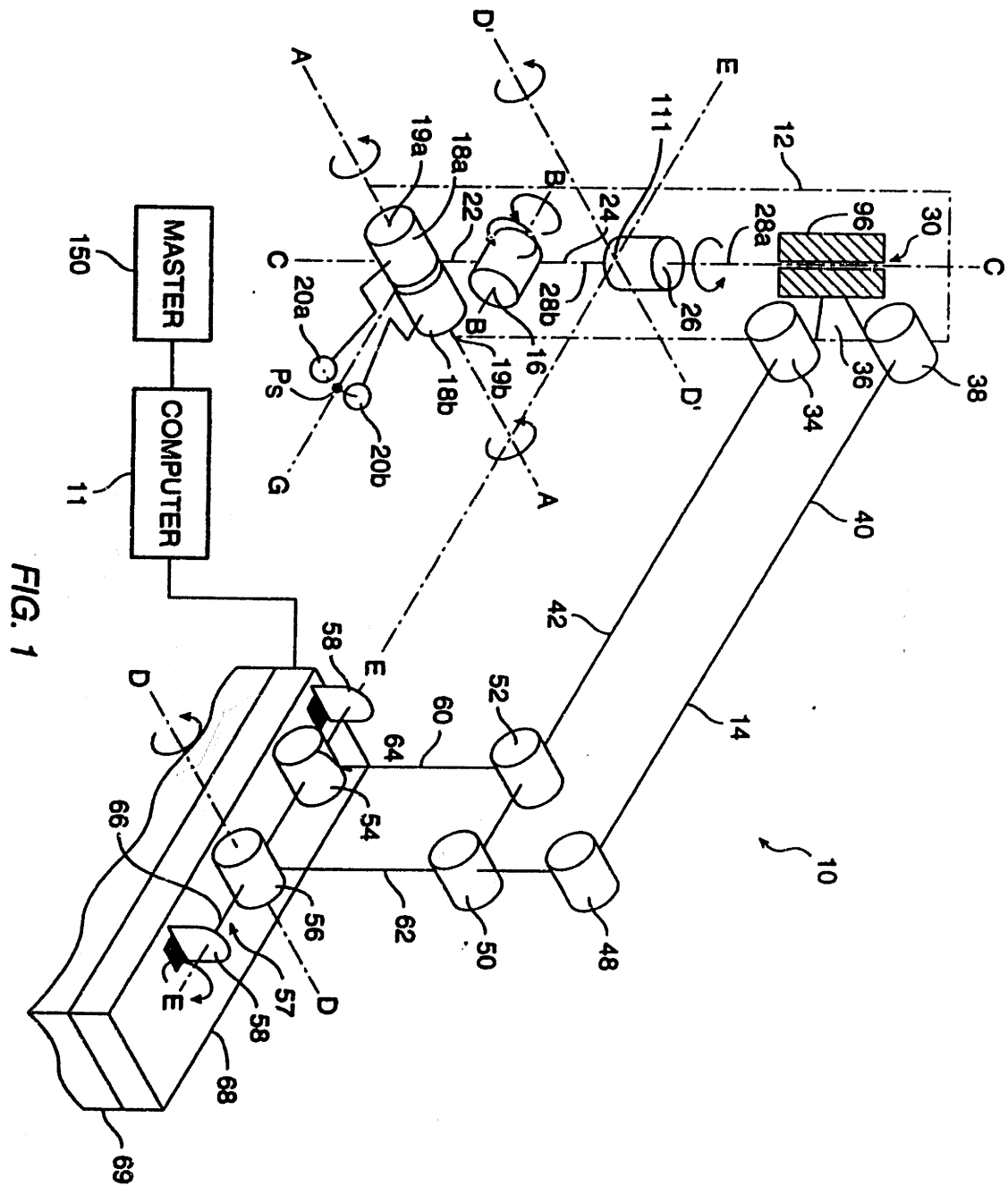
Figure 5-3: Schematic view of the Silver Falcon which shows the numbering scheme used in the descriptions.
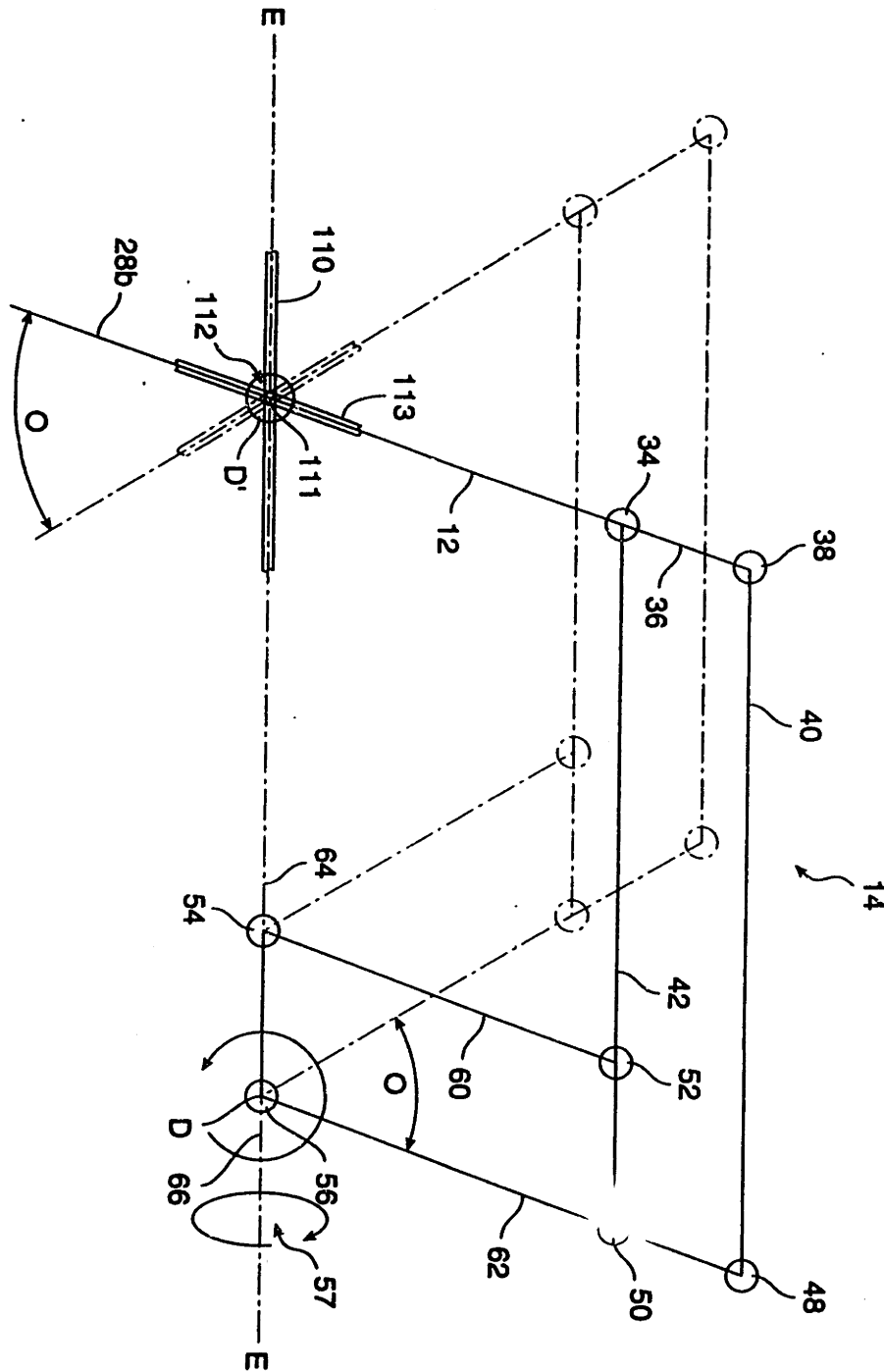
Figure 5-4: The remote center kinematics are formed by two coupled parallelograms. 110 represents the body wall, and 111 is the remote center. The remote center maintains the same relation with points 34 and 38 as does point 56 with points 50 and 48, and need not lie along a line.
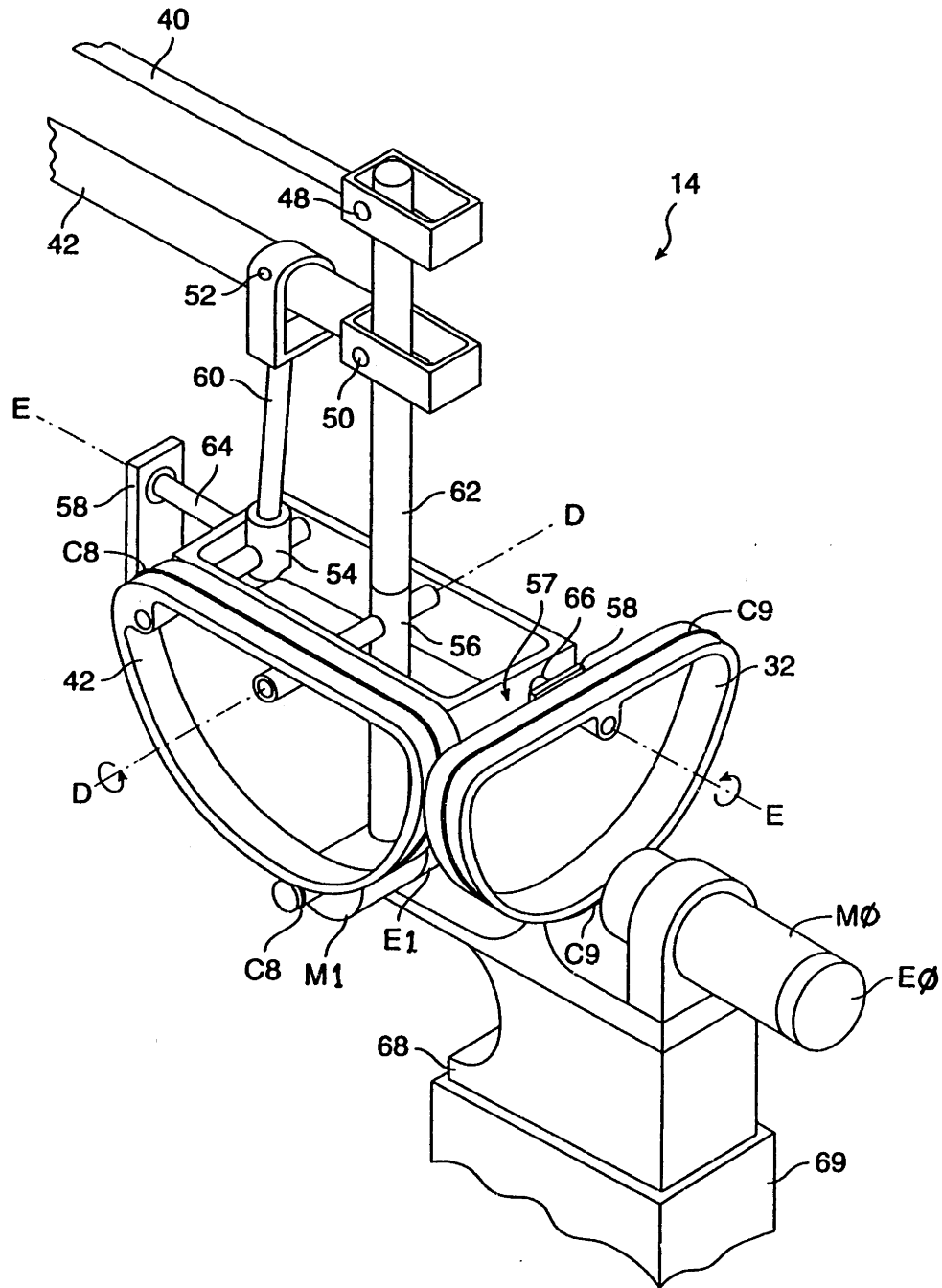
Figure 5-5: The two base positioner axes are both driven by backlash-free cable drives.
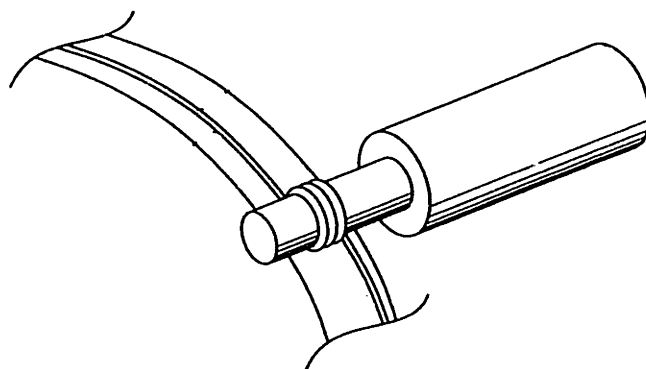
Figure 5-6: Cable drive used to drive a ring

counterbalance was incorporated to compensate for the remaining imbalance.

5.2.1.3   Spring Counter Balance

In practice, weight imbalance can be compensated for using an active gravity compensation, or by using a spring counterbalance. The spring counterbalance which was incorporated into the Silver Falcon is described below.

Figure 5-7 shows a schematic of the counterbalance. A cable is attached to a point on the bottom of member 56 beneath motor 6. This cable passes through a teflon bushing in the base support member 68, around two idler pulleys which are fixed to this base and to a spring whose opposite end is also fixed to the base. Angular motion of the parallelogram linkage about either axis D or axis E draws out cable and causes a deflection in the spring.

Let Δ_0 be the initial spring deflection, and Δ be the deflection above this amount due to motion of the two base axes. Also, let R be the radius at which the cable is attached to the member 56, let θ be the angular deflection of the member 56, let L be the length from this point to the teflon bushing when the θ is equal to zero, let d be this distance when θ is non-zero, and let α equal the angle between the cable and member 56. Then using the laws of cosines and sines:

$$d = \sqrt{(R^2 + (R + L)^2 - 2R(R + L)\cos\theta} \qquad (5.1)$$

$$\sin\alpha = \sin\theta\left(\frac{R + L}{d}\right) \qquad (5.2)$$
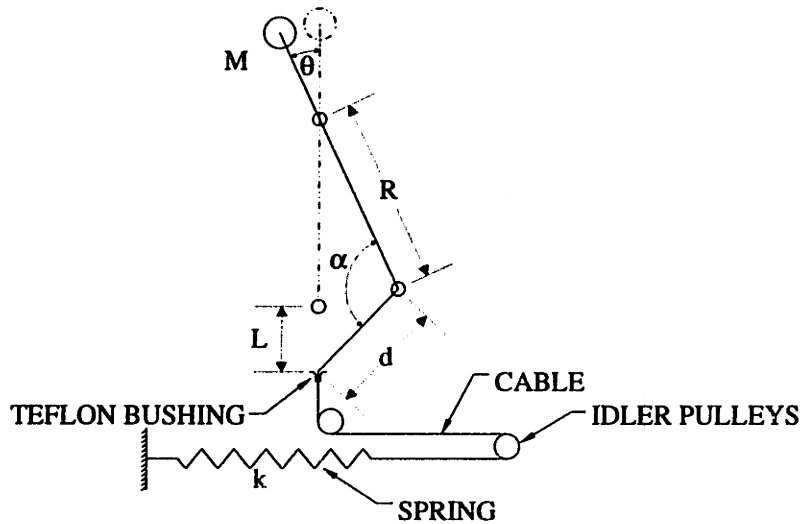
Figure 5-7: The spring counterbalance approximately balances gravity imbalance torques.

$$\tau_{spring} = k(\Delta + \Delta_0)R\sin\alpha \tag{5.3}$$

$$\tag{5.4}$$

The gravity torque is proportional to the sin of the angle of deflection:

$$\tau_{gravity} = K\sin\theta \tag{5.5}$$

We measured the following values:

$$
\begin{aligned}
k &= 111 \text{ N/m} \\
K_{bottom} &= 1.9 \\
K_{top} &= 2.1 \\
L &= 0.025 \text{ m} \\
R &= 0.121 \text{ m} \\
\Delta_0 &= 0.038 \text{ m}
\end{aligned}
$$

where K_{bottom} applies when joint 2 is in its bottom position and K_{top} applies when joint 2 is in its top position.

Figure 5-8 shows all three torques as a function of θ, given in radians. This graph corresponds well with what we feel. The spring is slightly strong for the bottom
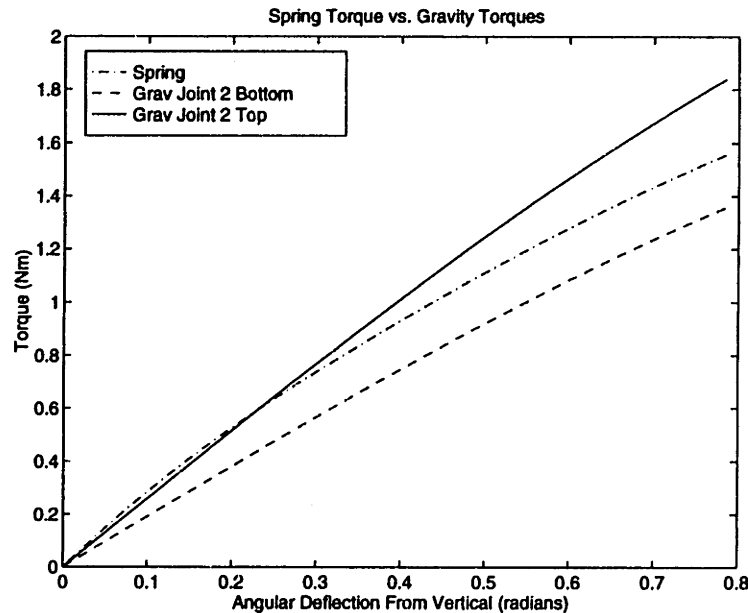
Figure 5-8: The spring counterbalance approximately balances gravity torques due to imbalance. Gravity torques are shown with the joint 2 axis in its bottom and top positions

position of joint 2, but feels better when joint 2 is in its top position. In either case, the error is within the friction in the base actuators so that the system does not move when displaced.

5.2.2 Wrist Unit

We now begin a detailed description of the wrist unit. Recall that the main goals of the wrist unit are: (a) to provide extra degrees of freedom within the body, distal of the incision point, for dexterity and (b) for these freedoms to be low in inertia and to have low friction to allow macro-micro control to be implemented.

Figure 5-9 shows the five-degree-of-freedom wrist unit. The wrist unit, 12, consists of two sections, a distal portion, 28b, which is connected via a rotary joint, 26, to a proximal portion, 28a. The distal portion consists of two fingers and a wrist, mounted on an instrument shaft through which cables pass to actuate the wrist and fingers.

The proximal portion consists of a linear sliding joint, 30, which allows the instrument to pass into and out of the body, and appropriate pulleys to terminate the cables which actuate the wrist and gripper. Five actuators, M2, M3, M4, M5, and
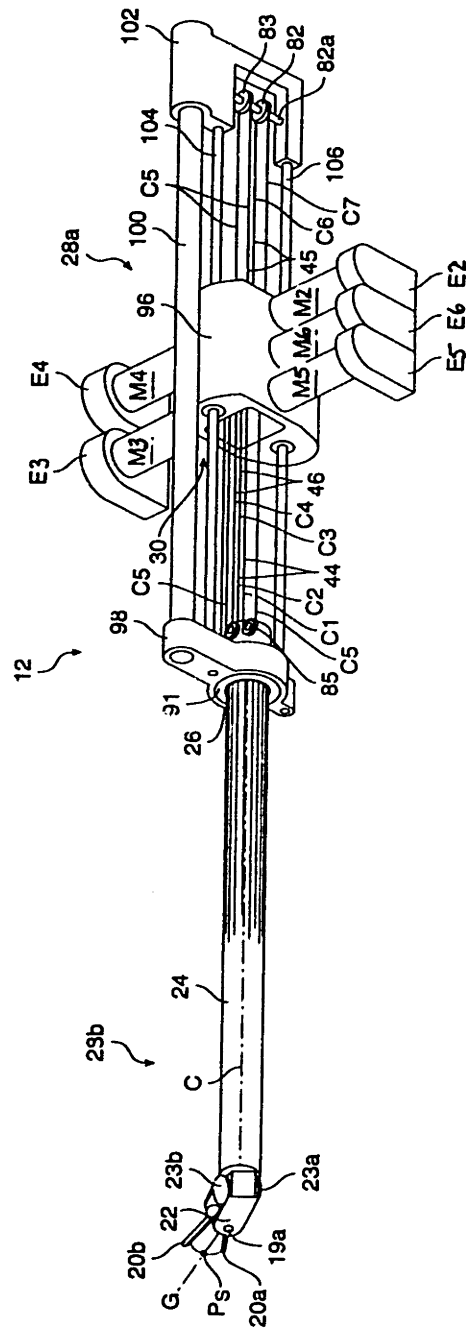
Figure 5-9: The wrist unit for the Silver Falcon has five degrees of freedom: translation in the direction of the instrument shaft, rotation about the instrument shaft, wrist pitch, and individual rotation of each finger.

M6 are used to power and control these freedoms and are rigidly face mounted to a bracket, 96, which in turn mounts to the base positioner.

5.2.2.1   Distal Portion

Lets look more closely at the distal portion, 28b, which includes the wrist, gripper, and instrument shaft. In order to more clearly describe the cabling scheme, I will first describe a simplified version of the wrist and gripper shown in Figure 5-10. We can see from this figure that the wrist is a roll-pitch-yaw wrist where the axis C is the roll, axis B is the pitch, and axis A is the yaw. Both the fingers rotate about axis A as described below. The actual version used in the Silver Falcon is described in Section 5.2.2.4 below. The two versions are in fact similar, though for reasons we will explain, the actual version used has substantially less friction than the version described below. The cabling scheme will be described in Section 5.2.2.3.

Referring to Figure 5-10, the wrist is mounted to a hollow aluminum instrument shaft, 24, mounted along axis C, through which four cables, C1, C2, C3, and C4 pass. The tongue, 24a is mounted to the wrist tube and supports a steel shaft in small ball bearings. The wrist member, 22, pivots on this shaft about axis B which is orthogonal to axis C. Two fingers, 20a and 20b, are attached to driven capstans, 18a and 18b, respectively. Each of these fingers operates independently. The fingers and driven capstans are in fact each machined from single pieces of stainless steel. The wrist member, 22, supports a steel shafts at axis A which in turn supports the driven capstans. Intermediate idler pulleys 70, 72, 74, and 76 lie along the shaft of axis B. Two small ball bearings are mounted in each driven capstan, and one in each idler pulley to minimize friction.

It is important to note that in this wrist the smallest pulleys are the intermediate idler pulleys, 70, 72, 74, and 76 which are roughly half the diameter of the shaft. One of the main objectives in designing a wrist is to keep the diameter of pulleys within the wrist as large as possible, where the upper limit will be the diameter of the instrument shaft. There are two reasons for this. First, steel cable has a minimum bending radius about which it may turn since repeated bending stresses in the cable will cause fatigue and failure in the individual cable fibers. This is well documented in cable catalogs and limits are given for pulley radius for given cable diameters of given constructions. For a small number of cycles, however, actually breaking the cable due to fatigue may not be an issue. The second reason is that there may be substantial friction caused by pulling cable over a small radius. The motion of cable fibers relative to each other increases as the pulley diameter decreases, while at the same time cable tension is distributed over a smaller area. Under load this internal rubbing of the individual cable fibers represents energy loss and manifests itself as
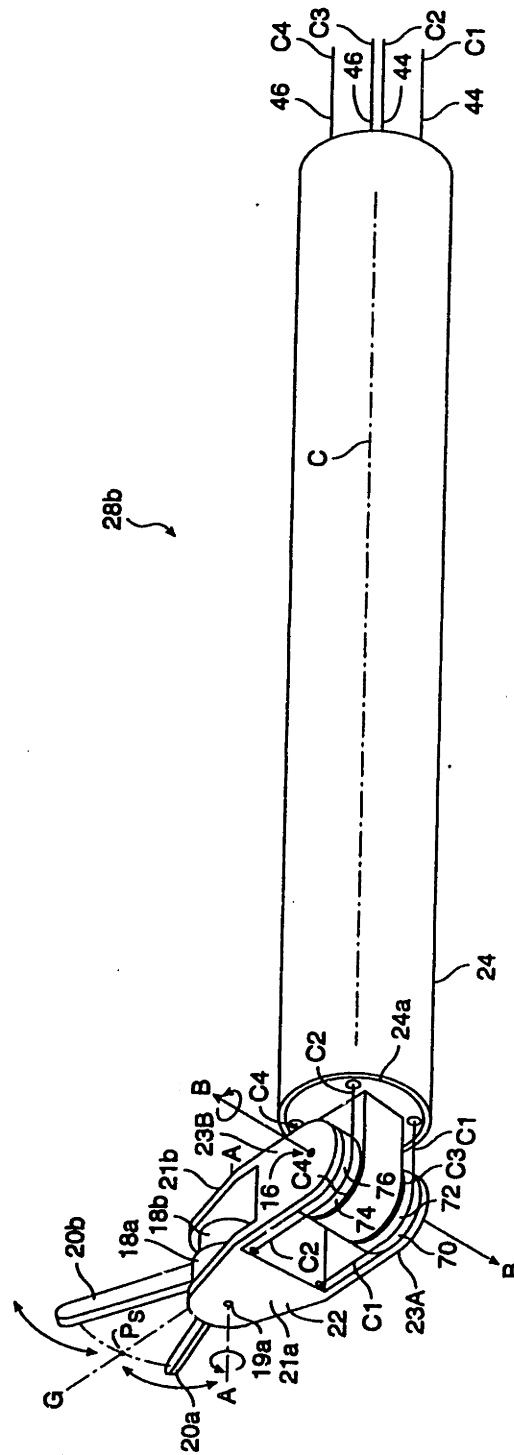
Figure 5-10: This is a simplified version of the silver falcon wrist used to describe the cabling concept.

friction in the overall drive.

We should note that the fingers in this device are serrated and designed to hold needles. However, they could be made as retractors, microforceps, dissecting scissors, blades, etc.

5.2.2.2 Proximal Portion

The proximal portion of the wrist comprises an actuator package which drives the wrist and fingers, rotation of the instrument shaft about its long axis, axis C, and translation along this axis.

The proximal portion of the wrist unit, 28a, includes the aluminum support brackets 98 and 102, which are connected via two 0.250 diameter stainless steel guide shafts. A single 4-point-contact bearing (Kaydon KAA10XL0) is housed in bracket 98 to support the instrument shaft, 24. Such bearings support radial, moment and axial loads and can be used in place of two radial bearings. Four ball bushings (Thomson SUPER-4) are mounted in motor bracket, 96, to form a bearing for the translational degrees of freedom. The brackets 96, 98, and 102 are line bored to assure parallelism of the shafts so that the ball bushings do not bind. The lengths of the shafts were chosen to allow nine inches of travel. The motors M2-M6 are face mounted to the outside of bracket, 96, which is essentially a rectangular hollow tube. Each motor has a threaded drive capstan which engages one cable as shown in Figure 5-11 and forms a friction drive. Two or three wraps is sufficient to prevent the cable from slipping on the capstans since the ratio of high to low tension sides of the cable increases exponentially with wrap angle:

$$\frac{T_1}{T_2} = e^{\mu\theta}$$

where T_1 is the high tension side, T_2 is the low tension side, μ is the coefficient of friction, and θ is the wrap angle. This relation holds for the case of impending slip where the tangential frictional force between the cable and the capstan is proportional to the normal force multiplied by the coefficient of friction μ.

Threading the pinions prevents the cable from rubbing on itself as it travels over the capstans. Also, the threads are semicircular in cross-section so that the cable deforms minimally as it rolls onto and off of the capstans. This is again to minimize friction generated within the cable itself. We use uncoated 7×19 construction .018 diameter stainless steel aircraft cable (SAVA Industries, NJ) in the wrist unit.[2] We

---

[2]I recently saw a sample of very nice 19×7 cable manufactured by Baird Industries in Hohokus,
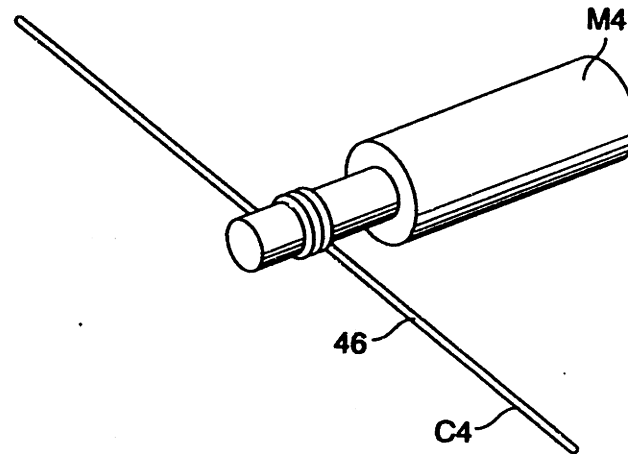
Figure 5-11: Drive layout for single motor and cable.

find that cable coatings add a substantial amount of friction to cable transmissions due to the compression of the coating as it rolls onto pulleys. At the same time, the static sliding friction between the cable and the driving capstans is reduced, which is unsatisfactory for a friction drive system. The motors are Maxon RE025-055-035 brushed d.c. motors with graphite brushes which have zero cogging and very low rotor inertia. The encoders are Hewlett-Packard HEDS-5500 series optical encoders with 1024 lines (4096 counts with quadrature) per revolution mounted on the rear of the motors, which are reliable and inexpensive. Motors M3-M6 actuate the four wrist cables, and motor M2 actuates rotation about the instrument shaft, axis C, as described below.

The cable actuation scheme for rotation about the instrument shaft, axis C, is shown in Figure 5-9, and 5-12. A single cable loop, C5, runs about idler pulleys 83, 84 and 85. Pulley 83 rides in a shaft which is mounted on a fork. This fork is attached via a tensioning mechanism (tensioned using a screw) to bracket 102 to adjust tension in the cable. The driven capstan, 90, is also threaded and fixed directly to the proximal end of the instrument shaft, 24. The pulleys 84 and 85 are fixed via a piece not shown onto the guide shaft, 104. This mechanism is similar functionally to a traditional spline, though in this case, the motor, M2, turns during linear motion of the instrument.

NJ. This cable was drawn through a mandrel and very round and smooth externally. It also used smaller fiber sizes to improve fatigue strength. I also saw a sample of tungsten cable from Baird which has a higher elastic modulus (roughly 2 times) and apparently is more abrasion resistant than stainless. At the time of this writing I have not had a chance to test these cables.
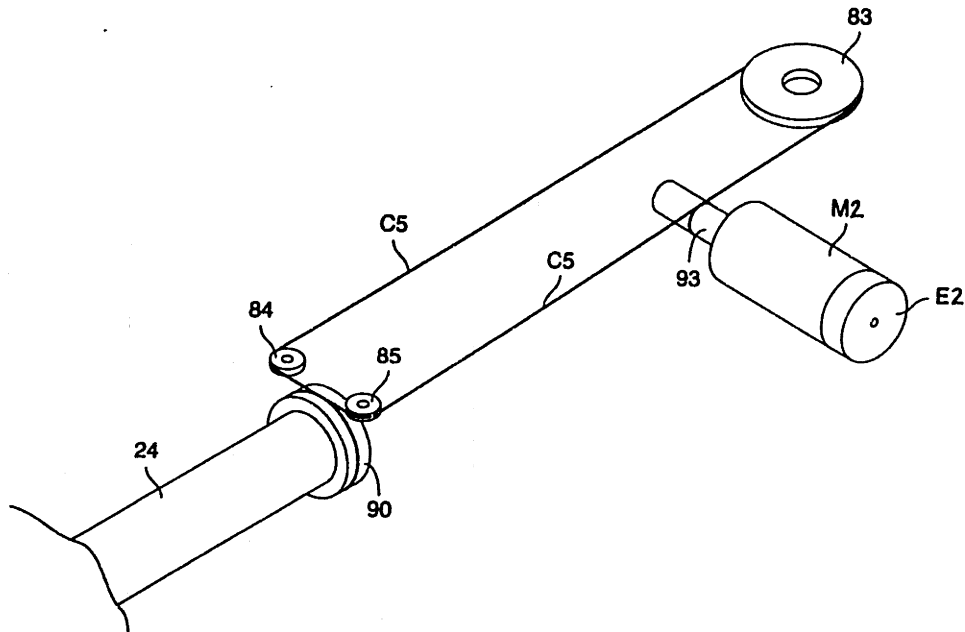
Figure 5-12: Rotation about the instrument shaft 24 is driven by motor M2 and a cable drive which acts in a similar fashion to a traditional spline.

5.2.2.3 Cabling Scheme - Simplified Version

Here we describe the $N + 1$ cabling scheme used in the wrist described above. The cable layout is shown in Figure 5-13. The fingers 20a and 20b, wrist member 22, and the translation of instrument 12 along axis C are driven by cables C1, C2, C3, and C4. Driving N freedoms with $N + 1$ cables is known as an $N + 1$ actuation scheme. This represents the minimum number of tension elements needed to actuate N freedoms. (Salisbury, 1982)

In Figure 5-13, the rotational motion about the instrument shaft, axis C, is omitted in order to more easily show cables C1-C4. Such rotation results only in twisting of the cables C1-C4 between motors M3-M6 and pulleys 70, 72, 74, 76. Due to the length of the instrument shaft, however, the resulting change in length of the cables is slight, and the length of the cables is long, so that the resulting resistance to rotational motion is on the order of bearing friction in joint 26, and substantially less than torque due to brush friction in motor M2. (Discussion of friction values and performance specifications in general may be found in Section 6.1). This twisting of cables C1-C4 does, however, limit rotation of the instrument shaft to ± 180° at which point the cables will rub on each other creating friction and wear.
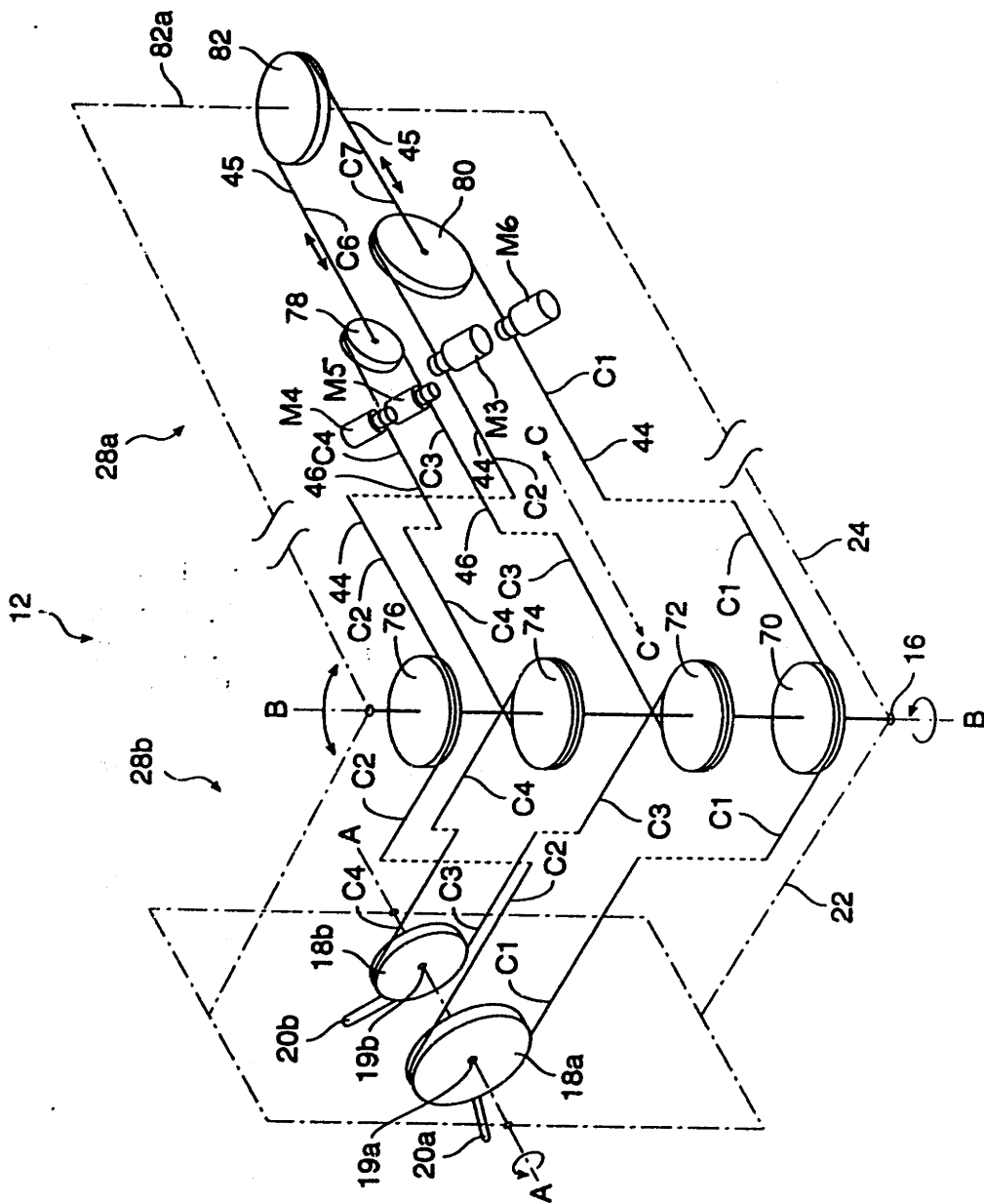
Figure 5-13: $N + 1$ cable actuation scheme for wrist. Four cables, C1 - C4 actuate three axes, each of two fingers about axis A and the wrist about axis B. Each of these four cables is driven with motors M3, M4, M5 and M6, but remain pretensioned using idler pulleys 78, 80, and 82.

As shown in Figure 5-13, cables C1 and C2 form two sides of a continuous cable loop 44. Cable C1 of loop 44 engages a proximal idler pulley 80, the drive shaft of motor M4, intermediate idler pulley 70 and driven capstan 18a. Cable loop 44 returns from driven capstan 18a as cable C2 and engages intermediate idler pulley 76, the drive shaft of motor M5 and proximal idler pulley 80. The cable is fixed under the head of a single #0-80 screw in order to fix it to the capstan. Conventional tin-lead solder can also work if an appropriate flux is used for stainless steel, though this does not allow room for later adjustment without re-cabling, and application of heat may detemper and weaken the cable.

Continuing with the description, cables C3 and C4 form two sides of a continuous loop of cable 46. Cable C3 of cable loop 46 engages proximal idler pulley 78, the drive shaft of motor M3, intermediate idler pulley 72 and driven capstan 18b. Cable loop 46 returns from driven capstan 18b as cable C4 and engages intermediate idler pulley 74, the drive shaft of motor M6 and proximal idler pulley 78.

The proximal idler pulleys 78 and 80 are tensioned by cables C6 and C7 which are fixed kinematically to the center of proximal idler pulleys 78 and 80. The pulleys in fact ride on shafts held in small forks into which the cables terminate. Each pulley uses a single ball bearing. Cables C6 and C7 form two sides of a single cable 45 which engages proximal idler pulley 82. Pulley 82 rides on a shaft held in a fork. This fork is mounted via a tensioning mechanism to the bracket 102 which allows turning of a screw in order to tension the cables. The cables are arranged so that this single tensioning point tensions all cables C1-C7.

The use of proximal idler pulleys 78, 80, and 82 is unusual in $N+1$ cabling schemes. Typically, a separate motor is used for each of the $N + 1$ cables, as suggested in (Burdea and Zhuang, 1991a). Using an extra motor has the advantage that the overall pretension in the system is actively adjustable, which is useful when using a relatively high friction transmission such as cable conduits as in the Salisbury Hand. However the disadvantages are that an extra motor is required, and tension is lost when motor power is turned off. This results in an unraveling of cables at the driving capstan where multiple wraps are used to drive the cable. A pretensioned $N + 1$ arrangement is much more convenient while maintaining the advantage of minimizing cables which must past through the shaft into the wrist and simplifying the wrist design.

In order for all the cables to align properly with all the pulleys, pulleys 78 and 80 were made different diameters. In addition, the mounting locations of motors M2-M6 on bracket 96 were selected carefully to ensure cables C1-C5 align exactly tangentially to the driving capstans on motors M2-M6. Since the cables make several wraps on each driving capstan, and each capstan is threaded accordingly, the cable will walk axially along the capstan as the motor turns. In practice, the axial cable motion
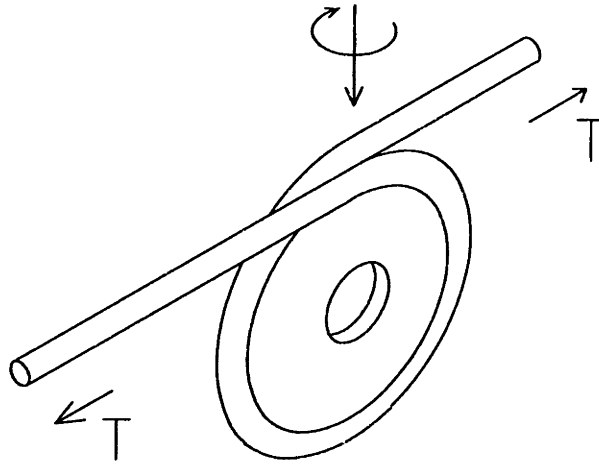
Figure 5-14: The α-wrap causes two problems. (a) the cable rubs on itself, and (b) it causes the pulley to tilt. If T is the tension on the cable, then there is a a torque on the pulley equal to T×d where d is the cable diameter.

is approximately 0.25 inches over the length of travel so that this does not cause a problem.

The movement of the wrist and fingers is caused by coordinated motion of the motors. If motors M4 and M5 act in opposition, finger 20b will rotate. Similarly if motors M3 and M6 act in opposition, finger 20a will rotate. These separate rotations acting against each other provide gripping. If motors M3 and M6 act in the same direction, and motors M4 and M5 act in the same direction, but in opposition to M3 and M6, then the wrist will pitch about axis B. Finally, if all motors M3, M4, M5, and M6 act together, the entire wrist unit will translate along axis C. The exact differential transformations for the wrist described below, which is actually used in the Silver Falcon, will be given in section 5.2.3.

5.2.2.4   Cable Scheme - Non-α Version

The cabling scheme described above has the problem that the cables are forced to cross over themselves and form a slight helix as they make complete wraps around the intermediate idler pulleys, 70, 72, 74, and 76. We call this type of wrap an α-wrap.[3] The helix causes two problems, see Figure 5-14. First, the cable tends to rub on itself which creates extra friction. Second, a torque is placed on the pulley which causes it

---

[3]The author first heard this term from Tom Cooper at Intuitive Surgical, Inc. The term was originally used to describe tape drive mechanisms.

to tilt about an axis orthogonal to the pulley shaft. This is because the cable comes onto the pulley approximately one cable diameter to the side of where it comes off of the pulley. Since the single pulley bearings are not designed to handle moments, tilting the pulley forces the pulley to rub on its neighboring pulley for support creating additional friction. Also the bearing itself is not meant to run tilted creating yet more friction.

As a result, a modified wrist was designed which eliminated α-wraps. A top view of this design is shown in Figure 5-15. The addition of four extra pulleys adds complexity and friction at the pulley bearings and due to bending of the cables on these pulleys. However, the fact that the pulleys are relieved of tilting moments and do not rub on each other for support more than compensates for the addition, resulting in reduced overall friction.

This represents the wrist implementation on the Silver Falcon. The kinematics relationships change slightly, though the change is straightforward. The relationships given in the next section reflect this change.

5.2.3 Differential Kinematics

Here we give the relationship between motor velocities and joint velocities, and similarly motor torques to joint torques for the wrist unit. These relationship are represented as linear transformations as follows:

$$\dot{q} = J_{motor \to joint} \dot{m} \tag{5.6}$$

$$\tau_m = J^T_{motor \to joint} \tau_j \tag{5.7}$$

where $\dot{m}$ are motor velocities, $\dot{q}$ are joint velocities, τ_m are motor torques, τ_j are joint torques, and $J_{motor \to joint}$ is a constant linear transformation.

We define the joints of the Silver Falcon 0-6 (seven joints total) as shown in Figure 5-2. Definitions of the positive direction of rotation are also given in the figure.

The speed ratios are defined as:

R_{LC}	268.04 rad/meter	Motor to cable velocity ratio
R_{SC}	396.75 rad/meter	Motor to cable velocity ratio
R_P	.00417 meter/rad	Cable velocity to wrist pitch velocity ratio
R_{SF}	1.519 rad/rad	Motor to finger ratio
R_{LF}	1.580 rad/rad	Motor to finger ratio
R_R	5.291 rad/rad	Motor to roll axis ratio

Figure 5-15: $N + 1$ Cable actuation scheme for the non-α wrist. This wrist reduces friction by avoiding all α-wraps within the wrist. The wrist structure 116 rotates about the axis labeled 16.

The relationship between motor velocities and joint velocities is:

$$
\begin{pmatrix} \dot{q}_2 \\ \dot{q}_3 \\ \dot{q}_4 \\ \dot{q}_5 \\ \dot{q}_6 \end{pmatrix} = \begin{pmatrix}
0 & \frac{1}{4R_{LC}} & \frac{-1}{4R_{SC}} & \frac{-1}{4R_{SC}} & \frac{1}{4R_{LC}} \\
\frac{-1}{R_R} & \frac{-R_{SC}}{4R_R R_{LC}} & \frac{1}{4R_R} & \frac{1}{4R_R} & \frac{-R_{SC}}{4R_R R_{LC}} \\
0 & \frac{1}{4R_{LC}R_P} & \frac{1}{4R_{SC}R_P} & \frac{1}{4R_{SC}R_P} & \frac{1}{4R_{LC}R_P} \\
0 & \frac{-1}{2R_{LF}} & \frac{-1}{2R_{SF}} & \frac{1}{2R_{SF}} & \frac{1}{2R_{LF}} \\
0 & \frac{-1}{4R_{LF}} & \frac{1}{4R_{SF}} & \frac{-1}{4R_{SF}} & \frac{1}{4R_{LF}}
\end{pmatrix} \begin{pmatrix} \dot{m}_2 \\ \dot{m}_3 \\ \dot{m}_4 \\ \dot{m}_5 \\ \dot{m}_6 \end{pmatrix}
\tag{5.8}
$$

where the above matrix is $J_{motor \to joint}$. The transpose relates joint torques to motor torques:

$$
\begin{pmatrix} \tau_{m2} \\ \tau_{m3} \\ \tau_{m4} \\ \tau_{m5} \\ \tau_{m6} \end{pmatrix} = \begin{pmatrix}
0 & \frac{-1}{R_R} & 0 & 0 & 0 \\
\frac{1}{4R_{LC}} & \frac{-R_{SC}}{4R_R R_{LC}} & \frac{1}{4R_{LC}R_P} & \frac{-1}{2R_{LF}} & \frac{-1}{4R_{LF}} \\
\frac{-1}{4R_{SC}} & \frac{1}{4R_R} & \frac{1}{4R_{SC}R_P} & \frac{-1}{2R_{SF}} & \frac{1}{4R_{SF}} \\
\frac{-1}{4R_{SC}} & \frac{1}{4R_R} & \frac{1}{4R_{SC}R_P} & \frac{1}{2R_{SF}} & \frac{-1}{4R_{SF}} \\
\frac{1}{4R_{LC}} & \frac{-R_{SC}}{4R_R R_{LC}} & \frac{1}{4R_{LC}R_P} & \frac{1}{2R_{LF}} & \frac{1}{4R_{LF}}
\end{pmatrix} \begin{pmatrix} \tau_{j2} \\ \tau_{j3} \\ \tau_{j4} \\ \tau_{j5} \\ \tau_{j6} \end{pmatrix}
\tag{5.9}
$$

There are several things to note from the above relationships.[4]

- Two motors contribute to the torque applied to each finger. As a result, given the same speed ratios, the gripping force possible with this design is twice that of a more conventional design where a single motor operates each finger, or a one-degree-of-freedom gripper. A caveat is that if torques are being supplied to other joints, the grip force possible is reduced.

  An additional advantage is that finger velocities are an average of two measurements which makes them smoother. From a velocity estimation standpoint, the encoder resolution is effectively doubled.

- Four motors contribute to the translational axis. This is good because this axis must use a portion of the torque available to counterbalance itself actively. It turns out that in order to do so, each motor uses less than 10% of its available torque. The position estimate is the average of four encoder readings so resolution is quadrupled.

- Four motors also contribute to joint 4 torques (pitch) which is good because the tips of the fingers are twice as far away from this axis than they are from the finger axes. Again position resolution is quadrupled.

---

[4]For reference, the Silver Falcon software calls R_P above R_Y. That is this pitch axis is referred to a yaw axis in the software. We have renamed it pitch here to be consistent with other descriptions given in this thesis.

5.3   Master

Our master manipulator is the PHANToM haptic interface described in (Massie and Salisbury, 1994), and shown in Figure 5-16. Figure 5-17 shows the Silver Falcon and PHANToM being used together. A schematic showing the PHANToM kinematics is shown in Figure 5-18. The cartesian axes in the figure are aligned with those shown in Figure 5-2 during use of the system. The system is shown in its zero position. The system is essentially a three-degree-of-freedom manipulator which is approximately counterbalanced using the weight of its own motors. The standard PHANToM uses a passive three-degree-of-freedom gimbal at the end of the actuated three-degree-of-freedom arm. We replaced the gimbal with a version of our own design which uses panel mount optical encoders (Bourns) to measure the gimbal positions. A seventh degree of freedom was also incorporated into the last link of the gimbal to control gripping motion of the slave manipulator. The master gripper uses a spring return so that the user can operate them somewhat like a pair of tweezers. Figure 5-19 shows a close up of the gimbal.

The link lengths are given by:

$$l_1 = 0.143 \text{ m}$$
$$l_2 = 0.178 \text{ m}$$

and the speed ratios are given by:

$$R_0 = 9.970$$
$$R_1 = 9.936$$
$$R_2 = 9.936$$

Each motor is capable of producing 29.61 mNm of maximum continuous torque. At 2 times max rated continuous torque (which is typically how we run the system), we can achieve maximum endpoint force values of:

$$f_{MX} = 4.1 \text{ N}$$
$$f_{MY} = 4.1 \text{ N}$$
$$f_{MZ} = 3.3 \text{ N}$$

Each encoder is a Hewlett-Packard optical encoder with 2000 counts/revolution (after quadrature). This gives an endpoint measurement resolution of:

$$r_x = 4.51 \times 10^{-5} \text{ m}(1.77 \times 10^{-3} \text{ in})$$
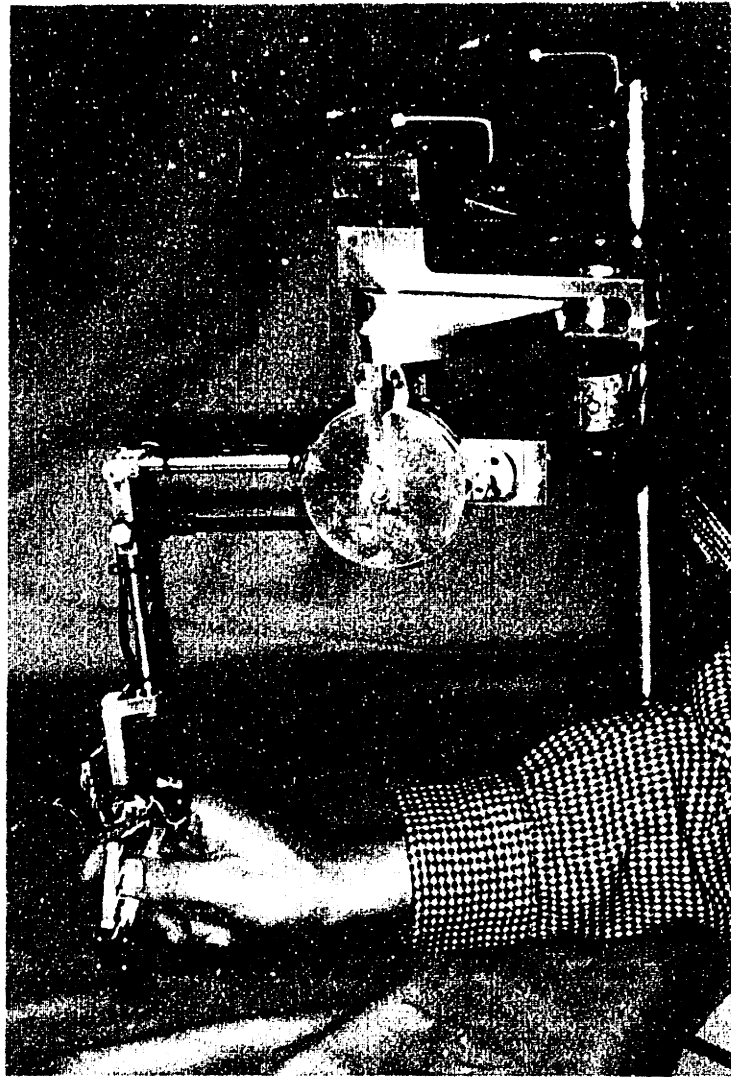
Figure 5-16: The PHANToM haptic interface modified for use as master manipulator for the Silver Falcon. The user's hand is holding a gimbal which measures three orientations. His index finger is resting on a spring-loaded paddle which controls the slave gripper.
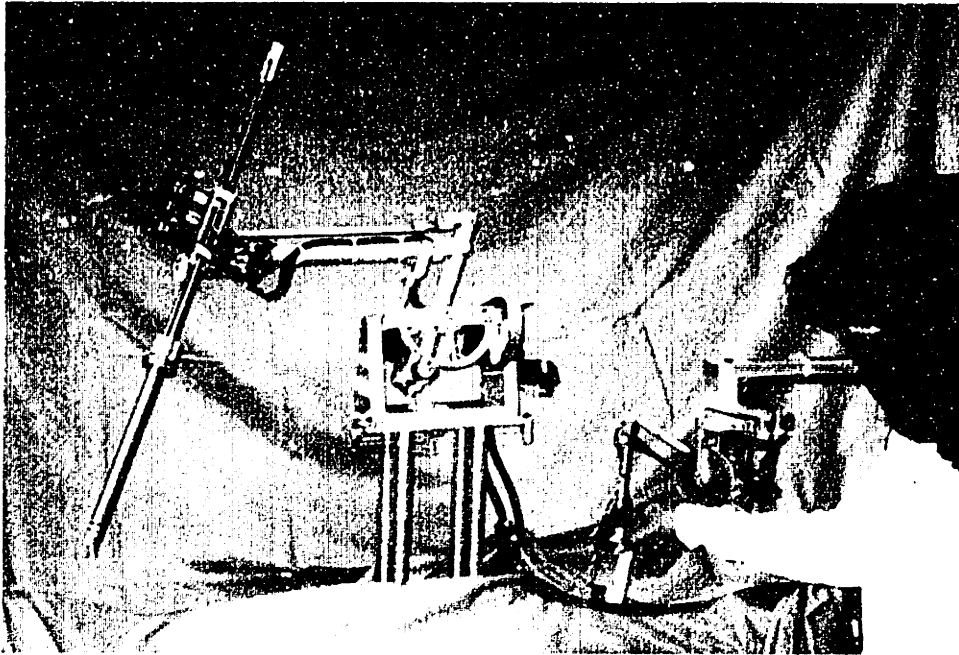
Figure 5-17: The Silver Falcon slave was used in conjunction with the PHANToM haptic interface. An instrumented gimbal and gripper were added to the end of the PHANToM so that it had a total of seven degrees of freedom (3 actuated).
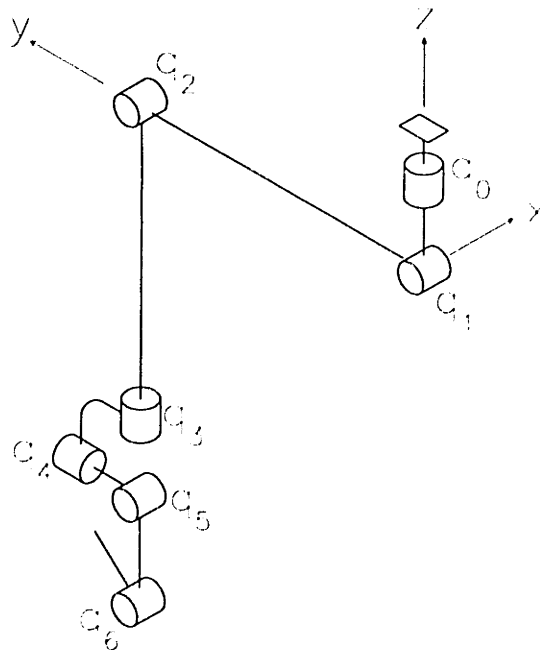
Figure 5-18: The PHANToM Haptic interface kinematics. The system is shown in its zero position.
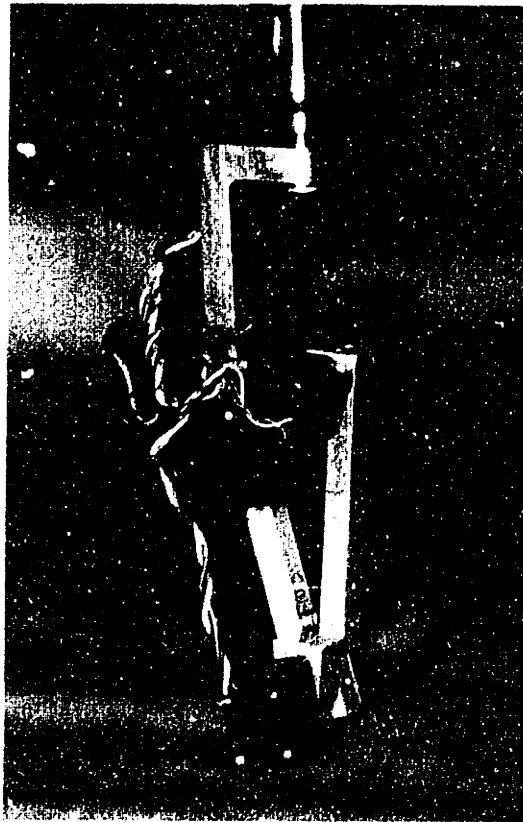
Figure 5-19: A passive gripper added to the end of the PHANToM Haptic interface to control gripping on the Silver Falcon.
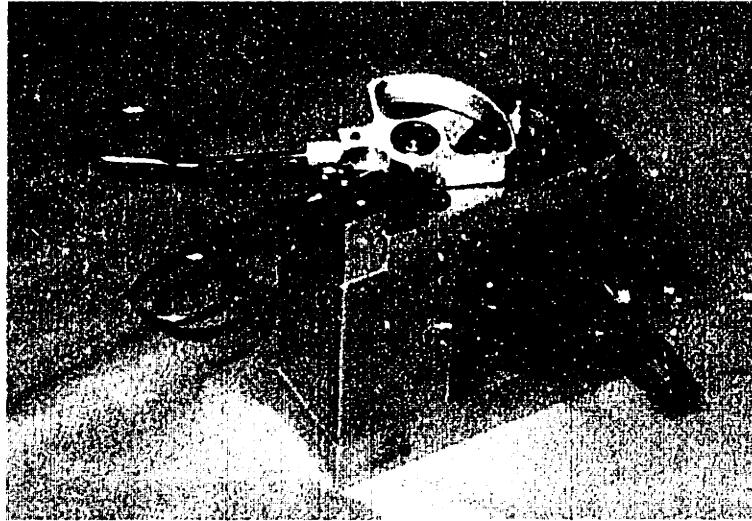
Figure 5-20: Actuated gripper "left-hand" master interface. This allows force re-
flection of the gripper to be felt by the user while still using the PHANToM haptic
interface as a master manipulator.

$$r_y = 5.63 \times 10^{-5} \text{ m} (2.22 \times 10^{-3} \text{ in})$$
$$r_z = 4.52 \times 10^{-5} \text{ m} (1.78 \times 10^{-3} \text{ in})$$

Because this passive gripper does not allow the user to feel forces, we developed a
second *actuated gripper* interface to control gripping. Because the master cannot
carry the weight of such an actuated gripper, it was mounted on a table stand so as
to be used with the user's left hand, while the PHANToM is used with the right hand.
The actuated gripper consists of a pair of standard needle holder handles attached to
a single rotary axis. One handle is fixed to ground, while the other is attached via a
cable transmission to a brushed d.c. electric motor (Maxon RE025-055-035, graphite
brushes). Figure 5-20 shows the actuated gripper.

5.4   Controller

The basis for the controllers implemented on this system was described in Chapter
4. Implementation on the full seven-degree-of-freedom Silver Falcon was done by
Dr. Günter Niemeyer of the MIT AI Lab, and will be described in a forthcoming
publication.

5.5 Summary

The Silver Falcon represents our first prototype teleoperator slave for minimally invasive surgery. It consists of two main subsystems. The first is a wrist unit which incorporates a wrist and grippers and an actuation and transmission system to power these. The second is a base positioning unit which carries the wrist unit and constrains the shaft of the wrist unit to lie along a remote center of rotation meant to coincide with the surgical incision point. This chapter described in detail the design of this system.

The system was used in conjunction with the PHANToM haptic interface, modified for use as a master manipulator. In the next chapter, we will describe the performance of these two systems individually, and working together as a master-slave teleoperator system.

Chapter 6

Silver Falcon Teleoperator Slave Performance

In Section 6.1 we describe the location of singularities and joint range of motion limits, and make a qualitative assessment of the range of motion with respect to surgical tasks. We then give a number of basic test results which describe friction, inertia, and servo stiffness of individual joints for the Silver Falcon and the PHANToM master. We also give individual joint step responses. These results essentially show how well various elements of the system were built on a joint by joint basis.

In Section 6.2 we discuss teleoperation performance using two main criteria. What does the operator feel when using the master to control the slave when it is not contacting anything (moving through freespace), and what does he feel when the slave makes contact with the environment. We also give discrimination test results to show the lowest levels of force at the slave which can be distinguished by the operator holding the master.

6.1 Basic System Performance

6.1.1 Singularities

We use a roll-pitch-yaw wrist. Therefore, there are two singular configurations at $q_4 = \pm\pi/2$. No output roll is possible at these singular configurations.

6.1.2   Joint Limits

The joint range of motions are:

q_0	$\pm 45°$
q_1	$\pm 45°$
q_2	$0 \text{ m} - 0.19 \text{ m}$
q_3	$\pm 175°$
q_4	$\pm 90°$
q_5	$\pm 90°$
q_6	$0° - 180°$

6.1.3   Motions for Suturing

It is impossible to say whether or not the kinematics we have chosen will suffice for all the motions which are performed during the course of actual surgery. However, we can consider the motions required for suturing as an example, as described in Section 3.1.2. There we saw that this motion consisted primarily of a roll motion combined with a push to pass the needle through tissue. Therefore, we need to avoid singularities in the Silver Falcon wrist which would prevent output roll.

As we have described, our wrist is a roll-pitch-yaw wrist with non-intersecting axes, and with two singular configurations at $q_4 = \pm 90°$. Therefore it is possible to operate at up to 90° joint deflections. Practically, we feel more comfortable allowing a surgeon to operate at roughly a $\pm 45°$ deflection, since they will invariably not be consciously avoiding singularities while operating. Referring to Figure 3-3, we can therefore deviate comfortably by $\pm 45°$ from the indicated instrument shaft orientation and still maintain the proper needle orientation during the suturing motion.

The Silver Falcon grip strength (0.48 N (1.0 lb) at the tip of the gripper jaws) was insufficient to hold needles securely, so it was impossible to test the system by suturing actual tissue. At best, we were able to throw sutures into soft foam. It appeared however, that the range of motion of the wrist was sufficient to allow us to suture from different angles without careful alignment of the "tissue" relative to the manipulator.

We look at joint by joint dynamics of both the Silver Falcon slave, and the PHAN-ToM master. While we are primarily concerned with evaluating the Silver Falcon, the overall system response is a direct function of both the slave and the master. We

will find a number of areas for improvement that will be addressed in our second design, the Black Falcon. In assessing dynamics, we will consider structural flexibility, transmission flexibility and friction. We will look at joint servo responses for both the slave and master manipulators.

Again, refer to Figure 5-2 for joint numbering and definition of cartesian axes.

6.1.4 Structural Stiffness

The structural stiffness was tested in the manipulator's zero position by clamping the base axes, axes 0 and 1, and deflecting the tip of the manipulator just above the wrist in the x and y directions using a digital force gage (Mark 10 Model BG2), and measuring deflection corresponding to a measured force. When centered in its workspace, the slave manipulator tip is 32.5 cm (12.8 in) below the remote center of rotation. To test z stiffness, we applied a vertical force to the motor mounting bracket, 96 in Figure 5-9. While the actual stiffnesses are certainly not linear, these rough measurements still give a good idea of overall stiffness and represent an overall upper limit to the slave stiffness which can be achieved.

In the x direction, we measured a 12.5 mm deflection with a 6 N force giving a 480 N/m stiffness. In the y direction, a 12.5 mm deflection with $3.1 - 3.3$ N force resulted in a 250 N/m stiffness. And in the z direction, a 2.5 mm deflection with 8.4 N gave a 3400 N/m stiffness.

These numbers, particularly in the x and y directions, are quite soft and show the difficulty of making a stiff slave which must be long and slender in order to pass through a small incision in the human body. The compliance in the x and y directions is primarily due to the Thomson ball bushings/steel rod bearing structure used to support the wrist unit. Two long 1/4 in diameter parallel steel rods simply do not provide much structural stiffness in bending or in torsion. The z compliance is due to flexibility in the remote center linkage.

6.1.5 Friction

The static backdrive friction was measured with our digital force gage in the x and y directions at the tip of the fingers both with the base clamped, and with it free. These values represent friction in the transmission and in the motors. Four or five trials were done in each case and averages were taken.

With the base clamped we found the friction in the wrist axes alone. The wrist friction f_{WX} in the x direction represents friction about axis 4. The wrist friction

in the y direction f_{WY} with the fingers closed represents friction about axis 5. The friction about each of the fingers, f_{SF}, f_{LF}, were similar and are referred to using the notation of Section 5.2.3. These values are:

$$f_{WX} = 0.30 \text{ N} \pm 0.1 \text{ N}$$
$$f_{WY} = 0.76 \text{ N} \pm 0.1 \text{ N}$$
$$f_{SF} = 0.35 \text{ N} \pm 0.1 \text{ N}$$
$$f_{LF} = 0.46 \text{ N} \pm 0.1 \text{ N}$$

With the base left free, the friction in the x direction was:

$$f_{BX} = 0.19 \text{ N} \pm 0.1 \text{ N}$$
$$f_{BY} = 0.20 \text{ N} \pm 0.1 \text{ N}$$

In this case most of the motion was in the base joints and not in the wrist joints. In the Silver Falcon, the friction in the wrist joints is actually higher than in the base joints in the x and y directions when measured at the tip of the manipulator. The friction in the z direction corresponds to that in joint 2 and is 2.0 N. The system was tilted so that this joint was horizontal in order to measure its friction. The friction in this joint is considerably higher because all five motors are backdriven simultaneously. Also, these cables are directly backdriven without the benefit of additional leverage as in the case of the wrist and fingers.

The friction in the master was measured in the x, y, and z directions f_{mx}, f_{my}, f_{mz}, as shown in Figure 5-18. We also measured the friction in the actuated gripper f_{ag}. The values found were:

$$f_{mx} = 0.18 \pm 0.05 \text{ N}$$
$$f_{my} = 0.15 \pm 0.05 \text{ N}$$
$$f_{mz} = 0.15 \pm 0.05 \text{ N}$$
$$f_{ag} = 0.07 \pm 0.03 \text{ N}$$

There are several primary causes of friction in the system:

- Brush friction in the motors. Our motors are Maxon RE025-055-035 brushed d.c. motors with a catalog value of 0.0086 Nm frictional torque. We typically measure smaller values however. On one motor we measured 0.02 ± 0.005 N at 1 in (0.0254 m)which gives 0.0005 Nm brush torque.

  Had we used precious metal brushes instead of graphite brushes, the brush friction, using catalog values, would be roughly 25% times less. Graphite brushed

motors have a higher peak torque capacity, but since we typically operate within one or two times continuous torque limits in order not to damage our motors, this capacity goes unused and precious metal brushes would be a smarter choice. The precious metal brushes are not available on the larger RE035 motors.

- Bearings add small amounts of friction. In particular the very small bearings used in the wrist have a low load capacity. We suspect that the high cable tension required to maintain frictional drive loads on the drive capstans increase friction in these bearings.

- If cable turns over very small diameter pulleys, internal friction is generated between the individual fibers of the cable. One possible mechanism is plastic deformation in the cable. The other is rubbing of the cable fibers against one another since they pass over different radii of curvature as they pass over the pulleys. We do not know the magnitude of this frictional component.

We know that changing cable tension makes a substantial difference in frictional levels, particularly in the wrist. The tradeoff is that low tension will allow one side of the cable go slack at higher torques, and slippage will occur if we rely on frictional drive capstan engagement. Increased pretension increases bearings loads, and loads on cable which wraps around capstans and pulleys and therefore friction within cable. If due to poor design, pulleys are made to rub on one another, these loads will also increase with increased cable tension, though we do not believe this occurs in our design.

6.1.6 Friction Compensation Algorithm

The friction compensation used is the same as that in the micro-macro testbed. In order to reduce the effects of static friction, we used a friction compensation algorithm which feeds forward a constant torque to each motor. The feed forward torque is increased linearly from zero to of 0.00072 Nm as velocity is increased. The feedforward torque is slightly less than that required to move any of the axes. The velocity at which this full feed forward torque is applied was adjusted empirically to give a smooth breakaway from zero velocity. If the value is zero, the system will feel very "sticky" near zero velocity. If this value is too high, the friction feedforward is ineffective.

6.1.7 Inertia

The joint inertias were measured by programming known stiffnesses into each joint servo and comparing the resulting experimental output responses to simulated re-

sponses with known values. The values were taken with the slave centered in its workspace, and are:

$$I_{s0} = 0.09 \text{ kgm}^2$$
$$I_{s1} = 0.08 \text{ kgm}^2$$
$$I_{s2} = 1.14 \text{ kg}$$
$$I_{s3} = 0.000033 \text{ kgm}^2$$
$$I_{s4} = 0.000010 \text{ kgm}^2$$
$$I_{s5} = 0.000011 \text{ kgm}^2$$
$$I_{s6} = 0.0000028 \text{ kgm}^2$$

When centered in its workspace, the slave manipulator tip is 32.5 cm (12.8 in) below the remote center of rotation. If we convert the joint 0 and 1 inertias I_{s0} and I_{s1} to cartesian inertias using this length, we find:

$$I_{sx0} = 0.85 \text{ kg}$$
$$I_{sy0} = 0.76 \text{ kg}$$

These are the inertias we feel if moving the slave manipulator by its tip.

The PHANToM inertias were measured directly in cartesian space and are given below. The inertia of the actuated gripper is given in joint space:

$$I_{mx} = 0.23 \text{ kg}$$
$$I_{my} = 0.16 \text{ kg}$$
$$I_{mz} = 0.18 \text{ kg}$$
$$I_{ag} = 0.000115 \text{ kgm}^2$$

6.1.8   Individual Joint Responses

To give an idea of servo performance, we give representative step responses for each joint of the Silver Falcon. The joint gains were tuned experimentally to be reasonably good and are given below. The magnitude of the responses corresponds to essentially

Figure 6-1: Silver Falcon Joint 0 response to a 0.07 rad step input.
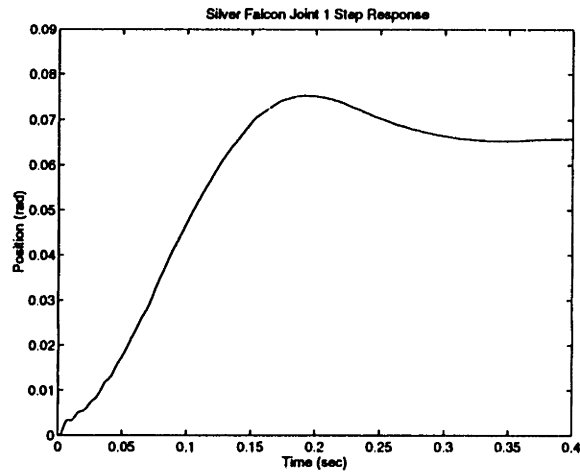
Figure 6-2: Silver Falcon Joint 1 response to a 0.07 rad step input.

the largest magnitude we could perform without torque limiting the motors.

$$K_{qs0} = 24 \text{ Nm/rad} \qquad B_{q0} = 1.2 \text{ Nms/rad}$$
$$K_{qs1} = 24 \text{ Nm/rad} \qquad B_{q1} = 1.2 \text{ Nms/rad}$$
$$K_{qs2} = 6000 \text{ N/m} \qquad B_{q2} = 60 \text{ Ns/m}$$
$$K_{qs3} = 2.4 \text{ Nm/rad} \qquad B_{q3} = 0.0084 \text{ Nms/rad}$$
$$K_{qs4} = 0.24 \text{ Nm/rad} \qquad B_{q4} = 0.0024 \text{ Nms/rad}$$
$$K_{qs5} = 0.48 \text{ Nm/rad} \qquad B_{q5} = 0.0048 \text{ Nms/rad}$$
$$K_{qs6} = 0.12 \text{ Nm/rad} \qquad B_{q6} = 0.0012 \text{ Nms/rad}$$

The master gains are:

$$K_{xm0} = 480 \text{ N/m} \qquad B_{xm0} = 0.72 \text{ Ns/m}$$
$$K_{xm1} = 480 \text{ N/m} \qquad B_{xm1} = 0.72 \text{ Ns/m}$$
$$K_{xm2} = 480 \text{ N/m} \qquad B_{xm2} = 0.72 \text{ Ns/m}$$
$$K_{qm6} = 3.0 \text{ Nm/rad} \qquad B_{qm6} = 0.0045 \text{ Nms/rad}$$

The length of the gripper handles is 0.079 m, so the cartesian space gripper servo stiffness at the tip of the handles is 480 N/m, and the damping is 0.72 Nms/rad.

Figures 6-1 and 6-2 show step responses for the base joints, axes 0 and 1. These responses are slightly underdamped and not particularly fast. The damping gains are limited primarily by the limited encoder resolution on these axes. This in turn limits

the stiffness gains and thus the overall speed of response. Use of higher resolution encoders would improve these responses.

A more involved change would be to increase the magnitude of the cable reductions on these axes from their current values of 19:1 for joint 0 and 19.3:1 for joint 1 in order to inertia match the motor rotors with the inertia of the pitch and yaw axes. Inertia matching the rotor inertia to the output link inertia maximizes the output link acceleration for a given input torque. The base motor rotor inertia (Maxon RE-035-034) is 6.96×10^{-6} kgm^2. For joint 0, the measured link inertia is almost entirely due to the output link inertia. That is:

$$
\begin{aligned}
I_{output} &= I_0 - I_{rotor} R^2 \\
&= 0.09 - 6.96 \times 10^{-6} 19^2 = .087 \text{ kgm}^2
\end{aligned}
$$

To inertia match the rotor inertia to that of the output link would require a reduction of:

$$
\sqrt{\frac{0.087}{6.96 \times 10^{-6}}} = 112
$$

which is not possible with single stage cable reduction in a reasonable size.

Finally, we can see that the overall dynamics are fairly clean, with the exception of some high frequency very low amplitude (roughly 80 Hz) oscillations at the beginning of the responses. This is due to flexibility of the steel drive cables.

Figure 6-3 is a 3.5 mm step response for joint 2. This is a very rapid response, but with a number of slower oscillations which prevent settling of the system. These oscillations are caused by flexibility of the base positioner structure and are actually visible. We can show this by repeating the step response while supporting the motor block by holding it against a 1/4 in diameter steel rod braced against the table on which the system is mounted, Figure 6-4. The structural oscillations are essentially gone.

Figure 6-5 gives the 0.05 radian step response for joint 3. This is a fairly straightforward 2nd order type response. Figures 6-6 gives a 0.3 rad step responses for joint 4. Note that the joint never quite reaches 0.3 radian due to stiction in the wrist mechanism.

Figures 6-7 gives a 0.1 rad step response for joint 5, motion of a point midway between the two fingers. This response is for both fingers moving together with the distance between them commanded to remain constant. This joint also does not reach its commanded value due to stiction in the wrist. Also, there is a slight oscillation superimposed on the response due to cable flexibility between the motor and the wrist
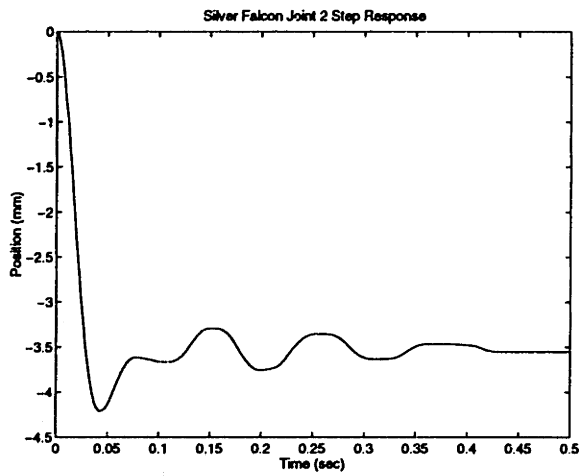
Figure 6-3: Silver Falcon Joint 2 response to a 3.5 mm step input.
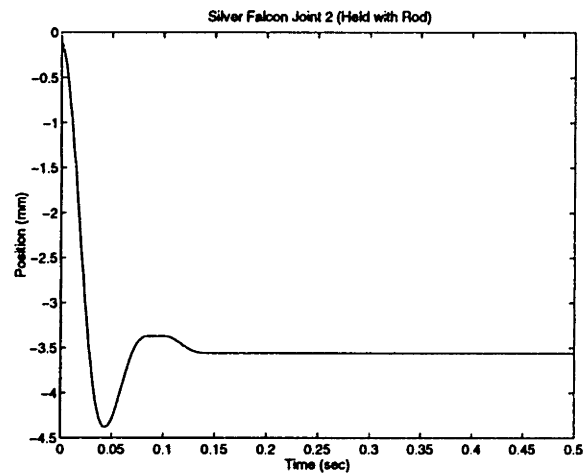
Figure 6-4: Silver Falcon Joint 2 response to a 3.5 mm step input with motor block braced against table with 1/4 inch steel rod.

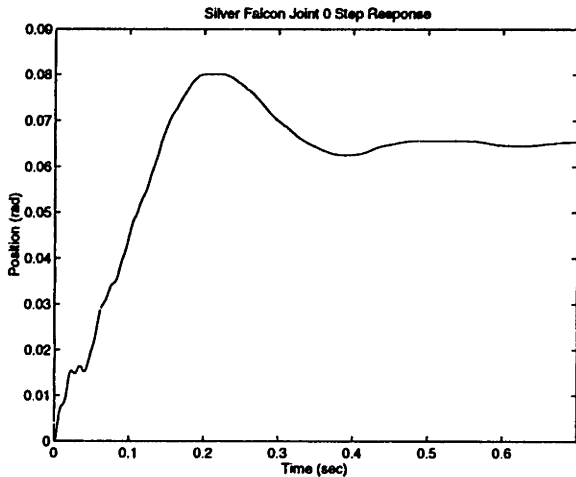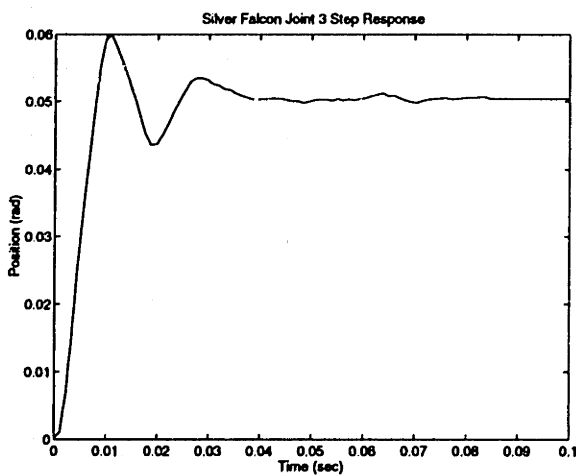Figure 6-5: Silver Falcon Joint 3 response to a 0.05 step input.
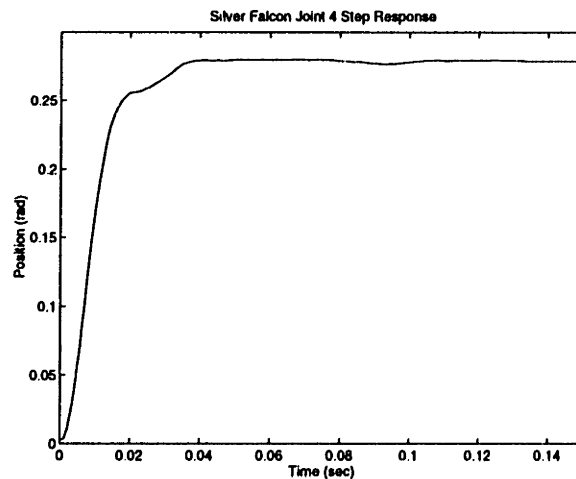
Figure 6-6: Silver Falcon Joint 4 response to a 0.3 rad step input.
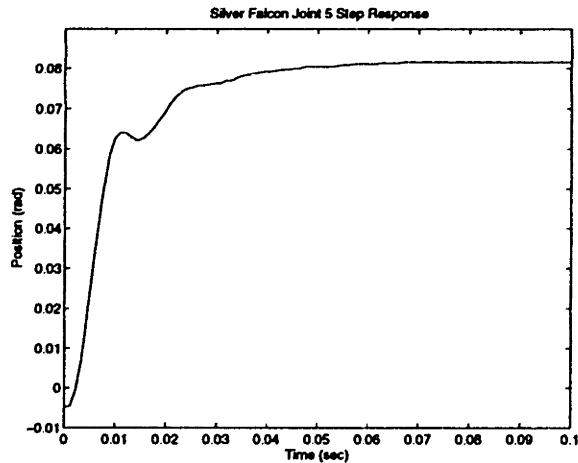
Figure 6-7: Silver Falcon Joint 5 response to a 0.1 rad step input.
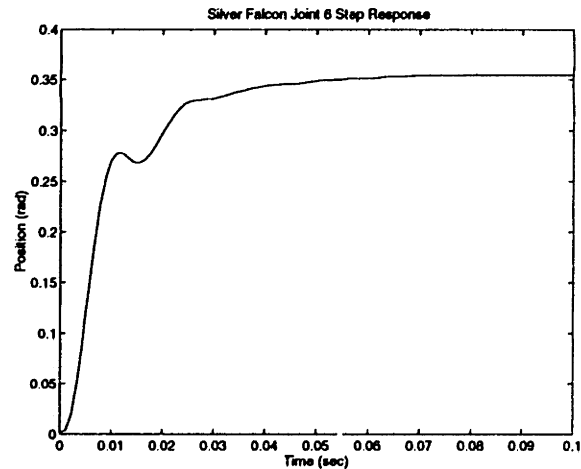
Figure 6-8: Silver Falcon Joint 6 response to a 0.4 rad step input.

stiction.

Figure 6-8 gives a 0.3 rad step response for joint 6, gripping. This plot is very similar though the joint comes to rest slightly beyond its setpoint due to wrist stiction. A similar oscillation due to cable flexibility can be observed here also.

The PHANToM joint step responses are given in Figures 6-9, 6-10, and 6-11. These responses show some slight non second order response characteristics. There are high frequency cable dynamics visible as small oscillations at the beginning of the joint 1 and joint 2 responses. Also, the joint 0 response appears slightly nonlinear. The PHANToM is most flexible in this direction structurally, which may account for this. Limited encoder resolution is visible in the responses.

Overall, there are several points to note about the PHANToM performance. First, the maximum stiffness which we can achieve when servoing joints to fixed positions is roughly 480 N/m. This is fairly soft. (Tan et al., 1994) demonstrated that humans feel stiffnesses of above roughly 25,000 N/m as infinitely rigid in static pushing tests. We have found that using our PHANToM haptic interface to feel virtual walls is easier than servoing to a fixed position, and we can achieve a "wall" stiffness of roughly 2000 N/m. This provides a satisfactory feeling of pushing on a "wall", though the wall does not feel infinitely rigid. A stiffness of 480 N/m is four times softer and corresponds to a fairly mushy wall. If this is the best our master can achieve, then we are fundamentally limited in achieving a rigid master-slave connection.

The master stiffness could be substantially improved by increasing rotor inertia by using either larger motors (Maxon RE035 instead of RE025), or by increasing the
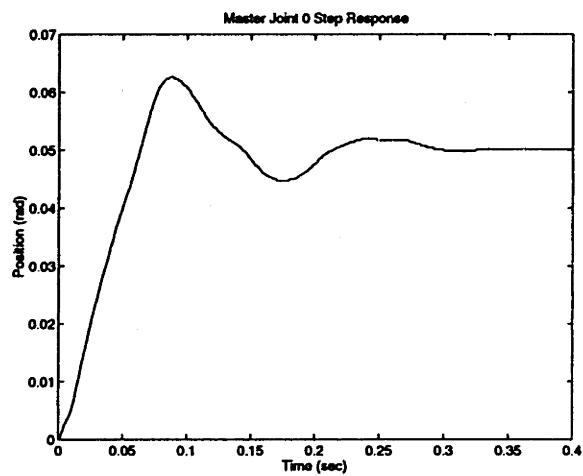
Figure 6-9: PHANToM Joint 0 response to a 0.05 rad step input.
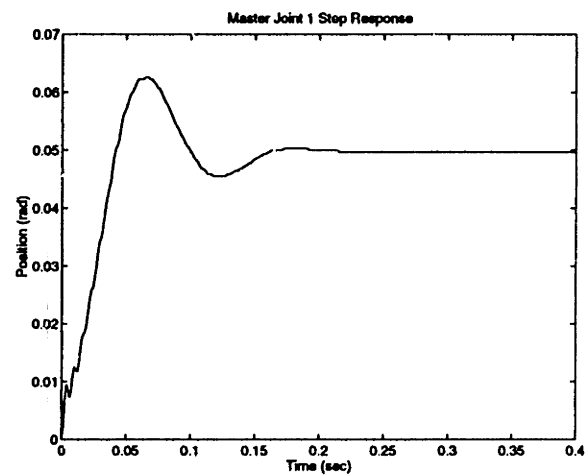
Figure 6-10: PHANToM Joint 1 response to a 0.05 rad step input.
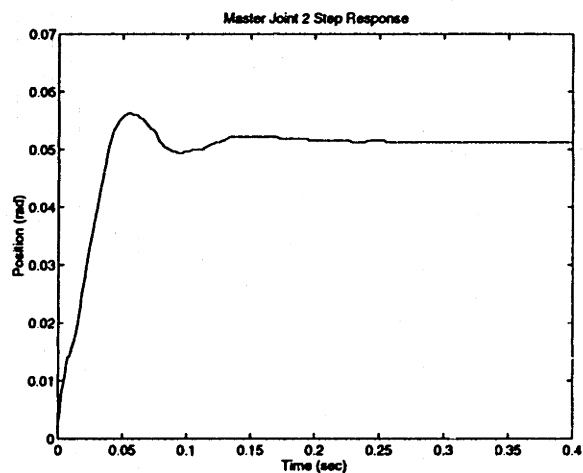
Figure 6-11: PHANToM Joint 2 response to a 0.05 rad step input.
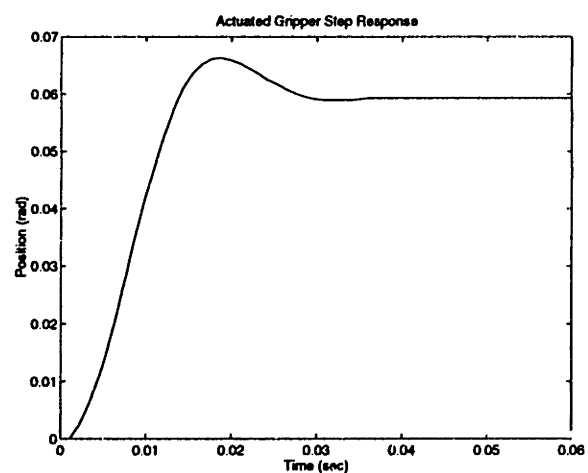
Figure 6-12: Actuated Gripper response to a 0.06 rad step input.

reduction used. Damping gains and hence corresponding stiffness gains could be increased by using higher resolution encoders such as Canon TR36 laser encoders with 14,400 counts per revolution. SensAble Technologies Inc. which currently manufactures and sells the PHANToM uses a higher resolution Hewlett-Packard encoder than on the version which I am using as a master. My version uses 500 count (2000 after quadrature) encoders while the newer version uses 1000 count (4000 after quadrature) encoders.[1]

The second point to note is that the PHANToM endpoint inertia is significant. As we discussed in Chapter 2, inertia is necessary to achieve stiffness in a servo system. However, the tradeoff is that with a system such as this, it will never feel as if we are touching objects directly with our fingers. There will always be a mass of at least, in our case, roughly 0.2 kg between our fingers and the environment which we sense through the teleoperator slave.

The actuated gripper step response is shown in Figure 6-12. This response is much faster than the other master responses, since the output link is lighter and the reduction is higher. The measured link inertia (not including motor rotor inertia) is 4.29×10^{-5} kgm^2. The optimal (inertia matched) reduction ratio is then:

$$\sqrt{\frac{4.29 \times 10^{-5}}{1.04 \times 10^{-6}}} = 6.42 \tag{6.1}$$

I designed the actuated gripper with a ratio of 8.33:1 "by eye" because the link and reduction are incorporated into one piece so that the inertia was unknown. It turned out this was fairly close, resulting in the good performance which we observe.

6.2 Force Reflection

When implementing a master-slave teleoperator with force reflection, there are several qualities which describe the quality of force reflection:

- Freespace motions of the system should feel free. The user who is operating the master should feel the master and little else. They should not feel as if they are "dragging" or "carrying" the slave along with them. Obviously, if no forces from the slave are sent to the master (force reflection is turned off and the master is used only as a positioning input), then this will be the case.

---

[1]For historical reference, the PHANToM which I am using is the original one which Thomas Massie made in the A.I. Lab machine shop in the Spring of 1993.

- Contact should feel conspicuous and forces between the slave manipulator and its environment should be accurately reproduced at the master. For example, if we make a hard contact with the slave we can observe bandwidth limitations in the master-slave connection by observing the sharpness of the resulting force response at the master.

- The system should be sensitive. The lowest level of force which can be felt should be as low as possible. How low depends on the task at hand. The ability to discriminate when contact occurs and how delicately contact occurs depends on this value.

- Because the system is multi-dimensional, these properties should be equally good in all directions. There should not be preferential directions of motion caused by anisotropic friction or inertia because this may mislead the surgeon while they operate.

Below we compare two different controllers which were implemented on the Silver Falcon and PHANToM, the Jacobian Transpose controller and the Inverse Jacobian controller. These were both described in Chapter 4. The Inverse Jacobian control gave us the best overall performance which we were able to achieve with our system. This comparison will show that:

- When implemented on the Silver Falcon, the Inverse Jacobian controller hides the inertia of the slave base positioner roughly twice as well as does the Jacobian Transpose controller and is therefore the better of the two.

- The Silver Falcon base positioner has a limited servo response which limits the Inverse Jacobian controller from better hiding the base positioner inertia from the user.

- Using the Inverse Jacobian control, forces are not felt in a direction pointing into the fingers of the wrist unit since there are no redundant degrees of freedom in this direction.

We then give discrimination test results showing the lowest forces which can be felt by a user through the system using the Inverse Jacobian controller.

In the plots given below, we are concerned with the forces output by the master and the slave manipulators. However, neither manipulator uses explicit force sensing at their output, so we cannot actually measure the force outputs. As a result we must estimate output forces using commanded joint torques. Fortunately, both systems were designed so that joint torques would provide good estimates of output forces.

The error between joint torques and output forces are caused by friction in the joints and motor brushes and by inertia in the systems links. Friction levels are given above in Section 6.1.5, and inertias are given in 6.1.7. For the slave, we use only wrist torque measurements to determine the slave endpoint force in order to avoid errors which would be caused by the inertia of the base positioner which is much larger. This is in effect the whole idea of macro-micro control. The exception is for forces in the direction of the fingers of the Silver Falcon. Redundant positioning degrees of freedom do not exist in this direction, so that the entire slave must move during these motions. In the plots shown here, the fingers are always pointing downwards, in the $-z$ direction, so we expect more error in this direction between the forces shown in the plots and the actual forces at the tip of the manipulator.

The gains used for the master were:

$$K_x = 480 \text{ N/m} \quad B_x = 0.72 \text{ Ns/m}$$
$$K_y = 480 \text{ N/m} \quad B_y = 0.72 \text{ Ns/m}$$
$$K_z = 480 \text{ N/m} \quad B_z = 0.72 \text{ Ns/m}$$

The gains used for the slave during Jacobian Transpose control were:

$$K_x = 240 \text{ N/m} \quad B_x = 0.36 \text{ Ns/m}$$
$$K_y = 240 \text{ N/m} \quad B_y = 0.36 \text{ Ns/m}$$
$$K_z = 240 \text{ N/m} \quad B_z = 0.36 \text{ Ns/m}$$
$$K_{grip} = 240 \text{ N/m} \quad B_{grip} = 0.36 \text{ Ns/m}$$

The gains used for the slave during Inverse Jacobian control were:

$$K_{q0} = 30 \text{ Nm/rad} \quad B_{q0} = 1.4 \text{ Nms/rad}$$
$$K_{q1} = 30 \text{ Nm/rad} \quad B_{q1} = 1.4 \text{ Nms/rad}$$
$$K_{q2} = 6000 \text{ N/m} \quad B_{q2} = 60 \text{ Ns/m}$$
$$K_{q3} = 2.4 \text{ Nm/rad} \quad B_{q3} = 0.0084 \text{ Nms/rad}$$
$$K_{q4} = 1.0 \text{ Nm/rad} \quad B_{q4} = 0.0060 \text{ Nms/rad}$$
$$K_{q5} = 0.4 \text{ Nm/rad} \quad B_{q5} = 0.0060 \text{ Nms/rad}$$
$$K_{q6} = 0.12 \text{ Nm/rad} \quad B_{q6} = 0.0012 \text{ Nms/rad}$$

6.2.1   Freespace Responses

The freespace response plots show how much force is transmitted to the user from the slave while they are moving the system through freespace. In an ideal system, this value would be zero. We commanded a sinusoidal position command to the slave (i.e. a virtual master following a sinusoid) and recorded the forces which were calculated

Figure 6-13: Freespace response for the Silver Falcon slave and PHANToM master in the x direction using the Jacobian Transpose controller. The solid line represents the master, and the dashed line represents the slave.

by the controller and sent back to the master. We recorded the commanded sinusoid, and the tracking response of the slave. We also recorded the commanded cartesian output force of the slave, which is our measured slave tip force, and the cartesian output force which was commanded to the master. These forces represent the forces which would be applied to the master if it were moved along a perfectly sinusoidal path, in order to overcome inertia and friction reflected back from the slave. In all cases, the commanded sinusoid has a frequency of 8.0 rad/sec and an amplitude of 2.0 cm.

6.2.1.1 Jacobian Transpose Controller

Figures 6-13, 6-14, and 6-15 show freespace responses in the x, y, and z directions using the Jacobian Transpose controller with a force scaling factor of 2:1. Recall that the Jacobian Transpose controller forces the user to feel the inertia of the slave in addition to that of the master, multiplied by the force scale factor used.

Consider Figure 6-13, the x direction freespace response. We can see that:

• The slave lags the master as it tries to track its motions.

Figure 6-14: Freespace response for the Silver Falcon slave and PHANToM master in the y direction using the Jacobian Transpose controller. The solid line represents the master, and the dashed line represents the slave.

Figure 6-15: Freespace response for the Silver Falcon slave and PHANToM master in the z direction using the Jacobian Transpose controller. The solid line represents the master, and the dashed line represents the slave.

- There are roughly +2.5 N and -3.5 N peak forces commanded to the master despite the fact that the slave is not touching anything.

The forces we feel in the slave are inertial forces, frictional forces, and forces required to bend electrical cabling. Gravity forces are cancelled (fedforward) in the controller, and not shown in the graphs. The spring counterbalance is not used in these tests.

We may do a rough calculation to estimate the inertia which is reflected to the master from the slave. The master trajectory in Figure 6-13 is sinusoidal with a frequency and amplitude of:

$$\omega = 8.0 \text{ rad/s}, \ A = 0.02 \text{ m}$$

The maximum acceleration is then:

$$\ddot{x} = \omega^2 A = 1.28 \text{ m/s}^2$$

The inertia of the slave tip in the center of its workspace in cartesian space was previously measured as 0.85 kg, and the force scale is 2. The resulting force which the master needs to apply is:

$$0.85 \text{ kg} \times 1.28 \text{ m/s}^2 \times 2 = 2.2 \text{ N}$$

which is approximately what we read in the lower graph in Figure 6-13. We are unsure as to why the plot does not show completely symmetric positive and negative force values, but suspect that this is due to forces required to bend the electrical cables.

Note that the user also feels the inertia of the master itself which is not shown in the plots. We know this is 0.23 kg in the x direction, so that the total inertia which the user feels in the x direction is 0.85 kg × 2 + 0.23 kg = 1.93 kg. This is a substantial inertia for the user to carry!

The y direction response is similar as shown in Figure 6-14, but the z response appears different in that torques applied to the master are larger, roughly ±4 N, and not as smoothly sinusoidal. The slave force in the lower graph is half (in fact exactly half) that of the master force. The master forces correspond directly to the tracking error in the slave. Because there is substantially more inertia and friction along the joint 2 (linear in-out) axis than in the x and y directions, the tracking performance is poorer. This translates directly into an increased force applied to the master. Since there are no wrist axes which move in the z direction, the slave force shown in the graph represents the force required to move this entire joint. Because of the force scale factor of 2, the master forces are exactly twice those required to move the slave joint. These forces are so large that it is difficult to move the slave without reaching the
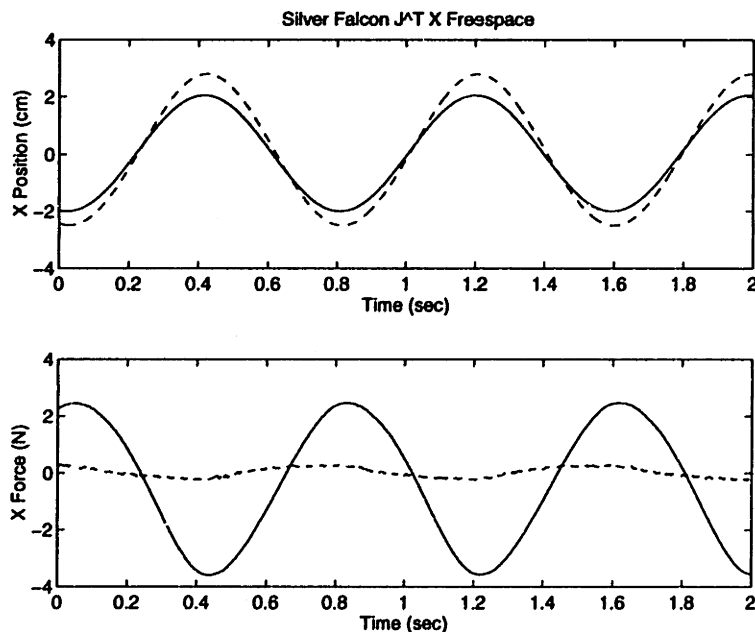
Figure 6-16: Freespace response for the Silver Falcon slave and PHANToM master in the x direction using the Jacobian Inverse controller. The solid line represents the master, and the dashed line represents the slave.

torque limits of the PHANToM master. These limits were set to twice the continuous motor torque, which when in the zero position are:

$$f_{MX} = 4.1 \text{ N}$$
$$f_{MY} = 4.1 \text{ N}$$
$$f_{MZ} = 3.3 \text{ N}$$

6.2.1.2 Inverse Jacobian Controller

Now we consider freespace motions for the Inverse Jacobian controller. Consider the x direction response shown in Figure 6-16. Again we notice that there is an error between the response of the slave and the motion of the master. However the error is somewhat less than in the previous Jacobian Transpose case.

As we would expect, the slave force is nearly zero, since the manipulator is not touching anything and we are using sensitive wrist axes to measure this force.

If we assume the user is feeling primarily inertia of the slave, then the equivalent

measured reflected inertia is approximately:

$$\frac{1.3 \text{ N}}{1.28 \text{ m/s}^2} = 1.1 \text{ kg}$$

We can calculate the inertia we would expect the user to feel by using the gains applied to the base axes of 30 Nm/rad and its measured inertia of 0.85 kg. Converting the base axis gain to an equivalent cartesian gain we have;

$$\frac{30 \text{ Nm/rad}}{0.325 \text{ m}^2} = 293 \text{ N/m}$$

The base inertia is scaled by a ratio of the base and master gains. This is multiplied by the base inertia to get a corresponding reflected inertia:

$$
\begin{aligned}
\frac{480 \text{ N/m}}{293 \text{ N/m}} &= 1.64 \\
1.64 \times 0.85 \text{ kg} &= 1.39 \text{ kg}
\end{aligned}
$$

A reasonable question would be why don't we feel less inertia? After all, one of the main benefits of the Inverse Jacobian control is to hide inertia. The reason is that the slave base actuators are not strong enough to properly track the master. The forces sent to the master are due to errors in the base joints, not in the wrist joints. Using the Inverse Jacobian controller, any tracking errors in the x direction should be due to wrist deflection. Since the wrist inertia is low, this deflection should be due to an outside force, and *should* be fed to the master as a force. However, if the base positioner does not properly track the master position, then this tracking error will be misinterpreted as a force despite the lack of contact between the slave and the environment. In this way, the base position tracking ability is important for the slave to accurately measure forces. Figure 6-17 shows a similar response for the y direction.

In the z direction, the graphs look different, see Figure 6-18. There is virtually no tracking error. This is because in this direction, which is along joint 2, we have four actuators/encoders contributing to this axis resulting in a stiff, high performance axis as we showed in Figures 6-3 and 6-4. (The slower motions made here do not appear to excite any structural dynamics.)

As in the case of the Jacobian Transpose controller, the slave forces appear non-zero even when the slave is moving in freespace. This is because we do not have a redundant micro freedom in this direction. Hence the slave torques represent the force required to move the base positioner instead of a light wrist joint.
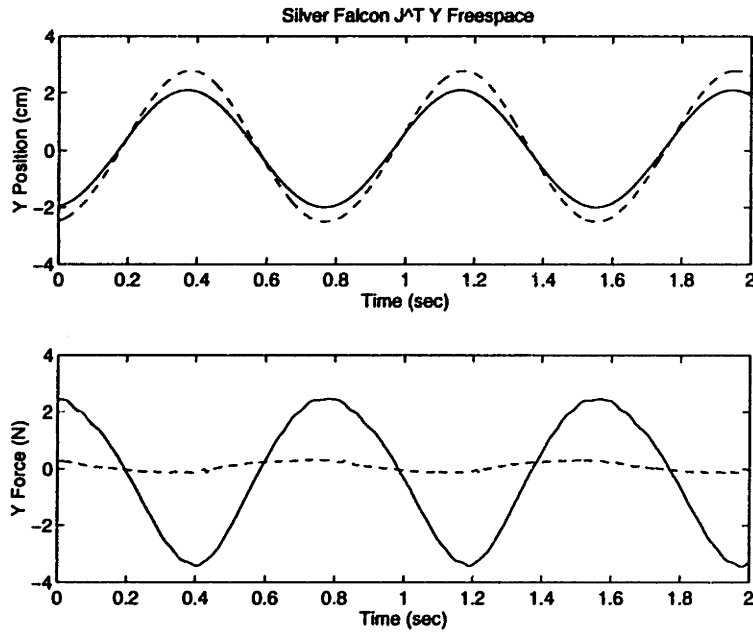
Figure 6-17: Freespace response for the Silver Falcon slave and PHANToM master in the y direction using the Jacobian Inverse controller. The solid line represents the master, and the dashed line represents the slave.
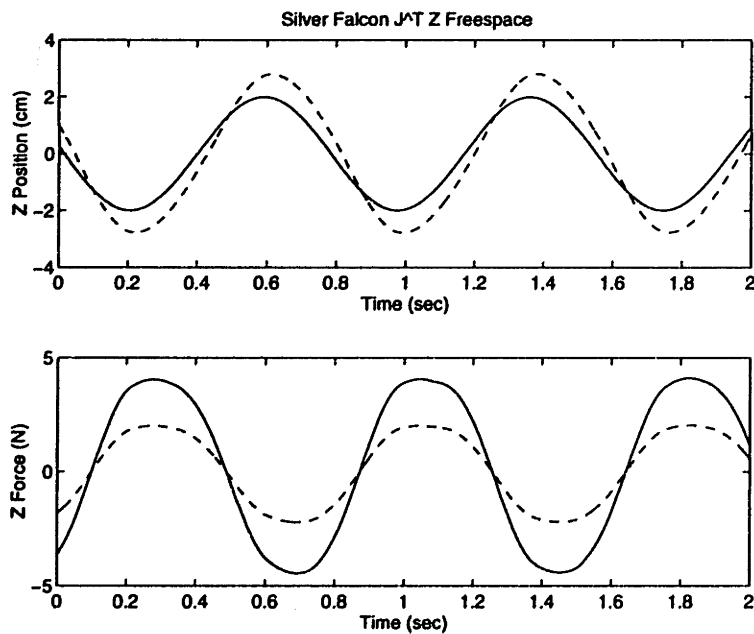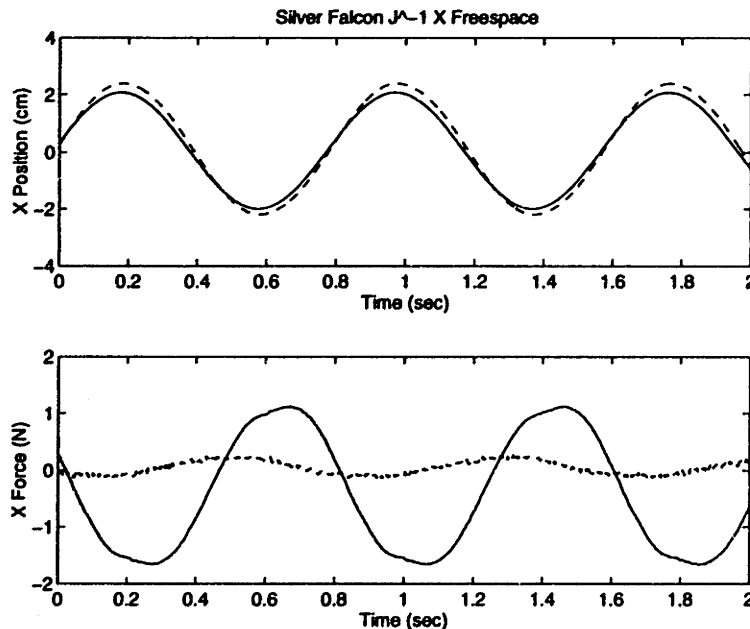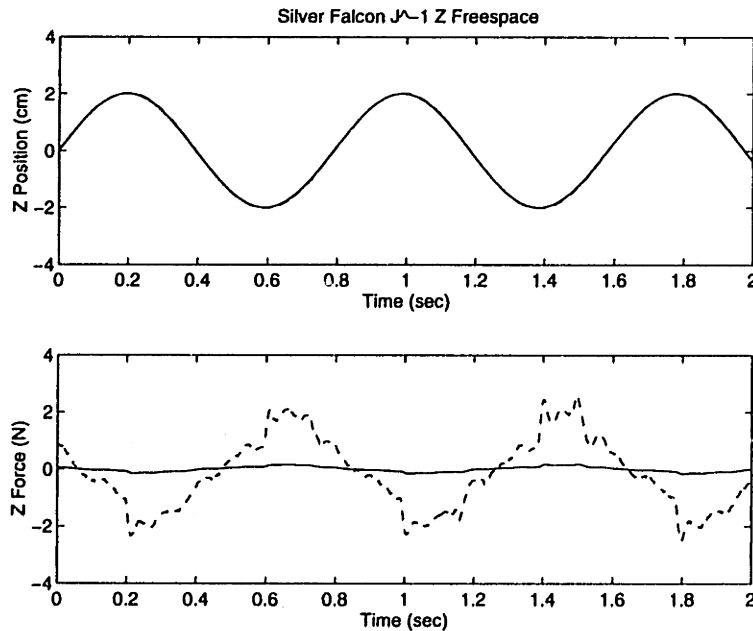
Figure 6-18: Freespace response for the Silver Falcon slave and PHANToM master in the z direction using the Jacobian Inverse controller. The solid line represents the master, and the dashed line represents the slave.
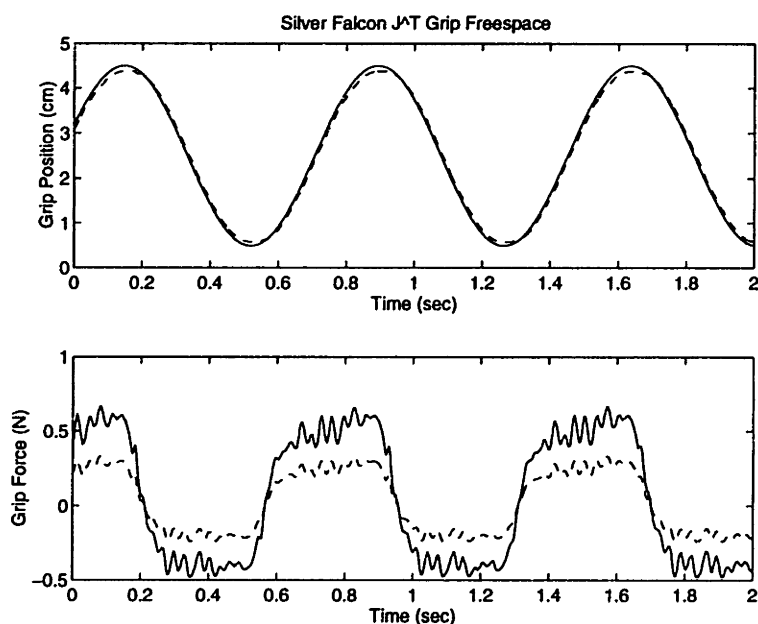
Figure 6-19: Freespace response for the Silver Falcon slave and PHANToM master for the gripper using the Jacobian Inverse controller. The solid line represents the master, and the dashed line represents the slave.

The master shows very small forces however. Because the base positioner has such good position response along joint 2, there is little tracking error. Because we rely on the wrist to provide force information, and because we do not have a micro freedom available in this direction, the only forces sensed are due to errors in the base positioner, which are small. Therefore, the controller sees very little force applied to the slave and applies very little force to the master. In the z direction, freespace motions feel very good. A lesson to learn from this is that if the positioning ability of the base positioner is very good, the freespace motions should also feel considerably better.

6.2.1.3   Gripper Freespace Response

Gripping motions are no different with either the Jacobian Transpose controller or with the Inverse Jacobian controller. In each case, because we have a one-degree-of-freedom input and a one-degree-of-freedom output, each form of control reduces to the basic force reflecting teleoperator described in Chapter 4. Of course grip forces will only be applied to the user if the actuated gripper is used. Freespace response for the gripping motion is shown in Figure 6-19. While the tracking response appears quite good in terms of magnitude, the error is closer to a square wave than a sinusoid

and there is a substantial vibration present. The square wave indicates that coulomb friction forces dominate which change direction as the velocity changes direction. The gripper dynamics are largely friction dominated because the wrist elements are so light, instead of inertia dominated as are the other axes. The vibration is caused by a repeated breaking of stiction forces.

Note that the friction force shown is between roughly 0.2 N and 0.3 N. However, we measured 0.35 N and 0.46 N in the fingers. So we would expect roughly 0.4 N of friction in the grip responses. Recall however that we are using a friction compensation algorithm which adds 0.00072 Nm of torque in motor space, which corresponds to 0.12 N at the fingertips when multiplied through the appropriate ratios. Given this, we would expect roughly 0.28 N of friction which correlates with the values in Figure 6-19.

6.2.2   Contact Responses

The contact response plots were made by moving the master by hand such that the slave moved into contact with a rigid aluminum block. As always, we use a 2:1 force scaling. Because the master is moved by hand, these plots are not precisely repeatable. Contact velocities and trajectories differ slightly between all the plots. Nevertheless, the qualitative results do not change. Repeatedly performing these contact plots results in qualitatively similar data. Each contact plot consists of freespace motion, contact, and relatively steady state application of force.

To summarize the results, in comparing the Jacobian Transpose and Inverse Jacobian controllers in the x and y directions, we find the Jacobian Inverse controller performs better during freespace motions. Based on results from the previous section, this is expected. They also differ somewhat though not strikingly during initial contact and not significantly during steady state contact.

Contact behavior in the z direction, where no micro wrist freedom exists at our chosen wrist orientation, is different than in the x and y directions. The Jacobian Transpose controller is particularly poor in freespace, but is force reflecting in the z direction. The Inverse Jacobian controller feels good in freespace, but is not at all force reflecting in the z direction.

6.2.2.1   Jacobian Transpose Controller

Figure 6-20 shows the contact response in the x direction. During freespace motion prior to contact, the force applied to the master deviates from the slave force because the user must move the slave inertia. Upon contact, the wrist tip stops against the
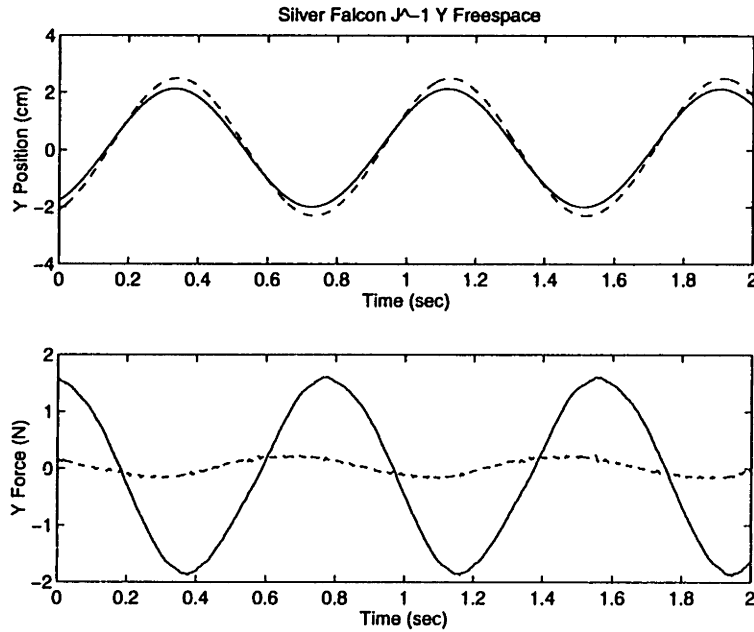
Figure 6-20: Contact response for the Silver Falcon slave and PHANToM master in the x direction using the Jacobian Transpose controller. The solid line represents the master, and the dashed line represents the slave.

aluminum block, but the slave inertia causes the base to continue moving. This causes a relatively large deflection in wrist, causing the slave force to reach 2.5 N. The inertia of the base unit bounces against the wrist servo stiffness and settles to a slave contact force of about 1 N and master force of about 2 N.

Note that in the position response, the slave does not appear to come directly to a rest during the contact, but rather has a rounded deceleration. This is in fact not the case. The slave tip comes to an abrupt stop when it hits the aluminum block as we can observe when watching the tests. However, the position is measured from encoder measurements. Therefore, the stiffness of the environment is modified by any structural flexibility in the system between the motors and the slave tip. This directly limits the crispness of the contact, and is evident in all the position response plots shown here with the exception of the gripper contact response plot in Figure 6-26.

The y direction contact response looks qualitatively similar though with less wrist deflection, possibly because of the greater friction in this axis, and because the contact speed was slower, see Figure 6-21

The z contact response looks considerably different. The freespace motion clearly requires greater forces in order to move the heavier joint 2 axis. The contact is fairly
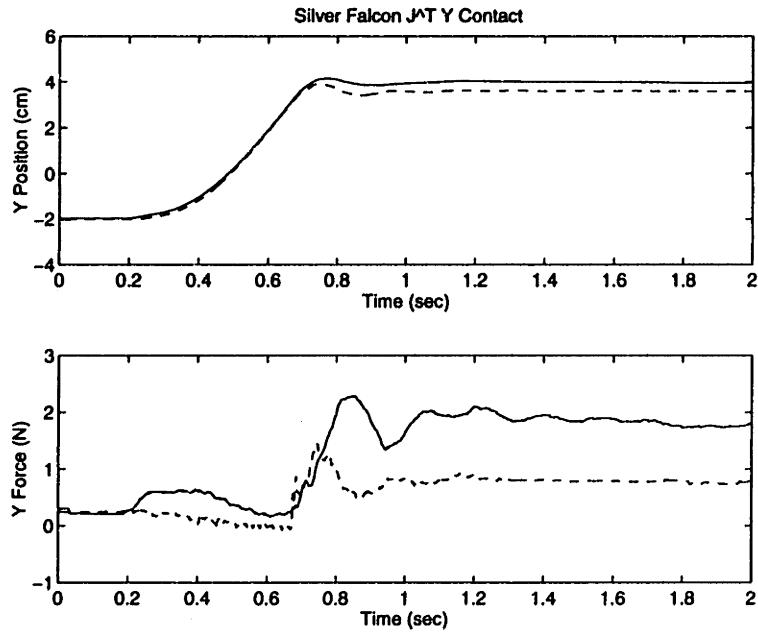
Figure 6-21: Contact response for the Silver Falcon slave and PHANToM master in the y direction using the Jacobian Transpose controller. The solid line represents the master, and the dashed line represents the slave.
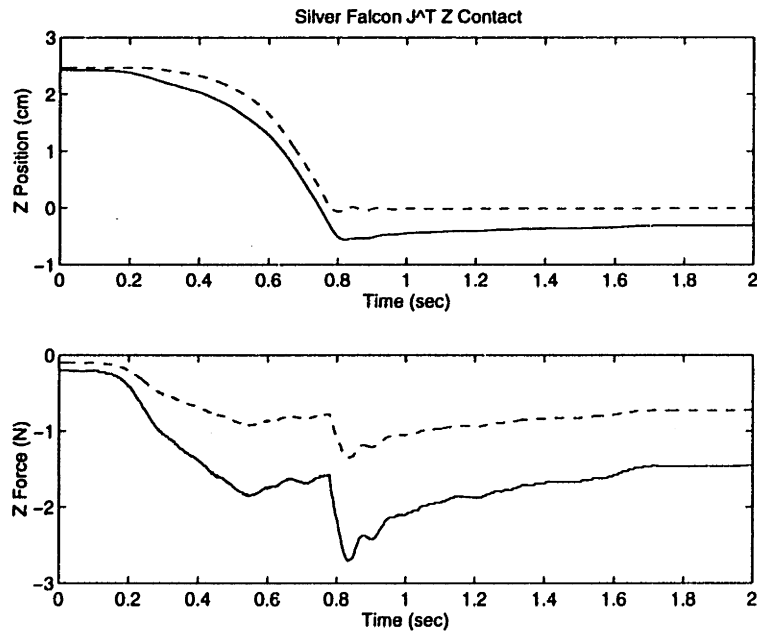
Figure 6-22: Contact response for the Silver Falcon slave and PHANToM master in the z direction using the Jacobian Transpose controller. The solid line represents the master, and the dashed line represents the slave.
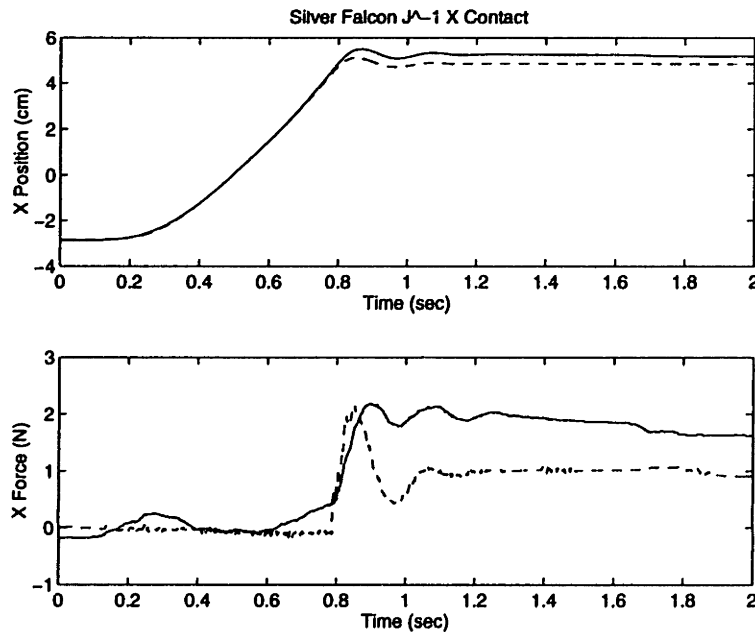
Figure 6-23: Contact response for the Silver Falcon slave and PHANToM master in the x direction using the Jacobian Inverse controller. The solid line represents the master, and the dashed line represents the slave.

sharp, but does not feel very distinct because the increase in force due to contact is only 1 N whereas 2 N of force were required just to move the slave inertia.

Note that since inertial forces required to stop the slave manipulator are not shown in these plots, and because there are no low inertia wrist elements flexing during this contact, the actual contact force is likely to be substantially higher than shown in Figure 6-22.

6.2.2.2 Inverse Jacobian Controller

The x and y direction contact plots are shown in Figures 6-23 and 6-24 respectively. These are similar to those using the Jacobian Transpose controller. There are two subtle differences. The magnitude of forces during freespace motions are slightly less, particularly in the x response, and the level of oscillation in the base position after contact is made is slightly less. These can both be explained by a reduced base inertia as felt by the master.

The z direction plots are different however, as shown in Figure 6-25. There is essentially no force reflection in the z direction. This is because there are no micro freedoms in the z direction with the wrist oriented in the zero position (with the
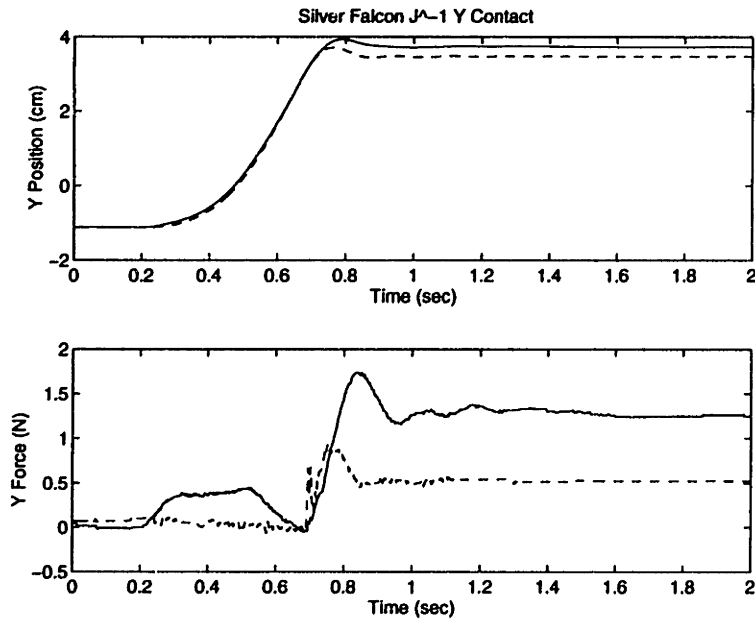
Figure 6-24: Contact response for the Silver Falcon slave and PHANToM master in the y direction using the Jacobian Inverse controller. The solid line represents the master, and the dashed line represents the slave.
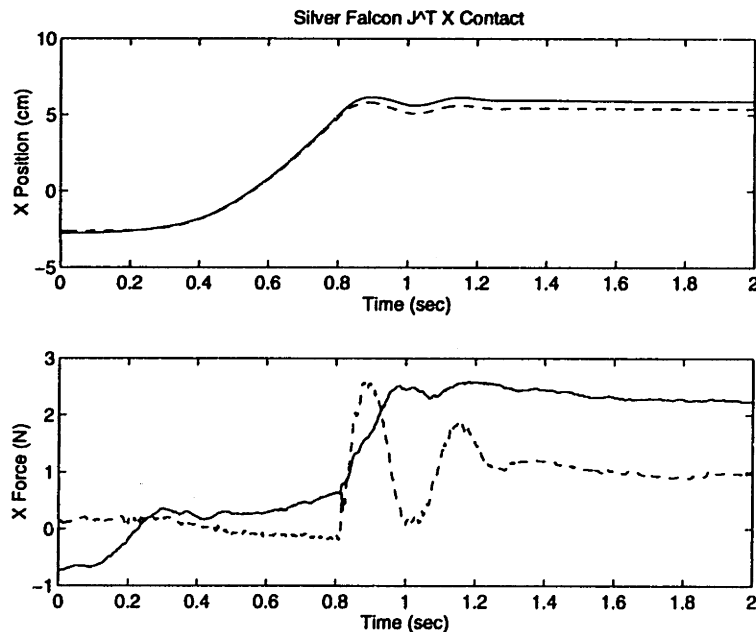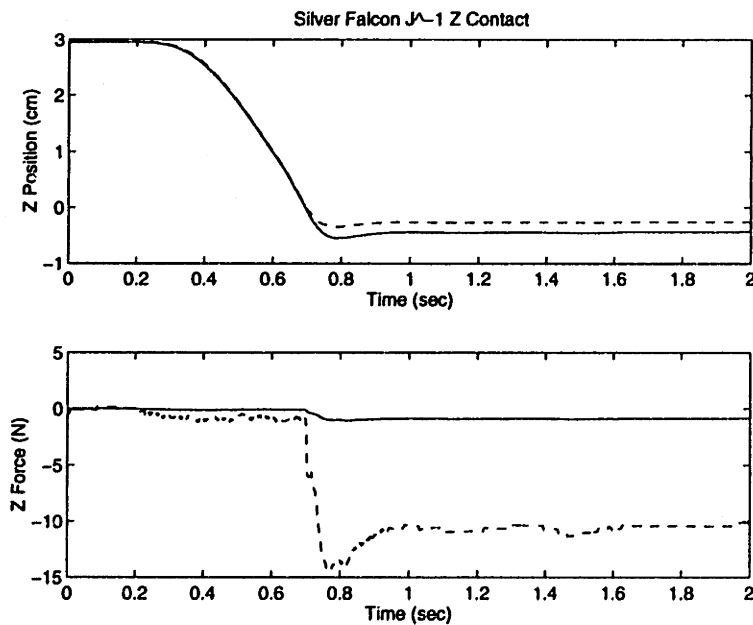

Figure 6-25: Contact response for the Silver Falcon slave and PHANToM master in the z direction using the Jacobian Inverse controller. The solid line represents the master, and the dashed line represents the slave.
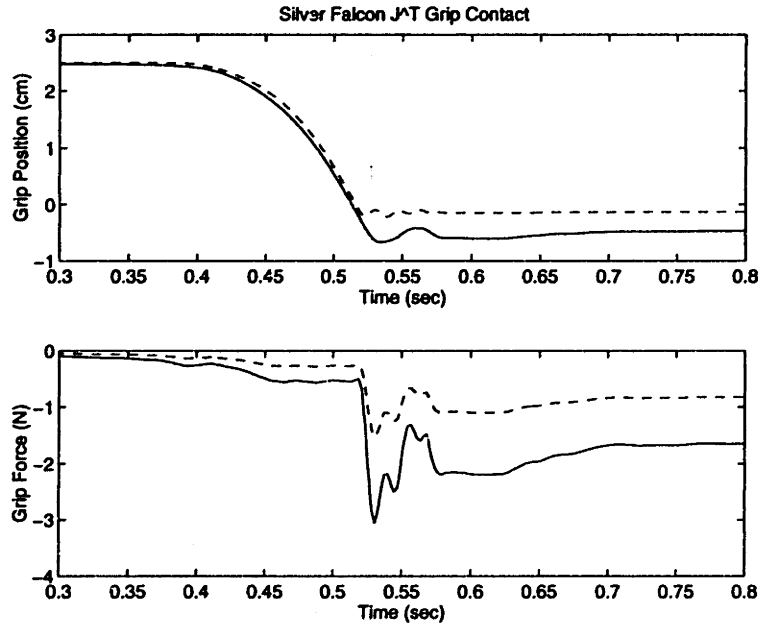
Figure 6-26: Contact response for the Silver Falcon slave and PHANToM master for the gripper using the Jacobian Inverse controller. The solid line represents the master, and the dashed line represents the slave.

fingers pointing straight down). Note that if the wrist were bent at $90°$, say by moving q_4 to $90°$, then the plot would look similar to Figure 6-23, though perhaps slightly better because the tracking performance of joint 2 is better than that of the joints 0 and 1 of the base positioner.

6.2.2.3 Gripper Contact Response

These plots show the slave gripper (joint 6) operated using the actuated gripper as a master. As we mentioned before, this is effectively the basic force reflecting teleoperator described in Chapter 4. Figure 6-26 shows the contact response. This figure shows a very quick motion. Note that the graph represents 0.5 seconds instead of 2.0 seconds as in the other graphs. When performing the test, we can visually observe that the fingers clamp together without oscillation. The plot shows a slight oscillation in the slave position response which most likely represents an oscillation between the inertia of the motor rotors and that of the servo. The actuated gripper position slightly overshoots and then settles to about -1.8 N, while the slave contact force (grip force) is maintained at half this value.

This response is probably the best feeling contact response of any shown in the

thesis. We feel a very crisp contact, as indicated by the very low forces prior to contact followed by a very sharp rise to -3 N force in roughly 10 ms.

We submit that the reason why this response feels good is that our measurement of the endpoint position of the slave is more accurate for the gripper than any other axes due to the relative lack of structural flexibility between the motors and gripper. Of course the actuated gripper is a very good master, given that it has less inertia and lower friction than the PHANToM.[2] To test whether the quality of the master, or the quality of our slave endpoint measurement improved the quality of the contact, we performed a qualitative experiment. The PHANToM x axis and the actuated gripper were swapped so that the PHANToM controlled gripping, y, and z slave motions, and the actuated master controlled the x motion of the slave. Both were programmed with the same stiffness gains (480 N/m). Now x contact was felt with the actuated gripper, and gripping contact was felt with the master. The grip contact, felt through the PHANToM, still felt good, whereas the x contact, felt through the actuated gripper, felt much as it did before. It appears as though the inertia and structural flexibility of the slave are more to blame for the lack of crispness in the force contact responses than is the quality of the master.

6.2.3   Discrimination Tests

With the wrist in its zero position (the fingers pointing straight down), we measured the ability to distinguish small forces. These tests were done using the Inverse Jacobian controller, which we felt to be our best controller. We attached a string to our digital force gage and gripped a loop tied in the other end of the string with the gripper jaws. I then moved the master so that the slave moved in the x, y and z directions until I just began to feel a force indicating that the string had become taught. My eyes were closed. The force levels were then recorded. This represents the smallest force which I could distinguish above the freespace forces. Six measurements were made in each direction and the values averaged. The values were:

$$f_{dx} = 0.23 \text{ N}$$
$$f_{dy} = 0.26 \text{ N}$$
$$f_{dz} = N.A.$$

In the z direction, the string slipped out of the fingers above 3 N without ever feeling any force at the master. This is expected since we have previously shown there is essentially no force reflection in a direction pointing directly into the fingers, and with

---

[2]Things become easier when you're working with only one degree of freedom.

the fingers pointing downwards, this corresponds to the z direction.

These values seem to correlate with the lowest values of static friction measured in these directions, which were 0.19 N in the x direction, and 0.20 N in the y direction.

6.3 Summary

The Silver Falcon provided us with a testbed to study a number of issues in teleoperation for MIS surgery:

- We tested and confirmed the feasibility of using a cable actuated wrist as an end effector suitable for MIS surgery.

- We found that the double parallelogram remote center kinematics works well to provide a remote center of rotation without using additional redundant joints.

- It is possible to use a kinematically dissimilar master and slave in conjunction with a cartesian controller.

- We found that macro-micro control works but requires a wrist with more degrees of freedom if we are to feel forces in all three directions. Using our roll-pitch-yaw wrist, motions in the direction of the fingertips do not have a micro freedom available.

- The standard Jacobian Transpose method of cartesian control simply transmits too much inertia to the user via the master to be useful.

- The Inverse Jacobian controller reduces the slave inertia transmitted to the surgeon via the master, but relies on having lightweight and low friction micro freedoms to provide force feedback.

- Force scaling is possible, but the force scale factor is limited largely by friction in the slave wrist. We used a force scale factor of 2:1 in all the results given in this chapter.

- Building the Silver Falcon gave us experience with a number of practical design issues including motor sizing, cable friction, bearing friction, motor brush friction, encoder resolution, and structural design.

There are a number a number of areas which call for improvement:

- We need to add a degree of freedom to the wrist if we intend to achieve 3 directions of macro-micro force feedback.

- The grip force was insufficient to securely hold needles. This is a fundamental practical issue, and must be addressed in a new system.

- A system used in the operating room will need interchangeable tools and instruments. This is a severe constraint and we need to study how this will affect the overall design.

- The structural rigidity must be improved, both of the main base unit and of the wrist unit.

- The base unit axes (0 and 1) should be designed for improved tracking performance.

- For safety, the system should be counterbalanced. In the event of a complete system shutdown with no power, the system should not move on its own. Because the slave may be tilted above a patient, it is difficult to design a spring counterbalance that will compensate for this reorientation. The most straightforward solution is gravitational counterbalancing.

Chapter 7

The Black Falcon Teleoperator Slave

This chapter presents a design description of the Black Falcon teleoperator slave. The Black Falcon incorporates lessons learned from designing and testing the Silver Falcon. The primary issues we addressed were allowing interchangeable tools, gravitationally counterbalancing the system, designing a wrist which would allow full three-degree-of-freedom macro-micro control, and increasing the overall size, rigidity and strength of the system. Below is a brief description of these features. A photo of the Black Falcon is shown in Figure 7-1.

7.1 Summary of Changes

- A similar remote center linkage was used on the Black Falcon as was used in the Silver Falcon.

- In order to counterbalance the system, we relocated all of the system motors to locations below the center of the main gimbal. The mass of the entire structure is arranged to be counterbalanced when the wrist unit is midway in its stroke.

- The wrist unit is now designed to be detachable. It is not however "quick-release" in any sense; it takes several minutes to unscrew it from the main unit. But this still allows new wrist designs and other instruments to be developed for the same system as part of future research projects.

- In order to allow macro-micro control in all three directions, a four-degree-of-freedom wrist was designed for the Black Falcon. To accommodate this wrist,
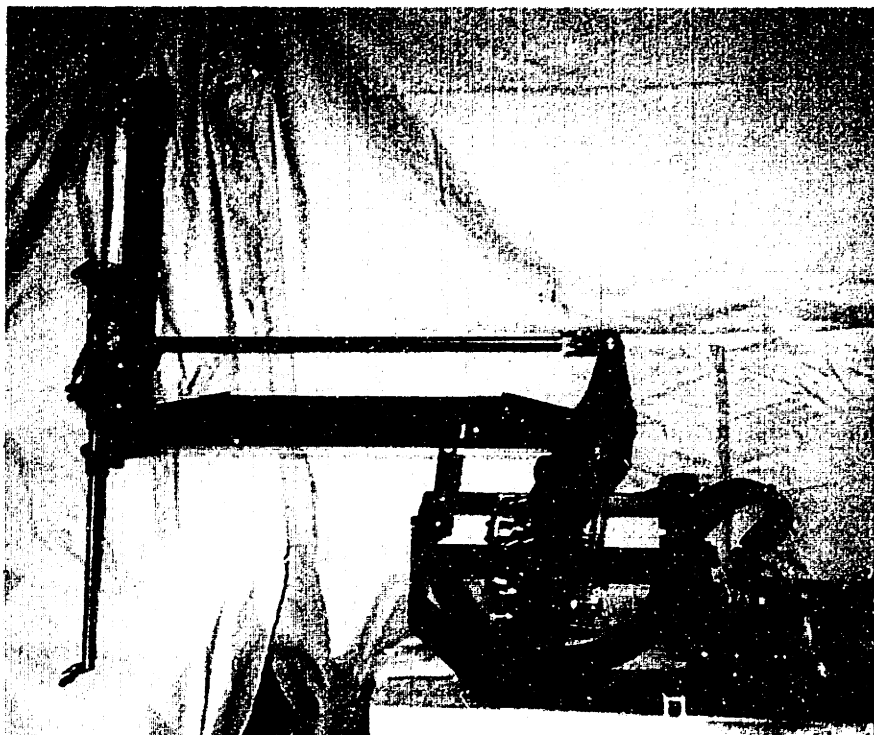
Figure 7-1: The Black Falcon

the overall system has 8 powered degrees of freedom instead of seven.

- The Black Falcon is structurally stiffer with higher actuator capacity than the Silver Falcon.

- The carriage which carries the wrist unit uses a much improved bearing and support structure design. It is structurally stiffer, has lower friction, and has a higher load capacity.

- The range of motion of the main pitch and yaw axes of the base have been increased roughly 15 degrees to ±60 degrees and ±80 degrees respectively.

- Grip force of the fingers has been increased to a maximum of 240 N (11.1 lbs). The Silver Falcon fingers did not have sufficient grip force to securely hold needles. While it was sufficient to test the primary concepts, actual surgical work was not be possible. The needle would often roll in the grip of the Silver Falcon, much to the frustration of surgeons using the system. The Black Falcon has no difficulty securely holding needles during suturing.

- Unfortunately, the added cabling and larger motors contribute to increased friction in the system.

- However, by modeling the Maxon RE035-071-034 motors with high resolution Canon TR36 laser encoders (14400 counts/rev), a friction compensation algorithm was developed which reduced brush friction by a factor of roughly four.

7.2 Black Falcon Design Description

7.2.1 Mechanism Overview

The following is an overview of the system, and more details will follow in subsequent sections. The Black Falcon consists of a two main subsystems, a base unit and a wrist unit. However, unlike the Silver Falcon, the base unit contains all of the actuators for the entire system and provides a mechanical interconnect for the wrist unit, which is a passive detachable instrument. The following components are referred to in Figure 7-2, and the kinematic structure including axis and link numbers are defined in the schematic drawing Figure 7-3. Note that the 8 joints are labeled 0-7. The system is grounded through a "U"-shaped base. A spindle, link 0, rotates within this base about axis 0. Motor M0 actuates this axis using a cable drive similar to that in the Silver Falcon. Link 1 rotates about axis 1 within the spindle. Link 1 holds motors M1-M7.
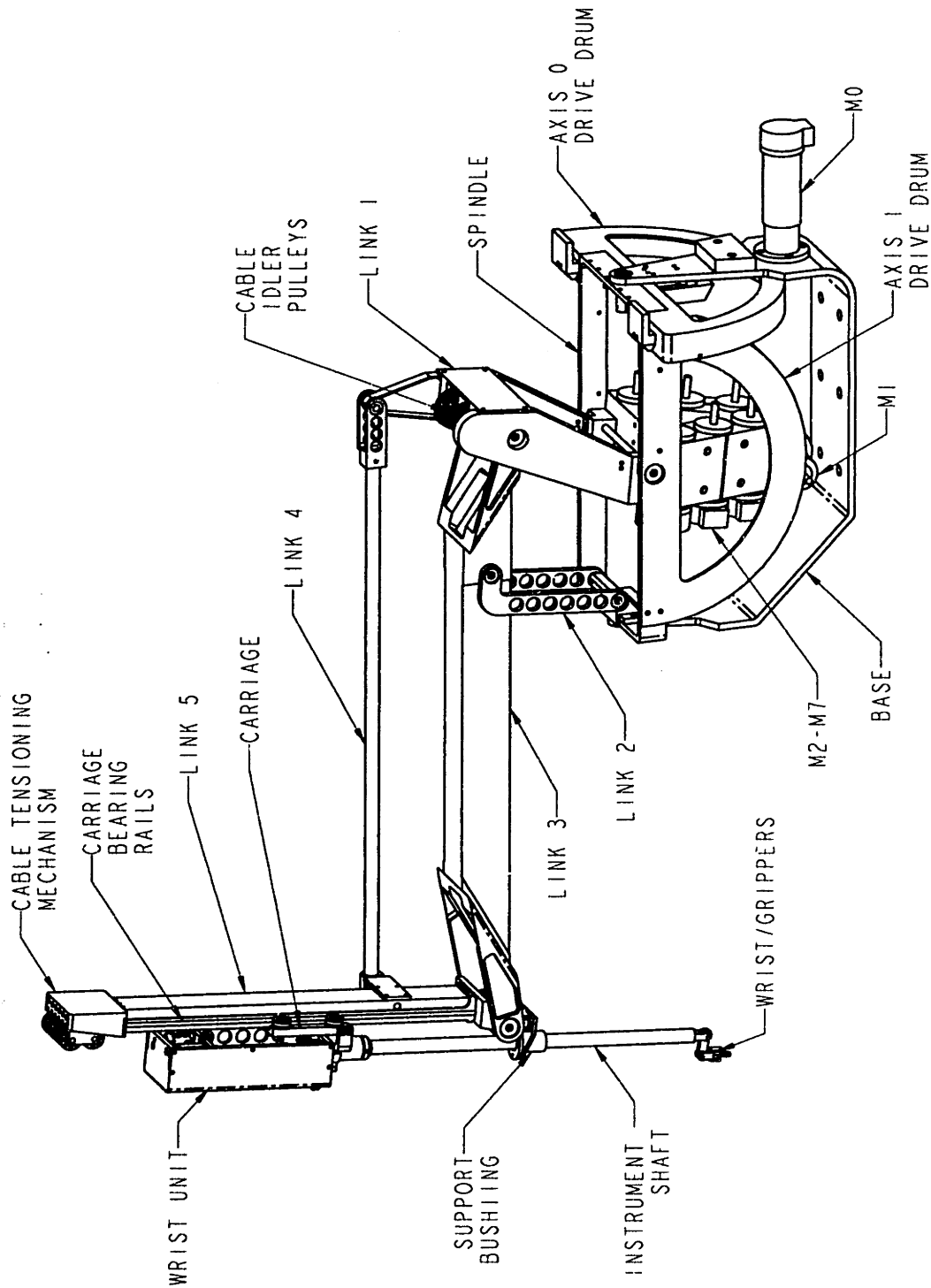
Figure 7-2: The Black Falcon consists of a counterbalanced base unit which carries all the motors for the system. A vertical carriage carries a detachable wrist unit which carries the end-effector.
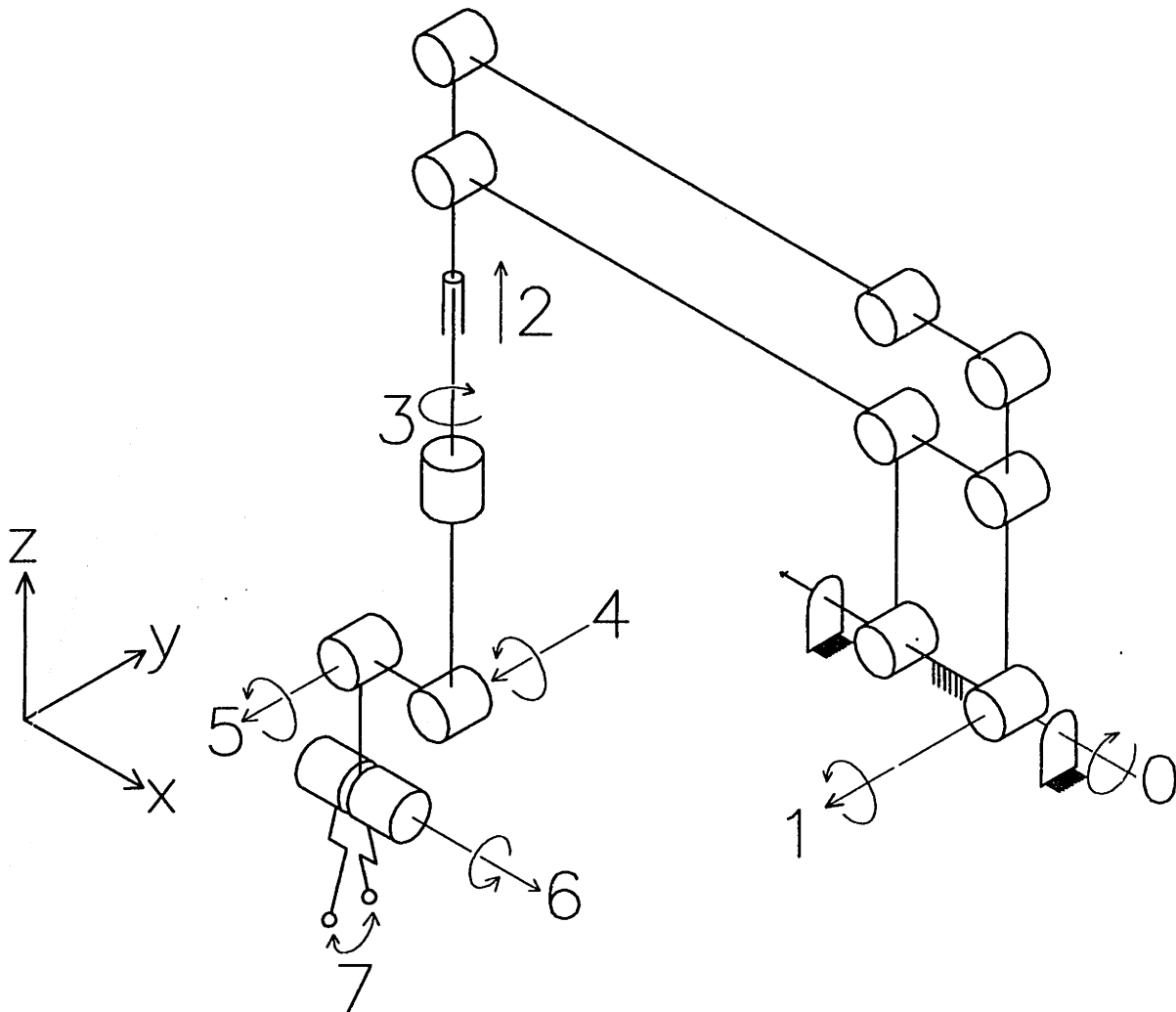
Figure 7-3: The Black Falcon base kinematics are similar to those of the Silver Falcon. However the wrist can now be interchanged, so the system can be redesigned with different wrist kinematics in the future. The current wrist has four degrees of freedom and is designed to allow macro-micro control in all three linear degrees of freedom. The joint orientations shown are referred to as the "zero" position of the manipulator. Note that we define all joint positions relative their its proximal link *except* joint 5, which is defined relative to ground.

Motor M1 drives axis 1 using a cable drive similar to axis 0. Motors M1-M7 are all mounted within link 1. The remote center kinematics are formed by links 1-5. Links 1, 3, and 5 are the main structural members, while links 2 and 4 act in tension and compression. Link 5 holds two bearing rails on which a carriage rides. The carriage holds the wrist unit which comprises a mechanical attachment, an instrument shaft, and an end-effector consisting of a wrist and grippers.

7.2.2   Base Unit

7.2.2.1   Remote Center Kinematics

We use a similar double parallelogram linkage to form a remote center of rotation, as in the Silver Falcon. However, there are offsets in the links now which allow us to place the carriage and link 5 behind the remote center (towards the base) in order to give room for the wrist unit.

7.2.2.2   Range of Motion and Workspace

The Black Falcon can pitch forward and backward about axis 1 by ±60 degrees, as shown in Figures 7-4 and 7-5. It can also yaw about axis 0 by ±80 degrees. Soft stops made from aluminum covered with soft foam rubber have been designed into these two main base axes as a safety measure.

The Black Falcon has a stroke of 20 cm (8 in) with the current version of the wrist unit, and a total carriage travel of 25.4 cm (10 in). The overall workspace is then a cone with an elliptical cross section, which has been truncated with a spherical bottom and top, see Figure 7-6. The centers of the spheres are at the remote center. The radial distance between spheres is the stroke. The location of the truncating surfaces depends on the length of the instrument. For example, if the instrument is shorter, we can access nearer to the remote center. We cannot effectively use the area near the remote center however, because of course the manipulator is singular there. The current wrist unit uses a 38 cm (15 in) instrument shaft which can operate from 3.8 cm (1.5 in) to 24 cm (9.5 in) from the remote center.

7.2.2.3   Structure

The structure has been made substantially more rigid. For example, the Silver Falcon link 3 was 1 in diameter aluminum round tubing with 0.035 in wall thickness, whereas the Black Falcon link 3 is 2 in aluminum square box tubing machined to 0.050 in wall
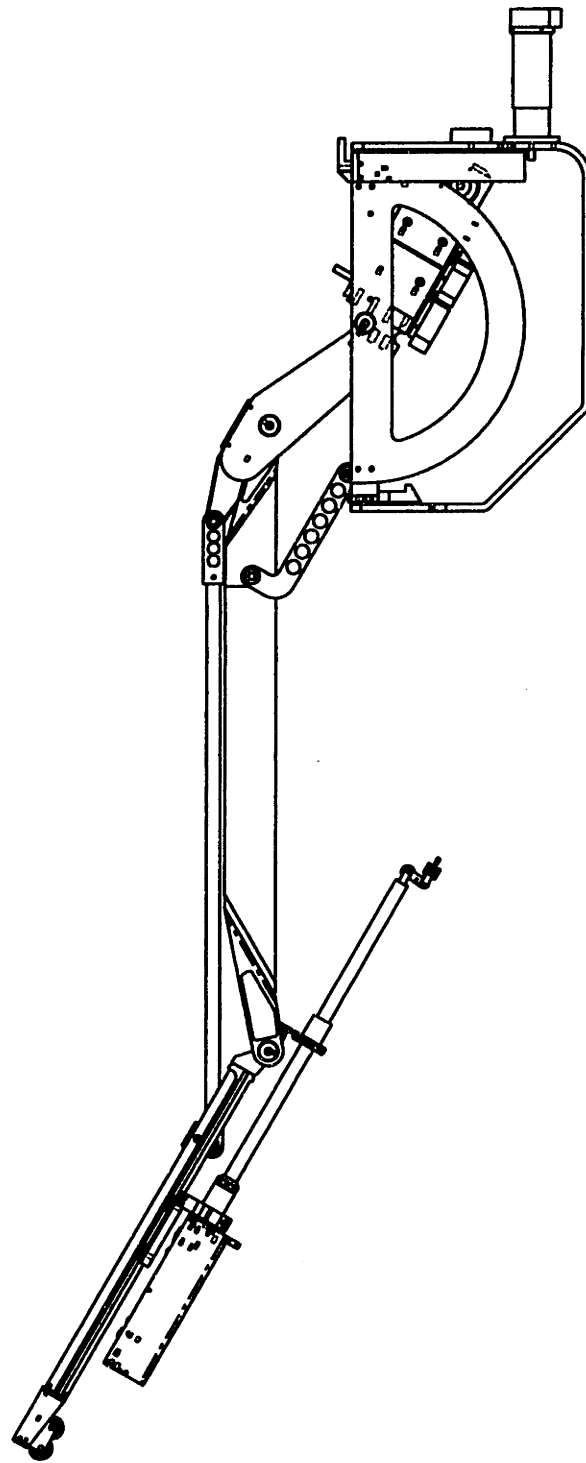
Figure 7-4: The Black Falcon can pitch 60 degrees forwards.
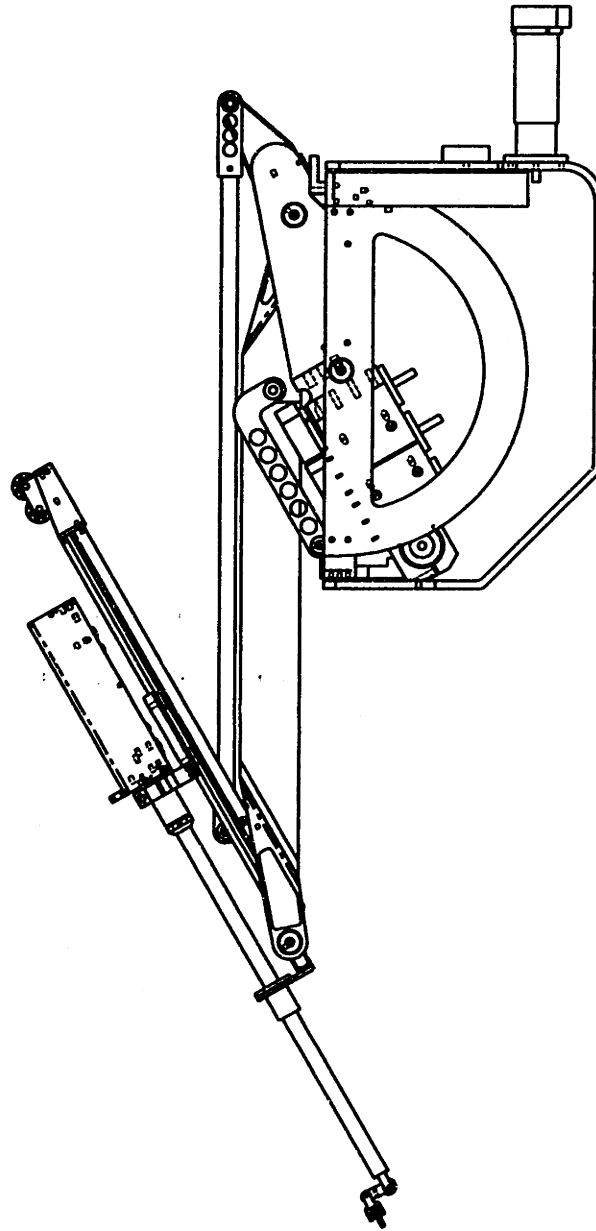
Figure 7-5: The Black Falcon can pitch 60 degrees rearwards. The motors are placed such that they form a "V" which straddles link 3 in order to maximize the rearward pitch angle while still allowing the weight to be placed where it can counterbalance the system.
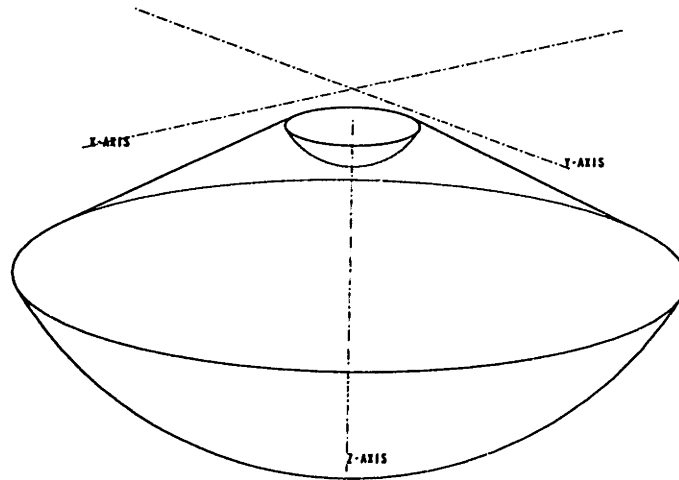
Figure 7-6: The workspace is a elliptical cone truncated with spherical bottom and top surfaces. The axes shown intersect at the remote center.

thickness. The pivot forks at the end of link 3 have been welded since we found much flexing in the bolted connections of the Silver Falcon. Link 5 is 1 in×1.5 in aluminum square tubing machined to 0.050 in wall thickness.

This beam is 23 in long with pivots connecting it to links 1 and 2 at a distance of 5.5 in apart. To calculate stiffness at the end where link 5 is attached, we assume the link 1 and 2 pivots are simple supports. The deflection δ at this end in response to a force P is given by:

$$\delta = \frac{Pa^2(a + l)}{3EI} \tag{7.1}$$

where in this case $a = 5.5$ in, and $l = 17.5$ in. The tube is 1.85 in×1.85 in (machined down from 2 in square) with a 0.050 wall thickness, so the area moment, I is given by:

$$(1.85^4 - 1.75^4)/12 = 0.0195 \text{ in}^4 \tag{7.2}$$

Given a modulus of elasticity for aluminum, E, of 10.3×10^6 psi, we find:

$$\delta = 0.00117P \text{ in} \tag{7.3}$$
$$k = 3800 \text{ lbs/in} = 150,000 \text{ N/m} \tag{7.4}$$

For example, a 2 lb endpoint force gives a 0.0023 in deflection.

Link 1 consists single aluminum block which houses the 7 motors M1-M7, with 2 aluminum uprights bolted to it. The cable idler pulleys noted in Figure 7-2 are mounted to a piece which braces the two uprights across their backs to add structural stiffness, see Figure 7-7.

We measured stiffness of the base structure by measuring the force (Wagner Force Dial, model FDK 160, Mark 10 Model BG2) required to deflect the end of link 3 by 1/8 in with the base held fixed. It was difficult to measure any deflection in the x direction. Because of the small distances over which forces could be applied, we can expect accuracy of these values to only about 20%.

$$k_{BY} \cong 5500 \text{ N/m} \tag{7.5}$$
$$k_{BZ} \cong 12000 \text{ N/m} \tag{7.6}$$

Humans find a stiffness of 25,000 N/m indistinguishable from being infinitely rigid, so this is ideally the number we might hope to achieve for the overall system including structural stiffness and servo stiffness of the slave and master. Practically, we would be happy to achieve a total stiffness on the order of 2000 N/m.

7.2.2.4 Base Actuators

The Black Falcon base axes are powered by motors M0 and M1 which are Maxon brushed d.c. servomotors (RE035-071-034) with 4.8:1 planetary gearheads. The additional cable and drum reduction adds approximately 29× reduction to give a total reduction of 137.92:1 for joint 0 and 137.41:1 for joint 1. (The slight difference is caused by manufacturing tolerance.) We typically measure speed reduction by measuring the output link angles using a digital level (Macklanburg-Duncan Pro SmartLevel) and comparing these with encoder readings for five or so points within the range of motion and taking a least squares fit of the results.

One problem with the Silver Falcon was the servo response of the base axes was underdamped due to a lack of encoder resolution and insufficient speed reduction. However, the Black Falcon was designed such that the base actuator rotor inertias were roughly matched to the output load inertia. That is:

$$R \cong \sqrt{\frac{I_{axis0}}{I_{rotor}}}$$

Of course, the inertia about axis 0 varies as axis 1 is moved through its workspace, so it

is impossible to match these inertias in all configurations. Using a ProEngineer™ model of the system, we found the inertia of the system about joint 0 when link 5 is vertical, not including motor inertia, to be 0.183 kgm^2.[1] When the system is pitched rearward by 60° , the inertia is 0.051 kgm^2. The motor rotor inertia is 6.96×10^{-6} kgm^2. Using these two values, we find the reductions required to match the link and rotor inertias at these two configurations to be:

$$R = \sqrt{\frac{0.183}{6.96 \times 10^{-6}}} = 162 \tag{7.7}$$

$$R = \sqrt{\frac{0.051}{6.96 \times 10^{-6}}} = 86 \tag{7.8}$$

$$\tag{7.9}$$

The average of these values is 124. Due to packaging constraints, we made the ratio slightly larger, at 137:1.

We will give experimentally measured inertias for all axes in Section 8.1.4. But we note here that the total joint 0 inertia (link inertia + reflected rotor inertia) calculated using ProE is equal to 0.315 kgm^2 when link 5 is vertical, and the measured joint 0 inertia is 0.32 kgm^2, which gives us confidence in the experimentally measured values and in our CAD system model.

The larger speed reduction also increases effective encoder resolution. On the base axes, we used Hewlett-Packard 5500 series optical encoders with 4096 counts per revolution (after quadrature). With a 137:1 speed reduction, this gives 561,152 counts per joint revolution, or an endpoint resolution of 1.57×10^{-6} m when the instrument shaft is 0.140 m below the remote center, which is the middle of its stroke. The positioning response is excellent as we will see in Section 8.1.5.

7.2.2.5 Wrist Unit Actuators

Figure 7-7 shows link 1 which houses motors M1-M7. The end-effector actuators are all placed within link 1. We use Maxon RE-035-071-034 brushed d.c. motors with Canon TR36 laser encoders. These encoders have 14400 counts per revolution (after quadrature).

Each of the six motors which drive the wrist unit axes is mounted with a threaded drive capstan. The capstan has a flexure clamp manufactured into it to clamp it to

---

[1]This design was done using ProEngineer CAD software, Parametric Technology Corporation, Waltham MA.
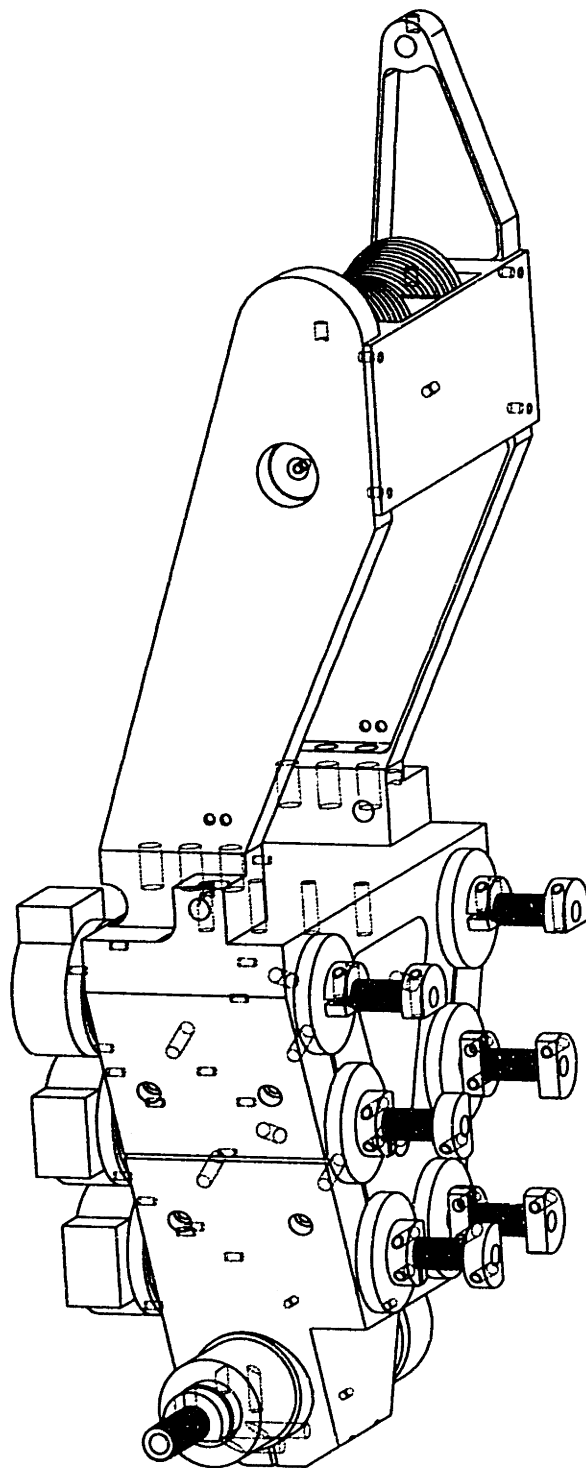
Figure 7-7: Link 1 clamps 7 of the 8 motors in a block machined from a single piece of aluminum. A triangular water-cooled counterweight fits into this piece. Two vertical uprights and a pulley support piece form the remainder of the structure. Each motor is fitted with a threaded cable drive capstan.
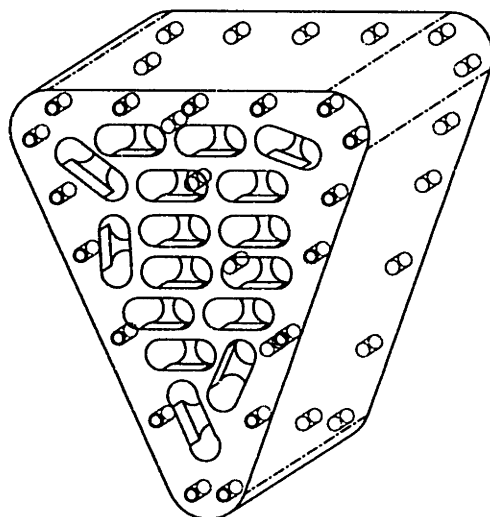
Figure 7-8: The counterweight incorporates radiator like passages for water cooling. It is copper for high thermal conductivity, and use two end plates to form a single continuous water channel.

the motor shaft. There are flats and screws at each end of the clamp which allow the cable to be terminated on the pinion at each end. The cable is then wound towards the center of the pinion from each end in opposite directions and comes off of the pinion at essentially the same location along the length of the pinion. In this way, slippage on the pinion is impossible, and the extra length required to maintain frictional wraps on the pinion are eliminated. The cable used on these axes is 0.024 in diameter 7×19 construction, stainless-steel cable (Sava Industries, Riverdale, NJ). The motors are placed parallel to one another. This is actually very convenient and allows all the drive cables to emanate from the rear of the link. This works very well with the base cabling scheme which will be described in Section 7.2.2.6.

The motors nearly gravitationally counterbalance the system. To complete and tune the counterbalancing, we placed an additional copper weight of 0.95 kg (2.1 lbs) inside link 1. The weight can be moved forward and backward for tuning. The weight incorporates water cooling passages in order to cool the motor block in link 1, see Figure 7-8. Since the motor block is a single piece of aluminum and covers the entire length of the motors, it provides a good heat sink, and can be cooled using the copper counterweight.

The Maxon motors use a rotor which consists of a wire basket set in epoxy. While this gives a low mechanical inertia, it also gives a low thermal inertia making the

motors prone to overheating. By water cooling the motors, we can optimally get a factor of four improvement in thermal power dissipation. At stall, this corresponds purely to I^2R losses in the rotor and therefore gives a factor of 2 improvement in maximum continuous torque output. We can see this with a simple calculation based on values from the Maxon Motor catalog. Let:

$$
\begin{aligned}
\delta_R &= \text{rotor temperature} \\
\delta_{Rmax} &= \text{max rotor temperature} \\
\delta_U &= \text{ambient temperature} \\
R_{TH} &= \text{total thermal resistance (rotor + ambient)} \\
R_R &= \text{rotor to housing thermal resistance} \\
R_A &= \text{housing to ambient thermal resistance} \\
r_R &= \text{rotor electrical resistance} \\
P_J &= \text{power} \\
I_R &= \text{motor rotor current}
\end{aligned}
$$

and using the following values:

$$
\begin{aligned}
\delta_{Rmax} &= 155°\text{C} \\
R_R &= 2.0°\text{C/W} \\
R_A &= 6.2°\text{C/W} \\
r_R &= 2.07\ \Omega
\end{aligned}
$$

We find:

$$
P_J = \frac{\delta_R - \delta_U}{R_{th}} \tag{7.10}
$$

$$
P_J = \frac{155°\text{C} - 25°\text{C}}{8.2°\text{C/}W} = 15.8\ \text{W} \tag{7.11}
$$

The maximum continuous motor current is then:

$$
I_R = \sqrt{P_J/r_R} = 2.77\ \text{A} \tag{7.12}
$$

which is slightly higher than the experimentally determined catalog value of 2.15 A. If we maintain the shell of the motor at 25°C, then the thermal resistance is just R_R and we have:

$$
P_J = \frac{155°\text{C} - 25°\text{C}}{2.0°\text{C/W}} = 65\ \text{W} \tag{7.13}
$$

$$I_R = \sqrt{\frac{65}{2.07\ \Omega}} = 5.6\ \text{A} \qquad\qquad (7.14)$$

Which represents an approximately $2\times$ increase in continuous torque output.

7.2.2.6 Base Cabling Scheme

We now describe the cabling scheme for each of the 6 motors M2-M7 which lie parallel to each other in link 1. Each of these motors drives a single cable loop. Figure 7-9 shows how this works for one motor. The loop begins by terminating on the motor pinion at point A. The cable continues upwards passing over pulley P1 and under pulley P3. It continues forward and passes under pulley P5, over pulley P7 and is brought forward by pulley P8. It then returns around pulleys which lie next to the pulleys it originally passed over, pulleys P6, P4, P2 and finally terminates on the motor pinion at point B. Pulleys P3 and P4 lie along a shaft which forms the pivot between links 1 and 3, and pulleys P5 and P6 lie on the shaft which forms the pivot between links 3 and 5. Pulleys P7 and P8 are fixed relative to each other, but can translate along link 5 in order to tension the cable loop. Pulleys P1 and P2 ride on a shaft which is fixed to link 1. Finally, the motor is also fixed to link 1. The nice feature of this cabling scheme is that as the system pitches forward about axis 1, there is no length change in this cable loop and no coupling between this motion and the motor rotation. [2]

In order to drive the wrist unit, a direct attachment is made between one side of the cable loop between pulleys P5 and P7. We will further describe this below in section 7.2.3.3 after first describing the carriage and wrist unit.

7.2.2.7 Carriage

In the Silver Falcon, we designed the bearing system used in the linear axis using Thomson ball bushings riding on 1/4 in diameter steel shafts. This system had several problems. The rigidity of two shafts running parallel to one another is low. Furthermore, the Thompson ball bushings have a dynamic load capacity of only 42 lbs. The Hertzian contact stresses between the balls and the shafts is particularly high in this case because the small balls ride on opposing curvature cylindrical shafts. The friction increases noticeably with loading. Finally, the bearing balls are exposed and

---

[2] A similar method of maintaining constant cable length through a parallelogram linkage was used in early mechanical master-slave teleoperators, such as the M8, in the mid 50's, (Vertut and Coiffet, 1986)
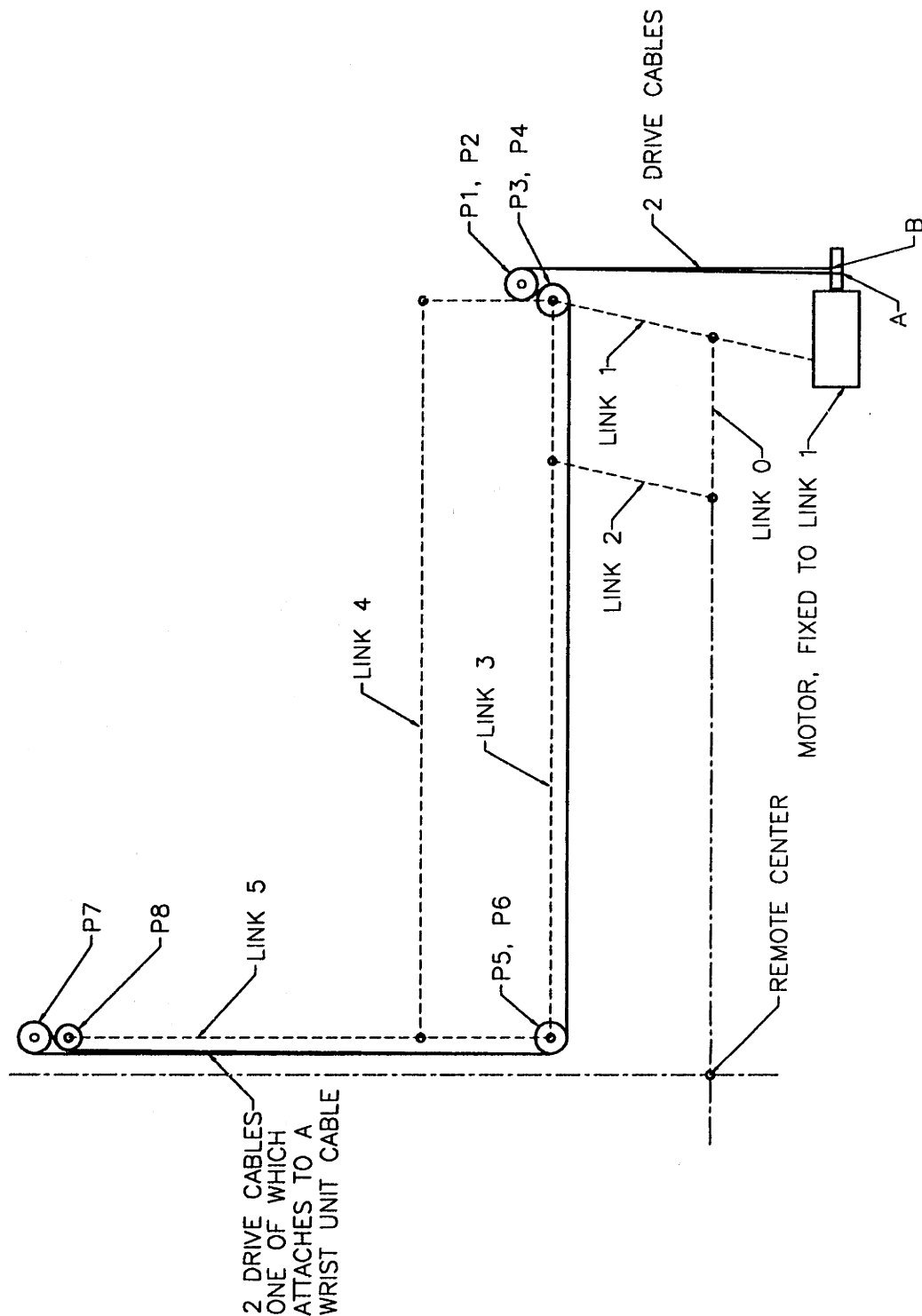
Figure 7-9: The cabling scheme for the base unit allows it to pitch forward and backward without moving the cables relative to the carriage. As a result there is no coupling between the base motion and that of the wrist degrees of freedom. The solid line represent mechanical cables, and the dashed lines represent the structure.

are prone to pick up debris or dust on the shafts as they roll by. As a result, they tend to gum up with age.

The new carriage for the Black Falcon uses a different bearing system, see Figure 7-10. Two 4 mm stainless steel rails are mounted in square slots machined into the sides of link 5 to provide bearings ways. The carriage itself uses four INA roller bearings mounted on studs (Part Numbers: LFR 50/5, KDD-4, LFZ 5, LFE 5-0.5) which ride on these steel rails. Two of the four studs are eccentric so that the bearings may be preloaded against the steel rails. The bearings themselves are shielded, so that dirt and dust do not interfere with rolling of the balls within them, and lubricant is retained. The curvature between the INA bearing outer races is designed to match the rails in order to reduce contact stresses. Each of the four bearings has a dynamic load capacity of 269 lbs. The aluminum tubing which comprises link 5 (the carriage beam) is machined from $1 \times 1.5 \times 1/8$ in wall aluminum extrusion and is exceedingly stiff in torsion and in bending. [3]

The carriage uses a simple flexure clamp to hold the wrist unit in place. It is designed so that cables run parallel to each other through a space between the carriage and the carriage beam. Finally, the carriage beam has a support mounted to the bottom of it to support the slender wrist shaft. The support incorporates a Teflon bushing to reduce friction between the two.

7.2.3 Wrist Unit

The wrist unit is shown in Figure 7-11. It is a separate assembly which can be detached from the base unit. The cables which drive the wrist form closed pretensioned loops within the wrist unit. The cables are mechanically attached to the base unit cables when the wrist unit is mounted onto the base unit. This attachment is made using simple screw clamps. It is by no means "quick-release", as it takes several minutes to make the attachment.

7.2.3.1 Wrist Kinematics

Figure 7-12 shows a four-degree-of-freedom wrist developed to improve the use of macro-micro control with the Black Falcon.[4] The wrist is essentially a roll-pitch-

---

[3] This bearing arrangement was suggested to the author by Steve Blumenkranz of Redwood City, CA. Thanks Steve!

[4] Note that it is of course possible to use a three degree-of-freedom wrist unit with the Black Falcon if desired, such that the kinematics become the same as those for the Silver Falcon, for example.
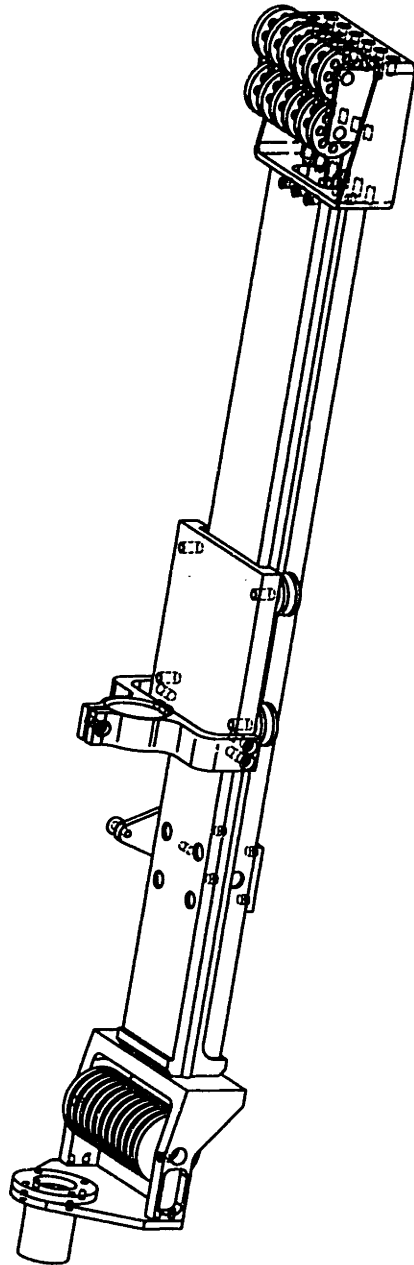
Figure 7-10: The wrist unit is supported on a carriage. This carriage is mounted on INA roller bearings which run on 4 mm steel shafts mounted into grooves machined the carriage beam, which is constructed of machined aluminum box tubing and welded to the lower fork.
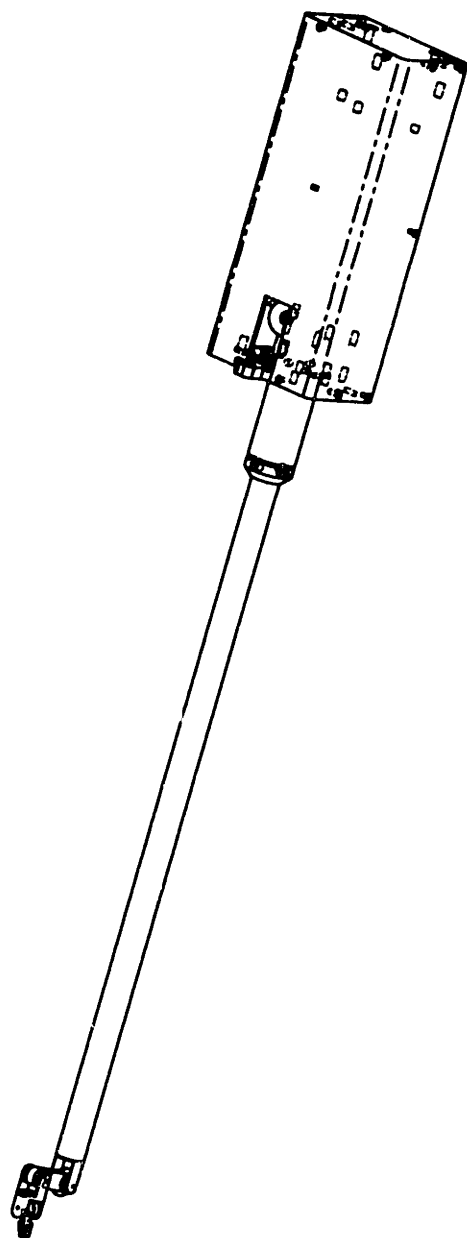
Figure 7-11: The wrist unit is a detachable assembly which clamps to the carriage. The cables directly align with the cables on the main unit and clamp to those cables for attachment.
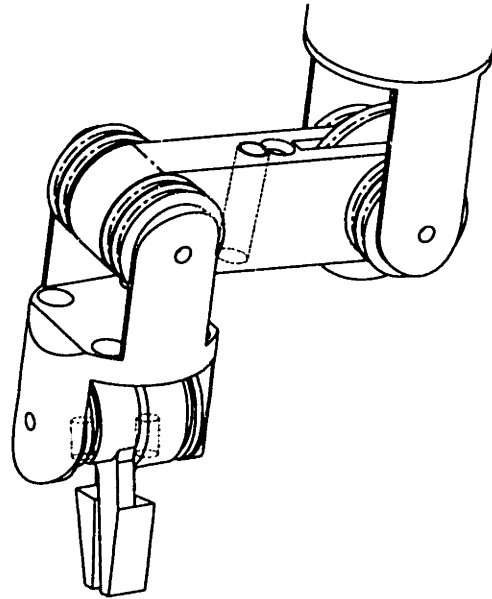
Figure 7-12: This four-degree-of-freedom wrist allows macro-micro control in all three directions within ±90° pitch and yaw motions in order to provide force reflection.

pitch-yaw wrist with the first roll being about the instrument shaft. The joint axes are labeled in Figure 7-13. Recall that to implement macro-micro control, the wrist must allow redundant motions in, ideally, each of three independent directions. The Silver Falcon did this for only two directions. As a result, there was always one direction, pointing directly into the fingers, where redundancy did not exist which resulted in poor force reflection in that direction. The new wrist avoids that problem by adding an extra pitch degree of freedom and maintaining a right-angle bend while re-orienting, Figure 7-14. Figure 7-14 shows a number of different orientations which the wrist can assume. By doing so, we maintain a redundant degree of freedom corresponding to motions directly into the fingers.

Unfortunately, such a wrist also has disadvantages. The main disadvantage is that the wrist obviously has a kink in it. There is typically a limited amount of space at the surgical site and the extra room which this wrist occupies may well be a problem. Second, the wrist has essentially the same singularities as does a roll-pitch-yaw wrist. For example, a singlular configuration occurs when the wrist pitch is at $\pi/2$, ($q_5 = \pi/2$) measured from the zero position shown in Figure 7-13, see Figure 7-15.

Since we have already studied these kinematics with the Silver Falcon, we did not reproduce them in a separate Black Falcon wrist unit.
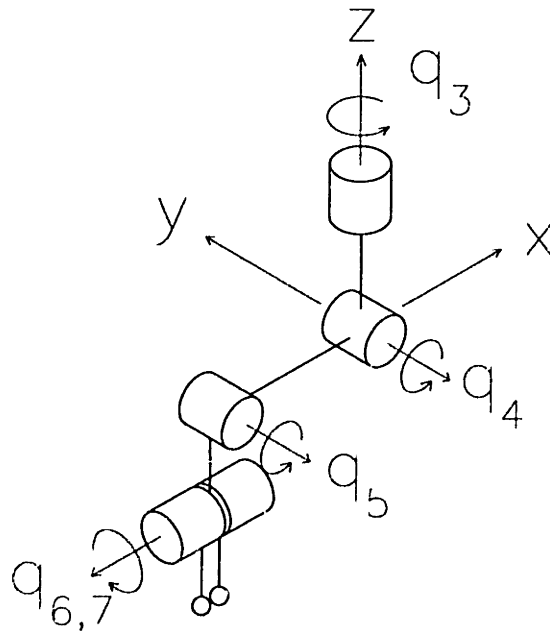
Figure 7-13: Kinematic diagram for the four DOF wrist. We define all joint angles relative to their proximal link *except* joint 5 which is defined relative to ground. Therefore in this figure the fingers point horizontally when $q_5 = \pi/2$ regardless of the position of q_4. The orientation shown is defined as the "zero" position of the wrist.
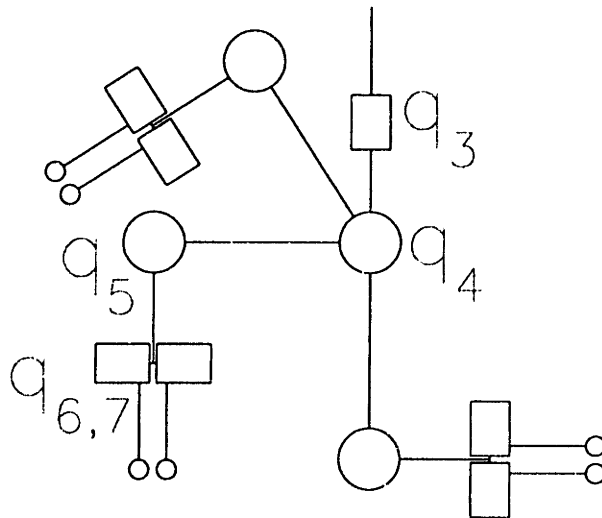
Figure 7-14: The wrist can reorient (pitch) while maintaining a right angle bend at q_5.
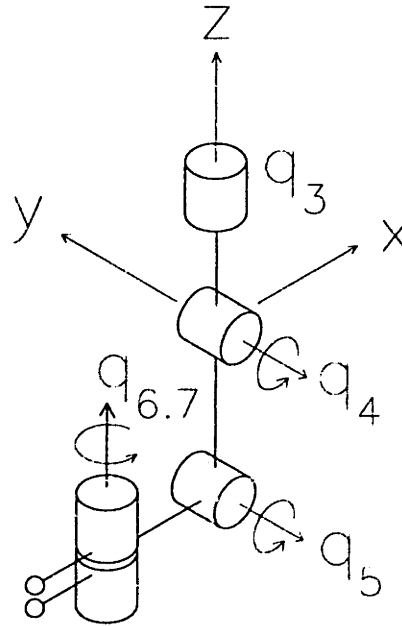
Figure 7-15: The wrist can still be placed in a singular configuration

7.2.3.2 Wrist Cabling and Mechanism

Figure 7-16 shows a schematic diagram of the cabling scheme for the Black Falcon's four-degree-of-freedom wrist. The cabling scheme is similar to that for the Silver Falcon with the addition of one joint. The cables for the distal joints simply pass thru this joint on idler pulleys. Two of the six cables which pass thru the instrument shaft actuate joint 4, the joint which has been added. Figure 7-17 shows a schematic of the cable used to drive joint 3, rotation about the instrument shaft.

In the Silver Falcon design, we found that the use of alpha wraps within the wrist added a considerable amount of friction. So we redesigned that wrist such that there were no alpha wraps, and this is the design presented in Chapter 5. However this comes at a cost of increasing the number of pulleys in the wrist and lengthening the wrist. If the four-degree-of-freedom wrist presented in this chapter were designed to avoid alpha wraps, 8 pulleys would be needed which would consume a considerable amount of space and add offsets to the kinematic structure. So to avoid the added friction we opted to use non-metallic cable, in particular Spectra fiber in the form of Spiderwire™ fishing line. This material is not as stiff as stainless steel cable, but it is smaller in diameter and is much smoother on its outside surface. As r · ·ilt, as the cable slides on itself, as is inevitable in an alpha wrap, very little ad·ⁱ· ·. ·l friction is added.
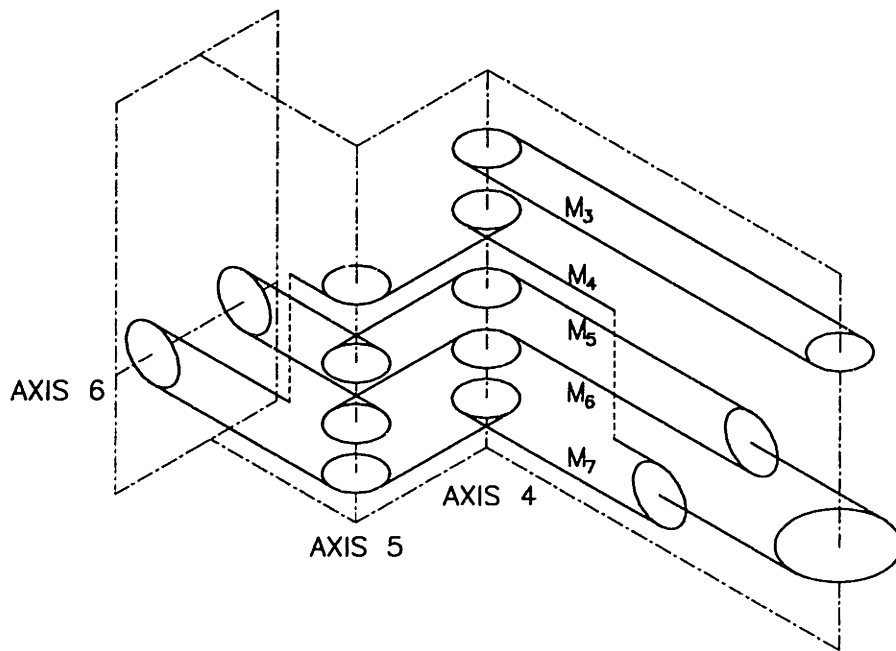
Figure 7-16: The wrist cabling is similar to that of the Silver Falcon, with the addition of one axis. This axis is controlled separately via an additional cable loop.
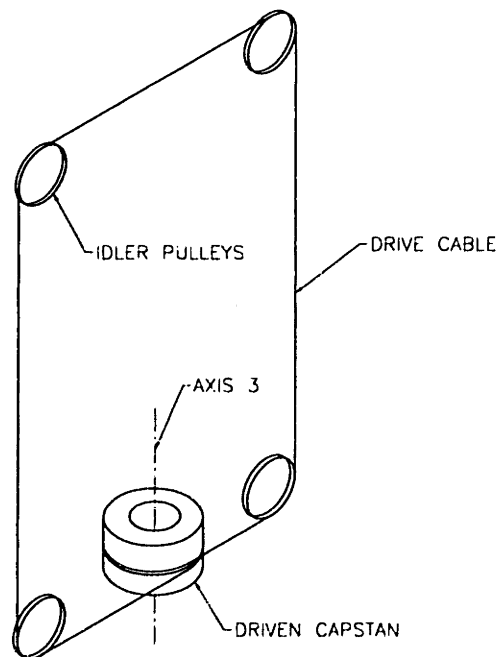
Figure 7-17: Joint 3, rotation about the instrument shaft, is actuated using a cable drive similar to that in the Silver Falcon. One point of the cable loop shown attaches to a drive cable on the base unit.

188 CHAPTER 7. THE BLACK FALCON TELEOPERATOR SLAVE

Another change between the wrist mechanism here and that used in the Silver Falcon is the bearings/pulleys used here. The Silver Falcon used a single ball bearing in each idler pulley, and pairs of ball bearings on the pulleys that supported each finger. In order to make this design closer to what might be used in an operating room, we decided to avoid the use of ball bearings. This makes sterilization easier, as there is less place for bacteria to grow, and we do not have to worry about losing bearing lubricant during the sterilization process.

Each finger is machined as a single piece with the pulley which drives it, and has a knurled surface to securely hold needles. They are stainless steel with clearance holes drilled in them, that ride on steel shafts made from drill rod. This is not a particularly good material combination, though we have not noticed any problems. The friction torque is low because the shafts are only 0.047 in diameter. The shafts should likely be replaced with Titanium Nitride coated stainless shafts to avoid galling. The idler pulleys are made from teflon and simply have clearance holes so that they ride ..moothly on drill rod shafts. Because they are thin, and the alpha wrapped cable produces a moment on the pulleys (see Figure 5-14) the pulleys must support themselves by leaning on each other. Despite the low coefficient of friction of teflon, this is still a major source of wrist friction. Because teflon is very soft, a teflon filled delrin might have been a better choice for this material. The main structural wrist components are machined from 303 stainless steel.

7.2.3.3 Base Unit - Wrist Unit Interface

Figure 7-18 shows a view of the top of the wrist unit. What we see is essentially a number of idler pulleys in various locations within this top structure. The effect is that the six cables which pass thru the instrument shaft and the extra cable loop which drives the wrist roll all pretension within this unit against various idler pulleys some of which move against screws to allow pretensioning. Six cable segments are aligned against the back of the wrist unit such that they precisely align with the six drive cables within the base unit which run parallel to link 5. These six cable segments are then mechanically fixed to their respective drive cables using screw clamps.

Figure 7-19 shows schematically the wrist unit to base unit connection for a single degree of freedom.

Because the cables in the wrist unit align with the cables in the base unit, no further mechanism is required to make an attachment other than a single small clamp per cable. In other words, no complex mechanical interlocking mechanism is required, and the actual connection between the wrist unit and the base unit is frictionless.

The downside is that it is fairly complicated design task to get the cables to run
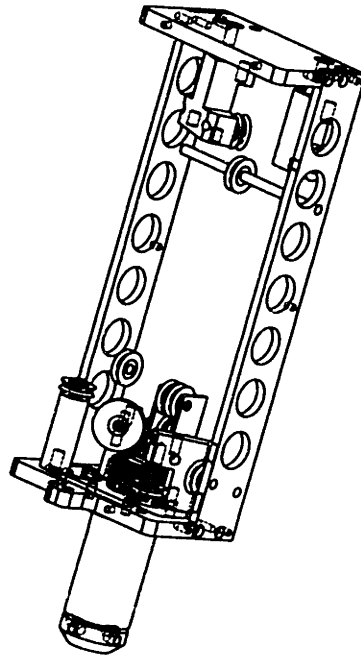
Figure 7-18: Detail of the top of the wrist unit assembly.

out of the shaft and parallel to each other and to mate with the base unit cables. Also, there is no "quick-release" capability.

7.2.3.4 Differential Kinematics

Here we give the relationships between the motor velocities and joint velocities for joints 2-7. The motor-joint mapping for joints 0 and 1 are simply speed ratios. Let **q** be the velocities of joints 2-7, let **c** be the velocities of the six drive cables which run parallel to link 5, and let R_3, R_4, R_5, and R_6 be speed ratios defined below. Recall that all the joint angles are measured with respect to the previous link *except* joint 5 which is measured with respect to the axis of the instrument shaft.

$$R_3 = 8.717 \times 10^{-3} \text{ m/rad}$$
$$R_4 = 6.252 \times 10^{-3} \text{ m/rad}$$
$$R_5 = 3.787 \times 10^{-3} \text{ m/rad}$$
$$R_6 = 3.094 \times 10^{-3} \text{ m/rad}$$
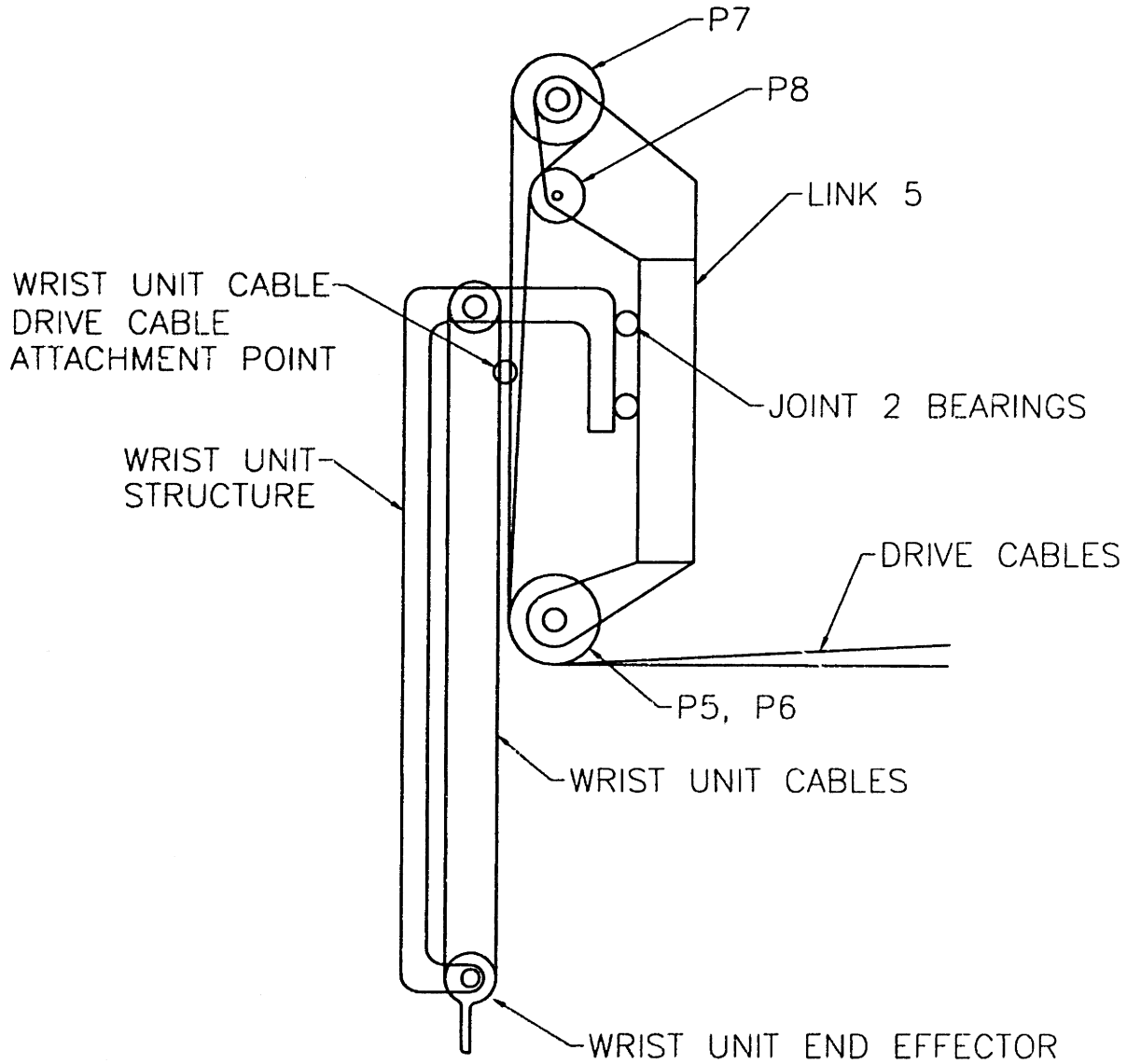
Figure 7-19: Schematic of the wrist unit - base unit attachment for a single degree of freedom. Six such attachements are made allowing for control of 5 wrist unit freedoms plus motion of the wrist unit vertically along the carriage. The locations of five of these attachments are shown in Figure 7-16, labeled M3 - M7. M2 drives the roll freedom (q_3) as shown in Figure 7-17

We then have:

$$\mathbf{q} = J\mathbf{c} \qquad (7.15)$$

where:

$$J = \begin{pmatrix} 1 & 0 & 0 & 0 & 0 & 0 \\ 0 & \frac{1}{R_3} & 0 & 0 & 0 & 0 \\ 0 & 0 & \frac{1}{R_4} & 0 & 0 & 0 \\ 0 & 0 & 0 & \frac{1}{R_5} & 0 & 0 \\ 0 & 0 & 0 & 0 & \frac{1}{R_6} & 0 \\ 0 & 0 & 0 & 0 & 0 & \frac{2}{R_6} \end{pmatrix} \begin{pmatrix} 0 & 1/4 & 1/4 & 1/4 & 1/4 & 0 \\ 0 & 1/4 & 1/4 & 1/4 & 1/4 & -1 \\ -1 & 1/4 & 1/4 & 1/4 & 1/4 & 0 \\ 0 & -1/4 & 1/4 & 1/4 & -1/4 & 0 \\ 0 & -1/4 & -1/4 & 1/4 & 1/4 & 0 \\ 0 & -1/4 & 1/4 & -1/4 & 1/4 & 0 \end{pmatrix} \qquad (7.16)$$

7.3 Summary

The Black Falcon teleoperator slave has a number of improvements over the Silver Falcon, and in general moves closer to an architecture which could be used for human surgical procedures. The pros and cons of these changes are summarized below.

- The structure is stiffer and stronger. This reduces flexibility which improves control performance and endpoint measurement.

- The actuators are stronger and better matched to the overall inertia, improving positioning performance and increasing grip strength so that needles may be securely held.

- The carriage uses an improved bearing system which increases stiffness and decreases friction.

- The first two axes of the system are counterbalanced. This increases safety and convenience since the system will not fall when motor power is shutdown.

- The wrist unit is detachable, though not "quick-release". This allows wrist units to be designed as part of future research projects. The architecture may be adapted to a quick-release design.

- The four-degree-of-freedom wrist was added to allow force reflection in all three directions.

Disadvantages which are apparent are:

- The remotization of the motors to the base of link1, the use of larger motors, and the non-alpha wrist design have contributed to increased friction in the wrist.

We will investigate the effects of these changes in the next chapter.

Chapter 8

Black Falcon Teleoperator Slave Performance

We now investigate the performance of the Black Falcon Teleoperator Slave. We begin by giving basic data on a joint by joint basis. Then we will perform tests to quantify force reflection performance as was done for the Silver Falcon. Finally, we will demonstrate ability to perform tasks, in particular, suturing and a more difficult task of moving a piece of soft plastic tubing along a "S"-shaped curved wire.

For our force reflection tests, we used the PHANToM Haptic interface which was described in Chapter 5. In order to perform motion scaling however, we found we needed a larger master workspace. Therefore, to demonstrate tasks such as suturing with motion scaling we used a larger version of the PHANToM, know as the Toolhandle (Zilles, 1995). The tool handle is essentially a scaled up PHANToM with 16 in link lengths instead of 5.5 in link lengths.

8.1   Basic System Performance

8.1.1   Joint Limits

The range of motion of each of the joints is given relative to the zero position defined in Figure 7-3.

q_0	$\pm 80°$
q_1	$\pm 60°$
q_2	8 in stroke

$$q_3 \qquad \pm 180°$$
$$q_4 \qquad -27° \;\; +40°$$
$$q_5 \quad -180° \; -q_4 \; +30° \; -q_4$$
$$q_6 \qquad \pm 100°$$
$$q_7 \qquad +200° \text{ jaw opening}$$

8.1.2   Structural Stiffness

The structural stiffness at the endpoint of the system is given below. These numbers are difficult to measure and are probably accurate to about 20%. We calculated stiffness by measuring the force required to deflect the instrument shaft by 1/16 in in the x direction and 1/8 in in the y direction using a force gage (Mark 10 Model BG2). The z direction structural stiffness is that found for the base unit in section 7.2.2.3, and is repeated below:

$$k_{WX} \; \cong \; 9500 \text{ N/m}$$
$$k_{WY} \; \cong \; 2800 \text{ N/m}$$
$$k_{WZ} \; \cong \; 12000 \text{ N/m}$$

These measurements were made with the wrist unit centered in its stroke. The point where force was applied was .15 m (6 in) below the teflon support bushing, and 0.086 m (3.4 in) below the remote center.

8.1.3   Friction

We measured the force required to backdrive each joint of the wrist with the base joints 0 and 1 held stationary, and when the manipulator was in its zero position (Figure 7-13). We made 4 - 6 measurements in each case and averaged the results. The forces we measured were:

- f_R is a force in the x direction applied in line with axis 5, which causes rotation about axis 3 only.

- f_X is a force at the finger tips in the x direction with the fingers closed. Axis 3 is held fixed, so only axis 6 may rotate.

- f_Y is a force at the finger tips in the y direction. Only axis 5 rotates.

- f_Z is a force at tip in z direction. Only axis 4 rotates.

- f_{q2} is the force required to backdrive the carriage and wrist unit together.

In the first case, we measured these forces with the system turned completely off.

$$
\begin{aligned}
f_R &= 0.63 \pm 0.04 \text{ N} \\
f_X &= 1.1 \pm 0.2 \text{ N} \\
f_Y &= 0.60 \pm 0.2 \text{ N} \\
f_Z &= 0.96 \pm 0.06 \text{ N} \\
f_{q2} &= 12.9 \pm 0.03 \text{ N}
\end{aligned}
$$

In the second case, we applied a friction compensation algorithm which we used throughout the remainder of the results given. This algorithm will not be described here in detail. It is essentially feeds forward a torque to each motor as a function of motor velocity and includes a model of the brush friction and brush flexibility. When this is implemented, the measured friction values are: [1]

$$
\begin{aligned}
f_R &= 0.48 \pm 0.1 \text{ N} \\
f_X &= 0.88 \pm 0.14 \text{ N} \\
f_Y &= 0.40 \pm 0.02 \text{ N} \\
f_Z &= 0.73 \pm 0.07 \text{ N} \\
f_{q2} &= 2.86 \pm 0.2 \text{ N}
\end{aligned}
$$

The friction is created in two places, within the wrist itself and in the motors as brush friction. The fact that joint 2 friction can be reduced by a factor of 4 indicates that this axis is dominated by brush friction because this is what the friction compensation algorithm compensates for. However, in the other cases where the compensation does not reduce overall friction substantially, the friction must be directly in the wrist.

8.1.4 Inertia

The inertias of each joint were calculated by plotting oscillatory step responses where very little damping and a known spring constant (position gain) were used. These were compared to a simulation of a spring mass damper system. The simulation mass

---

[1]This work is part of the controller implementation and was done by Günter Niemeyer. It will be presented in a forthcoming publication.

and damping were modified until a fit was found to find the actual mass and damping.

$$I_0 = 0.32 \text{ kgm}^2$$
$$I_1 = 0.25 \text{ kgm}^2$$
$$I_2 = 3.35 \text{ kg}$$
$$I_3 = 26.0 \times 10^{-6} \text{ kgm}^2$$
$$I_4 = 20.0 \times 10^{-6} \text{ kgm}^2$$
$$I_5 = 20.5 \times 10^{-6} \text{ kgm}^2$$
$$I_6 = 19.5 \times 10^{-6} \text{ kgm}^2$$
$$I_7 = 2.8 \times 10^{-6} \text{ kgm}^2$$

8.1.5 Individual Joint Responses

In order to give an idea of the position servo performance available with the Black Falcon, we first give individual joint responses for a fairly well tuned set of gains given below:

$$K_{qs0} = 3500 \text{ Nm/rad} \quad B_{q0} = 35 \text{ Nms/rad}$$
$$K_{qs1} = 3500 \text{ Nm/rad} \quad B_{q1} = 35 \text{ Nms/rad}$$
$$K_{qs2} = 20000 \text{ N/m} \quad B_{q2} = 200 \text{ Ns/m}$$
$$K_{qs3} = 1.5 \text{ Nm/rad} \quad B_{q3} = 0.015 \text{ Nms/rad}$$
$$K_{qs4} = 0.8 \text{ Nm/rad} \quad B_{q4} = 0.008 \text{ Nms/rad}$$
$$K_{qs5} = 0.3 \text{ Nm/rad} \quad B_{q5} = 0.003 \text{ Nms/rad}$$
$$K_{qs6} = 0.2 \text{ Nm/rad} \quad B_{q6} = 0.002 \text{ Nms/rad}$$
$$K_{qs7} = 0.05 \text{ Nm/rad} \quad B_{q7} = 0.0005 \text{ Nms/rad}$$

During master-slave teleoperation we used much lower joint 0 and 1 gains, because the system was no longer stable at these high gains. We suspect this is due to limited position measurement resolution in the PHANToM master. Consider that a joint 0 gain of 3500 N/m corresponds to an endpoint stiffness of 128,400 N/m when the tip of the fingers are at a distance of 0.17 m from the remote center. This is an extremely high endpoint stiffness. The endpoint resolution about joint 0 is the result of a 4096 count encoder and a 137:1 speed reduction, which gives 561,152 counts/rev or at 0.17 m a 3.03×10^{-7} m resolution. The inertia of this axis is high, at 0.32 kgm^2, so that the bandwidth of the response is only $\sqrt{3500/0.32} = 104$ rad/sec $\cong$ 17 Hz. With such high positioning resolution and inertia, it is no wonder we can achieve such
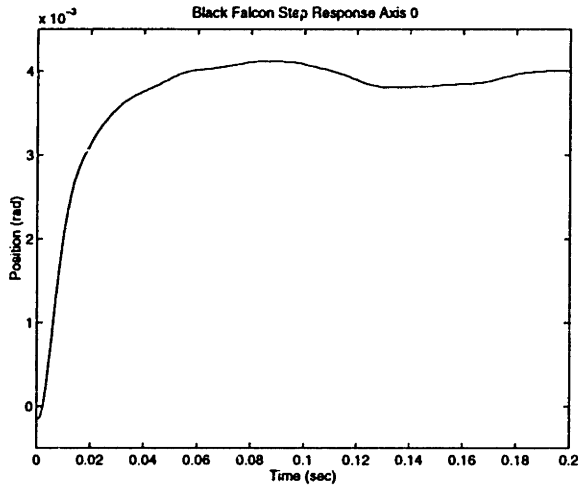
Figure 8-1: Joint 0 response to a 0.004 rad step input.
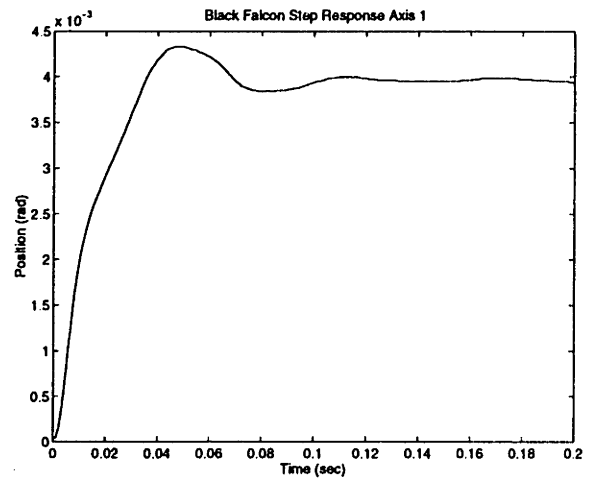
Figure 8-2: Joint 1 response to a 0.004 rad step input.
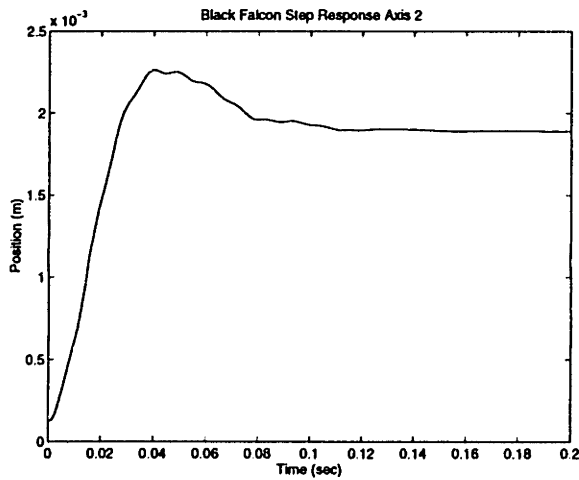
Figure 8-3: Joint 2 response to a 0.002 m step input. Gain used during force reflection tests.
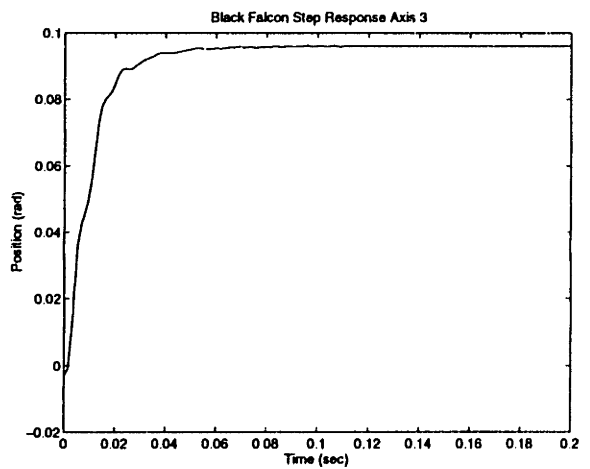
Figure 8-4: Joint 3 response to a 0.1 rad step input.
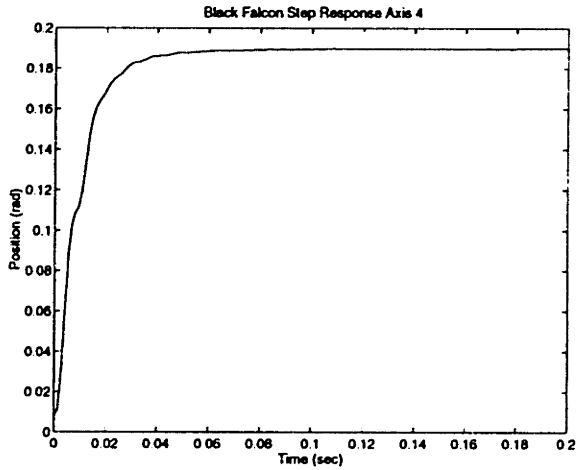
Figure 8-5: Joint 4 response to a 0.2 rad step input.
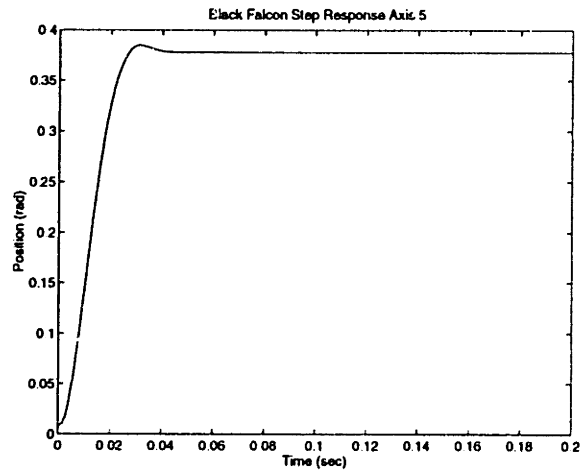
Figure 8-6: Joint 5 response to a 0.4 rad step input.
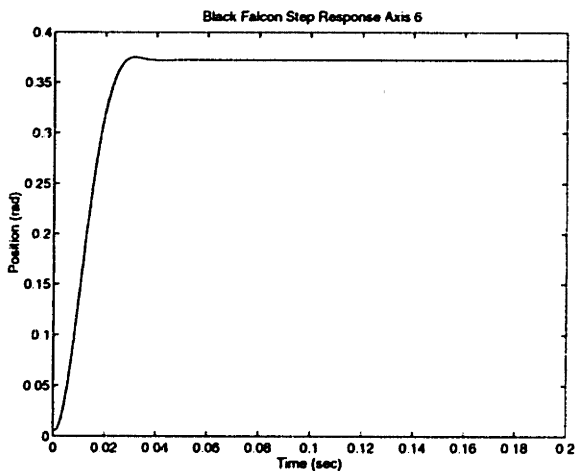
Figure 8-7: Joint 6 response to a 0.4 rad step input.
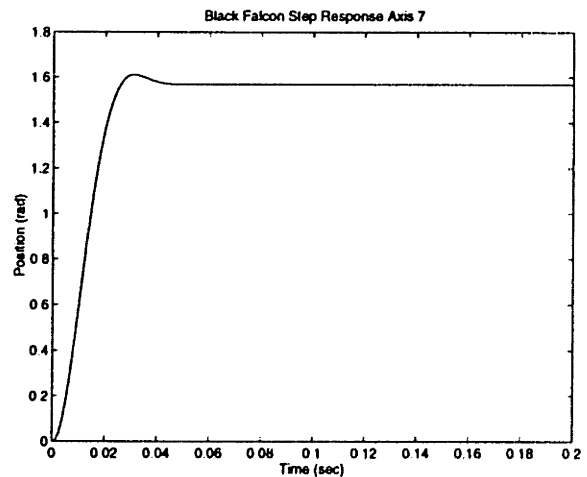
Figure 8-8: Joint 7 response to a 1.6 rad step input.

high stiffness. However, the PHANToM has an endpoint resolution of 4.511×10^{-5} m. Therefore, if the slave tracks the master at this high gain, each time the master moves by one encoder tick, the slave sees a force step of 5.8 N or 1.3 lbs. Tracking such a coarse input creates noticeable vibration in the system.

Also, the slave has a structural flexibility at roughly 8-12 Hz as we can see in Figures 8-1 and 8-2. We believe the vibration caused by tracking the coarse master input combined with these structural dynamics is causing instability at high gains and has forced us to detune the slave joint 0 and 1 gains to 200 Nm/rad, which corresponds to an equivalent endpoint stiffness of 6920 N/m. One encoder tick movement on the master now corresponds to a 0.31 N (0.07 lb) force step for the slave.

The second reason our gains are different during the force reflection tests is that we need to adjust them appropriately in order to have a 2:1 force scaling. Because we are now running joint P.D. gains (instead of a cartesian P.D. mapped to joints via J^T) we must set the joint gains to give an endpoint gain which is 1/2 that of the master, or 240 N/m. These gains are dependent on the configuration of the wrist. For our force reflection tests, where the manipulator was always nominally in its zero position (Figure 7-3) we used the gains given below:

$$
\begin{aligned}
K_{qs0} &= 200 \text{ Nm/rad} & B_{q0} &= 10 \text{ Nms/rad} \\
K_{qs1} &= 200 \text{ Nm/rad} & B_{q1} &= 10 \text{ Nms/rad} \\
K_{qs2} &= 20000 \text{ N/m} & B_{q2} &= 250 \text{ Ns/m} \\
K_{qs3} &= 0.12 \text{ Nm/rad} & B_{q3} &= 0.004 \text{ Nms/rad} \\
K_{qs4} &= 0.10 \text{ Nm/rad} & B_{q4} &= 0.003 \text{ Nms/rad} \\
K_{qs5} &= 0.20 \text{ Nm/rad} & B_{q5} &= 0.004 \text{ Nms/rad} \\
K_{qs6} &= 0.10 \text{ Nm/rad} & B_{q6} &= 0.003 \text{ Nms/rad} \\
K_{qs7} &= 0.04 \text{ Nm/rad} & B_{q7} &= 0.0007 \text{ Nms/rad}
\end{aligned}
$$

8.2 Force Reflection

In this section we discuss force reflection only for the Jacobian Inverse controller, see Chapter 4, as we found this gave the best results. When programmed with the Jacobian Transpose controller, it is essentially impossible to move the slave using the master due to its large apparent inertia. We also found some success using the Simulated Force Sensor controller, though we do not present results here.
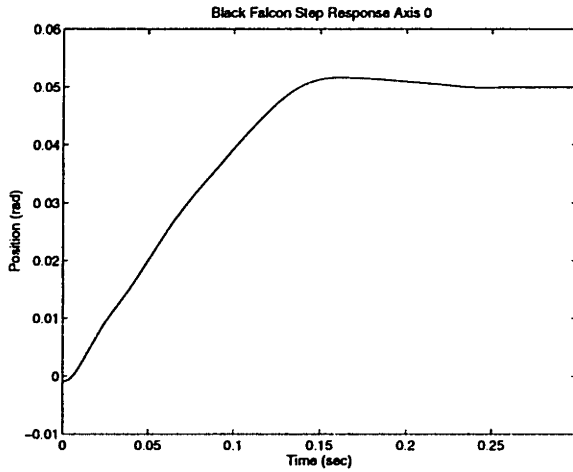
Figure 8-9: Joint 0 response to a 0.05 rad step input. Gains used during force reflection tests.
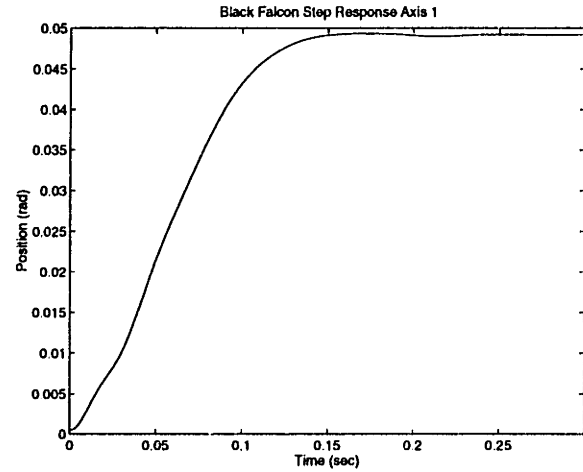
Figure 8-10: Joint 1 response to a 0.05 rad step input. Gains used during force reflection tests.
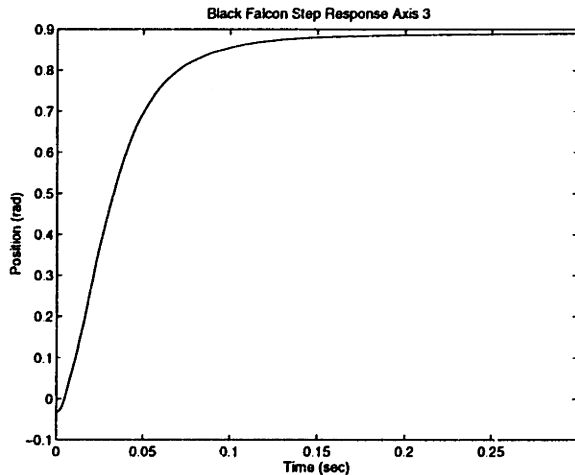
Figure 8-11: Joint 3 response to a 1.0 rad step input. Gains used during force reflection tests.
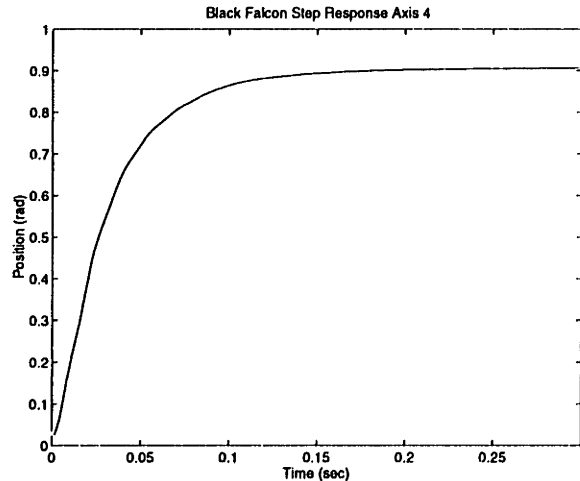
Figure 8-12: Joint 4 response to a 1.0 rad step input. Gains used during force reflection tests.
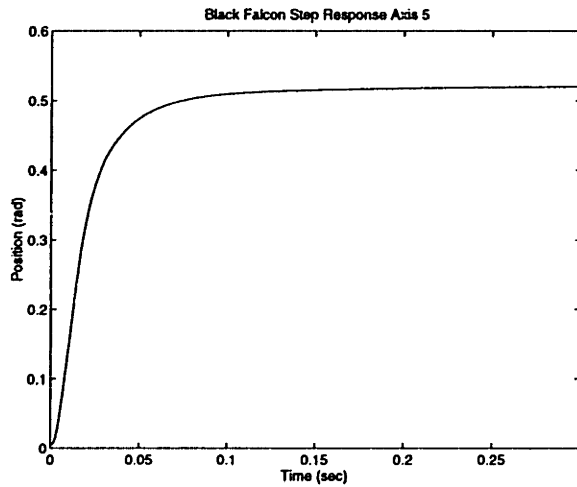
Figure 8-13: Joint 5 response to a 0.6 rad step input. Gains used during force reflection tests.
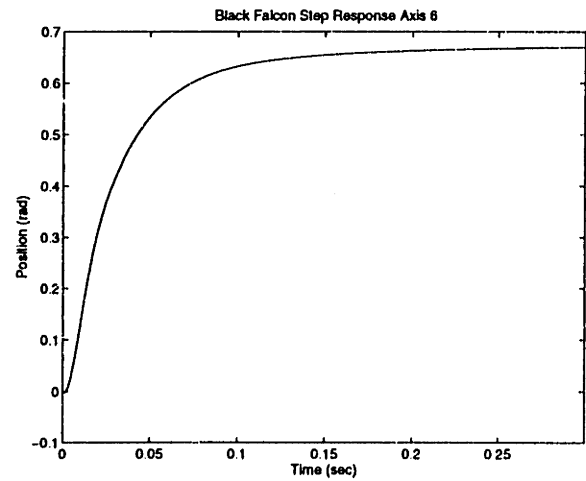
Figure 8-14: Joint 6 response to a 0.8 rad step input. Gains used during force reflection tests.
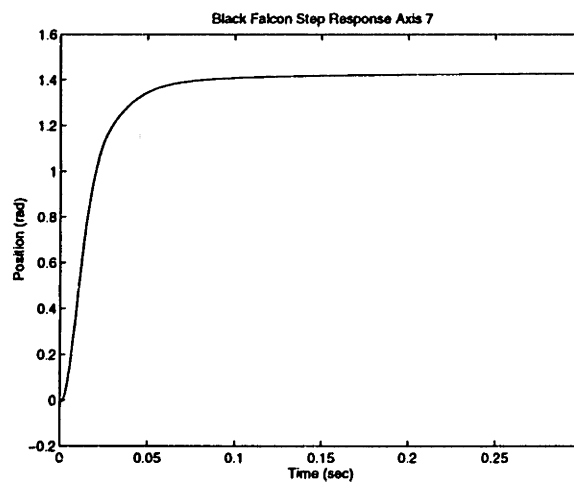
Figure 8-15: Joint 7 response to a 1.6 rad step input. Gains used during force reflection tests.

Figure 8-16: Freespace response for the Black Falcon slave and PHANToM master in the x direction using the Inverse Jacobian controller. The solid line represents the master, and the dashed line represents the slave.

8.2.1 Freespace Responses

These tests are identical to those done for the Silver Falcon in Chapter 6. We commanded an 8.0 rad/sec, 2 cm amplitude sinusoid to the slave and recorded the resulting slave motion. We also recorded the force commanded to the master through the controller and the force measured (using slave motor commands) at the slave tip. The actual force at the slave tip is of course zero.

Figures 8-16 and 8-17 show freespace response in the x and y directions, which are quite similar. As in the Silver Falcon, we see a substantial amount of tracking error which is presented as a force of roughly 1.5 N to the master. Our first reaction is that this error should not exist given that we went through some effort to improve the base tracking ability of the Black Falcon. Recall though that we *lowered* the base gains from a possible 3500 Nm/rad to 200 Nm/rad during these tests to achieve stability. The result is diminished base tracking and hence diminished freespace performance.

We can calculate the force which we would expect the master to see given the gains which we implemented. The base gains of 200 Nm/rad result in an equivalent
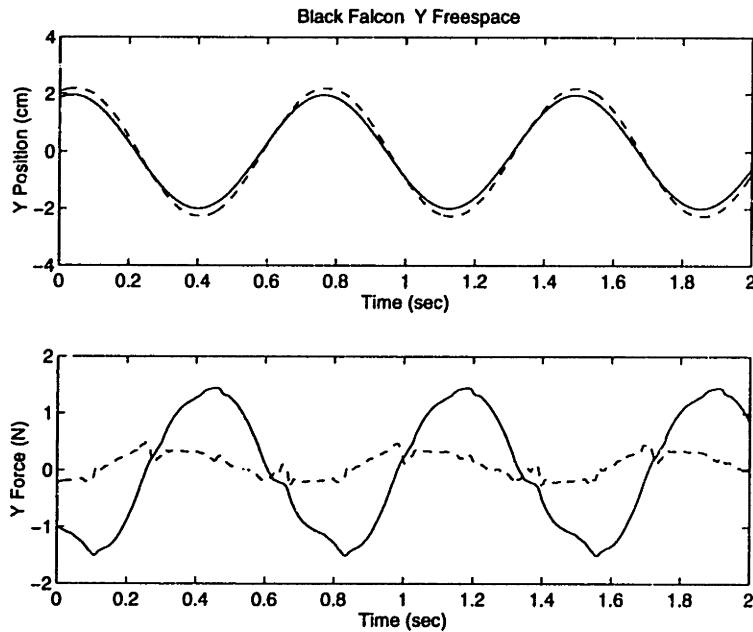
Figure 8-17: Freespace response for the Black Falcon slave and PHANToM master in the y direction using the Inverse Jacobian controller. The solid line represents the master, and the dashed line represents the slave.

endpoint stiffness of:

$$\frac{200 \text{ N/m}}{0.17^2} = 6920 \text{ N/m}$$

when the tip of the slave is 0.17 m from the remote center. The scaling between the base of the slave and the master is then:

$$\frac{6920 \text{ N/m}}{480 \text{ N/m}} = 14.4$$

The equivalent inertia of the base at the slave tip is:

$$\frac{0.32 \text{ kgm}^2}{0.17^2} = 11.1 \text{ kg}$$

Therefore the reflected inertia is:

$$\frac{11.1 \text{ kg}}{14.1} = 0.78 \text{ kg}$$
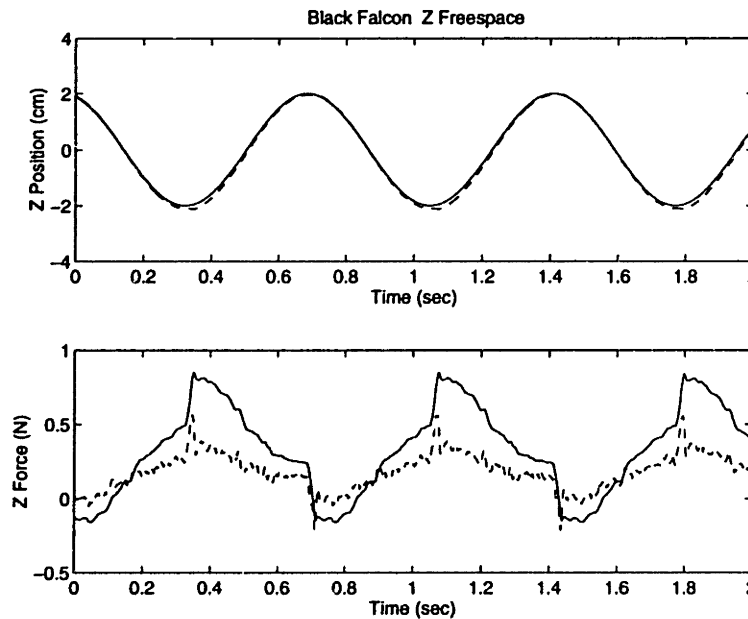
Figure 8-18: Freespace response for the Black Falcon slave and PHANToM master in the z direction using the Inverse Jacobian controller. The solid line represents the master, and the dashed line represents the slave.

At a peak acceleration of 1.28 m/s², we expect a force of:

$$0.77 \text{ kg} \times 1.28 \text{ m/s}^2 = 0.98 \text{ N}$$

The 1.5 N force which we observe is not surprising considering that only inertial forces are considered in the above analysis. We note that while we do feel forces which are only slightly less than with the Silver Falcon, the inertia is 13 times greater and being suppressed by a factor of 14.4.

The z axis tracking performance is considerably better, Figure 8-18. In absolute terms, the tracking error is less. This case is different from the x and y direction cases in that the error here is due to the micro axis more than the macro axis. The macro axis (joint 2) is in running at a high (20,000 N/m) gain which unlike in the joint 0 and 1 axes does not seem to cause vibration. This is likely because structural stiffness is higher in this direction and the inertia being moved is considerably less.

Joint 4 acts as the micro axis during the z direction tests. It is coupled to joint 2 (through the cable drive) such that when the direction of motion of joint 2 changes, a force equivalent to the joint 2 backdrive friction is introduced to the joint 4 and hence the output. This explains the cyclic sharp rise and fall in the output error plot when the direction of motion changes.
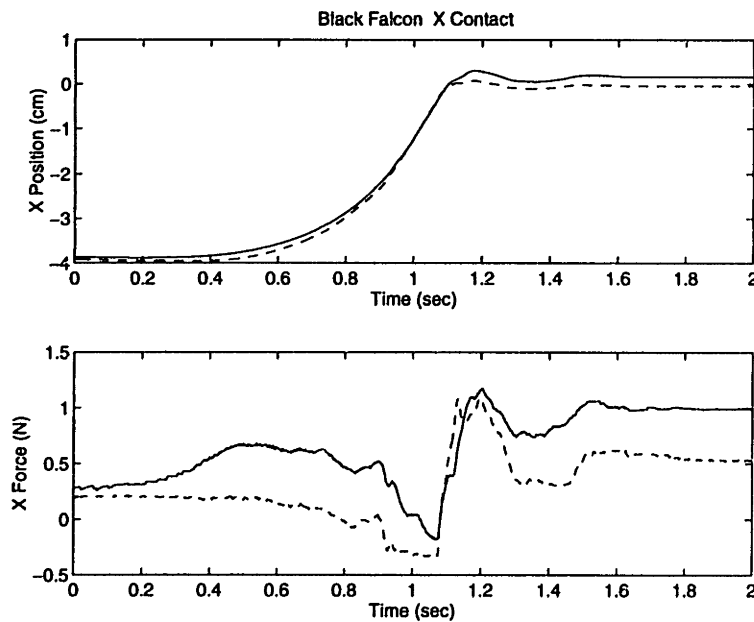
Figure 8-19: Contact response for the Black Falcon slave and PHANToM master in the *x* direction using the Inverse Jacobian controller. The solid line represents the master, and the dashed line represents the slave.

8.2.2 Contact Responses

During these contact experiments we use the PHANToM haptic interface, just as when testing the Silver Falcon. The tests were made by moving the PHANToM such that the slave came into contact with a rigid aluminum block. Because the movement is done by hand, the tests are not entirely repeatable. But we found that qualitatively, the responses look quite similar when the tests were run multiple times. A 2:1 force scaling was implemented.

Figures 8-19 and 8-20 show contact responses in the *x* and *y* directions. These responses look very similar. We have fairly substantial freespace forces which we expect from results from the previous section. The contact is however, quite good. We see sharp force increases in both the master and the slave which closely mimick each other. The steady state forces settles to 0.5 N and 1.0 N showing the 2:1 force scaling which was implemented.

Also note that there is little overshoot seen in the measured slave tip position as it contacts the aluminum block. This means our estimate of the endpoint position using joint measurements is good and shows that there is less structural flexibility than there was in the Silver Falcon.
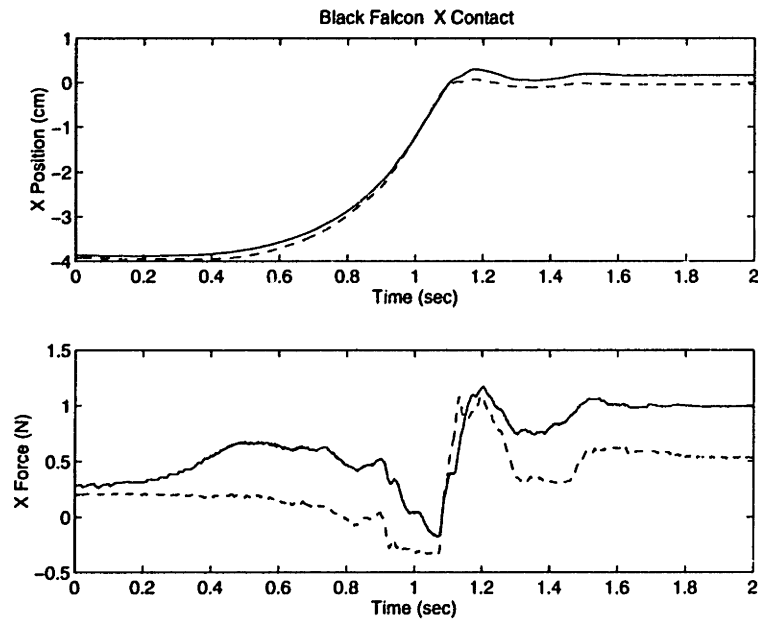
Figure 8-20: Contact response for the Black Falcon slave and PHANToM master in the y direction using the Inverse Jacobian controller. The solid line represents the master, and the dashed line represents the slave.

The z direction contact is shown in Figure 8-21, and is considerably better. This is in fact what we had hoped all the responses would look like. The tracking performance is excellent as expected with a 20000 N/m joint 2 gain. The resulting freespace forces are nearly zero. Then, when contact is made, a very sharp increase in force occurs in both the master and the slave which settles to a steady state value of 0.7 N in the slave and 1.4 N in the master as pressure is applied by the user.

A reasonable question to ask is why is this axis better than the others? We suggest the reason is simply the quality of the macro and micro freedoms involved. The macro freedom, joint 2, has a backlash free transmission, is lightweight, and has excellent encoder resolution because four encoder signals are averaged in determining its position. A gain of 20000 N/m means that inertia is suppressed by a factor of $20000/480 = 41.7$. The joint 2 inertia is only 3.35 kg, so that the user only feels 0.08 kg from the macro joint. If the inertia of axes 0 and 1 could be reduced, a difficult task admittedly, the overall performance of the system might be improved.

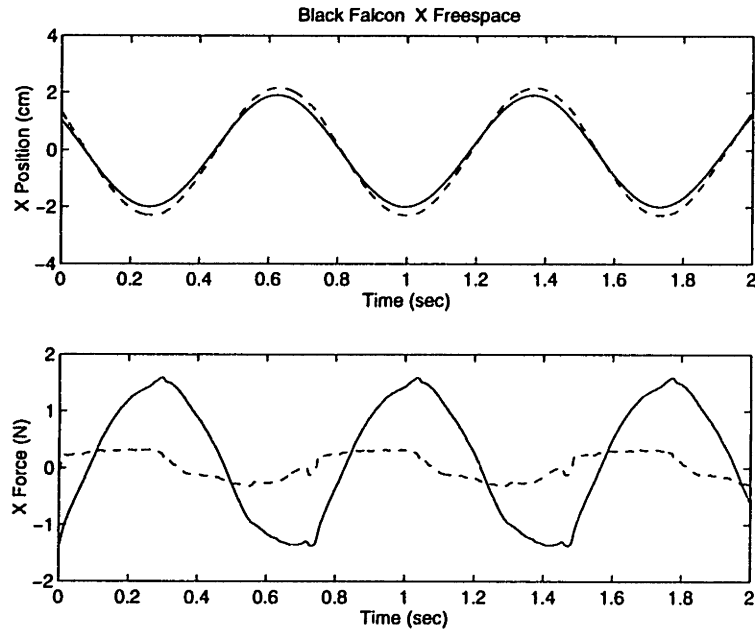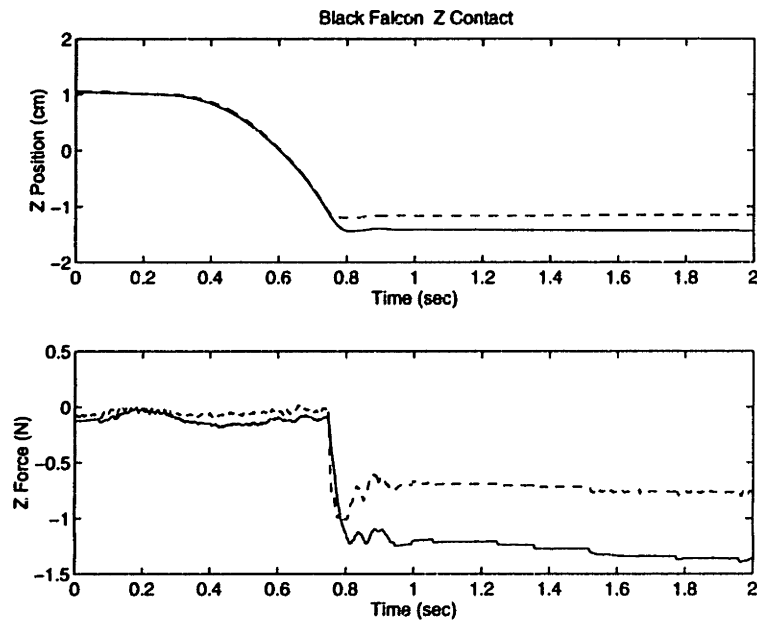**Figure 8-21:** Contact response for the Black Falcon slave and PHANToM master in the z direction using the Inverse Jacobian controller. The solid line represents the master, and the dashed line represents the slave.

8.2.3 Discrimination Tests

As in the Silver Falcon, we found that the lowest level of force which a user could discriminate correlates well with the wrist backdrive friction levels, given in section 8.1.3. In these tests, we duplicated the setup which we use below during suturing. We used the Toolhandle haptic interface as a master manipulator instead of the PHANToM (Zilles, 1995), running the Inverse Jacobian controller with a 5:1 motion scaling and a 2:1 force scaling. A loop of string was held in the fingertips at one end and attached to a digital force gage (Mark 10 Model BG2) at the other. With my eyes closed, I pulled until I first felt a force. The location of the sensor was moved every time so that I could not learn the position where the force would appear. Five values were taken in each direction and the values averaged. The error represents one standard deviation.

$$f_{dx} = 0.34 \pm 0.08 \ N \tag{8.1}$$

$$f_{dy} = 0.58 \pm 0.3 \ N \tag{8.2}$$

$$f_{dz} = 0.51 \pm 0.09 \ N \tag{8.3}$$

8.3   Features

Once a teleoperator is placed in the loop, a number of features can be added. Studying these features will require much future research to understand completely, but we discuss a few basic results below.

8.3.1   Alignment of Visual Image with Hand Motions

The most basic feature is to orient the visual image of the surgical site and slave tip motions with those of the surgeon's hand and master manipulator. If the surgeon were directly viewing the operating site, we would make master and slave motions coincide in an absolute reference frame. But if the slave is viewed on a monitor, then we need to rotate the reference frame of the slave such that it coincides with the viewing direction of the camera. The reference frame of the master is rotated such that it coincides with the reference frame of the monitor. Then a motion of the master directly towards the monitor, for example, will be a motion of the slave directly away from the camera and the image of the instrument tip on the monitor will coincide with motions of the master manipulator. In this way, motions made by the surgeon coincide with those that appear on the monitor. SRI went one step farther in their open telesurgery system by projecting a stereo image of the surgical site to the surgeon using a mirror. The system is aligned very carefully such that the slave instrument tips appear (in the mirror) to extend from the tools which the user is holding with their hands, which are partially visible from outside the sides of the mirror. This creates a powerful illusion. The SRI system does not have a wrist and does not increase range of motion over conventional laparoscopic surgery, yet it is much easier to perform tasks with it than with conventional instruments. I have used this system and feel that this is primarily due to this visual illusion. There is nothing in our system to preclude this type of presentation of the image to the user, but it does require building a surgical console in which a monitor, mirrors and masters can all be mounted.

8.3.2   Motion Scaling

Motion scaling is simple to implement. The slave is commanded to track scaled versions of the master motions. Rotational motions are not scaled. We typically want to allows large master motions to correspond to small slave motions, as this makes the slave more steady, in that jerky master movements are made smaller and less noticeable. It also effectively increases the position resolution of the master. We

tried values ranging from 1:1 to 5:1. The value to choose is task dependent. 5:1 might work well when the surgeon is performing 1/2 inch slave motions, but is inconvenient if he is making 2 inch slave motions. For suturing, which we discuss below, I found 2:1 motion scaling to work well.

8.3.3 Indexing

Indexing is the concept of detaching the master from the slave (via the controller) in order to reposition the master within its workspace. This is analogous to lifting a computer mouse from its pad (disengaging it from the cursor) and moving it back to the center of the mouse pad. This is again straightforward to implement, and makes sense for positions. It does not make sense to index orientations because if master and slave orientations become misaligned it becomes very difficult for the surgeon to determine how master motions correspond to slave motions. Position indexing is especially helpful when large motion scaling factors are used. We found ourselves indexing frequently when setting up the slave with respect to a given task.

8.4 Tasks

We demonstrated two tasks which show different aspects of the system. The first task was suturing, which is obviously relevant to MIS. When asked, surgeons uniformly ask whether or not suturing will be possible using our technology. Suturing is primarily a geometric task. That is, success depends on whether the system has sufficient degrees of freedom, workspace, and the appropriate kinematics to make the required motions.

The second test we tried is a tube and wire test, where we push a piece of clear plastic tubing along a wire bent into "S" shaped curves. This task requires similar mobility to suturing, but also requires contact with a much stiffer environment, namely a rigid metal wire. As a result, force reflection becomes much more important because small motions can create large forces which are difficult to detect visually.

We used the Toolhandle master during these tasks instead of the PHANToM. We simply moved the gimbal and gripper which we had built for the PHANToM to the Toolhandle. The reason was that we wanted to implement motion scaling, and the PHANToM did not have sufficient workspace. We also were able to mount the Toolhandle such that its last link points directly at the user, instead of straight down as with the PHANToM. This is a better configuration because the user's hand used to interfere with the last link of the PHANToM but does not interfere with the last link of the Toolhandle.
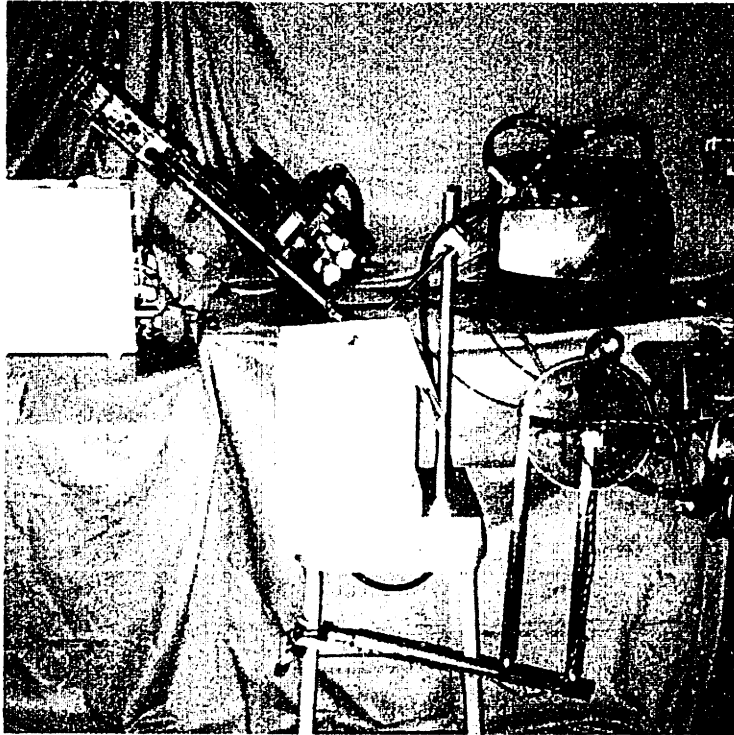
Figure 8-22: We used the Black Falcon Slave with the Toolhandle and instrumented gimbal/gripper as a master while performing tasks. The user sat facing to the right, holding the end of the Toolhandle (shown in the foreground in front of the stool) and could view the task directly. The chicken is sitting on top of several boxes on the stool, while the slave points down and to the right at roughly a 45 degree angle.

Both these tasks were performed with direct vision. That is, while we could view the task on a monitor, we found the lack of 3-D vision to make the task much more difficult. We arranged the master and slave so that the user directly views the task, as shown in Figure 8-22.

8.4.1   Suturing

To demonstrate our ability to suture along arbitrary suture lines, I made stitches in muscle tissue, specifically a chicken leg with the skin removed. We used an Ethicon Ethibond polyester suture (3-0) with a curved, tapered SH needle. I found I could make a row of stitches along different lines relative to the instrument shaft. For example, I could suture along a line parallel with the instrument shaft, as can be done with difficulty (by some surgeons) using conventional MIS instruments, see Figures 8-23 through 8-26.   Also, I could suture along a line perpendicular to the shaft
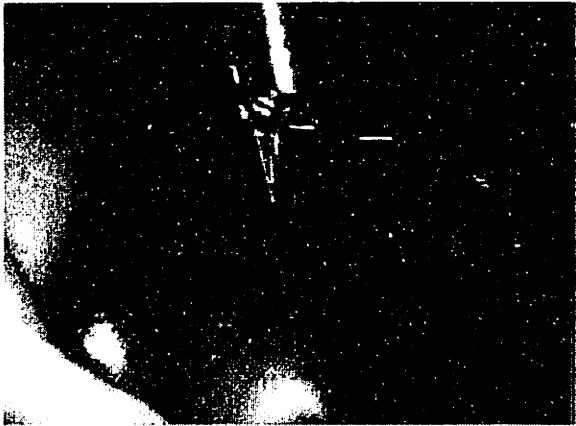
Figure 8-23: Suturing along a line roughly parallel with the instrument shaft. Beginning a stitch.
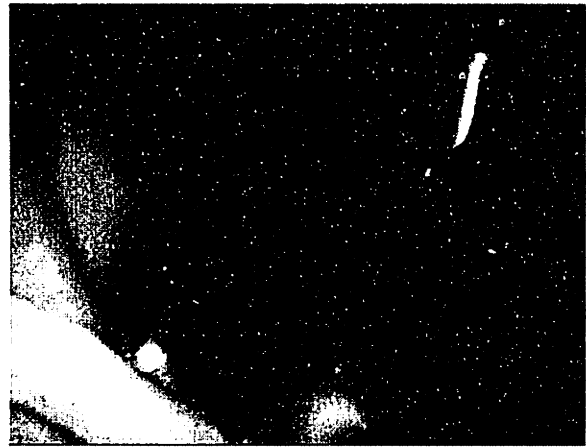
Figure 8-24: Suturing along a line roughly parallel with the instrument shaft. Rolling about the fingers and pushing the needle through the tissue.

Figure 8-25: Suturing along a line roughly parallel with the instrument shaft. Pulling the needle from the tip out of the tissue.

Figure 8-26: Suturing along a line roughly parallel with the instrument shaft. A completed row of stitches.

Figure 8-27: Suturing along a line per-pendicular with the instrument shaft. Beginning a stitch.
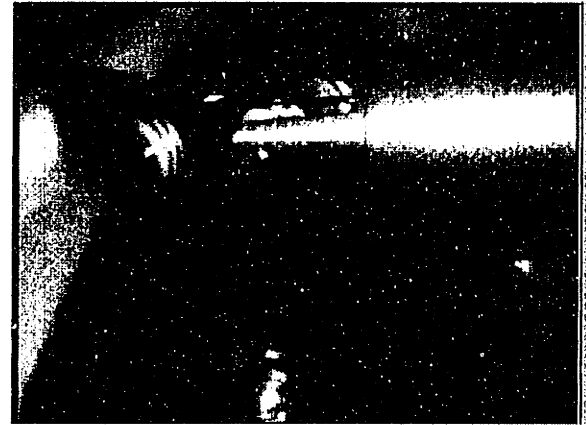
Figure 8-28: Suturing along a line per-pendicular with the instrument shaft. Pulling the needle from the tip out of the tissue.

which is essentially impossible using conventional MIS instruments, see Figures 8-27 through 8-30. It seemed clear that the instrument had sufficient degrees of freedom and that the geometry of the wrist allowed this to occur.

We tried suturing both with and without force reflection. Interestingly, we found force reflection to be more of an annoyance than a help. Our first comment is that the quality of our force reflection is simply is not good enough to help during suturing. Specifically freespace motions still do not yet feel free enough. There are background forces which cause fatigue during fine motions required for suturing.

The second problem is that there is a sufficient deadband in the forces which can be felt that most forces which are applied simply cannot be felt. Based on our discriminations tests, forces below roughly .39 N to .58 N cannot be felt. To give an idea of how soft the tissue is, we depressed it with a force sensor (Mark 10 model BG) with a cone shaped attachment with a 60° included angle. To depress the cone approximately 6 mm required anywhere from 0.22 N to 0.6 N. Since we can easily see deflections of less than 1 mm, we will see deflections and hence forces being applied long before we feel them.

Another way of stating this is that we can already do this task fairly well visually. Whether or not force reflection is necessary (better force reflection than we are able to provide) is questionable. It is unclear whether or not vision or touch is more important during the suturing task even when performed during open surgery.

Motion scaling used to reduce master motions at the slave makes fine motions eas-ier, but reduces the environment compliance sensed by the user. It is already difficult

Figure 8-29: Suturing along a line perpendicular with the instrument shaft. Beginning another stitch.

Figure 8-30: Suturing along a line perpendicular with the instrument shaft. A completed row of stitches.

to sense contact with soft tissue due to its low compliance - with further decreased compliance due to motion scaling it is essentially impossible. To compensate, we can implement force scaling which increases the compliance sensed by the user. However, some of the task forces are fairly large. For example it can take as much as one or two lbs of force (4.4 N- 8.8 N) to push our needle through tissue. We might use a similar amount of force to draw a suture tightly. We have found that these forces, when scaled up by a factor of two, require two hands to apply while simultaneously controlling three positions, three orientations, and a gripper. I found it convenient to use my left hand to support the end of the master while using my right hand to control fine motions. Therefore, if we use force scaling to achieve satisfactory levels of compliance, we find operation of the system is difficult with one hand and certainly operator fatigue.

8.4.2 Tube and Wire Test

Another qualitative demonstration is a task where a plastic (tygon) tube is slid over a curved wire which is mounted in a small piece of wood. Figures 8-31 through 8-34 show this task begin performed. This task is actually somewhat more difficult than suturing for several reasons:

- The required range of wrist motion is greater.

- The contact between the instrument and the wire is stiff. This means large forces can be generated which cannot be resolved using visual feedback. Force
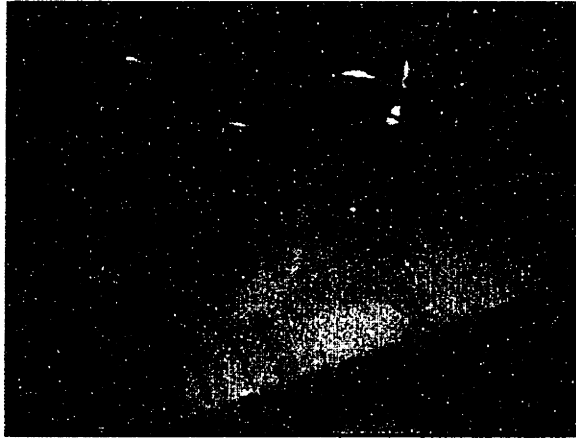
Figure 8-31: Sliding a tygon tube along a metal "S" shaped metal wire.

Figure 8-32: Sliding a tygon tube along a metal "S" shaped metal wire.
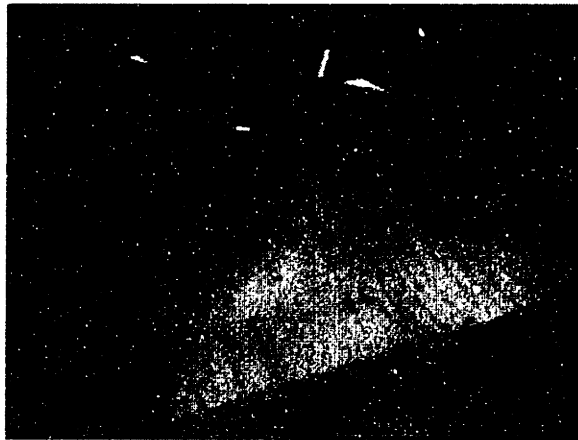
Figure 8-33: Sliding a tygon tube along a metal "S" shaped metal wire.
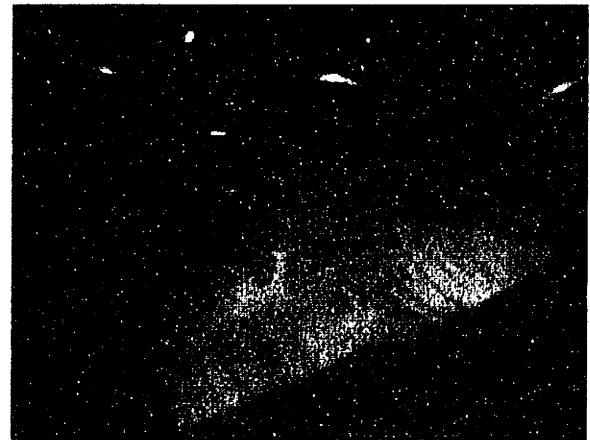
Figure 8-34: Sliding a tygon tube along a metal "S" shaped metal wire.

reflection is therefore more important during this task than during the suturing task.

- Substantial torques can be applied to the wire through the gripper, however we have no torque feedback. Again large forces can be applied to the stiff contact without the user knowing.

- The grip force must be modulated to successfully complete the task. If the tygon tube is gripped too strongly, it will bind on the wire and is unable to slide. Again, we have no gripper feedback (we are not using our actuated gripper here.) Thus grip force can only be modulated through visual feedback, that is by watching the tygon tube deflect.

With force reflection off, I found I could perform this task. However, I had to watch the instrument very carefully for deflections in the instrument in order to determine binding between the tubing and the wire.

With force reflection on, I found that when the tube binds, forces are fedback which stop the master from moving, so it becomes clear that the tube is stuck. However, because there is no torque feedback to tell me which way to reorient the wrist to free the tube, I could only watch very carefully and jiggle the tube in order to free it. In all fairness, this task is very difficult. I found it difficult to slide the tube over the wire when using a standard pair of open surgical needle holders, largely because it is difficult to modulate grip force with these instruments due to their large mechanical advantage. I could only slide the tube naturally when using my bare fingers.

8.4.3 Summary of Task Performance

While we have quantified performance using specific tests, the real proof of such a system is in trying it on real tasks. In this section we looked at two different tasks to further understand system performance. There are three areas which we can assess:

- Mobility: Does the system have enough and correctly placed degrees of freedom, and is there enough range of motion?

  We found that we certainly have the range of motion and degrees of freedom required to suture and to perform the tube and wire task described. I do not think we can ever have too much mobility, but since adding degrees of freedom comes at a very high design cost, we think the level we have achieved is sufficient.

- Force Reflection: How good is it and does it help? If it were better, would it help?

Force reflection, on the other hand, was found not to be particularly helpful during the suturing task. The environment is simply too soft for this to be useful since we can see deflections well before we can feel them. For the tube and wire task, the force reflection is marginally helpful. Since we do not have torque force feedback, if the tube is stuck, we do not know which way to reorient to free it. We can improve force reflection by reducing friction in the wrist unit. This is difficult, but I think possible. I do not think however that this will significantly change the utility of force reflection when handling soft materials.

Given our observations on mobility and force feedback, I think it would be better to use the first wrist pitch of the four-degree-of-freedom Black Falcon wrist to avoid singularities rather than to achieve force reflection. The would help insure that an output roll was always available which we know *is* critical during suturing, while force reflection is not.

- Vision: Do we have appropriate visualization of the operating site?

  Having high resolution 3-D vision is critical. We rely on vision and without it, we are simply in trouble. While this is not a focus of this thesis, given our experience, we are confident that it will be important in a fully functional system for human surgery.

8.5 Areas for Mechanical Design Improvement

8.5.1 Base Unit

- While each link was designed to be very stiff, the bearings which connect them were underdesigned from a stiffness point of view. We could raise the lowest structural natural frequency by increasing rigidity. Larger bearings, appropriately preloaded would increase the overall stiffness.

- The "spindle" and "base" pieces should also be redesigned for increased rigidity. In fact, I reinforced the spindle using two $3/8 \times 1 \times 11$ in aluminum bars to reduce torsional deflections about the x axis. This helped, but the base could still use reinforcement.

- I continue to dislike gears and would suggest a redesign where the base motors (axes 0 and 1) used two stage cable reductions instead of a single stage cable reduction and a gearhead reduction. The additional backlash may be contributing to an inability to raise base gains further during force reflecting master-slave operation.

8.5.2 Wrist Unit

- The wrist unit needs to be in general stronger. We do not use the full actuator potential of the base at this time. Partially because we have found that we do not need it in order to securely hold needles. But I am also wary of pretensioning the system more than we do due to strength of the wrist unit and the spectra cable we are using. More pretension would require stainless steel, or better yet, tungsten cable. This however tends to preclude a non-alpha wrist design due to the extra friction created by alpha wraps when used with metallic cable.

- The attachment between the wrist unit and the base unit cables is inconvenient and not 100% reliable. Currently, this attachment is made with screw clamps.

- We would like to further miniaturize the wrist.

- It is critical that we focus on reducing friction in the wrist if we intend to go forward with macro-micro type controllers for implementing force reflection.

- Finally, the geometry of the wrist must be studied in more detail. The kink introduced by our four-degree-of-freedom wrist design is inconvenient during suturing. It seems to get in the way and rub on the tissue. If correctly oriented, it actually helps keep the instrument shaft out of the tissue, but this is not always the case. While the concept is sound, we feel that the best way to design the wrist geometry to allow macro-micro control is still an open question.

Chapter 9

Conclusions

9.1   Summary

This thesis addresses teleoperator manipulator slave design for Minimally Invasive Surgery, (MIS).

There are several problems in current MIS, specifically:

1. The surgeon is deprived of three-dimensional depth cues and must learn the appropriate geometrical transformations to properly correlate hand motions to tool tip motions.

2. The surgeon's ability to orient the instrument tip is reduced. The incision point/cannula restricts the motions of the instrument from six DOF to four. As a result, the surgeon can no longer approach tissue from an arbitrary angle and is often forced to use secondary instruments to manipulate the tissue in order to access it properly or to use additional incision sites. Suturing become particularly difficult.

3. The surgeon's ability to feel the instrument/tissue interaction is nearly eliminated.

This work is based on the premise that despite surgeons' considerable skill and ability to work within the constraints of current MIS technology, the expansion of minimally invasive medical practice remains limited by the lack of dexterity with which surgeons can operate while using current MIS instruments.

We propose teleoperation as a solution. Specifically, this thesis focuses on the design of teleoperator slave manipulators. Chapter 4 discusses control algorithms

within the context of a three-degree-of-freedom testbed consisting of a two-degree-of-freedom slave and one-degree-of-freedom-master. The slave is designed with a low inertia distal micro freedom mounted to a large inertia macro freedom. We study several forms of macro-micro control which take advantage of the discrepancy in inertia.

In Chapter 5 we present the Silver Falcon telemanipulator slave, a seven-degree-of-freedom arm consisting of a two-degree-of-freedom base which pivots the device about the remote center of rotation created by the surgical incision. This base is coupled to a five-degree-of-freedom non-removable wrist unit. The wrist unit consists of actuation and transmission elements for a wrist and gripper which is attached to an instrument shaft which passed into the body. This system was tested using a PHANToM haptic interface as a master manipulator, modified with an instrumented gimbal and gripper to measure positions of seven degrees of freedom. Three directions of force feedback are available with this master.

There were a number of areas where the Silver Falcon was limited. The wrist kinematics allowed us to use macro-micro control in only two out of three directions meaning that there was always one direction in which the surgeon could not feel forces. There were also practical issues such as excessive structural flexibility, insufficient base servo performance, and the lack of sufficient grip strength to hold needles securely. Finally the wrist was designed as an integral part of the system and is not interchangeable with other instruments or sterilizable.

Our second teleoperator slave, the Black Falcon, is described in Chapter 7 and was designed to address some of these issues. This eight-degree-of-freedom arm is structurally stiffer and stronger with increased actuator capacity. The system is counterbalanced for safety by placing all of its actuators at its base and using cable transmissions to actuate the wrist and gripper. This also allows the wrist unit to be detachable to allow future development of wrist-units which perform other functions, such as cutting, grasping tissue instead of needles, and cauterizing. This basic concept also allows the actual portion of the instrument which enters the body to be sterilized. The wrist was redesigned with an additional degree of freedom to allow macro-micro control in all three linear degrees of freedom with the goal of allowing forces to be felt equally well in all three directions.

We found that the system had the appropriate kinematics and range of motion to allow suturing along arbitrarily oriented suture lines. Force reflection was however inadequate to help the suturing task. Force reflection is more useful during rigid contact tasks where force information is not available to the operator via visual cues. One such task, although not surgical, is sliding a plastic tube along a curved metal wire, a task which is difficult using direct manipulation with open instruments. We

could perform this task using the Black Falcon, albeit with difficulty. The lack of torque feedback from our master manipulator was a noticeable limitation during this task. Tests were carried out using both the PHANToM haptic interface and the Tool Handle (a scaled up version of the PHANToM) as a master each mounted with an instrumented gimbal and gripper.

9.2 Comments on Master Design

A few comments are warranted on the design of master manipulators for minimally invasive surgery, and in particular on the suitability of the PHANToM haptic interface for this purpose. In general we very much like the PHANToM, a three-degree-of-freedom arm which is nearly counterbalanced mechanically (the remainder can be done in software using motor torques) and which has low friction and no backlash in the transmissions. There are several areas where we might improve this system when used as a master manipulator:

- To have similar encoder resolution to the Black Falcon, resolution needs to be improved by roughly $100\times$. This would improve master-slave teleoperation by giving the slave a much smoother command to track. This would allow higher base gains to be implemented to improve both tracking and force reflection performance.

- Continuous force levels need to be increased by about $10-20\times$ to allow scaled force reflecting teleoperation.

- The structural stiffness of the master is low and could easily be increased by several times through improved design, especially bearing design at the joints.

- A higher-degree-of-freedom wrist is required. One of the most annoying problems while using the system was running into rotational limits of the master well before running into such limits on the slave. One solution is to use a kinematically identical master and slave so that singularities and joint limits are aligned. However reorientation of the slave relative to the patient would then require reorientation of the master to keep this benefit. The other solution is to increase the range of motion of the master wrist, most likely through the use of a four-degree-of-freedom wrist, that is through the addition of an output roll. In order to take advantage of this however, the gimbal must have at least one controlled joint (the input roll) in order to ensure that singularities are avoided.

- There is another reason to power the wrist joints. When the surgeon lets go of the master (which they have a surprising tendency to do), the master wrist will

simply fall. Even if it were balanced one could bump it easily. The slave wrist will then track this motion potentially causing damage to tissue. Assuming that sensors are incorporated to determine whether or not the surgeon is holding the master, then we have two options. First we can disconnect the two in software, so that when the master wrist falls, the slave wrist does not move. In this case re-engaging the system becomes a problem, in that the surgeon would have to realign the two (with some sort of visual cues displayed on the video monitors for example) before the controller would re-engage the system. The second option is that we power the master gimbal so that when the surgeon lets go, it simply freezes in position so that misalignment between the master and slave never occurs. Another advantage of this approach is that if the slave manipulator is repositioned with respect to the patient, the master manipulator can reposition and reorient itself automatically in order to maintain visual correspondence between the two.

The disadvantage to powering wrist is that it generates a substantial increase in design complexity and possibly weight.

- Finally, we may want to go one step further and not only power the wrist but design these degrees of freedom to allow precise application of forces in order to give the surgeon torque, as well as force, feedback. We would have to experiment with such a system to answer this question.

9.3   Future Work

9.3.1   Improved Force Reflection

The quality of force reflection could be improved, though it is unclear that this will necessarily improve surgical task performance. One option to improve force reflection is to pursue our current track and further improve the transmission characteristics of these systems, primarily in order to reduce friction. Brushless motor technology which typically has had many problems when applied to force control may have improved sufficiently to help here as well.

Another option is to incorporate additional modes of sensing into the system. This does not imply removing the good qualities (low friction and backlash free transmissions, lightweight distal joints) which we have strived to incorporate, but rather to augment them in order to further improve the system. Force sensing in particular has for many years been a subject of much interest, but has in my mind not fulfilled expectations. Perhaps improvement in the quality of sensing available will in the future

make the addition of force sensing a reliable, robust, and accurate way to augment the quality of our force reflection.

9.3.2 Enhanced Modes of Teleoperation

Replacing hand-held instruments with teleoperators opens the door to enhanced modes of surgery. In particular, we have a way of giving more information to the surgeon in a fairly natural way.

9.3.2.1 Visual Overlays

The first way is to include visual overlays into the surgeon's view of the operating site. Since this view is already planned to be in 3D, why not have images, MRI images of tumors for example, directly overlaid onto this view? This would be an incorporation of work such as (Grimson et al., 1996) into teleoperated MIS.

9.3.2.2 Haptic Overlays

The second is to add haptic overlays onto the workspace of the master manipulator. We can easily place walls or funnels within this workspace in order to guide the surgeon or to protect sensitive areas from accidental contact. The difficult part of both the visual and haptic overlay problems is actually getting the information accurately and registering it to the actual anatomy. Displaying the information is relatively simple.

9.3.2.3 Beating Heart Surgery

Another enhanced mode of surgery is operating on moving tissue. The classic example is operating on a beating heart, in order to avoid the need for a heart lung machine and the trauma and risk associated with circulating blood through it. If the motion of the heart can be measured, the slave can track this motion. In the reference frame of the slave, the heart is now still. The same thing can be done to the image of the heart, either by having the arm which holds the camera track the heart, or by nulling out motions in the image using the measured position of the heart. Then the illusion can be created for the surgeon that he is operation on a still heart, when it is in fact beating. As with many problems, the difficult part is the sensing, and in this case measuring where the heart is. For the slave to track this, we need information at servo rates, preferably at better than servo rates so that we may filter noisy data. How then can we determine six-degree-of freedom motion at say 2000 Hz? It will be difficult or

impossible to do this using a video image which typically supplies information at 30 or 60 Hz. We suggest using a small instrumented mechanical arm whose end (a small horseshoe shaped platform for example) is placed directly onto the heart. A serial or parallel linkage with optical encoders mounted at the joints could easily measure six degree of freedom motion at sampling rates in the kHz range. This arm would then both partially stabilize the heart and measure its motions precisely, at rates limited only by computational speed.

Appendix A

Will minimally invasive CABG be worthwhile? Lessons from laparoscopic cholecystectomy, coronary angioplasty and open CABG.

Introducing new, potentially expensive technology into medical practice is a cause for concern, especially in light of rapidly growing health care costs. Today, health care costs in the U.S. are estimated as being roughly 15% of the GDP.

The technology presented in this thesis has not yet been introduced into medical practice. However, I am concerned that if and when it is, that it is done for the right reasons. One particularly touted application is Coronary Artery Bypass Grafting, (CABG). Whether it will be worthwhile is impossible to answer at this point. Much is yet to be learned. In order to better understand the costs and benefits involved, we studied several well known MIS procedures, and two new currently practiced forms of MIS CABG.

A.1 Introduction

There is a great deal of interest today in minimally invasive coronary artery bypass graft surgery (CABG), (Winslow, 1997). We are referring specifically to two different currently practiced forms of heart surgery. The first is "MIDCAB" surgery (Minimally

Invasive Direct Coronary Artery Bypass) where a mini-thoracotomy (10 cm incision) is made in the chest and a short portion of one rib is removed to access the heart. The heart is accessed using standard instruments. A primary proponent of this type of surgery is Cardio Thoracic Systems (CTS), of Cupertino, CA. The second is "port-access" CABG surgery as advocated by Heartport, Inc. where more typical minimally invasive surgical instruments are used. Both procedures are new and in contrast with open CABG where a full sternotomy is performed and the ribcage literally split in two.

As the new procedures and technologies are introduced, some questions will naturally arise: Will patient outcomes be improved? Will there be an increased risk of complications? Will MIS CABG save money or will it be more expensive than traditional CABG? Will surgeons accept these procedures? Will patients demand them? Are these procedures really necessary, or is the primary push coming from the medical instrument industry? To better understand some of these questions and what the relevant costs and benefits might be, we take an historical look at the use of minimally invasive surgery for cholecystectomy, comparing laparoscopic and open techniques, and for cardiac surgery, comparing open CABG to percutaneous transluminal coronary angioplasty (PTCA).

MIS procedures have been touted as directly reducing costs to payers in terms of decreased hospital stay. However, there have also been higher reported complications and questionable improvements in efficacy. At the same time, we have seen and surgeons have predicted for several years the increased use of MIS techniques, (Bloom et al., 1995).

We find that in the case of laparoscopic cholecystectomy, a consensus has been reached by the medical community that this is a useful and viable procedure which patients prefer, (NIH, 1993). However the actual quantitative savings in terms of hospital costs and long term outcomes appear to be slight with estimates ranging from essentially 0% to 20%, (Bass et al., 1993), (Fisher et al., 1991). The primary cost savings is in reduced hospital stay which is offset considerably by the higher cost of instruments. The consensus seems to be that the increased cost due to increased risk of bile duct injury apears to have diminished as surgeons have become more experienced with the procedure. Patient satisfaction and cost due to reduced time away from work, while important, do not typically enter the published studies.

When comparing CABG to medical therapy alone to treat coronary artery disease, it is clear that CABG improves quality of life, but unclear that it increases life expectancy except in severe cases such as triple vessel disease or occlusion of the left main coronary artery. Given their large number (roughly 400,000 annually in the United States) the procedure is clearly well accepted.

When comparing angioplasty to CABG, it is unclear as to which is in fact less expensive. The primary reason is that the rate of restenosis in angioplasty is high requiring subsequent angioplasty or CABG. It is likely that the less invasive nature of angioplasty drives surgeons to administer it (and patients to request it), despite published comparisons of costs and effectiveness.

Finally, it is too early to make clear statements about the cost effectivenes of new MIS cardiac procedures. A preliminary estimate indicates that the cost saved due to reduced hospital stays is not sufficient to offset additional instrument costs. The cost savings to the patient or their employer due to a faster return to work (in the case they are working) could be substantial, but is unlikely to drive the technology since the hospital or payer do not see these savings. The desire to improve outcomes and to keep abreast with the latest technology may well be the deciding factors in driving these techniques into the market.

A.2 Laparoscopic versus Open Cholecystectomy

A.2.1 Introduction

Until 1991, the primary treatment of symptomatic gallstones was surgery to remove the gallbladder, which resulted in a roughly 5-day hospitalization and 3-6 week period of convalescence. Alternative treatments have since been developed including oral bile acid dissolution, contact solvent dissolution, mechanical extraction through a catheter, and fragmentation by shock wave lithotripsy combined with oral bile acid dissolution. These treatments all leave the opportunity of recurring gallstones since the gallbladder is left in place, (NIH, 1993).

Laparoscopic cholecystectomy was first performed in the U.S. in 1988. Using this technique, the abdomen is first inflated with CO_2, an endoscopic camera and surgical instruments are inserted through small incisions (.5 inch) in the abdomen to view the operating site and to perform the necessary manipulations to remove the gallbladder. It was estimated in 1993 that 80% of cholecsystectomies were performed this way, and today the percentage is most likely above 95%.

A.2.2 Published Comparisons

A number of studies compare cost effectiveness and efficacy of laparoscopic cholecystectomy with that of open cholecystectomy. We find that despite the much publicized potential for cost savings, the actual cost advantage of laparoscopic over open chole-

Type of Clinical Event	Open Chole Probability	Lap Chole Probability
Operative mortality	0.002	0.0008
Major nonfatal operative complication	0.10	0.033
Postchelecystectomy syndrome	0.05	0.05
Retained gallstones	0.01	0.01
Successful T-tube extraction	0.95	-
Mortality from T-tube extraction	0	-
Recurrent stone in bile duct	0.01	0.01
Successful removal of bile duct stone by endoscopic sphincterotomy	0.90	0.90
Mortality from endoscopic sphincterotomy	0.01	0.01
Mortality from re-exploration of billiary tree	0.018	0.018
Biliary stricture formation	0.01	0.025
Mortality from choledochoenterostomy	0.02	0.02
Stricture recurrence after repair	0.20	0.20
Conversion from open to lap surgery	-	0.042

Table A.1: Probabilities of Clinical Events During Cholecystectomy (Bass et al., 1993)

cystectomy is slight and could be easily subsumed by additional costs due to complications. There is evidence that patient satisfaction and a desire to keep abreast of technology as opposed to economic benefits to paying organizations or hospitals appear to be a prime motivator for the widespread acceptance of the procedure, (Escarce et al., 1995).

(Bass et al., 1993) performed a cost-effectiveness analysis comparing laparoscopic cholecystectomy with open cholecystectomy. They used a decision analysis type approach, estimating probabilities of outcomes, made quality-of-life adjustments, and estimated costs of different health states. Reviewing the results is interesting in order to find where the potential costs and benefits are for MIS procedures in general.

They first assigned probabilities to clinical events and gave references regarding how these probabilities were assigned, see Table A.1. Base estimates are for 45 year old women. These probabilities indicate that 1) a major non fatal complication is 3 times more likely in open cholecystectomy, and yet 2) biliary stricture formation is 2.5 times more likely in laparoscopic cholecystectomy. This indicates the basic tradeoff between the increased potential for complication due to the surgical wound in open surgery versus the increased possibility of making mistakes during MIS procedures.

They then identified types of morbidity and assigned utility values, Table A.2.

Type of Morbidity	Utility Value
Complications	
Complications of surgery	0.77
Postcholecystectomy syndrome	0.79
Surgical scar	0.988
Procedures	
Laparoscopic chole	0.91
Open chole	0.77
Endoscopic sphincterotomy	0.95
T-tube extraction of stone	0.83
Reexploration of biliary tree	0.77
Biliary stricture surgery	0.64

Table A.2: Utility Estimates (Bass et al., 1993)

This confirms our notion that morbidity due to the open procedure is higher than that for the laparoscopic procedure. Using their probability and quality of life estimates, they found the expected gain in quality adjusted survival with laparoscopic cholecystecomy over open cholecstectomy for 45 year old women to be just 0.29 months (52.16 versus 51.89), or just a fraction of a percent of the total gain due to either procedure. So based on quality alone, this analysis does not show a significant difference between either procedure.

Bass et al. estimates costs from their experience in the state of Maryland. For a 45 year old individual with acute or chronic biliary pain and documented gallbladder stones, the differences in projected average total charges at the end of 1 month were less for the laparoscopic procedure than for open procedure by $651.00 ($4431 vs. $5082) for women, and $1271 ($5118 vs $6389) for men. Though it is not stated explicitly, I believe the estimates are given in 1993 dollars. Over 5 years the savings due to the laparoscopic procedure were $171 for women and $794 for men. The difference is greater if only patients with acute cholecystis are considered ($1019 for men and women combined). However if they considered using a pre-operative retrograde cholangiography and sphincterotomy (raising charges by $667), then for 45 year old women charges were increased on average by $496.

To summarize, the differences are slight. The addition of cholangiography, which is standard in teaching hospitals, can make laparoscopic procedure more expensive than the open one, not less. The primary complication is bile duct injury which has

a substantial effect on the analysis because of the high costs associated with it. In support of the laparoscopic procedure, however, we note that Bass et al uses a 2.7 day average hospital stay for the lap chole, whereas most reports today estimate a 1 day stay. Also, the analysis does not include indirect costs such as time lost from work which might make a substantial difference in favor of lap chole.

Another perspective on the likelihood of complications is given by Bernard et al, (Bernard and Hartman, 1993). Complications which are not discussed in Bass et al are: major vascular injury (aorta, vena cava), hematoma or hemorrhaged bowels, bladder perforation, and incarcerated bowels (through the instrument ports). Apparently these totaled 158 for New York State between August 1990 and March 1992. Almost 72% resulted in open surgical repair. 18% resulted in conversion to open cholecystectomy during the same procedure. This data was available because N.Y. State health law requires such incidents to be reported to the State Health Department.

Until January 1992, a separate identification code did not exist for laparoscopic cholecystectomy. [1]. So the total number of laparoscopic cholecystecomies during that time was not reported in Bernard et al, but they do report that between January 1, 1992 and October 29, 1992, 19,697 cholecystectomies were reported and 13,159 were coded as laparoscopic cholecystectomies. Due to time delay in reporting, they expect the numbers to be much higher. They also show, between April and October 1992, that there were 22 major complications reported due to open cholecystecomy vs. 90 complications during laparoscopic cholecystectomy, with 5 major bile duct injuries or leaks during open chole compared to 44 during lap chole. This data contradicts the results found by Bass et al. Both studies were published in the same April 1993 issue of the American Journal of Surgery.

We might suppose that New York State is different. However the data presented is real (albeit retrospective and using fairly small sample sizes). Bass et al estimated complication rates because they found actual data to be difficult to acquire as no randomized trials had been done to that time.

Despite this one fairly negative report, most other reports support the view that laparoscopic cholecystectomy is a valid and useful procedure. For example the NIH formed a Consensus Development Panel on Gallstones and Laparoscopic Cholecystectomy which supports this view, (NIH, 1993). They state that: "Laparoscopic cholecystectomy provides distinct advantages over open cholecystectomy. It decreases pain and disability without increasing mortality or overall morbidity. Although the rate of common bile duct injury appears to be increased, this rate is still sufficiently small

---

[1] The Statewide Planning and Research Cooperative System, SPARCS, processes data from N.Y. state hospitals

to justify the use of laparoscopic cholecystectomy in the treatment of symptomatic gallstones."

Williams et al (Jr. et al., 1993) also supports this view and states: "LC appears to be a safe procedure with a low incidence of complications including bile duct injury when performed by adequately trained surgeons".

Steiner et al (Steiner et al., 1994) states that using data from 1985-1992, "In Maryland, although the adoption of laparoscopic cholecystectomy has been accompanied by a 33 percent decrease in overall operative mortality per procedure, the total number of cholecystectomy-related deaths has not fallen because of a 28 percent increase in the total rate of cholecystectomy". In other words, in terms of overall societal costs, there has been an increase in the rate of cholecystectomies, which likely offsets any savings due to individual procedural costs.

The question of costs for MIS procedures is a subject of debate with much argument concerning the costs of the specialized instruments used to perform laparoscopic surgery. For example, Traverso (Traverso, 1995) studied costs for laparoscopic surgery over a one year period and found that 28% of OR costs could be attributed to disposable instruments. He recommends that reusable instruments be used to decrease costs (Traverso, 199). In contrast, Reichert (Reichert, 1993) suggests that when the full costs of labor and time required to maintain and sterilize reusable instruments are considered, that disposables justify their cost and decrease risks associated with the difficulty in sterilizing these complicated instruments. Voyles in fact reports published hospital costs for laparoscopic cholecystectomy which vary by a factor of 4 between different hospitals, (Voyles, 1993)

We note finally that, despite a lack of quantitative evidence at the time, laparoscopic cholecystectomy was rapidly adopted and accepted amongst general surgeons. Diffusion of the procedure amongst general surgeons went from several % in 1990 to 81% in 1992, (Escarce et al., 1995). More than three fourths of the adopters questioned in this report stated a "desire to keep up with the state-of-the-art and improved patient outcomes as very or extremely important reasons for adopting laparoscopic cholecystectomy."

A.2.3 Summary

A consensus has been reached by the medical community that laparoscopic cholecystectomy is a useful and viable procedure which patients prefer. However the actual quantitative savings in terms of hospital costs and long term outcomes appear to be slight. All of the following issues are relevant:

- Decreased morbidity and improved patient satisfaction with laparoscopic cholecystectomy.

- Decrease time lost from work with laparoscopic cholecystectomy.

- Increased risk of complications such as bile duct injury with laparoscopic cholecystectomy.

- Increased risk of complication due to wound trauma due to open cholecystectomy.

- Decreased cost of hospitalization in laparoscopic cholecystectomy.

- Increased cost of instruments in laparoscopic cholecystectomy.

- Technological imperative - the feeling in the surgical community that one must remain current with the technology.

A.3 Coronary Artery Disease

The second area we look at is cardiac surgery, in particular we look at the comparisons which have been made between coronary artery bypass grafting surgery (CABG) and medical therapy and also comparisons between CABG and percutaneous transluminal coronary angioplasty (PTCA). In the near future, I expect the introduction of minimally invasive CABG will produce similar comparisons. Below we discuss published reports on the efficacy of CABG versus medical therapy, and of angioplasty versus CABG.

The methods of assessment for CABG, in addition to the procedure, have gone through a period of evolution according to Preston (Preston, 1989). CABG was developed in the late 60's, and early assesments in the early 70's were largely anectodal. The first large randomized study, the Veterans Administration Study, was reported in 1976 (Murphy et al., 1977), followed by the European Coronary Surgery Study (ECSS) (Varnauskas, 1988), and the NIH-sponsored Coronary Artery Surgery Study (CASS) (CASS, 1983a; CASS, 1983b), discussed below. It is interesting that, as Preston states, initially cardiologists asked cardiac surgeons to support their claims that CABG was an efficacious treatment when compared to medical therapy. But the tables turned after the introduction of angioplasty, with cardiac surgeons asking cardiologists to justify the recommendation of angioplasty.

A.3.1 Efficacy Studies

A.3.1.1 CABG versus Medical Therapy

The first question is whether or not CABG prolongs life, or whether the primary benefit is to improve quality of life when compared to medical therapy. Weinstein et al (Weinstein and Stason, 1982) states that the Veterans Administration (VA) Cooperative Study and the European Coronary Surgery Study Group indicate that surgery prolongs life in patients with coronary artery disease involving three vessels or the left main coronary artery. In contrast, the CASS reports surivival data which states: "In contrast to the European Collaborative Study, the CASS does not show a significant decrease in survival rates for patients with three-vessel disease and ejection fractions greater than 0.50, or in patients with two- or three-vessel disease involving the left anterior descending coronary artery.", (CASS, 1983a).

The CASS reported specifically on both survival data (CASS, 1983a) and on the quality of life (CASS, 1983b) associated with CABG as compared to treatment with medication alone. This study followed 780 patients with $\geq$ 70% stenosis of one or more operable vessels for a mean of 5.5 (3.8-7.7) years and used the following factors for comparison:

- Chest pain: classified as occurring during four different cases ranging from strenuous physical activity to occuring with any activity or at rest.

- Activity limitation: classified by levels of limitation during normal daily activities.

- Heart failure: recorded if patients reported ankle edema, dyspnea, or orthopnea.

- Graded exercise tests: a series of treadmill exercises.

- Employment status: unemployed, part time employed or full time employed.

- Recreational status: classified as strenuous, moderate, mild, or sedentary.

While there were no significant differences noted in heart failure, employment status, or recreational status between the surgical or medical groups, there was marked difference between chest pain status, activity status, and graded exercise tests. For example, roughly 20% more patients who underwent surgery reported no chest pain after five years than did those who underwent medical therapy alone averaged over patients with one, two, and three vessel disease. The need for extensive drug therapy

causes problems with compliance, may itself reduce quality of life, and adds cost for the life of the patient.

The conclusion is that CABG definitely improves quality of life when compared to medical therapy alone, but most likely does not improve life expectancy in one and two vessel disease. The CASS left some question as to whether or not it improves life expectancy in left main disease or in three vessel disease. In speaking with surgeons today however, there seems to be littlex doubt that in the case of three vessel or left main disease that CABG improves life expectancy.

A.3.1.2 CABG versus Coronary Angioplasty

For reference, there have been a number of trials comparing angioplasty with CABG. These include the Randomized Intervention Treatment of Angina (RITA) trial (Hampton et al., 1993), the German Angioplasty Bypass Surgery Investigation (GABI) (Hamm et al., 1994), the Coronary Angioplasty Bypass Revascularization Investigation (CABRI), the Argentine Randomized Trial of Percutaneous Transluminal Coronary Angioplasty versus Cornary Artery Bypass Surgery in Multivessel Disease (ERACI) (Rodriguez et al., 1993) and the Bypass Angioplasty Revasularization Investigation (BARI) (BARI, 1991).

The main points of comparison between angioplasty and CABG can be seen by looking at data from Hamm et al, (Hamm et al., 1994). In this study, patients with at least two major vessels supplying different myocardial regions of the heart were studied. Hospitalization was 19 days for CABG versus 5 for PTCA. Q-Wave myocardal infarction was more common in CABG (8.1%) than in PTCA (2.3%). In hospital mortality was 2.3% in CABG versus 1.1% in PTCA. 93% of CABG patients were free from angina at discharge versus 82% for PTCA. 6% of CABG patients required further intervention within one year (1% CABG and 5% PTCA) versus 44% of PTCA patients (18% CABG and 3% PTCA).

It is clear, from this study and others, that while CABG is a substantially more traumatic experience for the patient, the likelihood that the patient will be free from angina is much higher.

A.3.2 Cost-Effectiveness Studies

A.3.2.1 CABG vs. Medical Therapy

Weinstein et al (Weinstein and Stason, 1982) performed a cost-effectiveness analysis of coronary artery bypass surgery versus medical therapy in 1982 which tries to measure

	Gone	Improved	Same or Worse
Medical	16%	32%	52%
Surgical			
year 1	63%	20%	17%
year 2	45%	11%	44%

Table A.3: Outcomes for Medical Therapy vs. CABG, from Weinstein et al, (Weinstein and Stason, 1982)

	1vd	2vd	3vd	LMD
surgical	20.7	20.3	20.4	19.5
medical	20.9	19.7	17.2	12.6
difference	-0.2	+0.6	+3.2	+6.9

Table A.4: Expected Increase in Life Expectancy for CABG over Medical Therapy, from Weinstein et al, (Weinstein and Stason, 1982)

cost-effectiveness in terms of quality-adjusted life years (QALY's) and assigns a net cost per added QALY. They consider the following outcomes for life expectancy: operative mortality, survival after surgery, and survival with medical management. They try to asses quality by assigning a weight to each level of angina in order to derive a measure of quality adjusted life-years. Based on the data in Table A.3 on relief from symptoms and life expectancy, they find values for quality-adjusted life expectancy for surgical versus medical therapies for one, two, three vessel disease and left main disease, Tables A.4, A.5.

Essentially, their quality of life assessments serve to modify their survival data, but do not seem to have a large effect on overall advantage, in life years, of one

	1vd	2vd	3vd	LMD
surgical	17.1	16.8	16.9	16.2
medical	16.6	15.7	13.7	10.0
difference	+0.5	+1.1	+3.2	+6.2

Table A.5: Quality Adjusted Expected Increase in Life Expectancy for CABG over Medical Therapy from Weinstein et al., (Weinstein and Stason, 1982)

	1vd	2vd	3vd	LMD
$000	30	17.5	7.2	3.8

Table A.6: Net Cost per Quality-Adjusted Life Year Gained Using Surgery instead of Medical Therapy for Q = 0.7, from Weinstein, (Weinstein and Stason, 1982)

procedure over the other.

Weinstein defines four sources of costs:

- Cost of surgery itself.

- Differences in the cost of medical management with and without surgery.

- Savings due to the prevention of coronary artery disease, especially myocardial infarction.

- Differences in costs of repeated or subsequent operations.

He then finds the net cost per quality adjusted life year gained by using surgery instead of medical therapy for various levels of angina. For example, for patients with severe angina (Q = 0.7), Table A.6. The majority of the cost difference is due to the cost of surgery as opposed to savings on medical therapy. If increased quality-adjusted life expectancy is in question, the above analysis is meaningless. This is likely to be the case in one and two vessel disease.

To summarize this information, if a substantial increase in life expectancy exists, then cost effectiveness based on this study turns out to be essentially the cost of surgery divided by the increase in life expectancy. Of course, if the efficacy of two treatments is equal in terms of QALY's, then while differential cost-effectiveness is undefined, the lower cost treatment can still be selected.

A.3.2.2 CABG vs. Coronary Angioplasty

Reeder (Reeder et al., 1984) compares the cost of percutaneous coronary angioplasty with that of bypass surgery. This is a one year retrospective study of 79 patients who underwent PTCA and 83 patients who underwent CABG in order to compare costs and to some degree reported benefits between the two.

Costs included those due to initial hospitalization, follow-ups, later procedures and hospitalization for restenosis either using PTCA or CABG. Over the course of

one year, the average cost for PTCA was found to be 15% lower than for CABG (not adjusted for quality of life). However, the costs for PTCA ranged from a roughly 50% lower cost for patients who did not require subsequent restenosis to a 52% higher cost for those who required subsequent restenosis via CABG. An overall 33% restenosis rate (both via PTCA and CABG) was reported.

The authors suggest that a substantial savings could occur if the percentage of patients requiring restenosis were reduced. At the time this seemed likely because the procedure was still young. However, other more recent studies (King et al., 1994) report the levels of restenosis required in PTCA over the course of three years is over 50%, suggesting this is unlikely.

Quality of life was reported as essentially equal between PTCA and CABG treatments. Patients seemed equally satisfied (or dissatisfied) with their health status. However, the percentage of patients who returned to work (who were working prior to treatment) was significantly higher amongst PTCA patients (95% for PTCA versus 75% for CABG). We can speculate that the trauma induced by CABG is sufficient to deter patients from returning to work even after (or perhaps because of) a relatively long period of post operative convalescence.

A.3.3 Summary

We have looked at some published comparisons between treatments of coronary artery disease via medical therapy, percutaneous transluminal coronary angioplasty (PTCA), and coronary artery bypass grafting (CABG) surgery.

It is clear that CABG improves quality of life when compared to medical therapy alone, but unclear that it increases life expectancy except in severe cases such as triple vessel disease or occlusion of the left main coronary artery. This comes at a substantial monetary cost, and while it is the subject of debate, it appears to be the consensus among physicians that it is worth the cost.

When comparing angioplasty to CABG, it is unclear as to which is in fact less expensive. The primary reason is that the rate of restenosis in angioplasty is high requiring subsequent angioplasty or CABG. The obviously less invasive nature of angioplasty compared to CABG likely drives cardiologists to administer it (and patients to request it). It is unclear whether a real comparison of costs and effectiveness is made during these decisions. It is clear that these procedures are complimentary and should be administered on the basis of individual circumstances.

A.4 New Cardiac Technology

This finally brings us to new minimally invasive techniques for cardiac surgery. Up to this point we have found that minimally invasive technology was rapidly accepted in the case of laparoscopic cholecystectomy and coronary angioplasty prior to any controlled trials to prove efficacy and cost effectiveness. The decrease in recovery time and trauma to the patient seem like clear advantages. Surgeons cite a desire to keep abreast with the technology and to improve patient outcomes, and the perception that these techniques decrease costs to the payer, typically insurance companies, primarily through a reduction in hospital stay.

In fact, the decrease in cost was not that initially perceived in either case. The costs during MIS procedures could be greater due to the cost of follow up procedures and costs associated with complications, and the cost of instrumentation is typically higher for instruments used in MIS procedures.

For new MIS cardiac procedures, we find that these same tradeoffs exist. The cost of instruments is very high, but at this point it is difficult to say whether or not it will be worth it because complications data has been difficult to find in the absence of controlled trials. The procedures are in fact less than a year old, and the companies making instruments in the area have not released specific complications data.

It is clear though that the promise of CABG which does not require a standard (split ribcage) sternotomy is in high demand, (Winslow, 1997) The promise is to have a procedure with the effectiveness of open CABG, but with a recovery closer to that of angioplasty. It is difficult to assess whether the cost of decreased hospital stay and recovery time will sufficiently offset the cost of instrumentation, though I will briefly estimate this below.

A.4.1 New Technology

Obviously, I feel that a major new technology is teleoperated MIS which has been presented in this thesis. However, here I only discuss currently practiced methods.

There are two different approaches which are currently practiced and being called "Minimally Invasive Cardiac Surgery" at this point in time. The first is done through a mini-thoracotomy, whereby a relatively small (6 cm) incision is made in the chest wall and short (1-2") portion of rib is removed to create access to the heart. CABG's have been done through this approach both on cardio-pulmonary bypass (CPB), and while the heart remains beating.

Cardio Thoracic Systems (or CTS, in Cupertino, CA) specialize in beating heart

CABG using a mini-thoracotomy. This is often called MIDCAB (Minimally Invasive Direct Coronary Artery Bypass). About 1400 CTS MIDCAB procedures had been performed through June 1997, 900 of which were done in the first quarter of 1997. There is essentially no new technology involved in this procedure. The enabling device is essentially a horseshoe shaped spatula used to physically stabilize the heart so that the surgery may be done on the beating heart.

The second approach, which I am more interested in, is known as "port-access" and is closer to what we think of as MIS surgery where instruments are inserted through trocars (or ports) as in laparoscopic cholecystectomy. The primary company involved with this type of surgery is Heartport, (Redwood City, CA). Heartport prefers to use CPB while performing CABG. Without physically stabilizing the heart, as done by CTS, it is very difficult (even through open visualization) to operate on a beating heart. Heartport also states that doing CABG under CPB is the "gold standard" and allows the entire heart to be accessed in order to perform multiple bypasses.

The Heartport product line is considerably more extensive. Their products include:

1. A system for doing MIS CPB consisting of catheters and a balloon aortic clamp.

2. A Port-access MVR (mitral valve repair) system consisting of a thoracoscope, specialized instruments and a tissue retractor.

3. A Port-access CABG system consisting of a thoracoscope, specialized instruments, and a tissue retractor.

A.4.2 Complications and Efficacy

The data regarding procedures done with Heartport systems consists of press reports with a few preliminary reports from surgeons using the system. There have been no controlled trials to date. As of March 31, 1997, approximately 650 cardiac surgery procedures had been performed using the various systems above. 300 of these were performed in the first quarter of 1997. About 250 of these were mitral valve procedures. Until January 1997, approximately 20% of the CABG operations were double- or triple-vessel. The first Heartport quadruple bypass was reported on March 20, 1997.

According to a press report dated October 8, 1996 (http: //www.pslgroup.com/dg /cdf6.htm) the Heartport systems are becoming routine at the Cardiovascular Institute at the Dresden University Hospital. Data based on the first 30 patients to undergo port-access surgery had hospital stays of 5 days on average as compared

with 7 to 10 day stays after the open procedure. Operating room time was 4.5 hours, "slightly longer" than during the open procedure. 3 to 6 months after the procedures, there was no mortality and one patient required reoperation with the open-chest approach.

In a letter sent to the New England Journal of Medicine, surgeons from the same Dresden institution reported that based on experience with 12 patients, "minimally invasive bypass surgery appears to be feasible without an increase in risk to the patient," and that "safety and efficacy of cardiopulmonary bypass and cardioplegic arrest are the same as in conventional bypass surgery", (Reichnspurner et al., 1997). Obviously at this stage, without controlled trials, we must assume some level of opinion is involved in these statements.

Heartport themselves state only that post-surgical hospitalization may be shortened "from about six days to about three or four days" and that "patients may experience less pain and trauma, have a reduced risk of complications, and have only minimal scarring from the small 'port' incisions."

A.4.3   A Brief Cost Assessment

It is difficult to assess costs given the limited data available. Based on experience with laparoscopic cholecystectomy and coronary angioplasty, we would expect that the primary cost savings results from reduced hospital stay, and the primary additional cost is price of new instrumentation. Additional costs which are more difficult to measure are the cost of increased or decreased complications and costs which are saved (by the employer or employee) by a faster return to work.

In the case of Heartport, each kit for femoral artery catheterization for CPB costs $5000.00, one of which is required per procedure. Heartport supplies reusable instruments to the hospital, trains the surgical team, and gives out educational and promotional materials in return for a contract to purchase 30 kits. Let us assume, based on comments by Reichenspurner that hospital stay may be reduced from 7-10 days to 5 days using the Heartport system. (Heartport themselves give a similar estimate of "6 or more to three or four days".) We then have a 3-5 day savings in hospital stay. Further assume that ICU stay is the same in either procedure so this savings occurs in regular bed savings at a cost of $800/day. This gives a hospital stay savings of $2400.00 - $4000.00. Considering that the Heartport instruments may replace some other instruments, then this savings may roughly offset the higher cost of the Heartport instruments. A major cost savings does not seem to exist here.

The other major factor which is typically not included in cost analyses of laparoscopic cholecystectomy and coronary angioplasty is the cost to the employer or

employee of lost days at work. The main reason to perform MIS CABG is to avoid sternotomy. Heartport states that normal activity might be resumed in 1 - 2 weeks instead of 4 - 12 weeks, which represents a savings of 2 - 11 weeks. If we assume a savings per day of $100.00, then for 10 - 55 reduced days of convalescence, we have a $1000.00 - $5500.00 savings. If the daily savings are $1000.00, we have $10,000.00 - $55,000.00 savings, and for $3000.00 a day the savings would be $30,000.00 - $165,000.00. This represents a substantial savings, though of course it depends on the value we attribute to lost days of work. While this cost is real, it is difficult to see it driving the use of the technology since neither the hospital nor the payer see it.

If we consider models for laparoscopic cholecystectomy and coronary angioplasty however, I would speculate that patient satisfaction, the desire for surgeons to improve patient outcomes despite lacking appropriate data, and the general desire to keep abreast with the latest technologies will be sufficient to drive the diffusion of these techniques into the market.

A.5 Conclusions

The original question was "Will minimally invasive CABG using technology currently on the market be worthwhile".

Considering the first question, I feel the answer is yes, though not for the reasons I originally expected. The first assumption is that the overall complication rate will not be substantially different than in the open case. We might expect fewer wound related complications in MIS CABG, but possibly greater procedure related complications as well which will diminish as surgeons become more skilled and the procedures become further developed.

The main cost will then be due to increased cost of MIS instrumentation, and the main savings will be due to decreased hospital stay. This is from the perspective of the hospital or payer organization. While the perception might initially be different, I believe these costs will essentially cancel. A hidden savings, not seen by the hospital or payer, but rather by the patient or their employer due to the reduced period of convalescence. If the patient is not employed, this still represents a measure of patient satisfaction.

Therefore, the introduction of these techniques, even if they financially break even from the point of view of the hospital/payer, they appear to be worthwhile from an individual patient perspective and from a societal perspective because of the decreased convalescence times involved. Based on our experience with laparoscopic cholecystectomy and coronary angioplasty, patient satisfaction (which correlates with

decreased convalescence) combined with doctors' desire to improve outcomes and to stay abreast with the technology will drive this technology into the marketplace.

Bibliography

An, C. (1986). *Trajectory and Force Control of a Direct Drive Arm*. PhD thesis, Department of Electrical Engineering and Computer Science, MIT.

Asada, H. and Kanade, T. (1982). Design of direct-drive mechanical arms. *ASME Journal of Vibration, Acoustics, Stress, and Reliability in Design*, 105:313–316.

Asada, H. and Slotine, J. (1986). *Robot Analysis and Control*. John Wiley and Sons.

Asada, H. and Youcef-Toumi, K. (1984). Analysis of multi-degree of freedom actuator systems for robot arm design. *ASME Journal of Dynamic Systems, Measurement, and Control*, 106:225–230.

BARI (1991). Protocol for the bypass angioplasty revascularization investigation. *Circulation*, 84:SupplV:V–1–V–27.

Bass, E. et al. (1991). Cost-effectivenes of extracorporeal shock-wave lithotripsy versus cholecystectomy for symptomatic gallstones. *Gastroenterology*, 101:189–199.

Bass, E. B., Pitt, H., and Lillemoe, K. (1993). Cost-effectiveness of laparascopic cholecystectomy versus open cholecystectomy. *The American Journal of Surgery*, 165:466–471.

Bejczy, A. and Jr., J. S. (1983). Controlling remote manipulators through kinesthetic coupling. *Computers in Mechanical Engineering*, pages 48–60.

Bernard, H. and Hartman, T. (1993). Complications after laparascopic cholecystectomy. *The American Journal of Surgery*, 165:533–535.

Bloom, B., Fendrick, A., and McLane, C. (1995). Predicting effects of minimal invasive therapy. *Health Policy*, 33:179–187.

Blumstein, J. (1982). Responsibility and accountability in provider-patient relationships. *Circulation*, 66 Suppl III:III–91–III–101.

Boff, K., Kaufman, L., and (eds), J. T. (1986). *Handbook of Perception and Human Performance*. John Wiley & Sons.

Bolanowski, S., Gescheider, G., Verrillo, R., and Checkosky, C. (1988). Four channels mediate the mechanical aspects of touch. *The Journal of the Acoustical Society of America*, 84(4):1680–1694.

Burdea, G. (1996). *Force and Touch Feedback for Virtual Reality*. John Wiley and Sons.

Burdea, G. and Zhuang, J. (1991b). Dextrous telerobotics with force feedback - an overview. part 1 human factors. *Robotica*, 9:171–178.

Burdea, G. and Zhuang, J. (1991a). Dextrous telerobotics with force feedback - an overview. part 2 control and implementation. *Robotica*, 9:291–298.

Buttolo, P. and Hannaford, B. (1995). Pen-based force display for precision manipulation in virtual environment. In *Proceedings IEEE Virtual Reality Annual International Symposium*, North Carolina.

CASS (1983a). Coronary artery surgery study (cass): A randomized trial of coronary artery bypass surgery, survival data. *Circulation*, 68(5):939–950.

CASS (1983b). Coronary artery surgery study (cass): A randomized trial of coronary artery bypass surgery, quality of life in patients randomly assigned to treatment groups. *Circulation*, 68(5):951–960.

Club, S. S. (1991). A prospective analysis of 1518 laparascopic chelecystectomies. *The New England Journal of Medicine*, 324:1073–1078.

Cohen, H. (1982). On the quality of life: Some philosophical reflections. *Circulation*, 66, Suppl III:III–29–III–33.

Cohen, H., Solnick, M., and Stephenson, A. (1982). The financing of coronary artery bypass surgery. *Circulation*, 66, Suppl III:III–49–III–55.

Colgate, J. and Hogan, N. (1989). An analysis of contact instability in terms of passive physcial equivalents. In *Proc. IEEE International Conference on Robotics and Automation*, pages 404–409.

Costello, G. (1985). Wire rope. In *Mechanical Design Systems Handbook, 2nd ed.* McGraw-Hill.

Cuschieri, A., Dubois, F., Mouiel, J., et al. (1991). The european experience with laparascopic cholecystecomy. *The American Journal of Surgery*, 161:285–287.

Davidoff, A. et al. (1992). Mechanisms of major biliary injury during laparascopic cholecystectomy. *Annals of Surgery*, 215(3):196–202.

DiPietro, D. (1988). Development of an active compliant underwater manipulator. Master's thesis, Department of Mechanical Engineering, MIT.

Eppinger, S. (1988). *Modeling Robot Performance for Endpoint Force Control*. PhD thesis, Department of Mechanical Engineering, MIT.

Escarce, J. et al. (1995). Diffusion of laparascopic cholecystectomy among general surgeons in the united states. *Medical Care*, 33(3):256–271.

FerroTec, I. (1996). *Thermoelectric Product Catalog and Technical Reference Manual*.

Fisher, K., Redick, E., and Olsen, E. (1991). Laparascopic cholecystectomy: Cost analysis. *Surgical Laparascopy and Endoscopy*, 1(2):77–81.

Flatau, C. et al. (1972). Compact servo master-slave manipulator with optimize communication links. In *Proceedings of the 20th Conference on Remote Systems Technology*, page 296.

Flatau, C. R. (1973). Design outline for mini-arms based on manipulator technology. Technical report, MIT Artificial Intelligence Laboratory, AI-TR 300.

Fulton, J. (1955). *A Textbook of Physiology*. W.B. Saunders Co., Philadelpha.

Goertz, R. (1954). Mechanical master-slave manipulator. *Nucleonics*, 12(11):45,46.

Goertz, R. and Thompson, R. (1954). Electronically controlled manipulator. *Nucleonics*, 12(11):46,47.

Grimson, W., Ettinger, G., White, S., Lozano-Perez, T., III, W. W., and Kikinis, R. (1996). Automatic registration for multiple sclerosis change detection. In *IEEE Workshop Biomedical Image Analysis*, volume 15-2, pages 129–140, Seattle, WA.

Hamlin, G. J. and Sanderson, A. C. (1994). A novel concentric multilink spherical joint with parallel robotics applications. In *Proc. IEEE International Conference on Robotics and Automation*, pages 1267–1272.

Hamm, C. et al. (1994). A randomized study of coronary angioplasty compared with bypass surgery in patients with symptomatic multivessel coronary disease. *The New England Journal of Medicine*, 331:1037–43.

Hampton, J. et al. (1993). Coronary angioplasty versus coronary artery bypass surgery: the randomised intervention treatment of angina rita) trial. *Lancet*, 341:573–580.

Hannaford, B. (1989). A design framework for teleoperators with kinesthetic feedback. *IEEE Transactions of Robotics and Automation*, 5(4):426–434.

Hannaford, B. (1991). Kinesthetic feedback techniques in teleoperated systems. In *Control and Dynamic Systems, vol 40*. Academic Press.

Hannaford, B., Wood, L., McAfee, D. A., and Zak, H. (1991). Performance evaluation of a six-axis generalized force-reflecting teleoperator. *IEEE Transactions on Systems, Man, and Cybernetics*, 21(3):620–633.

Hill, J. W., Green, P. S., Jensen, J. F., Gorfu, Y., and Shah, A. S. (1994). Telepresence surgery demonstration system. In *Proc. IEEE International Conference on Robotics and Automation*, pages 2302–2307.

Hunter, I. W., Jones, L. A., Sagar, M. A., LaFontaine, S. R., and Hunter, P. J. (1995). Opthalmic microsurgical robot and associated virtual environment. *Computers in Biology and Medicine*, 25(2):172–182.

Hunter, I. W., Lafontaine, S., Hunter, P. M. N. P. J., and Hollerbach, J. M. (1989). Manipulation and dynamic mechanical testing of microscopic objects using a tele-micro-robot system. In *Proc. IEEE International Conference on Robotics and Automation*, pages 1553–1557.

Hunter, I. W., LaFontaine, S. R., Nielsen, P. M. F., Hunter, P. J., and Hollerbach, J. M. (1990). Manipulation and dynamic mechanical testing of microscopic objects using a tele-micro-robot system. *IEEE Control Systems Magazine*, 10(2):3–9.

Hunter, J. G. and Sackier, J. M. (1993). *Minimally Invasive Surgery*. McGraw-Hill, Inc.

Jr., L. W., Chapman, W., Bonau, R., Jr., E. M., boyd, R., and Jacobs, J. (1993). Comparison of laparascopic cholecystectomy with open cholecsystectomy in a single center. *The American Journal of Surgery*, 165:459–465.

Kazerooni, H. (1985). *A Robust Design Method for Impedance Control of Constrained Dynamic Systems*. PhD thesis, Department of Mechanical Engineering, MIT.

King, S. et al. (1994). A randomized trial comparing coronary angioplasty with coronary bypass surgery. *The New England Journal of Medicine*, 331:1044–50.

Kleinbeck, S. and Hoffart, N. (1994). Outpatient recovery after laparascopic chole-cystectomy. *AORN Journal*, 60(3):394–402.

Kontarinis, D. A. (1995). *Tactile Displays for Dextrous Telemanipulation*. PhD thesis, Harvard University.

Legorreta, A., Silber, J., Costantino, G., Kobylinski, R., and Zatz, S. (1993). In-creased cholecystectomy rate after the introduction of laparascopic cholecystec-tomy. *Journal of the American Medical Association*, 270(12):1429–1432.

Levin, M. D. (1990). Design and control of a closed-loop brushless torque activator. Technical report, MIT Artificial Intelligence Laboratory, AI-TR 1244.

Long, G. L., Paul, R. P., and Fisher, W. D. (1989). The hamilton wrist: A four-revolute-joint spherical wrist without singularities. In *Proc. IEEE International Conference on Robotics and Automation*, pages 902–907.

Mason, M. and Salisbury, J. K. (1985). *Robot Hands and the Mechanics of Manipu-lation*. MIT Press.

Massie, T. H. and Salisbury, J. K. (1994). The phantom haptic interface: A device for probing virtual objects. In *Dynamic Systems and Control*, pages 295–299, Chicago, Il. ASME.

McMahon, A., Gramsay, G., Baxter, J., and Galloway, D. (1994). Laparascopic and minilaparotomy cholecystectomy: A randomized trial comparing posteroperative pain and pulmonary function. *Surgery*, 115(5):533–539.

Mehta, S. N. (1997). Robotics may spur less-invasive surgery. *The Wall Street Journal*.

Minsky, M. (1995). *Computational Haptics: The* Sandpaper System for Synthesizing Texture for a Force-Feedback Display. PhD thesis, School of Architecture and Planning, MIT.

Morrell, J. B. (1996). *Parallel Coupled Micro-Macro Actuators*. PhD thesis, Mechan-ical Engineering, MIT.

Murphy, M., Hultgren, H., and Detre, K. (1977). Treatment of chronic stable angina. a preliminary report of survival data of the ransomized veterans administration cooperative study. *The New England Journal of Medicine*, 297:621–27.

Narasimhan, S. (1988). Dextrous robotic hands: Kinematics and control. Technical report, MIT Artificial Intelligence Laboratory, AI-TR 1056.

Neisius, B., Dautzenberg, P., Trapp, R., and Buess, G. (1995). Robotic telemanipulation for laparascopy. In *Proceedings of the 1995 IEEE Engineering in Medicine and Biology 17th Annual Conference and 21st Canadian Medical nad Biological Engineering Conference*, volume 17-2, pages 1199–1200.

Neugebauer, E., Troidl, H., Spangenberger, W., Dietrich, A., Lefering, R., and Group, T. C. S. (1991). Conventional versus laparascopic cholecsytectomy and the randomized clinical trial. *The British Journal of Surgery*, 78:150–154.

Niemeyer, G. (1996). *Using Wave Variables in Time Delayed Force Reflecting Teleoperation*. PhD thesis, Department of Aeronautics and Astronautics, MIT.

NIH (1993). Nih consensus conference - gallstones and laparaoscopic cholecystectomy. *Journal of the American Medical Association*, 269(8):1018–1024.

Paul, B. J. (1987). A systems approach to the torque control of a permanent magnet brushless motor. Technical report, MIT Artificial Intelligence Laboratory, AI-TR 1081.

Pratt, G. A. and Williamson, M. M. (1995). Series elastic actuators. In *Proceedings of the IEEE/RSJ International Conference on Intelligent Robots and Systems (IROS-95)*, volume 1, pages 399–406, Pittsburg, PA.

Preston, T. (1989). Assessment of coronary bypass surgery and percutaneous transluminal angioplasty. *International Journal of Technology Assesment in Health Care*, 5:431–442.

Rapaport, E. (1982). An overview of issues. *Circulation*, 66, Suppl III:III-3-III-5.

Reeder, G. et al. (1984). Is percutaneous coronary angioplasty less expensive than bypass surgery? *The New England Journal of Medicine*, 311(18):1157–1162.

Reichert, M. (1993). Laparoscopic instruments. *AORN Journal*, 57(3):637–655.

Reichnspurner, H., Gulielmos, V., Daniel, W., and Schuler, S. (1997). Letter: Minimally invasive coronary bypass surgery. *The New England Journal of Medicine*, 336(1):67–68.

Rodriguez, A. et al. (1993). Argentine randomized trial of percutaneous transluminal coronary angioplasty versus coronary artery bypass surgery in multivessel desease (eraci). *Journal of the American College of Cardiology*, 22:1060–7.

Rosheim, M. E. (1989). *Robot Wrist Actuators*. John Wiley and Sons.

Salcudean, S. and Yan, J. (1994). Towards a force-reflecting motion-scaling system for microsurgery. In *Proc. IEEE International Conference on Robotics and Automation.*

Salisbury, J. (1982). *Kinematic and Force Analysis of Articulated Hands.* PhD thesis, Stanford University.

Salisbury, J. and Craig, J. (1982). Articulated hands: Force control and kinematic issues. *International Journal of Robotics Research,* 1(1).

Salisbury, J. K., Eberman, B., Levin, M., and Townsend, W. (1989). The design and control of an experimental whole-arm manipulator. In *Robotics Research: The Fourth International Symposium.*

Salisbury, K., Eberman, B., Levin, M., and Townsend, W. (1990). An experimental whole-arm manipulator. In Winston, P. H. and Shellard, S. A., editors, *Artifical Intelligence and MIT Expanding Frontiers,* chapter 33, pages 228–249. MIT Press, Cambridge, MA.

Sastry, S., Cohn, M., and Tendick, F. (1997 To Appear). Millirobitcs for remote, minimally invasive surgery. *Journal of Robotic Systems.*

Schempf, H. (1990). *Comparative Design, Modeling, and Control Analysis of Robotic Transmission.* PhD thesis, Oceanography and Oceonographic Engineering, MIT.

Schenker, P. and Charles, S. (1995). Development of a telemanipulator for dexterity enhanced microsurgery. In *Second International Symposium on Medical Robotics and Computer Assisted Surgery.*

Sharon, A. (1988). *The Macro/Micro Manipulator: An Improved Architecture for Robot Control.* PhD thesis, Department of MechanicalEngineering, MIT.

Sharon, A., Hogan, N., and Hardt, D. (1988). High bandwidth force regulation and inertia reduction using a macro/micro manipulator system. In *IEEE,* pages 126–132.

Sharon, A., Hogan, N., and Hardt, D. (1993). The macro/micro manipulator: An improved architecture for robot control. *Robotics and Computer Integrated Manufacturing,* 10(3):209–222.

Sheridan, T. (1992). *Telerobotics, Automation and Human Supervisory Control.* MIT Press.

Sherrick, C. and Cholewiak, R. (1986). Cutaneous sensitivity. In *Handbook of Perception and Human Performance - Sensory Processes and Perception*, volume 10, pages 12–30. John Wiley & Sons, Inc, New York.

Steiner, C., Bass, E., Talamini, M., Pitt, H., and Steinberg, E. (1994). Surgical rates and operative mortality for open and laparascopic cholecystectomy in maryland. *The New England Journal of Medicine*, 330(3):403–408.

Tallon, R. (1996). Laparascopic cholecystectomy: A technological assesment. *Nursing Management*, 27(4):52–54.

Tan, H., Pang, X., and Durlach, N. (1992). Manual resolution of length, force, and compliance. *"Advances in Robotics*, 42:13–18.

Tan, H., Srinivasan, M., Eberman, B., and Cheng, B. (1994). Human factors for the design of force-reflecting interfaces. *ASME Journal of Dynamic Systems and Control*, DSC-55(1).

Tan, H. Z. (1996). *Information Transmission with a Multi-Finger Tactual Display*. PhD thesis, Department of Electrical Engineering, MIT.

Tan, H. Z., Durlach, N., Shao, Y., and Wei, M. (1993). Manual resolution of compliance when work and force cues are minimized. In *The ASME Winter Annual Meeting*.

Taylor, R. H. et al. (1995). *Remote Center-of-Motion Robot For Surgery*. United States Patent #5,397,323.

Taylor, R. H., Funda, J., Eldridge, B., LaRose, D., and Gomory, S. (Dec 1994). A telerobotic assistant for laparoscopic surgery. *"IEEE EMBS Magazine"*.

Townsend, W. T. (1988). *The Effect of Transmission Design on the Performance of Force-Controlled Manipulators*. PhD thesis, Dept. Mechanical Eng., MIT.

Traverso, L. W. (199). Technology and surgery, dilemma of the gimmick, true advances, and cost effectiveness. *Surgical Clinics of North America*, 76(1):129–138.

Traverso, L. W. (1995). A prospective cost analysis of laparascopic cholecystectomy. *The American Journal of Surgery*, 169:503–506.

Varnauskas, E. (1988). Twelve-year follow-up of survival in the randomized european coronary surgery study. *The New England Journal of Medicine*, 319:332–333.

Vertut and Coiffet (1986). *Robot Technology, Vol 3A, Teleoperations and Robotics: Evolution and Development*. Prentice Hall.

Volpe, R. and Khosla, P. (1992). An experimental evaluation and comparison of explicit frocecontrol strategies for robotic manipulators. In *Proc. IEEE International Conference on Robotics and Automation*, pages 1387–1393.

Voyles, C. (1993). The laparascopic buck stops here. *The American Journal of Surgery*, 165:472–473.

Weinstein, M. and Stason, W. (1982). Cost-effectiveness of coronary artery bypass sugery. *Circulation*, 66, Suppl III:III–56–III–66.

Whitney, D. (1985). Historical perspective and and state of the art in robot force control. In *Proc. IEEE International Conference on Robotics and Automation*, pages 262–268.

Winslow, R. (1997). Hope and hype follow heart-surgery method that's easy on patients. *The Wall Street Journal*, page A1.

Zilles, C. (1995). Haptic rendering with the toolhandle haptic interface. Master's thesis, Department of Mechanical Engineering, MIT.